Volume 96 Number 11 November 2015

BAMS

Bulletin of the American Meteorological Society

ODDS FOR WHITE CHRISTMAS

SUDDEN STRATOSPHERIC WARMING

THE HURRICANE THRESHOLD

THE MATTERHORN

COMPLEX FLOWS, COMPLEX TERRAIN

ATMOSPHERIC RADIATION INSTRUMENTATION

UV PYRANOMETERS

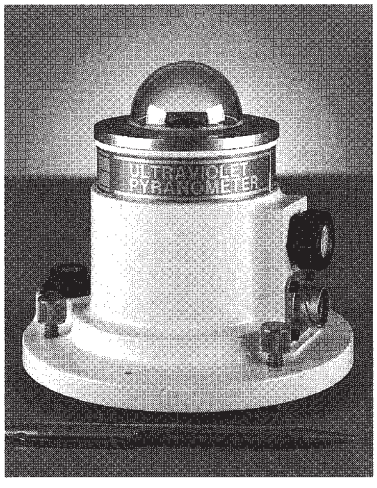

Thermally stabilized for long-term reference-grade measurements of global solar UV irradiance. Spectral sensitivity of 280 to 320 nm in the UVB and 320 to 400 nm in the UVA. High-level 0-5 VDC output signal. Hundreds in use in networks throughout the world.

FILTER SPECTROMETERS

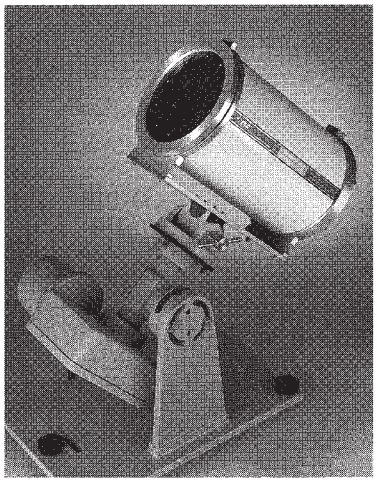

Measure direct normal solar irradiance at up to ten narrow-band wavelengths from 300 to 940 nm. Energy absorbing prefilters and state-of-the-art interference filters are environmentally sealed and thermally controlled to ensure long term stability. Mounts on most trackers.

MULTIFILTER ROTATING SHADOWBAND RADIOMETERS

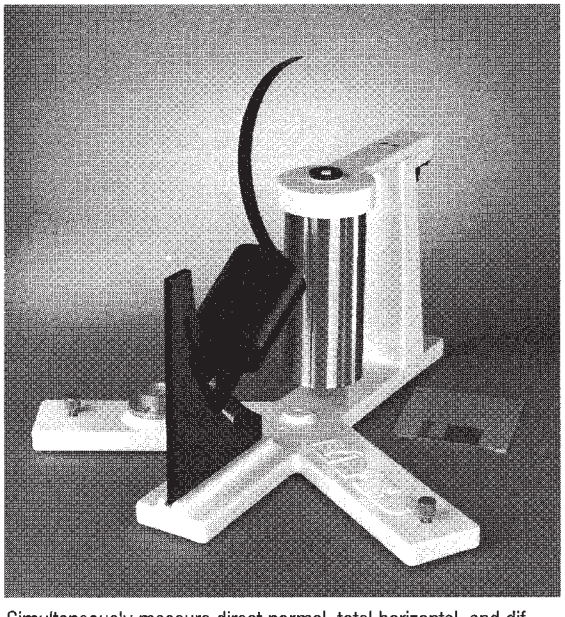

Simultaneously measure direct normal, total horizontal, and diffuse horizontal spectral irradiance using a unique algorithm and computer-controlled shadowband. Independent interference filter-diode detectors from 300 nm to 940 nm provide optical depth, aerosol, column ozone and water vapor data.

TOTAL SOLAR PYRANOMETERS

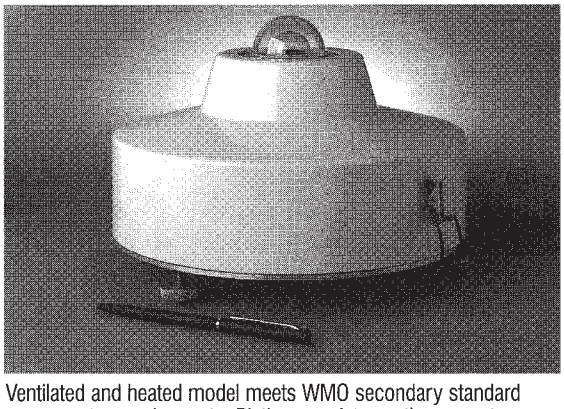

Ventilated and heated model meets WMO secondary standard pyranometer requirements. Platinum resistance thermometers replace older thermopile technology, resulting in an excellent cosine response and a high level output signal that is totally independent of ambient temperature changes.

YES produces an advanced line of atmospheric radiation instrumentation for reference-grade measurements in the UV through the visible and into the near-IR. Our instruments are field proven in networks throughout the world and form the core of the U.S. government's UVB monitoring network. All instruments are fully characterized in our state-of-the-art Optical Calibration laboratory.

E-mail, call, fax or write for detailed technical brochures on our products.

YES
YANKEE ENVIRONMENTAL SYSTEMS, INC.

Airport Industrial Park
101 Industrial Blvd., Turners Falls, MA 01376 USA
Tel: (413) 863-0200 Fax: (413) 863-0255
E-mail: info@sunlight.yesinc.com http://www.yesinc.com

BAMS
Bulletin of the American Meteorological Society
VOLUME 96, NUMBER 11, NOVEMBER 2015

IN BOX

MAP ROOM

ARTICLES

ON THE COVER

Mountains and adjacent valleys have complex, interacting atmospheric flows on multiple scales, often leading to sudden, highly local changes in weather. The Mountain Terrain Atmospheric Modeling and Observations (MATERHORN) program answers applications-driven questions about this difficult environment by investigating predictability in models, conducting field observations at Dugway Proving Ground, and developing new technology and parameterizations. For more information, see the article by Fernando et al., starting on p. 1945. (Photo: Leonard & Carolina Montenegro)

MEETING SUMMARIES

CONTENTS

FOLLOW AMS

http://facebook.com/ametsoc

http://twitter.com/ametsoc

http://blog.ametsoc.org

The *Bulletin of the American Meteorological Society* is the official organ of the Society, devoted to editorials, articles of interest to a large segment of the membership, professional and membership news, announcements, and Society activities. Editing and publishing are under the direction of Keith L. Seitter, executive director. Contributors are encouraged to send proposals to be considered for publication. For guidance on preparation and style, see the Authors' Resource Center online at www.ametsoc.org/pubs/arcindex.html.

The Bulletin of the American Meteorological Society (ISSN 0003-0007) is published monthly by the American Meteorological Society, 45 Beacon St., Boston, MA 02108-3693. Periodical postage paid at Boston, MA, and at additional mailing offices. Subscription price to members is included in annual dues. Subscription price to nonmembers is available on request; single issues are $12.50 each for members, $20 for nonmembers (prices incl. shipping and handling). Address all business communications to the Executive Director, AMS, 45 Beacon St., Boston, MA 02108-3693 (617-227-2425). POSTMASTER: Send address changes to Bulletin of the American Meteorological Society, 45 Beacon St., Boston, MA 02108-3693.

LETTER FROM THE EDITOR: THRESHOLD OF CHANGE

The seasons have turned. I can feel it in the air—the humidity has dropped, the sunlight is no longer intense, the nights have chilled. I have even switched the thermostat to "on" for the mornings.

The realization was sudden, but the days have actually been changing gradually. Not everyone would agree on the precise moment when this new season revealed itself. Despite the calendar, we all see the light, the cold, and the leaves differently. Setting the thermostat, however, is definitive—a tangible moment, a threshold crossed.

Thresholds are important to our way of thinking. No matter what the date or temperature, some of us hold off on conceding the arrival of winter until snow blankets the ground—hence one reason for the importance of a White Christmas, a holiday that, in the Northern Hemisphere at least, confirms winter's arrival. Happily, for the snow lovers, Imke Durre and Michael Squires show us in this issue (p. 1853) that if your threshold for "white" allows snowfall, not just snow cover, to qualify, then your White Christmas is significantly more likely over a much larger portion of the United States.

Sudden Stratospheric Warming does not gradually creep up on us like the seasons, but it is apparently not enough to be a major upheaval of temperature or reversal of circulation to satisfy the needs of science. Amy Butler and colleagues note (p. 1913) that no single standard definition of SSWs exists, and they argue for establishment of a "standard threshold" for major SSWs…"to ensure a consistent metric of polar stratospheric variability."

Another type of threshold figures in the article by Angelyn Moore and colleagues (p. 1867). They report on a National Weather Service initiative to increase GPS soundings in Southern California. By boosting density of moisture measurements, they found improvements in flash flood forecast and warning capabilities. Along the way, the local observing system passed a threshold of sufficient information,

One of the most memorable of thresholds in all of meteorology is the 26.5°C mark for sea surface temperatures—a minimum over which storm systems can develop into full blown tropical cyclones. That temperature mark has been enshrined in the scientific literature for almost 70 years, but it has not actually been accepted as exact. It may merely have been chosen for convenience, being so close to 80°F. There is even a matter of how to define the proper period and area of the relevant SST.

In this issue, Ron McTaggart-Cowan and colleagues (p. 1929) point out that roughly 5% of tropical storms around the world have developed over water that was cooler than that threshold. They propose a way around the SST threshold dilemma by looking at another metric altogether that recognizes the different pathways by which baroclinic systems transition into tropical systems when SSTs are low. While their solution has simplicity and evidence on its side, you're forgiven if you fear you will miss being able to click on and off the easy "80°F" switch that is etched in your memory. Cross this threshold of change and hurricane seasons may never be the same.

—*Jeff Rosenfeld,* Editor-in-Chief

ABSTRACTS

WHITE CHRISTMAS? AN APPLICATION OF NOAA'S 1981–2010 DAILY NORMALS

Are we going to have a white Christmas? That is a question that scientists at the National Oceanic and Atmospheric Administration (NOAA) receive each autumn from members of the media and general public. NOAA personnel typically respond by way of a press release and map depicting the climatological probability of observing snow on the ground on 25 December at stations across the contiguous United States. This map has become one of the most popular applications of NOAA's 1981–2010 U.S. Climate Normals.

The purpose of this paper is to expand upon the annual press release in two ways. First, the methodology for empirically calculating the probabilities of snow on the ground is documented. Second, additional maps describing the median snow depth on 25 December as well as the probability and amount of snowfall are presented.

The results are consistent with a climatologist's intuitive expectations. In the Sierras, Cascades, the leeward side of the Great Lakes, and northern New England, snow cover is a near certainty. In these regions, most precipitation falls as snow, and the probability of snowfall can exceed 25%. At higher elevations of the Rocky Mountains and at many locations between the northern Rockies and New England, snowfall is considerably less frequent on Christmas Day, yet the probability of snow on the ground exceeds 50%. For those who would like to escape the snow, the best places to be in late December are in Southern California, the lower elevations of the Southwest, and Florida. (*Page 1853*)

IMPROVING FLASH FLOOD FORECASTS: THE HMT-WPC FLASH FLOOD AND INTENSE RAINFALL EXPERIMENT

Despite advancements in numerical modeling and the increasing prevalence of convection-allowing guidance, flash flood forecasting remains a substantial challenge. Accurate flash flood forecasts depend not only on accurate quantitative precipitation forecasts (QPFs), but also on an understanding of the corresponding hydrologic response. To advance forecast skill, innovative guidance products that blend meteorology and hydrology are needed, as well as a comprehensive verification dataset to identify areas in need of improvement.

To address these challenges, in 2013 the Hydrometeorological Testbed at the Weather Prediction Center (HMT-WPC), partnering with the National Severe Storms Laboratory (NSSL) and the Earth System Research Laboratory (ESRL), developed and hosted the inaugural Flash Flood and Intense Rainfall (FFaIR) Experiment. In its first two years, the experiment has focused on ways to combine meteorological guidance with available hydrologic information. One example of this is the creation of neighborhood flash flood guidance (FFG) exceedance probabilities, which combine QPF information from convection-allowing ensembles with flash flood guidance; these were found to provide valuable information about the flash flood threat across the contiguous United States.

Additionally, WPC has begun to address the challenge of flash flood verification by developing a verification database that incorporates observations from a variety of disparate sources in an attempt to build a comprehensive picture of flash flooding across the nation. While the development of this database represents an important step forward in the verification of flash flood forecasts, many of the other challenges identified during the experiment will require a long-term community effort in order to make notable advancements. (*Page 1859*)

NATIONAL WEATHER SERVICE FORECASTERS USE GPS PRECIPITABLE WATER VAPOR FOR ENHANCED SITUATIONAL AWARENESS DURING THE SOUTHERN CALIFORNIA SUMMER MONSOON

During the North American Monsoon, low-to-midlevel moisture is transported in surges from the Gulf of California and Eastern Pacific Ocean into Mexico and the American Southwest. As rising levels of precipitable water interact with the mountainous terrain, severe thunderstorms can develop, resulting in flash floods that threaten life and property. The rapid evolution of these storms, coupled with the relative lack of upper-air and surface weather observations in the region, make them difficult to predict and monitor, and guidance from numerical weather prediction models can vary greatly under these conditions. Precipitable water vapor (PW) estimates derived from continuously operating ground-based GPS receivers have been available for some time from NOAA's GPS-Met program, but these observations have been of limited utility to operational forecasters in part due to poor spatial resolution. Under a NASA Advanced Information Systems Technology project, 37 real-time stations were added to NOAA's GPS-Met analysis providing 30-min PW estimates, reducing station spacing from approximately 150 km to 30 km in Southern California. An 18–22 July 2013 North American Monsoon event provided an opportunity to evaluate the utility of the additional upper-air moisture observations to enhance National Weather Service (NWS) forecaster situational awareness during the rapidly developing event. NWS forecasters used these additional data to detect rapid moisture increases at intervals between the available 1–6-h model updates and approximately twice-daily radiosonde observations, and these contributed tangibly to the issuance of timely flood watches and warnings in advance of flash floods, debris flows, and related road closures. (*Page 1867*)

NATURAL GAS PRICES AND THE EXTREME WINTERS OF 2011/12 AND 2013/14: CAUSES, INDICATORS, AND INTERACTIONS

Day-to-day volatility in natural gas markets is driven largely by variability in heating demand, which is in turn dominated by cool-season temperature anomalies over the northeastern quadrant of the United States ("Midwest–East"). Energy traders rely on temperature forecasts at horizons of 2–4 weeks to anticipate those fluctuations in demand. Forecasts from dynamical models are widely available, so the markets react quickly to changes in the model predictions. Traders often work with meteorologists who leverage teleconnections from the tropics and the Arctic to improve upon the model forecasts. This study

demonstrates how natural gas prices react to Midwest–East temperatures using the anomalous winters of 2011/12 and 2013/14. These examples also illustrate how energy meteorologists use teleconnections from the Arctic and the tropics to forecast heating demand.

Winter 2011/12 was exceptionally warm, consistent with the positive Arctic Oscillation (AO). March 2012 was a fitting exclamation point on the winter as it featured the largest warm anomaly for the United States above the twentieth-century climatology of any month since 1895. The resulting lack of heating demand led to record surpluses of natural gas storage and spurred prices downward to an 11-yr low in April 2012. In sharp contrast, winter 2013/14 was unusually cold. An anomalous Alaskan ridge led to cold air being transported from Siberia into the United States, despite the AO generally being positive. The ensuing swell in heating demand exhausted the surplus natural gas inventory, and prices rose to their highest levels since the beginning of the global recession in 2008. (*Page 1879*)

SEASONAL FORECASTING OF GLOBAL HYDROLOGIC EXTREMES: SYSTEM DEVELOPMENT AND EVALUATION OVER GEWEX BASINS

Seasonal hydrologic extremes in the form of droughts and wet spells have devastating impacts on human and natural systems. Improving understanding and predictive capability of hydrologic extremes, and facilitating adaptations through establishing climate service systems at regional to global scales are among the grand challenges proposed by the World Climate Research Programme (WCRP) and are the core themes of the Regional Hydroclimate Projects (RHP) under the Global Energy and Water Cycle Experiment (GEWEX). An experimental global seasonal hydrologic forecasting system has been developed that is based on coupled climate forecast models participating in the North American Multimodel Ensemble (NMME) project and an advanced land surface hydrologic model. The system is evaluated over major GEWEX RHP river basins by comparing with ensemble streamflow prediction (ESP). The multimodel seasonal forecast system provides higher detectability for soil moisture droughts, more reliable low and high flow ensemble forecasts, and better "real time" prediction for the 2012 North American extreme drought. The association of the onset of extreme hydrologic events with oceanic and land precursors is also investigated based on the joint distribution of forecasts and observations. Climate models have a higher probability of missing the onset of hydrologic extremes when there is no oceanic precursor. But oceanic precursor alone is insufficient to guarantee a correct forecast—a land precursor is also critical in avoiding a false alarm for forecasting extremes. This study is targeted at providing the scientific underpinning for the predictability of hydrologic extremes over GEWEX RHP basins and serves as a prototype for seasonal hydrologic forecasts within the Global Framework for Climate Services (GFCS). (*Page 1895*)

DEFINING SUDDEN STRATOSPHERIC WARMINGS

Sudden stratospheric warmings (SSWs) are large, rapid temperature rises in the winter polar stratosphere, occurring predominantly in the Northern Hemisphere. Major SSWs are also associated with a reversal of the climatological westerly zonal-mean zonal winds. Circulation anomalies associated with SSWs can descend into the troposphere with substantial surface weather impacts, such as wintertime extreme cold air outbreaks. After their discovery in 1952, SSWs were classified by the World Meteorological Organization. An examination of the literature suggests that a single, original reference for an exact definition of SSWs is elusive, but in many references a definition involves the reversal of the meridional temperature gradient and, for major warmings, the reversal of the zonal circulation poleward of 60° latitude at 10 hPa.

Though versions of this definition are still commonly used to detect SSWs, the details of the definition and its implementation remain ambiguous. In addition, other SSW definitions have been used in the last few decades, resulting in inconsistent classification of SSW events. We seek to answer the questions: How has the SSW definition changed, and how sensitive is the detection of SSWs to the definition used? For what kind of analysis is a "standard" definition useful? We argue that a standard SSW definition is necessary for maintaining a consistent and robust metric to assess polar stratospheric wintertime variability in climate models and other statistical applications. To provide a basis for, and to encourage participation in, a communitywide discussion currently underway, we explore what criteria are important for a standard definition and propose possible ways to update the definition. (*Page 1913*)

REVISITING THE 26.5°C SEA SURFACE TEMPERATURE THRESHOLD FOR TROPICAL CYCLONE DEVELOPMENT

A high sea surface temperature is generally accepted to be one of the necessary ingredients for tropical cyclone development, indicative of the potential for surface heat and moisture fluxes capable of fueling a self-sustaining circulation. Although the minimum 26.5°C threshold for tropical cyclogenesis has become a mainstay in research and education, the fact that a nonnegligible fraction of storm formation events (about 5%) occur over cooler waters casts some doubt on the robustness of this estimate. Tropical cyclogenesis over subthreshold sea surface temperatures is associated with low tropopause heights, indicative of the presence of a cold trough aloft. To focus on this type of development environment, the applicability of the 26.5°C threshold is investigated for tropical transitions from baroclinic precursor disturbances in all basins between 1989 and 2013. Although the threshold performs well in the majority of cases without appreciable environmental baroclinicity, the potential for development is underestimated by up to 27% for systems undergoing tropical transition. An alternative criterion of a maximum 22.5°C difference between the tropopause-level and 850-hPa equivalent potential temperatures (defined as the coupling index) is proposed for this class of development. When combined with the standard 26.5°C sea surface temperature threshold for precursor-free environments, error rates are reduced to 3%–6% for all development types. The addition of this physically relevant representation of the deep-tropospheric state to the ingredients-based conceptual model for tropical cyclogenesis improves the representation of the important tropical transition-based subset of development events. (*Page 1929*)

THE MATERHORN: UNRAVELING THE INTRICACIES OF MOUNTAIN WEATHER

Emerging application areas such as air pollution in megacities, wind energy, urban security, and operation of unmanned aerial vehicles have intensified scientific

SEND US YOUR THOUGHTS

We encourage readers to write to us with comments on what they read (or would like to read) in *BAMS*, as well as comments on AMS events and initiatives, or simply thoughts about what's happening in the world of atmospheric, oceanographic, hydrologic, and related sciences. When writing via e-mail, please send your messages to letterstotheeditor@ametsoc.org, or write to Letters to the Editor/*BAMS*, American Meteorological Society, 45 Beacon St., Boston, MA 02108. Your submissions will be considered for the "Letters to the Editor" column of *BAMS*.

and societal interest in mountain meteorology. To address scientific needs and help improve the prediction of mountain weather, the U.S. Department of Defense has funded a research effort—the Mountain Terrain Atmospheric Modeling and Observations (MATERHORN) Program—that draws the expertise of a multidisciplinary, multi-institutional, and multinational group of researchers. The program has four principal thrusts, encompassing modeling, experimental, technology, and parameterization components, directed at diagnosing model deficiencies and critical knowledge gaps, conducting experimental studies, and developing tools for model improvements. The access to the Granite Mountain Atmospheric Sciences Testbed of the U.S. Army Dugway Proving Ground, as well as to a suite of conventional and novel high-end airborne and surface measurement platforms, has provided an unprecedented opportunity to investigate phenomena of time scales from a few seconds to a few days, covering spatial extents of tens of kilometers down to millimeters. This article provides an overview of the MATERHORN and a glimpse at its initial findings. Orographic forcing creates a multitude of time-dependent submesoscale phenomena that contribute to the variability of mountain weather at mesoscale. The nexus of predictions by mesoscale model ensembles and observations are described, identifying opportunities for further improvements in mountain weather forecasting. (*Page 1945*)

NOWCAST

NEWS AND NOTES

Worsening Air Quality and Changing Weather in U.S. Parks

Air pollution, haze, and a changing climate are combining to plague U.S. national parks, according to a report recently released by the National Parks Conservation Association (NPCA). The analysis found that three-fourths of the studied parks have air that is unhealthy at least occasionally, 90% are experiencing weather that is unprecedented over the last century, and all of them have haze pollution that hinders visibility.

The study looked at 48 parks throughout that country that are most protected by the U.S. Clean Air Act. These parks are all covered by the Regional Haze Rule, a 1999 initiative to improve air quality in national parks and wilderness areas. By studying data taken from 2008 to 2013, the report found 36 of the parks at times experienced at least "moderate" ozone pollution (as based on the EPA's Air Quality Index), and four parks—Joshua Tree, Kings Canyon, Sequoia, and Yosemite, all in California—regularly had unhealthy ozone levels during that time. Meanwhile, haze pollution was found to affect the visibility at every park studied, with the dirty air clouding an average of 50 miles of scenery.

"Our parks remain under threat from air pollution, harming visitors' health, reducing visibility, and driving the impacts of climate change," says Ulla Reeves of NPCA's Clean Air Campaign.

The study also compared park data on temperature and precipitation taken in recent decades to that taken over the last century and found that almost every park has become hotter, drier, or wetter in the recently studied period.

The report assigned a letter grade to each park for each of three categories: "healthy air," "seeing clearly," and "changing climates." In all, 30 of the 48 parks received a "D" or worse in at least one of the three categories.

The full report can be found at www.npca.org/assets/pdf/NPCA-Polluted-Parks-July-2015.pdf.

Marine Organisms a Significant Source of Cloud Aerosols

Across Earth's oceans, powerful winds blow sea spray into the atmosphere, and at lower and middle latitudes this water is often enriched by organic matter produced by abundant phytoplankton. A new study in *Science Advances* has found that in the Southern Ocean in summer, these tiny aerosol particles stimulate a significant increase in cloud droplets in the region. Clouds with more droplets naturally reflect more sunlight and stifle solar radiation, a process revealed in this study that could be useful in climate research.

There are a number of different aerosols that seed cloud droplets, including sea salt and two marine organisms that are produced by phytoplankton: sulfates and organic matter aerosols. To distinguish the roles of these different types of aerosols, researchers utilized computer models and satellite measurements of cloud droplets taken from the Southern Ocean between 35°S and 55°S, from Brazil to the southernmost tip of Argentina.

"Satellite data allows us to observe events that occur over the course of months and on a scale of thousands of kilometers in the remotest regions on the planet," notes study coauthor Daniel

ECHOES

"I think the most exciting thing about this study is just to see what lightning can do."

—Reto Gieré, Earth and environmental sciences professor at the University of Pennsylvania, on a study that found a lightning strike changed the crystal structures of the rock it hit. The linear atomic-level structures, called shock lamellae, have previously been associated only with meteor strikes. The scientists sampled the rock, from southern France, and found that the layer underneath the fulgurite had parallel stripes, which tipped them off to the shock lamellae. Gieré explains the deformation was caused by the massive wave of stress the lightning strike brought on. The study was published in *American Mineralogist*. [Source: redorbit.com]

McCoy. "It really gives us an unparalleled glimpse of the Earth System's complexity."

By contrasting the concentrations of the three aerosols with the droplet measurements, the researchers developed a mathematical equation indicating how the sulfates and organic matter influence cloud droplet concentrations. They found that entering simulated aerosol data into the new model recreated the actual cloud droplet data quite well. The model showed that the sea salt was the primary source of the aerosols and produced about the same amount throughout the year. But the organic matter and sulfates produced more cloud droplets in the summer than during the winter, which led to the production of about twice as many cloud droplets in the summer. The researchers noted that areas in the Southern Ocean that were abundant with green phytoplankton were adjacent to atmospheric locations with many water droplets.

The greater number of summer cloud droplets led to an increase in the amount of sunlight reflected back into space of about 10 watts per meter squared during that season, which according to the article "is comparable to the annual mean increases expected from anthropogenic aerosols over heavily polluted regions of the Northern Hemisphere." Over the full year, the increase in reflected sunlight from the phytoplankton was about 4 watts per meter squared.

"It is a strong effect," says study coauthor Susannah Burrows of the Pacific Northwest National Laboratory. "But it makes sense because most of the area down there is ocean, with strong winds that kick up a lot of spray and lots of marine microorganisms producing these particles. And continental aerosol sources are mostly so far away that they only have a limited impact. Really, the marine aerosols are running the show there."

Indeed, past research into marine aerosols has generally been hindered by the influence of man-made pollution in coastal measurements, so the Southern Ocean was chosen for this study specifically because of the lack of human impacts there.

McCoy notes that the findings are "interesting in a climate sense, because the amount of sunlight that is being reflected by these clouds is to some extent determined by the number of cloud droplets," adding that the study's important climate implication "is that it gives us a way of understanding in a top-down, observationally based way what the interaction is between phytoplankton and cloud properties."

A second recent study, published in *Nature*, found that phytoplankton also can stimulate ice formation in clouds. That research, which focused on the Arctic Ocean, Western Atlantic, and North Pacific, combined direct measurements of biological matter taken from those regions with computer models of the atmosphere and discovered that a common type of phytoplankton releases organic material that nucleates ice. [Sources: DOE/Pacific Northwest National Laboratory, livescience.com]

ECHOES

"To be on the ground for two-and-a-half to three hours is phenomenal . . . and to miss everything is basically a miracle."

—Mike Macdonald, Environment Canada meteorologist, on the tornado that traveled across the Canadian province of Manitoba in July. Tornadoes rarely touch down for more than a few minutes in Canada, so the twister that stayed on the ground for almost three hours was a rare event. Since its path was in a rural part of the country, there were no injuries or deaths reported, only damaged buildings and roads. The tornado was part of an atypical weather pattern for that time of the year, which also brought cold and snow to parts of the U.S. Rocky Mountains along with damaging winds and hail to the northern Plains. The World Meteorological Organization's Randy Cerveny noted that "the path length distance of the Manitoba tornado might be shorter, but the duration may be comparable" to the longest-lasting twister on record, the Tri-State Tornado, which struck the U.S. Midwest in 1925 and was active for about 3.5 hours. [Source: *USA Today*]

Study Finds Coral Reefs Can Generate Huge Storm Waves

During Typhoon Haiyan in 2013, a series of tsunami-like waves flooded the town of Hernani in the Philippines. This was a surprising event, considering that a coral reef about a half-kilometer wide sits in the Pacific Ocean just offshore from Hernani, seemingly providing protection from waves. So what caused the giant waves, spaced apart by several minutes, to form? Rather than storm surge, which floods generally in a single influx of seawater, new research in *Nature Communications* reveals that the reef actually exacerbated the waves' enormity due to a particular type of wave-breaking process. The finding should be beneficial to the protection of coastal areas sheltered by reefs during powerful storms.

New Micromet Products

CSAT3B

Sensor head with integrated electronics

Improved sonic temp, accuracy & stability

Integrated inclinometer

31022 Zero Air Generator

Portable source of CO_2 and H_2O-free air

Zero any IRGA (IRGASON, LI-7500A, etc)

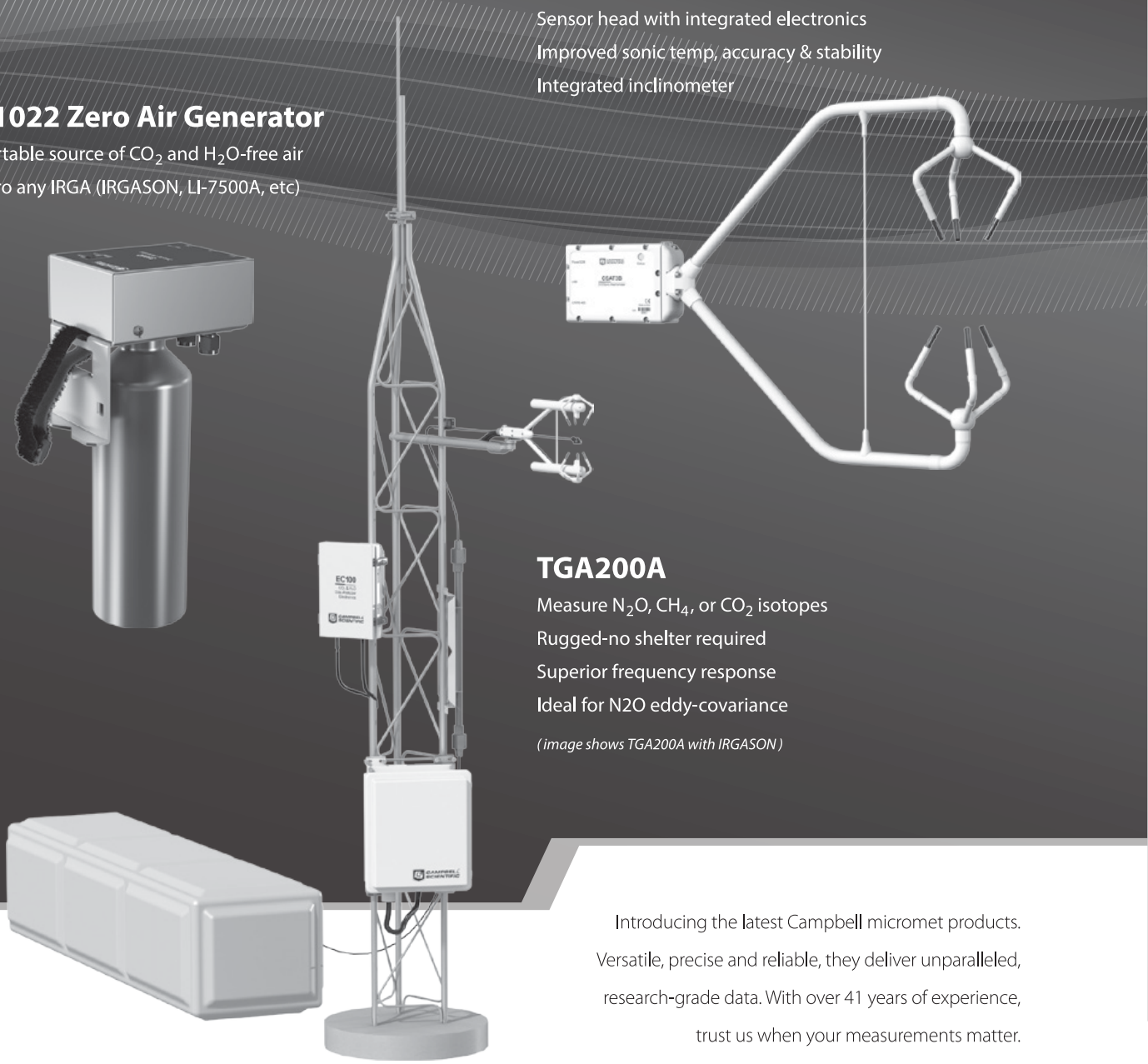

TGA200A

Measure N_2O, CH_4, or CO_2 isotopes

Rugged-no shelter required

Superior frequency response

Ideal for N2O eddy-covariance

(image shows TGA200A with IRGASON)

Introducing the latest Campbell micromet products. Versatile, precise and reliable, they deliver unparalleled, research-grade data. With over 41 years of experience, trust us when your measurements matter.

Call or visit: **435.227.9060**

campbellsci.com/bams

CAMPBELL SCIENTIFIC®

WHEN MEASUREMENTS MATTER

Volker Roeber and Jeremy Bricker of Tohoku University in Japan used a computer model to recreate the waves that struck Hernani. They found that their size and spacing was attributable to "surf beat," which occurs when longer waves in the open ocean catch up with shorter waves and create wave groups known as sets. The long group waves "can have wavelengths of several kilometers, but their height is much lower than that of the individual storm waves . . . similar to what characterizes nearshore tsunamis," explains Roeber.

But this was no ordinary surf beat. The steep, ocean-facing slope of the reef offshore from Hernani allows for a very short wave-breaking zone. The modeling showed that short storm waves broke and lost energy when encountering the reef, but the long group waves flowed over the reef nearly unaltered, creating an energized surf beat. Not only did the long waves retain almost all of their energy, but they also grew into turbulent—and devastating—breaking waves upon encountering the beach. The numerical models found the energy of these types of waves "to be very similar to waves from past tsunamis in the Pacific," according to Roeber.

The study revealed that each wave could have been even larger if the period of the group waves had coincided with the natural oscillation period of the reef—which would have occurred if the reef was about half as wide. It also found that the reef still protected the shoreline during moderate storms; the exacerbating effect only occurred during severe storms.

The findings could compel disaster management agencies to reassess their storm surge models, which "do a great job for what they were designed for, but…simply cannot account for the phenomena such as what we have seen in Hernani," states Bricker. [Source: Tohoku University]

African Fires Hamper Convection, Stifle Clouds and Rain

Farmers in Africa have long started fires to clear land and enhance productivity. These fires can have wide-reaching effects, and a new study in *Geophysical Research Letters* has found that they act to reduce rainfall and intensify drought during the region's dry season.

Researchers studied images taken from 2006 to 2010 on NASA's *Terra* spacecraft of smoky areas in Northern Africa (south of the Sahara Desert and north of the equator), and they also looked at photos from the companion *Aqua* satellite as well as the Tropical Rainfall Measuring Mission. They selected images showing varying cloud cover and four different types of weather conditions, and compared the evolution of cloud cover in those images to others with statistically identical weather conditions, but without the smoke. They then validated their results with a global atmospheric model. They found that during the smoky time periods, "[f]ire-emitted particles crippled the atmosphere's ability to build clouds and thunderstorms, and that ultimately caused a decrease in rainfall during what's already a seasonal drought," explains the study's lead author, Michael Tosca of the Jet Propulsion Laboratory.

On the other hand, regardless of weather conditions, there was more cloud cover during less smoky time periods. Smoke from African fires is profuse with black carbon particles, which liberally absorb sunlight and heat the surrounding air. This warm, dirty layer of air suppresses convection and, subsequently, the production of rain clouds.

"We are able not only to show that the clouds decrease in the presence of [these] aerosols, but that [the] aerosols inhibit convection," says Tosca. While he pointed out that these results had been suggested in earlier model studies, "it's really cool to see it in actual data."

He also noted that the dry land caused by the lack of rainfall makes it "easier for farmers to ignite more fires, which data show they probably do," and which then creates a cyclical effect that could ultimately lead to regional climate warming. [Source: NASA]

ECHOES

"It's critical to building people's confidence that what they do and say and think about climate can matter."

—Miranda Massie, a lawyer and creator of the Climate Museum Launch Project. The plan involves creating a museum in New York City that contains exhibits chronicling climate change. Massie got the idea after Hurricane Sandy in 2012, and the museum has now been approved by the New York Board of Regents and sketched out by architects. The goal of the museum is to cover the science in an accessible, interesting way and allow visitors to make connections with what they see in the museum to the outside world. The building process is going to take about six years, but when done Massie hopes it will serve indefinitely as a hub of climate awareness. [Source: Climate Central]

Highlights from the Royal Meteorological Society Journals

RMetS
Royal Meteorological Society

Browse Featured Articles from ***Quarterly Journal of the Royal Meteorological Society*** on Wiley Online Library

- **The effect of urbanisation on the climatology of thunderstorm initiation**
  Alex M. Haberlie et al.
- **Estimating low-frequency variability and trends in atmospheric temperature using ERA-Interim**
  A. J. Simmons et al.
- **High-latitude influence of the quasi-biennial oscillation**
  James A. Anstey and Theodore G. Shepherd

Coming soon to the App store! FREE Apps from ***Weather*** and ***Quarterly Journal***

Enjoy an entirely new browsing and reading experience. Keep up to date with the most important developments in the field, wherever you are, whenever you want.

Atmospheric Science Letters will be converting to Open Access in 2016

Going forward, manuscripts accepted for publication will be published open access and authors will be required to pay an APC.

OPEN

Benefits of publishing Open Access:

- Publish quickly and efficiently
- Increase the reach of your research: freely available on Wiley Online Library
- High-quality and authoritative standards:
  - Maintain the rigour of your work through traditional peer review standards and clear editorial policies
  - Get an expert publishing team on your side
- Increase your impact through easy sharing options such as social networking
- Retain copyright for the articles you publish under a Creative Commons License
- Automatically comply with open access mandates

WILEY

New Books in the Advancing Weather and Climate Science Series

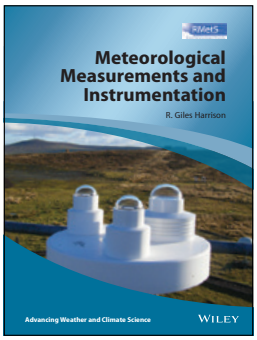

Meteorological Measurements and Instrumentation

Giles Harrison

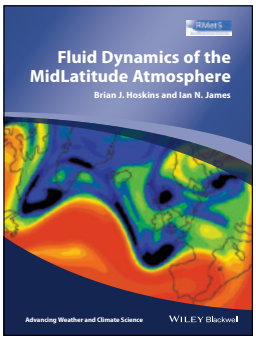

Fluid Dynamics of the Mid-Latitude Atmosphere

Brian J. Hoskins, Ian N. James

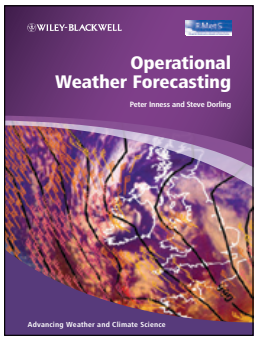

Operational Weather Forecasting

Peter Michael Inness, Steve Dorling

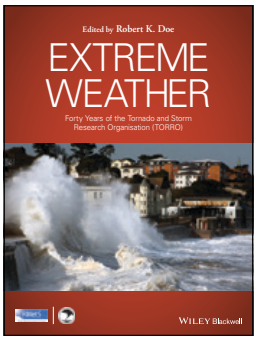

Extreme Weather: Forty Years of the Tornado and Storm Research Organisation (TORRO)

Robert K. Doe

Climate Science Books from Wiley

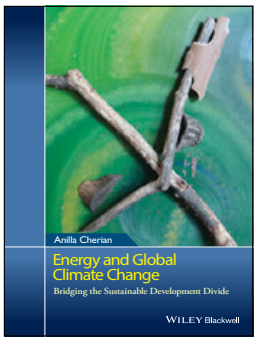

Energy and Global Climate Change: Bridging the Sustainable Development Divide

Anilla Cherian

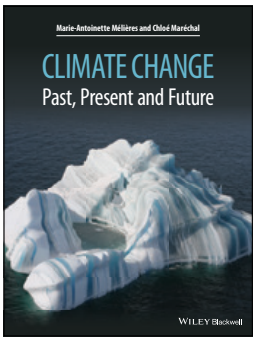

Climate Change: Past, Present, and Future

Marie-Antoinette Melières, Chloe Marechal

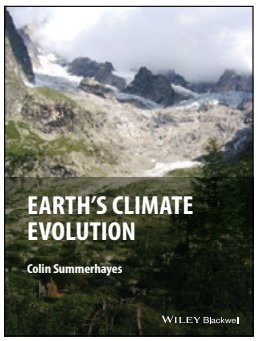

Earth's Climate Evolution

Colin P. Summerhayes

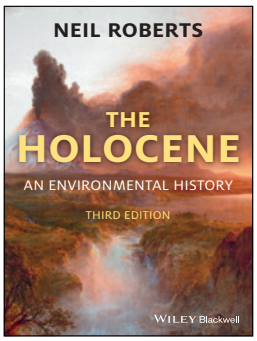

The Holocene: An Environmental History, 3rd Edition

Neil Roberts

Co-published with the American Geophysical Union

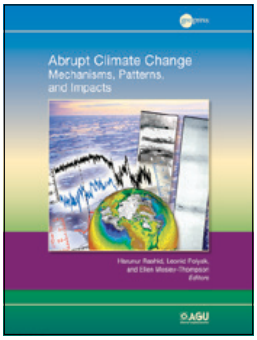

Abrupt Climate Change: Mechanisms, Patterns, and Impacts

Harunur Rashid, Leonid Polyak, Ellen Mosley-Thompson

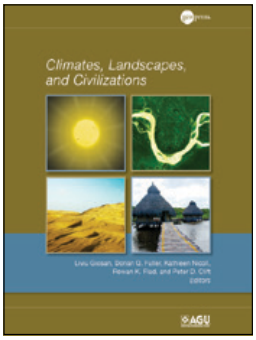

Climates, Landscapes, and Civilizations

Liviu Giosan, Dorian Q. Fuller, Kathleen Nicoll, Rowan K. Flad, Peter D. Clift

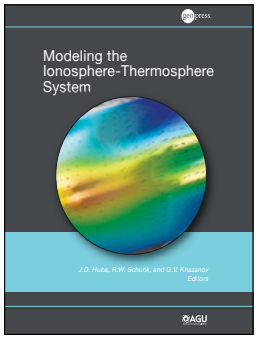

Modeling the Ionosphere-Thermosphere

J. D. Huba, R. W. Schunk, G. V. Khazanov

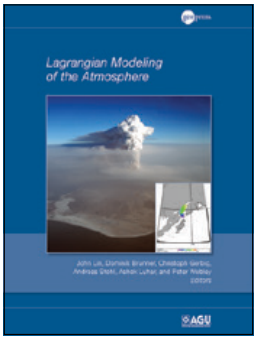

Lagrangian Modeling of the Atmosphere

John Lin

188208

AMS titles now available as eBooks at springer.com

AMS BOOKS

RESEARCH | APPLICATIONS | HISTORY

www.ametsoc.org/amsbookstore

Springer

Scan to see AMS eBook titles at springer.com

AMERICAN METEOROLOGICAL SOCIETY

White Christmas?

An Application of NOAA's 1981–2010 Daily Normals

By Imke Durre and Michael F. Squires

For many, Christmas is directly associated with snow. Christmas cards, carols, stories, and movies tend to depict a "white Christmas." Often these depictions portray a snow-covered landscape or falling snow. In most parts of the United States, however, a white Christmas is actually far from certain. Where, then, are the best places for experiencing snow on the ground or snowfall on Christmas Day? Where is there likely to be sufficient snow for skiing at that time? In which parts of the country might holiday travel be impeded by snow? These are the questions that this paper attempts to answer on the basis of NOAA's 1981–2010 U.S. Daily Climate Normals (Arguez et al. 2012).

For a number of years, NOAA's National Centers for Environmental Information (NCEI, formerly NCDC) has responded to requests for information about the odds of a white Christmas. An NCDC Technical Report from 1995 (Ross et al. 1995) provides probabilities of occurrence for snow depths equal to or exceeding various thresholds, using observations taken between 1961 and 1990 at several hundred cities across the continental United States. More recently, NCEI has issued a press release every December centered around a map of the probability of measurable (≥ 1 in., or 2.54 cm) snow depth across the country. Since 2011, the map has been based on the 1981–2010 Daily Normals, which include data from several thousand U.S. stations.

The purpose of this paper is to provide a more detailed assessment of the probability of a white Christmas than is possible in the annual press releases, and to document the methodology used to calculate the underlying daily climatological statistics.

AFFILIATIONS: Durre and Squires—NOAA National Centers for Environmental Information, Asheville, North Carolina
CORRESPONDING AUTHOR: Michael F. Squires, National Centers for Environmental Information, 151 Patton Avenue, Asheville, NC 28801
E-mail: Mike.Squires@noaa.gov

DOI:10.1175/BAMS-D-15-00038.1

METHODOLOGY. The results presented herein include two types of statistics taken from the 1981–2010 Daily Normals: probabilities of occurrence and medians of nonzero amounts. The statistics are computed empirically from once-a-day snow depth measurements as well as from 24-h totals of snowfall and precipitation at stations operated by the U.S. National Weather Service (Arguez et al. 2012; Durre et al. 2013). The Global Historical Climatology Network–Daily (GHCN-Daily) dataset (Menne et al. 2012) is the source of these data. Shown in this paper are results from the subset of stations where at least 25 of the years between 1981 and 2010 meet the relevant data completeness requirements (appendix A), and no more than three consecutive years fail to meet those requirements. The computational procedures are outlined here and described further in the appendices.

The climatological probability of occurrence for a calendar day is the percentage of years in which a particular event occurred on that day. For a 30-year period, however, using only the observations taken on exactly that day would yield a maximum sample size of 30 values, fewer when a station's record is incomplete. To increase the sample size, a 29-day window centered on the day of interest is used instead. Thus, the probability of a measurable snow depth on 25 December is based on measurements from 11–31 December and 1–8 January during 1981–2010. Once the probabilities have been calculated using the appropriate 29-day window for each day of the year, they are smoothed with a 29-day running mean in order to reduce random day-to-day variability (appendix A).

Medians of nonzero snow depth and snowfall amounts provide an indication of typical amounts

when snow depth or snowfall are present. They are computed within the same moving 29-day windows that are used in the computation of probabilities. A median for a specific day and variable is calculated only when nonzero amounts account for at least 10% of the total sample across all years and days in the window. As a result, medians are available only at stations and times of year at which this threshold is met. Furthermore, when the sample size is too small for one or more days within the snow season, some additional processing steps are employed to eliminate the resulting gap in the annual cycle (appendix B).

The combination of a 29-day window and 29-day running mean was chosen after sensitivity tests with different window sizes and smoothing filters. Based on visual inspection of resulting annual cycles of the various statistics included in the 1981–2010 Normals, the chosen combination strikes the best balance between dampening day-to-day sampling fluctuations and resolving the climatologically significant features of the annual cycle. To test the sensitivity of the statistics for 25 December in particular, the analyses shown in this paper were repeated for the stations listed in Table 1 using a five-day window together with a five-day running mean, requiring at least four of the five possible values to be available in each of at least 10 years. All of the probabilities thus obtained were within 5% of those shown in Table 1, and differences were less than 1% when the probability itself was small. Similarly, medians based on the five-day window were often identical to, and never more than half an inch different from, those computed with a 29-day window. Thus, the climatological patterns of probabilities and medians for 25 December are retained even with the use of a window that is 29 days long.

RESULTS. Figure 1 depicts the climatological probability that a snow depth of at least 1 in. (2.54 cm) was observed at locations across the contiguous United States on Christmas Day during 1981–2010. In addition, snow cover probabilities and related statistics for that calendar day at some specific locations are presented in Tables 1 and 2. A better than 50% chance of measurable snow on the ground was limited to the northern tier of states and higher elevations of the West. Values exceeded 75% at high mountain locations, in parts of North Dakota and Northern Minnesota, in the lee of the Great Lakes, and across northern New England. Crater Lake, Steamboat Springs, and Marquette are examples of locations where snow cover on Christmas Day was a virtual or complete certainty (Table 1).

Table 1. Probabilities of occurrence and medians of measurable snow depth and snowfall for selected U.S. cities where the probability of measurable snow on the ground on 25 Dec exceeds 20%. Entries are sorted in order of decreasing probability of snow on the ground. Medians are based on nonzero values only. By convention, measurable snowfall is defined as snowfall ≥ 0.1 in., measurable snow depth as snow depth exceeding 1 in.

City	Probability of Snow depth > 0	Median of Snow depth > 0	Probability of Snowfall > 0	Median of Snowfall > 0
Crater Lake, OR	100%	53"	52%	4.1"
Steamboat Springs, CO	98%	15"	44%	2.1"
Marquette, MI	97%	12"	61%	1.1"
Tahoe City, CA	87%	14"	23%	3.2"
Caribou, ME	86%	7"	42%	0.9"
Red Lodge, MT	85%	7"	17%	2.0"
Minot, ND	80%	3"	23%	1.0"
Burlington, VT	65%	4"	42%	0.8"
Los Alamos, NM	54%	5"	16%	1.5"
Salt Lake City, UT	53%	3"	28%	1.0"
Milwaukee, WI	48%	3"	26%	0.6"
Yankton, SD	47%	4"	11%	1.0"
Pittsburgh, PA	32%	2"	30%	0.6"
St. Louis, MO	21%	3"	13%	0.6"

Table 2. Probabilities of occurrence of measurable snow depth, snowfall, and precipitation for selected U.S. cities where the probability of measurable snow on the ground on 25 Dec is less than 10%. Entries are sorted in order of decreasing probability of snow on the ground and decreasing probability of precipitation. Measurable snowfall and snow depth are defined as in Table 1; measurable precipitation includes amounts ≥ 0.01 in.

City	Probability of Snow Depth	Probability of Snowfall	Probability of Precipitation
Oklahoma City, OK	8%	5%	17%
Portland, OR	4%	2%	68%
Raleigh, NC	1%	1%	29%
Birmingham, AL	<1%	1%	34%
San Antonio, TX	<1%	<1%	24%
Berkeley, CA	0%	0%	34%
Orlando, FL	0%	0%	21%
Tempe, AZ	0%	0%	13%

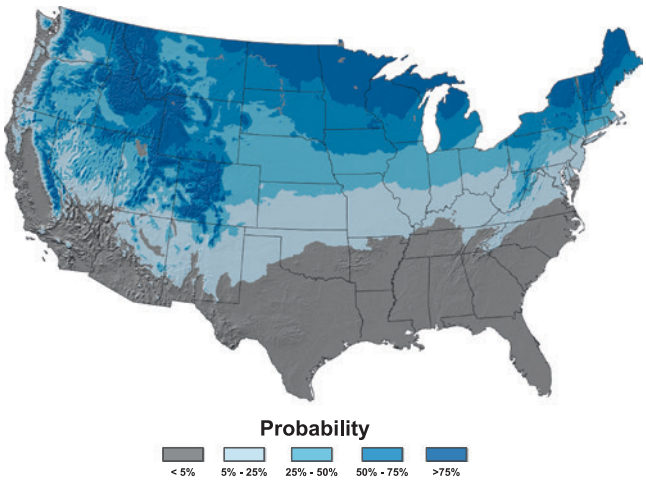

Fig. 1. Map of the climatological probability of at least 1 in. (2.54 cm) of snow on the ground on 25 Dec across the contiguous United States, derived from NOAA's 1981–2010 U.S. Daily Climate Normals. For this and all subsequent figures, station values are interpolated to a grid using thin plate splines (Vose et al. 2014).

East of the Rocky Mountains, the snow cover probability decreases from the high values in the North to values near zero in an area extending from Texas (excluding the panhandle) east to the Carolinas (Fig. 1, Table 2). In between these regions, there is a wide band with probabilities between 5% and 50%, as exemplified by Milwaukee, Yankton, Pittsburgh, and St. Louis (Table 1). From the Rockies westward, the influence of topography is apparent, with little or no chance of snow cover across southern Arizona and most of California, and probabilities below 50% at low elevations as far north as Oregon and Washington (e.g., 4% at Portland, Oregon).

The 1981–2010 25 December medians of nonzero snow depth observations are shown in Fig. 2. Not surprisingly, the large-scale spatial patterns in Figs. 1 and 2 roughly correspond to each other. The highest median values, exceeding 9 in. (22.86 cm), are found in the lee of Lake Superior and at high elevations in the Rockies, Sierras, and Cascades. Examples of such locations include Steamboat Springs and Tahoe City (Table 1), where the typically deep snow has led to the establishment of popular ski areas. Among the 1981–2010 Normals stations, the largest median snow depth on 25 December is 53 in. (134.62 cm) at Crater Lake, Oregon. East of the Rockies, a band of 1-to-3-in. (2.54-to-7.62-cm) snow depth medians extends eastward from the Colorado plains to the East Coast. Medians of 4 to 9 in. (10.16 cm to 22.86 cm) are found north of that region between the Rockies in the West and Maine in the East.

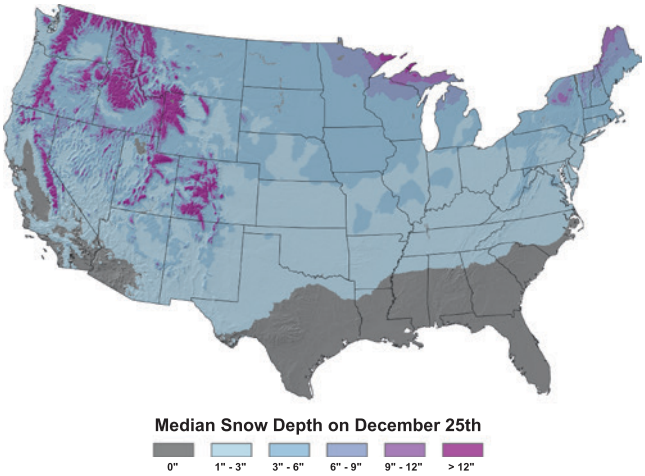

Fig. 2. Map of median snow depth when snow is on the ground on 25 Dec. For consistency with the original measurement units, medians are provided in inches. (1 in. = 2.54 cm).

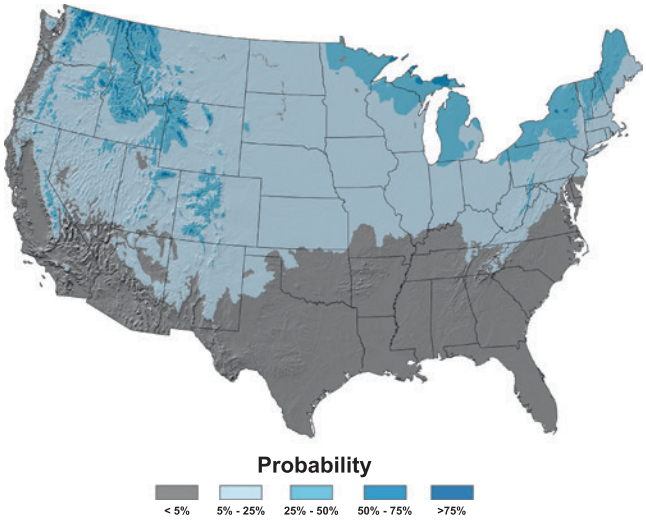

Fig. 3. Same as Fig. 1, but for the climatological probability of at least 0.1 in. (0.254 cm) of snowfall.

While the most popular definition of a white Christmas is the presence of significant snow cover, it is also instructive to consider the climatological probability of snowfall on 25 December since many cultural references to Christmas invoke an image of snowflakes, and travel is more likely to be impacted by new snow than by snow already on the ground. As shown in Fig. 3, the probability of measurable (≥ 0.1 in.) snowfall on 25 December is less than 25% for most of the country outside of mountainous regions and the Great Lakes. From central Texas to the Carolinas, it was essentially zero during 1981–2010. The only places where the probabilities exceeded 50% were isolated mountain locations in the West, some stations on the lee side of Lake Superior and Lake Ontario, and some stations in northern New England.

Over many parts of the United States, the probability of measurable snowfall (Fig. 3) is considerably less than the probability of measurable (≥ 0.01 in.) total precipitation, shown in Fig. 4, indicating that precipitation in these regions frequently falls as rain. Locations where more than half of the precipitation events involve snowfall are found in the mountains of the West as well as north of a line arching from New Mexico through western Kansas and northern Illinois into interior New England (Fig. 4). When snow does fall, it is often relatively light, as reflected in the median snowfall amounts in Table 1. Only some mountain locations in the West experienced snowfall in excess of 3 in. (7.62 cm) more than half of the time when snow fell on 25 December during 1981–2010.

SUMMARY. Although the 1981–2010 statistics in no way represent a forecast for future conditions, they can nevertheless serve as a guide for setting expectations regarding which parts of the contiguous United States are most likely to experience a white Christmas. They suggest, for example, that the places where one is most likely to experience both snow on the ground and falling snow are in the Sierras and Cascades, on the leeward side of the Great Lakes, and in northern New England. At high elevations of the Rocky Mountains and at most locations between the northern Rockies and New England, the probability of measurable snow depth is greater than 50%, while the probability of snowfall is generally less than 25%. By contrast, snow is at best extremely rare on 25 December in Southern California, the lower elevations of the Southwest, and Florida (Table 2).

While the results presented here focus solely on 25 December, they are generally representative of conditions during the last half of December and early January. Therefore, they are relevant not only to those concerned about snow on Christmas Day, but also to those planning a vacation or family visit during this popular travel season. Readers interested in probabilities of occurrence or median values for other times of year or for specific locations other than those shown in Tables 1 and 2 are referred to the full set of NOAA's 1981–2010 U.S. Climate Normals available

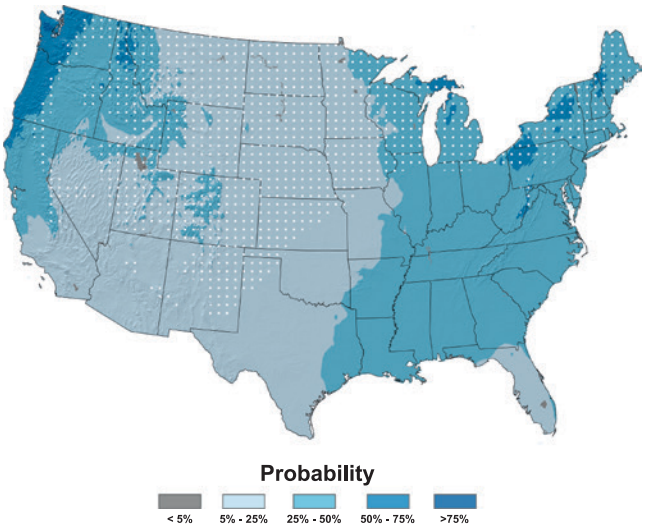

Fig. 4. Same as Fig. 1, but for the climatological probability of at least 0.01 in. (0.0254 cm) of precipitation. Stippling indicates regions where more than 50% of precipitation falls as snow.

on NCEI's website (www.ncdc.noaa.gov/data-access/land-based-station-data/land-based-datasets/climate-normals/1981-2010-normals-data). Since conditions in any specific year may differ significantly from the climatological norm, however, those with flexibility in the short term may wish to also consult NOAA's real-time snowfall maps at www.weather.gov.

ACKNOWLEDGMENTS. We thank Anne Markel for editing assistance. We also wish to thank Xungang Yin and several anonymous reviewers for their thoughtful comments.

APPENDIX A: CALCULATION OF DAILY CLIMATOLOGICAL PROBABILITIES OF OCCURRENCE. For a particular station and variable, the daily probabilities are calculated according to the following four-step procedure.

1) *Sample selection:* For each day of the year except 29 February, the sample used includes data from within +/–14 days of the day in question and from all years that have values on at least 20 calendar days within that 29-day window. A minimum of 10 such years is required for each window (Durre et al. 2013).
2) *Calculation:* The climatological probability of occurrence is then equal to the percentage of nonzero values within the pool. Due to the limited sample size for 29 February, the probability for that day is set to the average of the probabilities for 28 February and 1 March.
3) *Smoothing:* To reduce fluctuations from one calendar day to the next that are associated with sampling variability, the empirical probabilities are smoothed with a 29-day running mean. After several other types of filters had been tested, this particular filter was found to yield the desired level of smoothing while retaining variations on the time scale of weeks.
4) *Synchronization:* The use of the 29-day window and subsequent smoothing can result in small nonzero probabilities for snowfall or snow depth in months during which snow was never reported in the underlying observations. In such cases, the affected probabilities are set to zero. Similarly, at the beginning of the snow season, another check sets to zero any nonzero probabilities of snow on the ground that appear before the probability of snowfall has increased from zero.

As an example, consider the probability of snow on the ground on 25 December during 1981–2010 at Milwaukee (Table 1). For this calculation, observations were available on all of the 29 days in the window in 28 of the 30 years and on 27 of the 29 days in another year, yielding a total of 839 observations. Of these, 392 were nonzero values, resulting in an empirical probability of 46.8%, which was transformed to 47.7% by the subsequent smoothing of the raw probabilities.

APPENDIX B: COMPUTATION OF DAILY MEDIANS OF NONZERO AMOUNTS. The procedure for calculating daily medians of the nonzero amounts of one element at one station is described below.

1) *Sample selection:* The median of a particular day is calculated from the same sample of values used to compute the probability of occurrence (see #1 in appendix A).
2) *Calculation:* If at least 10% of the values in the sample for a particular calendar day are nonzero, these nonzero amounts are sorted from lowest to highest, and the median is identified (Durre et al. 2013). Otherwise, the median is set to missing. The median for 29 February is set to the average of the corresponding medians for 28 February and 1 March.
3) *Smoothing:* The resulting daily medians are smoothed with a 29-day running mean. To allow for the smoothing of even those medians that directly precede or follow a time of the year during which medians are missing, the running mean is calculated whenever medians are available on at least 15 of the 29 days. Medians that cannot be smoothed in this manner are set to missing.
4) *Interpolation:* Gaps in the resulting medians that are shorter than 15 days are filled in using linear interpolation between the corresponding medians immediately preceding and following the gap. At locations in the northern Great Plains, midwinter gaps in snowfall medians that extend over more than 15 days are also filled in since the medians before and after the gap typically do not differ significantly from each other.
5) *Cleanup:* To avoid fragmented annual cycles, continuous stretches of medians shorter than 15 days are removed, and all medians are set to missing if there is no continuous stretch of (empirical and interpolated) medians that is at least 30 days long.

FOR FURTHER READING

Arguez, A., I. Durre, S. Applequist, R. S. Vose, M. F. Squires, X. Yin, R. R. Heim, Jr., and T. W. Owen, 2012: NOAA's 1981-2010 U.S. climate normals: An overview. *Bull. Amer. Meteor. Soc.,* **93,** 1687–1697, doi:10.1175/BAMS-D-11-00197.1.

Durre, I., M. F. Squires, R. S. Vose, X. Yin, A. Arguez, and S. Applequist, 2013: NOAA's 1981-2010 U.S. Climate Normals: Monthly precipitation, snowfall, and snow depth. *J. Appl. Meteor. Climatol.,* **52,** 2377–2395, doi:10.1175/JAMC-D-13-051.1.

Menne, M. J., I. Durre, R. S. Vose, B. E. Gleason, and T. G. Houston, 2012: An overview of the Global Historical Climatology Network-Daily Database. *J. Atmos. Oceanic Technol.,* **29,** 897–910, doi:10.1175/JTECH-D-11-00103.1.

Ross, T., N. Lott, and M. Sittel, 1995: White Christmas? National Climatic Data Center Tech. Rep. 95-03, 13 pp.

Vose, R. S., and Coauthors, 2014: Improved historical temperature and precipitation time series for U.S. climate divisions. *J. Appl. Meteor. Climatol.,* **53,** 1232–1251, doi:10.1175/JAMC-D-13-0248.1.

Improving Flash Flood Forecasts

The HMT-WPC Flash Flood and Intense Rainfall Experiment

BY FAYE E. BARTHOLD, THOMAS E. WORKOFF, BRIAN A. COSGROVE, JONATHAN J. GOURLEY, DAVID R. NOVAK, AND KELLY M. MAHONEY

Despite advancements in numerical modeling and the increasing prevalence of convection-allowing guidance, warm season (June–August) quantitative precipitation forecasts (QPF) remain challenging (Fritsch and Carbone 2004). While overall threat scores have increased steadily over the past 50 years, the majority of that improvement has occurred during the cold season (December–February), with only incremental improvements during the warm season (Fig. 1). The difference in forecast skill and rate of improvement is likely driven by the spatial and temporal scale of precipitation events during each season (Sukovich et al. 2014). While precipitation during the cold season tends to be driven by synoptic-scale events (e.g., extratropical cyclones), precipitation during the warm season is often driven by small-scale convective processes (e.g., thunderstorms) that are more difficult for numerical models to accurately simulate.

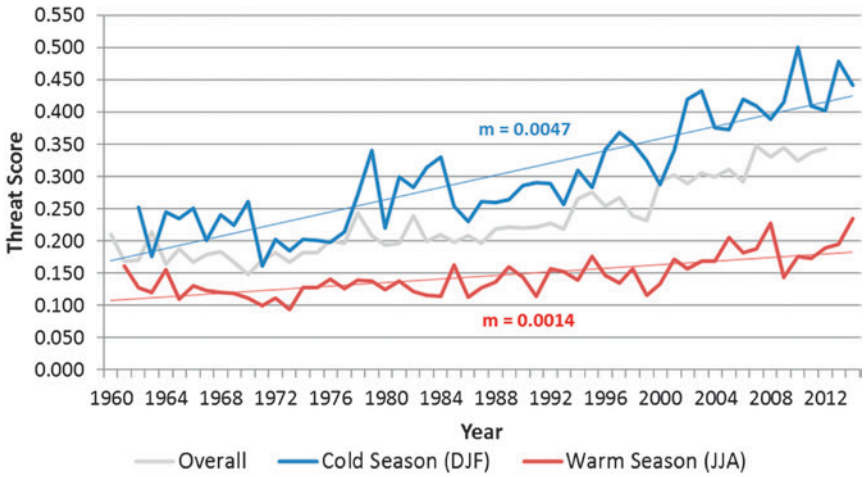

FIG. 1. Comparison of Day 1 WPC 1.0 in QPF threat scores from 1961 to 2014 during the cold season (blue) and warm season (red). The annual average threat score (gray) is provided for reference.

Flash flooding, defined as a rapid and extreme flow of high water into a normally dry area, or a rapid water level rise in a stream or creek above a predetermined flood level that begins within six hours of the causative event (NOAA 2012), introduces another variable into the forecast equation. In addition to accurate QPF information, the hydrologic aspect of a flash flood

AFFILIATIONS: BARTHOLD*—I.M. Systems Group, Inc., Rockville, Maryland, and NOAA/NWS/Weather Prediction Center, College Park, Maryland; WORKOFF+—Systems Research Group, Inc., Colorado Springs, Colorado, and NOAA/NWS/Weather Prediction Center, College Park, Maryland; COSGROVE—NOAA/NWS/National Water Center, Silver Spring, Maryland; GOURLEY—NOAA/OAR/National Severe Storms Laboratory, Norman, Oklahoma; NOVAK—NOAA/NWS/Weather Prediction Center, College Park, Maryland; MAHONEY—Cooperative Institute for Research in the Environmental Sciences, University of Colorado Boulder, and NOAA/ESRL/Physical Sciences Division, Boulder, Colorado

***CURRENT AFFILIATION:** NOAA/NWS/WFO New York, NY, Upton, New York
+**CURRENT AFFILIATION:** FirstEnergy, Akron, Ohio
CORRESPONDING AUTHOR: Faye E. Barthold, NOAA/NWS/WFO New York, NY, 175 Brookhaven Avenue, Upton, NY 11973
E-mail: faye.barthold@noaa.gov

DOI:10.1175/BAMS-D-14-00201.1

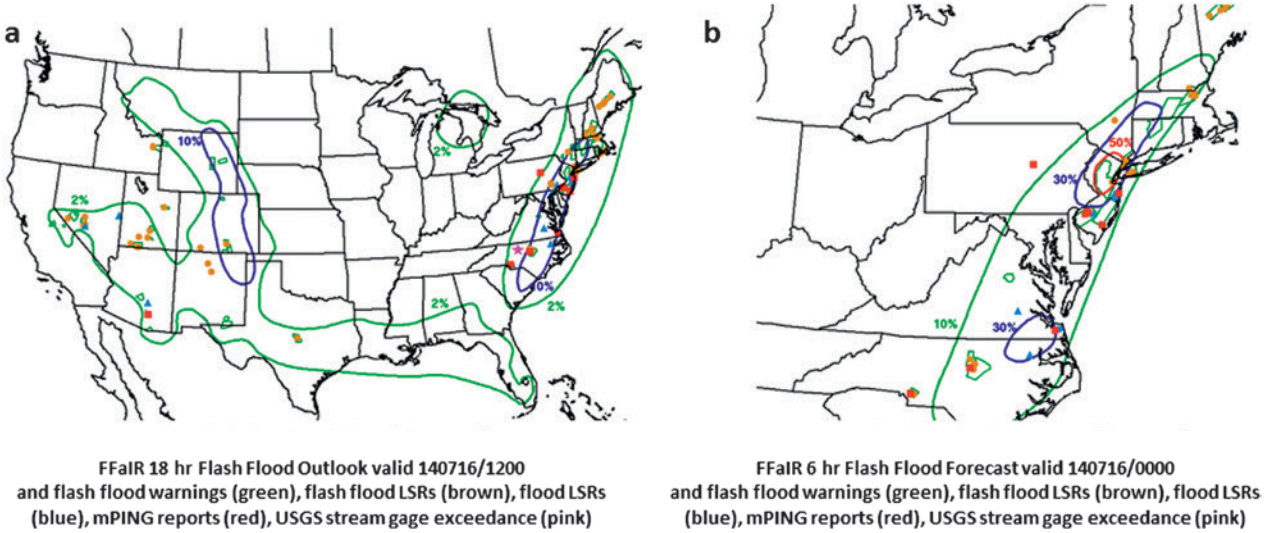

Fig. 2. Example of an experimental (a) 18-h probabilistic flash flood outlook forecast valid 1200 UTC 16 Jul and (b) 6-h probabilistic flash flood forecast valid 0000 UTC 16 Jul from the 2014 Flash Flood and Intense Rainfall Experiment. Both forecasts were defined as the probability of flash flooding within 40 km of a point. The experimental forecast contours are overlaid on the corresponding flash flood warnings (green) and observations including flash flood LSRs (brown), flood LSRs (blue), mPING reports (red), and USGS stream gauge exceedance (pink).

forecast represents a challenge on its own as recent rainfall, soil type, slope, land use, basin size, degree of urbanization, etc., all play a role in determining the flash flood threat. This combination of meteorological and hydrologic challenges allows flash flooding to remain one of the deadliest weather phenomena, typically resulting in more fatalities each year than either tornadoes or hurricanes.

Compounding these forecast challenges is the lack of a real-time comprehensive flash flood verification dataset. At present, flash flood observations are available from a variety of different sources (e.g., National Weather Service, U.S. Geological Survey) in a variety of different forms, each with varying levels of detail and accuracy. The development of a real-time dataset that combines the best available observations is vital to assessing the quality of current flash flood forecasts and identifying areas in need of improvement.

As the national center responsible for providing QPF and flash flood forecast guidance, NCEP's Weather Prediction Center (WPC) and the Hydrometeorology Testbed at WPC (HMT-WPC) are uniquely positioned to address the challenges associated with flash flood forecasting. WPC currently issues two products that address the flash flood threat: the Excessive Rainfall Outlook (ERO) and the Mesoscale Precipitation Discussion (MPD). The ERO is issued at scheduled intervals throughout the day as part of WPC's Day 1–3 QPF product suite and indicates the probability of exceeding flash flood guidance (FFG) at a point across the contiguous United States (CONUS). With the potential of multiday lead times, these products are intended to provide several days of advance notice about the potential for flash flooding. To address the near-term flash flood threat, WPC began issuing MPDs in April 2013. These event-driven forecasts highlight regions where heavy rainfall may lead to flash flooding over the next 1–6 h and are designed to enhance situational awareness among local National Weather Service (NWS) offices, emergency managers, and the media.

THE FLASH FLOOD AND INTENSE RAINFALL (FFAIR) EXPERIMENT. In an effort to improve flash flood forecasts and verification both at WPC and across the NWS, HMT-WPC partnered with the National Severe Storms Laboratory (NSSL) and the Earth System Research Laboratory (ESRL) in 2013 to develop and host the first annual Flash Flood and Intense Rainfall (FFaIR) Experiment. The FFaIR Experiment brings together participants from the operational forecasting, model development, and

research communities during the month of July to explore the challenges associated with flash flood forecasting. In particular, the experiments have focused on

- evaluating the utility of high-resolution convection-allowing models and ensembles for short-term flash flood forecasts,
- exploring new tools and approaches for combining meteorological and hydrologic information, and
- exploring improvements to WPC's operational suite of flash flood forecast guidance.

During the experiment, participants used a combination of operational and experimental model output to issue a series of experimental forecasts (Fig. 2). These forecasts, along with the corresponding model guidance, were then subjectively evaluated to gain insight about the utility of the experimental data under real-time operational conditions. The experimental forecasting environment provides an opportunity to test new forecast tools—such as neighborhood probabilities—and gather feedback about different verification approaches that can help inform future improvements to flash flood forecasts.

NEIGHBORHOOD FFG EXCEEDANCE PROBABILITIES. With the creation of WPC's MPDs, there was a need to develop guidance that combines QPF and hydrologic information to aid forecasters in identifying areas at risk for flash flooding. Using the concept of the "neighborhood maximum" technique (e.g., Schwartz et al. 2009, Schwartz et al. 2010, Ebert 2008), HMT-WPC uses convection-allowing model guidance to develop probabilistic forecast tools highlighting areas where QPF may approach or exceed FFG, which indicates the average amount of rain needed over an area during a specific time period to initiate flooding on small streams (Sweeney 1992). The neighborhood maximum technique is a postprocessing procedure that identifies the maximum value of a parameter within a user-defined search radius of each grid point. Once identified, the original value of the grid point is then replaced by its neighborhood maximum value; the benefit of this technique is to help account for spatial and temporal errors that are inherent in high-resolution forecasts.

HMT-WPC applies this approach to the QPF from members of the ~4-km grid spacing Storm Scale Ensemble of Opportunity (SSEO, Jirak et al. 2012), created by the Storm Prediction Center (SPC). Generated at 0000 and 1200 UTC, the seven-member SSEO combines various operational (NCEP ARW and NMMB high-resolution windows and NAM Nest) and nonoperational (NSSL WRF-ARW and EMC WRF-NMM) deterministic convection-allowing models. For flash flood purposes, the neighborhood maximum QPF (nQPF) fields are compared against CONUS 3-h and 6-h gridded FFG; these CONUS FFG grids are 5-km mosaic grids that combine the gridded FFG (Schmidt et al. 2007) that is generated by each NWS River Forecast Center (RFC). The result is a product indicating the neighborhood probabilities of QPF exceeding FFG (nPQPF > FFG), and highlights areas at risk for flash flooding.

To understand how to combine QPF and FFG into a forecast tool, HMT-WPC has evaluated different versions of the nPQPF > FFG tool in the FFaIR Experiment by comparing experimental forecast guidance to various flash flood verification metrics such as QPE, QPE > FFG, QPE recurrence intervals, flash flood warnings (FFW), and flash flood observations (e.g., NWS local storm reports). These evaluations have included exploring the use of various search radii (point, 20 km, and 40 km) in the neighborhood maximum technique (Fig. 3), as well as using different percentages of FFG (75%, 90%, or 100% of FFG values) as the exceedance threshold (Fig. 4). Having participants test and evaluate various permutations of the nPQPF > FFG products in a real-time environment has been critical in the continued development and improvement of the product.

Results of the FFaIR Experiment have shown that forecasters prefer using a 40-km search radius for nPQPF > FFG because it best highlights the potential for flash flood events (Fig. 3d). Forecasters also found that using 100% of FFG as a threshold value is the most effective way to identify areas at risk of flash flooding (Fig. 4d). They also noted that while the 75% threshold could provide helpful information about the potential for flash flooding in more uncertain situations, it had a tendency to highlight the potential for flash flooding over too large of an area. Beginning 1 June 2014, HMT-WPC began producing a modified version of the SSEO four times a day (0000, 0600, 1200, 1800 UTC) that utilizes the latest convection-allowing models and FFG, and replaces the EMC WRF-NMM (due to its noted high QPF bias) with the High Resolution Rapid Refresh (HRRR) model. As a result of the experiment, all of these products are currently available to WPC forecasters.

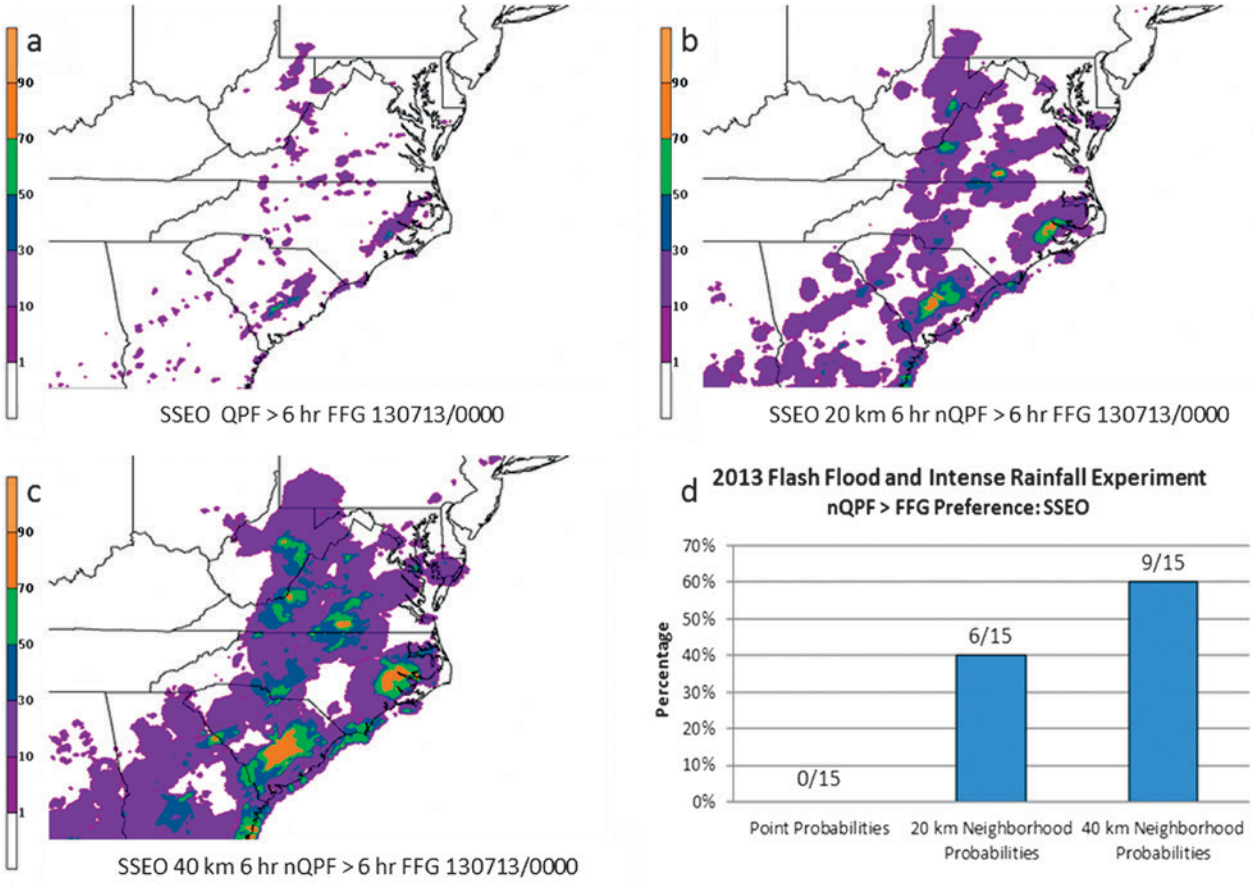

Fig. 3. Ensemble probability of 6-h QPF exceeding 6-h FFG from the SSEO valid at 0000 UTC on 13 Jul 2013 using (a) point probabilities, (b) neighborhood probabilities at a 20-km search radius, and (c) neighborhood probabilities at a 40-km search radius. (d) Shows results of subjective verification conducted in the 2013 FFaIR Experiment in which participants were asked daily which search radius (point, 20 km, or 40 km) provided the best guidance in terms of highlighting areas that received flash flooding.

FLASH FLOOD VERIFICATION. In addition to the development of new forecast tools, obtaining a complete and accurate assessment of when and where flash floods occur is a critical task (Gourley et al. 2013) for calibrating forecasts and improving forecast skill. Unfortunately, a single comprehensive source of real-time flash flood verification data does not currently exist. As such, it was decided to leverage three CONUS-wide hydrologic data sources to create a new merged, real-time verification dataset: NWS flash flood Local Storm Reports (LSRs), NSSL Meteorological Phenomena Identification Near the Ground (mPING, Elmore et al. 2014) reports, and United States Geological Survey (USGS) stream gauge measurements.

LSRs are an official NWS product, although reports can be subjective in nature and are dependent on people witnessing an event; darkness, low population density, etc., can limit reporting. Additionally, event categorization (flash flood versus flood versus heavy rain) can be inconsistent across the NWS, and location and time stamp errors can also occur. mPING reports, a method of crowdsourcing weather information developed by NSSL, are also dependent on submission by end users. Unlike LSRs, they do not undergo quality control and do not differentiate between floods and flash floods, although NSSL's examination of the reports indicates that they are mainly flash floods.

The third component of the database centers on USGS stream gauge reports. To the best knowledge of the authors, this represents the first CONUS-wide effort to leverage this resource for real-time verification of flash flooding. The dataset is composed of stage and discharge data collected at all-weather automated USGS stream gauges across the CONUS every 5–60 min.

To extract natural flash flood event signals, real-time data from USGS basins smaller than 2,000 km^2 are

passed through a series of sequential filters. Flooding is judged to occur if 1) discharge exceeds the minor flood stage discharge, 2) the stage exceeds the NWS minor flood stage, or 3) discharge exceeds the two-year recurrence discharge. This latter filter is used only when the flood stage is unavailable, as it is only a rough indictor of bank-full status. Streams that fall into the "flooding" category then pass through a ≥ 3 ft hr^{-1} rate-of-rise check to differentiate between floods and flash floods, and must be preceded or followed by a ≥ 1 ft hr^{-1} rate-of-rise to insure that the signal is not a one-time spurious data spike. This series of filters is based on a limited review of approximately 150 flash flood cases and will be refined as the database matures.

These datasets are stored in a searchable Postgres database that is updated throughout the day to capture the latest observations. During the 2014 FFaIR Experiment, this database was used to plot point observations of flash flooding to aid in the subjective evaluation of the experimental forecasts and model guidance (Fig. 2). This helped promote discussion about the best applications of the various datasets available to evaluate flash flooding. In addition, the development of this database also provided an opportunity to explore a new approach to probabilistic flash flood verification through the SPC-pioneered Practically Perfect analysis technique (Brooks et al. 1998, Hitchens et al. 2013). This experimental technique uses a Gaussian weighted function to convert the location of user-selected flash flood observations into a probabilistic forecast with the goal of producing the forecast a forecaster would have issued had the location of all reported flash flooding been known in advance (Fig. 5).

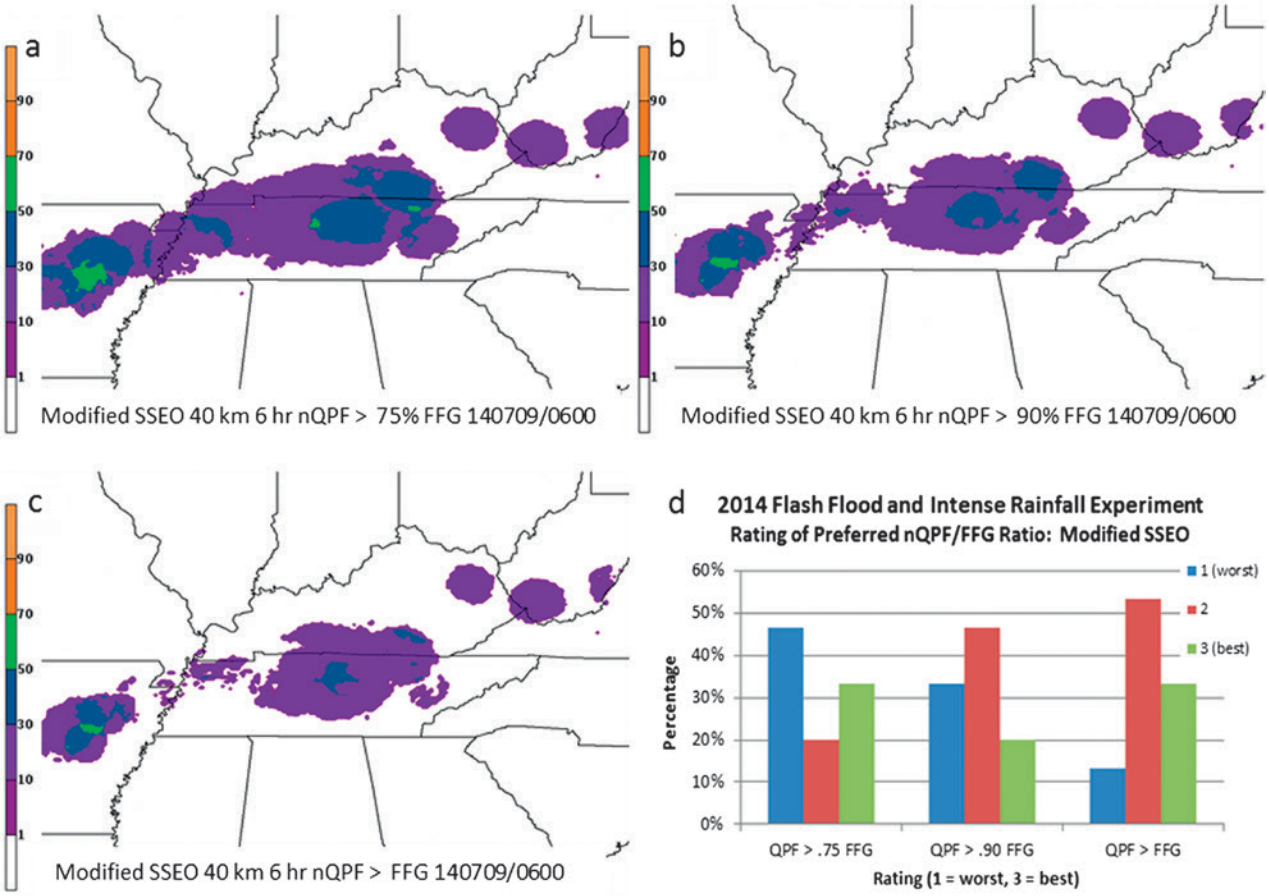

Fig. 4. Ensemble probability of 6-h QPF exceeding 6-h FFG from the modified SSEO valid at 0600 UTC on 9 Jul 2014 using (a) 75% of FFG (b) 90% of FFG, and (c) FFG as the exceedance threshold. (d) Results of subjective verification conducted in the 2014 FFaIR Experiment in which participants were asked daily which FFG threshold (FFG, 75% of FFG, or 90% of FFG) provided the best guidance in terms of highlighting areas that received flash flooding.

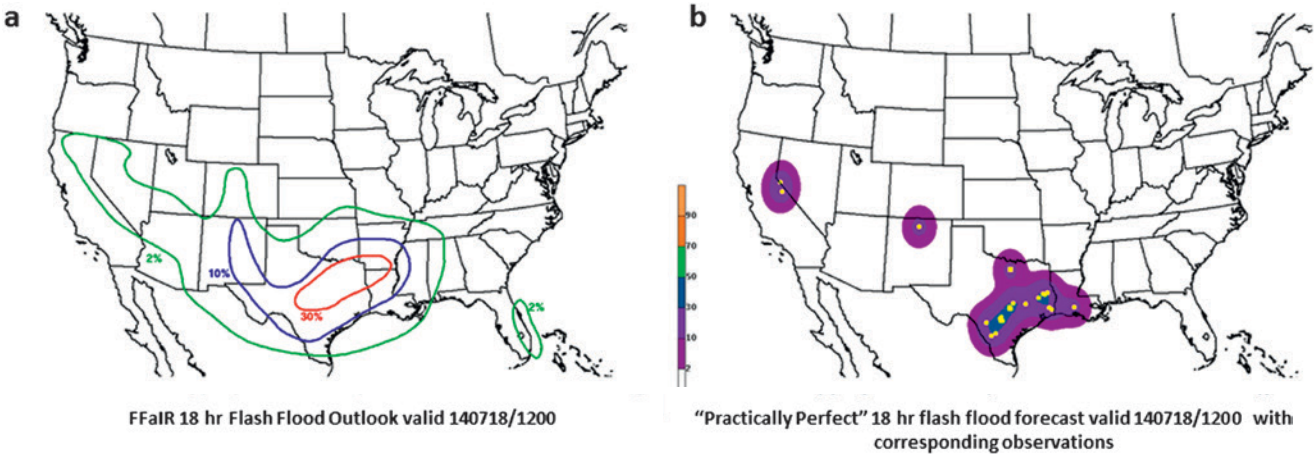

Fig. 5. Example of an (a) experimental 18-h probabilistic flash flood outlook forecast valid 1200 UTC 18 Jul, and (b) the corresponding experimental probabilistic flash flood forecast verification from the Practically Perfect analysis technique. The observations used to derive the Practically Perfect analysis are overlaid on (b).

FINAL THOUGHTS. Despite advancements in convection-allowing numerical modeling and precipitation forecasting in general, flash flooding remains one of the most difficult, yet most important, phenomena to forecast accurately. HMT-WPC initiated the FFaIR Experiment in 2013 to investigate ways to advance flash flood forecasting, better understand ways to communicate the flash flood threat, and develop a method to improve flash flood verification.

In its first two years, the FFaIR Experiment has made steady progress in aiding the development and testing of flash flood forecasting and verification tools. Through its experimental forecasting exercises and verification activities, FFaIR has shown that coupling QPF and hydrologic guidance (e.g., FFG) through the use of the neighborhood probability technique is a useful forecast tool for identifying areas of flash flood risk across the county. As a result, these neighborhood probabilities are now used by WPC forecasters in the process of generating both Mesoscale Precipitation Discussions (MPD) and the Day 1 Excessive Rainfall Outlook (ERO). Additionally, the development of a database which collects various flash flood observations in real time is a valuable resource for improving the awareness and accuracy of identifying where flash flooding occurs. These observations are now being used internally at WPC in the subjective verification of the ERO and MPD products.

While the development of these new forecast tools and the availability of a real-time flash flood verification database represent important steps forward, improvements in the quality of flash flood forecasts will not be made until the meteorological and hydrologic communities come together to address the remaining forecast challenges:

- *Improved hydrologic guidance*—Although FFG is readily available, it has numerous limitations, and the development of improved hydrologic datasets targeted toward flash flood applications is necessary.
- *Improved warm-season model QPF guidance*—Continued investment in the development of convection-allowing models, including the establishment of an operational storm scale ensemble, is vital to supporting the continued improvement of flash flood forecasts.
- *Improved flash flood forecast tools*—While neighborhood probabilities of QPF > FFG are useful, additional approaches to combining meteorological and hydrologic data need to be explored to increase forecast accuracy and lead time.

Although overcoming these challenges will require community-wide long-term development efforts, work is already under way to address some of these issues. For example, NSSL's Flooded Locations and Simulated Hydrographs (FLASH) project (Hong and Gourley 2015) and the NOAA Office of Hydrologic Development's Distributed Hydrologic Model-Threshold Frequency (DHM-TF) project (Reed et al. 2007) are focusing on the direct simulation of routed streamflow. Additionally, the Weather Research and Forecasting Model Hydrological modeling extension package (WRF-Hydro, Gochis et al.

2014) is advancing the use of convection-allowing model and ensemble data to directly force distributed hydrologic models.

Adding to the challenge, the current approach to the flash flood forecast problem is inconsistent across the NWS. These inconsistencies are present beginning with the definition of flash flooding (how should urban and poor-drainage street flooding be handled?) and continue into the forecasting and reporting of these events. For example, when heavy rain occurs in an urban area, there are a plethora of products available to a local NWS forecast office to communicate the threat: Flash Flood Warning, Urban and Small Stream Advisory, and Flood Warning. The best product to use often depends on the impact, which may be unknown. In addition, the product definitions themselves have overlap. Similarly, the classification of reported events may depend on unknown attributes (how fast did the water rise, is this a poor drainage area, etc.). The subjectivity involved in choosing the type of forecast product and classifying the observations results in a confusing picture of flash flooding across the nation and contributes to the challenge of both flash flood forecast verification and forecast improvement.

With the help of both the meteorological and hydrologic communities, HMT-WPC will continue to foster an environment of collaboration between forecasters, researchers, and model developers through the annual FFaIR Experiment. Building off of these initial lessons learned, future FFaIR Experiments will focus on testing the use of additional hydrologic guidance and convection-allowing ensembles, investigating the best ways to convey the flash flood risk through probabilistic forecasts, and exploring enhancements to the verification database to develop a more complete record of flash flooding across the nation.

ACKNOWLEDGMENTS. This work was supported by NOAA's Hydrometeorology Testbed (HMT) program and the U.S. Weather Research Program (USWRP). The authors thank all past FFaIR Experiment participants for their enthusiasm and valuable insight into the flash flood forecast problem. In addition, Michael Smith (National Water Center), Russ Schumacher (Colorado State University), and two anonymous reviewers provided helpful feedback to improve the quality of this paper.

FOR FURTHER READING

Brooks, H. E., M. Kay, and J. A. Hart, 1998: Objective limits on forecasting skill of rare events. *Preprints, 19th Conf. on Severe Local Storms,* Minneapolis, MN, Amer. Meteor. Soc., 552–555.

Ebert, E. E., 2008: Fuzzy verification of high resolution gridded forecasts: A review and proposed framework. *Meteor. Appl.,* **15,** 51–66, doi:10.1002/met.25.

Elmore, K. L., Z. L. Flemig, V. Lakshmanann, B. T. Kaney, V. Farmer, H. D. Reeves, and L. P. Rothfusz, 2014: MPING: Crowd-sourcing weather reports for research. *Bull. Amer. Meteor. Soc.,* **95,** 1335–1342, doi:10.1175/BAMS-D-13-00014.1.

Fritsch, J. M., and R. E. Carbone, 2004: Improving quantitative precipitation forecasts in the warm season: A USWRP research and development strategy. *Bull. Amer. Meteor. Soc.,* **85,** 955–964, doi:10.1175/BAMS-85-7-955.

Gochis, D. J., W. Yu, and D. N. Yates, 2014: The WRF-Hydro model technical description and user's guide, version 2.0. NCAR Technical Document, 120 pp.

Gourley, J. J., and Coauthors, 2013: A unified flash flood database across the United States. *Bull. Amer. Meteor. Soc.,* **94,** 799–805, doi:10.1175/BAMS-D-12-00198.1.

Hitchens, N. M., H. E. Brooks, and M. P. Kay, 2013: Objective limits on forecasting skill of rare events. *Wea. Forecasting,* **28,** 525–534, doi:10.1175/WAF-D-12-00113.1.

Hong, Y., and J. J. Gourley, 2015: *Radar Hydrology: Principles, Models, and Applications.* 1st ed. CRC Press, 180 pp.

Jirak, I. L., S. J. Weiss, and C. J. Melick, 2012: The SPC storm-scale ensemble of opportunity: Overview and results from the 2012 Hazardous Weather Testbed Spring Forecasting Experiment. *Preprints, 26th Conf. on Severe Local Storms,* Nashville, TN. Amer. Meteor. Soc. P9.137.

NOAA, 2012: Hydrologic Services Program, Definitions and General Terminology. National Weather Service Manual 10-950, 5 pp, [Available online at www.nws.noaa.gov/directives/sym/pd01009050curr.pdf.]

Reed, S., J. Schaake, and Z. Zhang, 2007: A distributed hydrologic model and threshold frequency-based method for flash flood forecasting at ungauged locations. *J. Hydrol.,* **337,** 402–420, doi:10.1016/j.jhydrol.2007.02.015.

Schmidt, J. A., A. J. Anderson, and J. H. Paul, 2007: Spatially variable, physically-derived flash flood guidance. *Preprints, 21st Conf. on Hydrology,* San Antonio, TX, Amer. Meteor. Soc., 6B.2.

Schwartz, C. S., and Coauthors, 2009: Next-day convection-allowing WRF model guidance: A second look at 2-km versus 4-km grid spacing. *Mon. Wea. Rev.,* **137,** 3351–3372, doi:10.1175/2009MWR2924.1.

——, and ——, 2010: Toward improved convection-allowing ensembles: Model physics sensitivities and optimizing probabilistic guidance with small ensemble membership. *Wea. Forecasting,* **25,** 263–280, doi:10.1175/2009WAF2222267.1.

Sukovich, E. M., F. M. Ralph, F. E. Barthold, D. W. Reynolds, and D. R. Novak, 2014: Extreme quantitative precipitation forecast performance at the Weather Prediction Center from 2001 to 2011. *Wea. Forecasting,* **29,** 894–911, doi:10.1175/WAF-D-13-00061.1.

Sweeney, T. L., 1992: Modernized areal flash flood guidance. NOAA Tech. Rep. NWS HYDRO 44, Hydrologic Research Laboratory, National Weather Service, NOAA, 21 pp.

National Weather Service Forecasters Use GPS Precipitable Water Vapor for Enhanced Situational Awareness during the Southern California Summer Monsoon

BY ANGELYN W. MOORE, IVORY J. SMALL, SETH I. GUTMAN, YEHUDA BOCK, JOHN L. DUMAS, PENG FANG, JENNIFER S. HAASE, MARK E. JACKSON, AND JAYME L. LABER

A Global Positioning System (GPS) network in Southern California, newly densified to an average station spacing of 30 km, enhanced situational awareness for local National Weather Service (NWS) forecasters during 2013 summer monsoon rainfall events. The North American Monsoon (NAM) occurs in summer due to strong heating of the Sierra Madre and Rocky Mountains driving a transition to mean low-level flow from the south (Adams and Comrie 1997). During this season, moisture associated with tropical easterly waves (Fuller and Stensrud 2000; Favors and Abatzoglou 2013) and remnant Pacific tropical cyclones (Corbosiero et al. 2009) is advected northward into the southwestern United States from the Gulf of California at low levels and westward from the Gulf of Mexico at midlevels. The origin and evolution of moisture surges from the Gulf of California into the southwestern United States have been investigated by Higgins et al. (2004), who identified a positive precipitation anomaly moving northward along the Mexican coastline that is correlated with the moisture surge. Favorable synoptic conditions for the surge generation and propagation along the Sierra Madre Occidental (SMO) include passage in the NAM region of tropical easterly waves (Ladwig and Stensrud 2009) or westerly moving mid-to-upper-level lows, termed "inverted troughs" (Bieda et al. 2009), that lead to moisture convergence over the SMO (Pytlak et al. 2005). It is thought that the development of mesoscale convective systems (MCS) and organized convection over the SMO produce cold outflow boundaries that contribute to surges of moist air into the southwestern United States (Douglas and Leal 2003; Finch and Johnson 2010; Schiffer and Nesbitt 2012).

In comparison to California, Arizona receives a greater amount of monsoon rainfall, and it also comprises a larger fraction of annual rainfall there (Means 2013). However, monsoonal moisture regularly reaches southern California and causes heavy rainfall, particularly when interacting with mountain ranges (Tubbs 1972). Orographic lift, channeling, lee-side convergence, and upslope convergence over the mountains all play a role (Whiteman 2000). Thunderstorms in Southern California tend to initially form along mountain ridges as upslope flow generates a convergence zone at or near the ridgeline. This typically oc-

AFFILIATIONS: MOORE—Jet Propulsion Laboratory, California Institute of Technology, Pasadena, California; SMALL—National Oceanographic and Atmospheric Administration, National Weather Service Forecast Office, San Diego, California; GUTMAN*—National Oceanographic and Atmospheric Administration Earth System Research Laboratory, Boulder, Colorado; BOCK, FANG, AND HAASE—Cecil H. and Ida M. Green Institute of Geophysics and Planetary Physics, Scripps Institution of Oceanography, La Jolla, California; DUMAS, JACKSON, AND LABER—National Oceanographic and Atmospheric Administration, National Weather Service Forecast Office, Oxnard, California
*Retired
CORRESPONDING AUTHOR: Angelyn W. Moore, 4800 Oak Grove Dr. MS 238-600, Pasadena, CA 91109
E-mail: Angelyn.W.Moore@jpl.nasa.gov

DOI:10.1175/BAMS-D-14-00095.1

A supplement to this article is available online (DOI:10.1175/BAMS-D-14-00095.2)

curs when a Gulf of California moisture surge provides sufficient precipitable water (PW), instability, and dynamic forcing to the region. Boundary interaction becomes very important as the sea breeze interacts with terrain-generated flows and outflow boundaries (Small and Maxwell 2014). Features such as easterly waves and upper-level lows can also destabilize the air mass enough to allow thunderstorms to develop, and potentially reach severe levels generating flash floods.

The mission of the NWS includes issuing weather watches and warnings to protect lives and property, and NWS forecasters use a variety of weather models and observations in making watch and warning decisions during monsoon events. Under rapidly changing conditions, model solutions and forecast guidance can vary greatly with respect to the timing, intensity, and duration of precipitation. Commonly cited factors include differences in model resolution, convective parameterizations, and cloud microphysics. Less commonly recognized is the need for more accurate and comprehensive initial conditions provided by upper-air observing systems at temporal and spatial resolutions consistent with the models assimilating them. This is especially true in regions of complex orography like Southern California. Given the incomplete or conflicting guidance that current model solutions often provide and their focus on longer-range (6–24 h) probabilistic predictions, most decisions about whether to issue flash flood watches and warnings are based on real-time data that give the forecaster confidence whether a threatening situation has developed or is about to develop. However, rapidly evolving low-to-midlevel regional moisture surges leading to flash flood conditions in this region can be particularly difficult to detect using satellite, radar, and surface dewpoint observations. Further, moisture observations around the Gulf of California and inland locations in Mexico, where convection often initiates, have historically been sparse and/or irregularly monitored. Radiosonde sites in San Diego, Yuma, Phoenix, Tucson, and Las Vegas are crucial for detecting monsoonal moisture surges (Dixon 2005), but are too widely spaced to precisely locate the horizontal boundaries between moist and dry air, and have limited temporal resolution because most are launched at 12-h intervals. [At the U.S. Army Yuma Proving Ground (YPG), radiosondes are launched irregularly in support of the local mission, and many observations only become available to the NWS and WMO retrospectively and with a variable delay.] As a result, inadequate real-time atmospheric moisture information can hinder the accuracy of flash flood watches and warnings during NAM events, and new methods that measure PW with high temporal resolution are of considerable interest. Additional sites in the Peninsular Ranges west of the Colorado and Mojave deserts in the southwestern United States are now equipped to provide near-real-time PW information from GPS receivers. We describe in particular a July 2013 NAM event that resulted in flash floods in the mountainous desert regions of Southern California. The new GPS PW measurements provided forecast guidance and contributed tangibly to NWS forecasters issuing timely flash flood watches and warnings.

Fig. 1. A typical continuous GPS station in Southern California. [Photo credit: D. Glen Offield, Scripps Institution of Oceanography]

GPS METEOROLOGY. Continuous GPS (CGPS) stations for observing crustal motion in the western United States now number more than 1,200. These stations are permanently mounted on bedrock (Fig. 1) or deeply anchored to improve stability. In Southern California, most stations are now part of the Plate Boundary Observatory, the geodetic component of the National Science Foundation's EarthScope Pro-

gram, operated by UNAVCO (http://unavco.org), or the Southern California Integrated GPS Network operated by the U.S. Geological Survey and Scripps Institution of Oceanography. The autonomous stations continuously record signals from the GPS satellites and transfer the data to a central facility, where position is estimated at cadences from daily to once per second to precisely identify ground motion during and between earthquakes. The GPS positioning technique is based upon measuring signal travel time from the GPS satellites to the receiving antenna to estimate the geometric distance between them. However, the signal is also subject to delays due to the total electron content (TEC) in the ionosphere and the amount of moisture and total density of the troposphere. In estimating the position of the ground station to accuracy better than 2 mm, it is necessary to account for these atmospheric delays (Davis et al. 1985). Dual-frequency receivers allow the ionospheric delay to be determined, and the remaining tropospheric effects estimated from the residual delay are the foundation of GPS meteorology. The total tropospheric delay (TD) observed by GPS is the integrated refractivity of the atmosphere, N, over the signal ray path

$$\mathrm{TD} = \int_{s=\text{raypath}} N ds = \int_{s=\text{raypath}} \left(k_1 \frac{P}{T} + k_2 \frac{e}{T} + k_3 \frac{e}{T^2}\right) ds$$

where P is the atmospheric pressure, T is temperature, e is water vapor partial pressure, and the k's are empirically determined physical constants in an expression for N (Bevis et al. 1994). Therefore, this estimated tropospheric signal delay provides information about the unknown moisture above the station.

All GPS signals arriving at the site with an elevation angle greater than 7 degrees, within an inverted cone (Fig. 2) centered on the receiving antenna, are considered in determining the zenith (vertical) delay. Typical modern receivers track 12 or more satellites simultaneously. The tropospheric delay observed for a given satellite at angle θ from vertical is modeled as

$$\mathrm{TD}\ (\theta) = \mathrm{ZHD} \times m_h(\theta) + \mathrm{ZWD} \times m_w(\theta)$$

where ZHD is the zenith hydrostatic delay, ZWD is the zenith wet delay, and m_h and m_w are mapping functions that describe the variation of ZHD and ZWD with varying elevation angle (Böhm et al. 2006). ZHD is a function of surface pressure, which is measured directly at the site, allowing ZWD to be isolated. Further, ZWD is proportional to PW, with the multiplier being

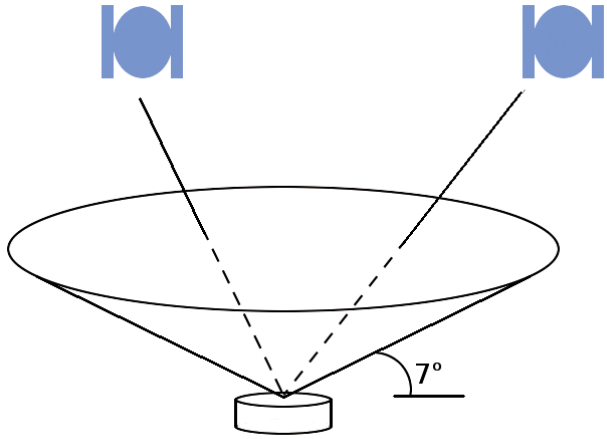

Fig. 2. All signals arriving at a GPS antenna with elevation angle greater than 7 degrees, within an inverted cone centered on the receiving antenna, are considered in determining the zenith tropospheric delay. Typical receivers track 12 or more satellites.

a function of mean water vapor–weighted atmospheric temperature, which can be approximated as a linear function of surface air temperature derived from climatology (Bevis et al. 1992). Thus, given a zenith total delay estimate at the GPS station, along with surface pressure and temperature measurements, the PW parameter familiar to meteorologists can be calculated at high temporal resolution (intervals of 5 to 30 min) to track moisture-associated weather conditions. Studies using the postprocessed estimates of PW from a dense geodetic network of GPS sites in California have examined monsoon conditions in great detail, but not with the timeliness necessary for operational use (Means 2013).

When initially installed in the early-to-mid-1990s, most stations only transferred data to central archives for processing on a daily basis. A collaboration between the Scripps Institution of Oceanography's Orbit and Permanent Array Center and the National Oceanic and Atmospheric Administration (NOAA) Earth System Research Laboratory (ESRL) began in the mid-1990s to implement the GPS meteorology data analysis using available stations and establish its accuracy, beginning with a 40-station demonstration network (Duan et al. 1996; Fang et al. 1998; Wolfe and Gutman 2000). Gradually, communications were upgraded to allow timelier processing. By 2005, the NOAA GPS-Met program was routinely providing and disseminating half-hourly PW from approximately 300 stations nationwide for assimilation into National Centers for Environmental

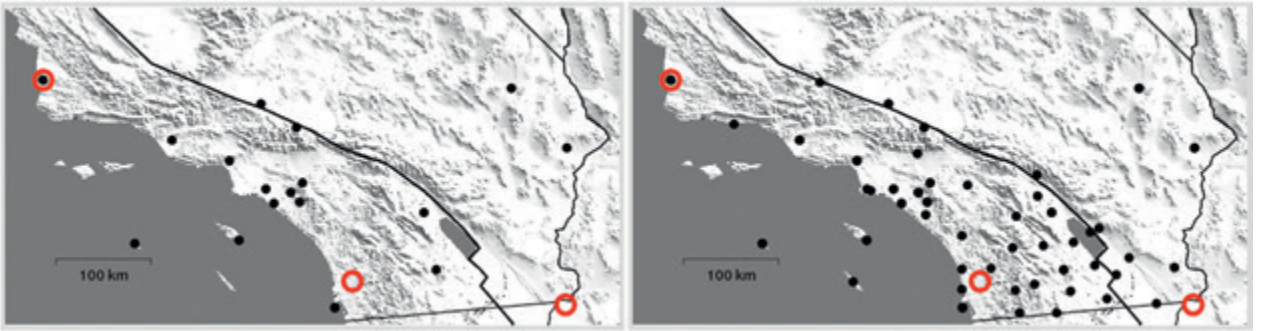

Fig. 3. (left) Southern California stations analyzed by the NOAA GPS-Met project prior to the start of this project. (right) The station set following the inclusion of 37 additional stations. Red circles indicate radiosonde sites at Vandenberg, San Diego, and Yuma. Heavy black line indicates the San Andreas fault.

Prediction (NCEP) models, and delivering continuous time series via the NOAA web page at http://gpsmet.noaa.gov. The results showed positive impact in winter, increasing as the number of sites increased in the central and eastern United States (Gutman et al. 2004); however, it was more difficult to confirm improvement in summertime precipitation, which is dominated by thermodynamic processes and greater spatial moisture variability. This was especially true in the southwestern United States due to a relative absence of independent observations needed for verification (Smith et al. 2007). Preliminary experiments assimilating GPS PW in convective-permitting models are attempting to address several of these issues (Kawabata et al. 2007). Several studies of moisture enhancements in cold-season heavy precipitation events along the west coast of North America followed (Marcus et al. 2007; Ralph et al. 2010; Neiman et al. 2013) and the California Department of Water Resources Hydrometeorology Testbed Legacy project (HMT-Legacy) added several stations to the California GPS-Met station set in this time frame (White et al. 2013). Communications improvements have continued, and approximately 600 stations in the western United States now stream raw GPS data with latency of less than a second (http://sopac.ucsd.edu/readi.shtml). Under a National Aeronautics and Space Administration (NASA) Advanced Information Systems Technology (AIST) project beginning in 2012, 37 more Southern California stations were included in NOAA's GPS-Met analysis providing 30-min estimates of PW to forecasters and modelers, as a test bed for the regional use of GPS PW in operational weather forecasting during weather conditions involving moisture extremes, and in particular to study their value in improving forecasts of monsoon rainfall. Figure 3 depicts the station sets before and after the additions. West of the San Andreas fault, typical station spacing is now 20–40 km. NWS Weather Forecast Offices (WFOs) in San Diego and Los Angeles/Oxnard are participating as technology infusion partners in the project to examine the utility of this dataset in their routine forecasting activities.

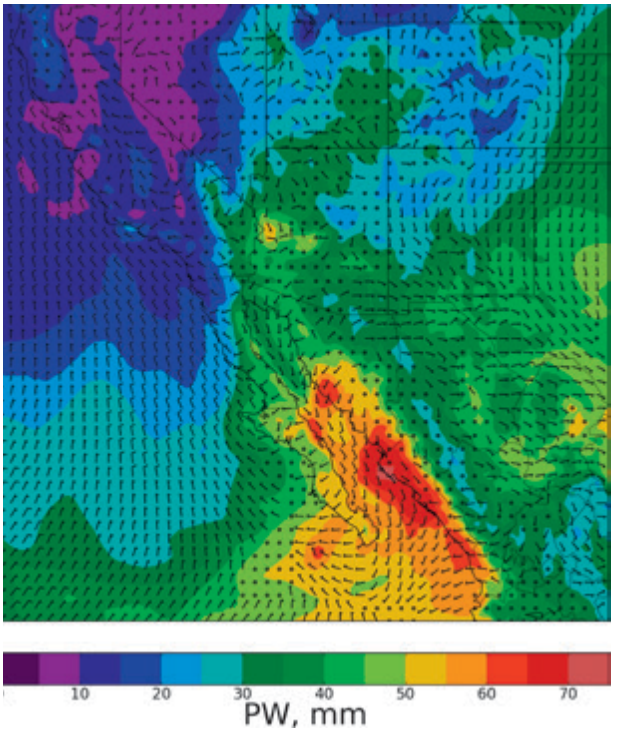

Fig. 4. National Centers for Environmental Prediction (NCEP) Rapid Refresh (RAP) model precipitable water with 10-m winds at 0000 UTC 19 Jul 2013, illustrating the transport of moisture from the Gulf of California into the area of Southern California. The NCEP models assimilate available scatterometer winds in the Gulf region.

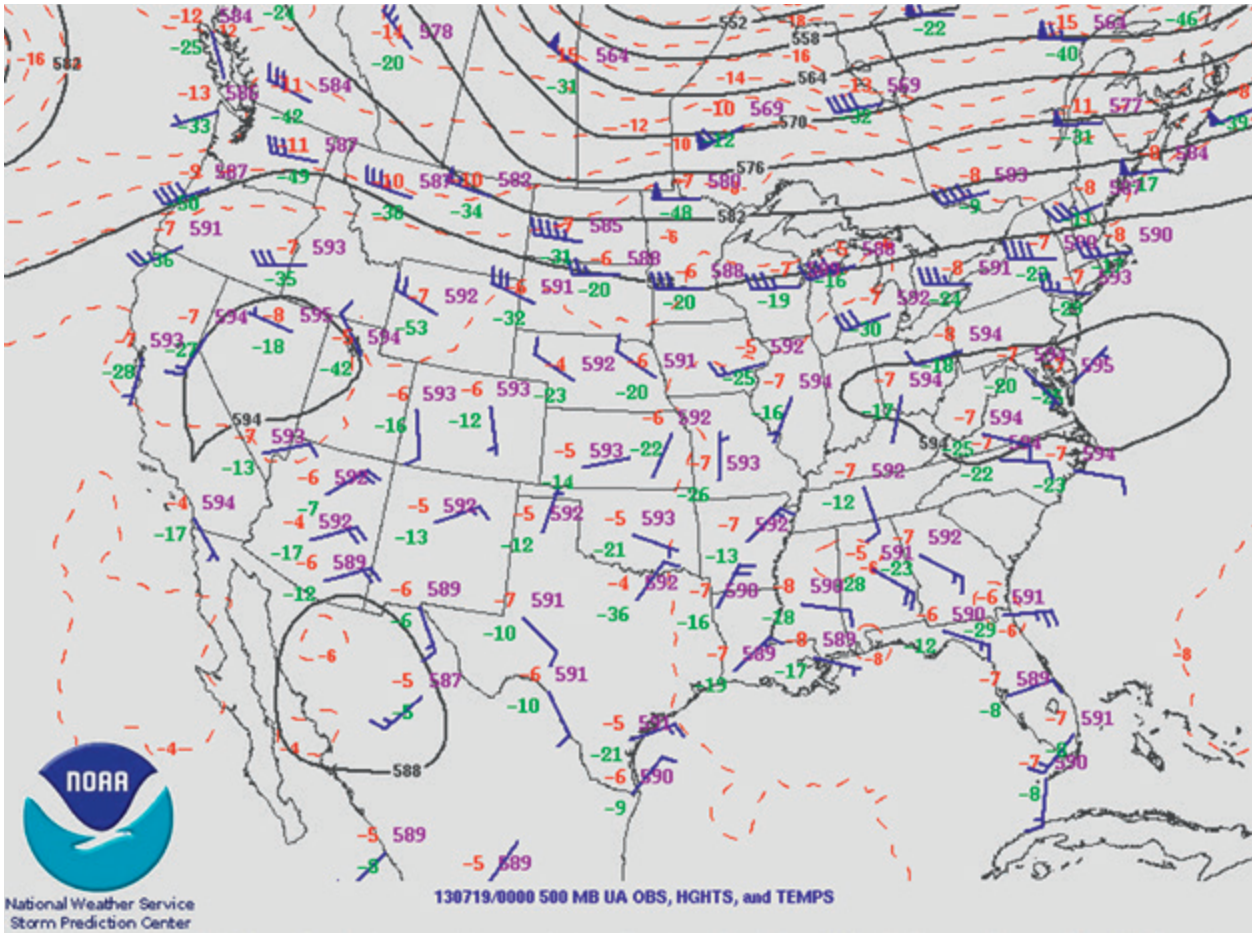

Fig. 5. 500-mb upper-air analysis at 0000 UTC 22 Jul 2013, showing the location of the upper-level low in northern Mexico. [Image credit: NOAA NWS Storm Prediction Center]

GPS PW IMPROVES SITUATIONAL AWARENESS IN A JULY 2013 EVENT. An example highlighting the use of GPS PW is a North American Monsoon event that began to develop on 18 July 2013, when an upper-level low pressure system moved into northern Sonora, Mexico, and weak southerly winds in the Gulf of California transported significant amounts of moisture into the area of Yuma, Arizona (Arellano et al. 2013) (Fig. 4). On 19 July, the upper low (manifesting itself as a wave) had moved west over the Gulf of California and the Baja Peninsula (Fig. 5). An MCS developed in central Arizona, and by 21 July it had moved northwestward toward the Southern California coast. Figure 6 shows the progression of the wave that moved through Southern California on 21 July as seen by the 500-hPa heights and the 300-hPa equivalent potential vorticity (EPV) from the 12-km North American Mesoscale model (NAM12) between 0600 UTC 21 July 2013 and 0000 UTC 22 July 2013. During the period of maximum heating, a high EPV feature rotated around the upper low and moved through Southern California, likely enhancing the convection generated over the region. The low-level forcing mechanism for the convection was probably the convergence near the ridgelines of the mountains. Optimal atmospheric conditions indicated by high GPS PW along with the forcing provided by the wave resulted in heavy rainfall, flash flooding, and debris flows in Riverside and San Diego counties beginning at about 0400 Pacific Daylight Time (PDT) (1100 UTC) 21 July. Precipitation totals over 30 min and one hour exceeded the 1,000-yr recurrence levels on 22 July at Llano, California in the Antelope Valley, where vehicles became stuck due to flash flooding.

This event presented an opportunity for NWS forecasters to utilize the expanded Southern California GPS PW dataset. The southernmost observations available to detect low-to-midlevel moisture arriving into the forecast areas from the Gulf of California

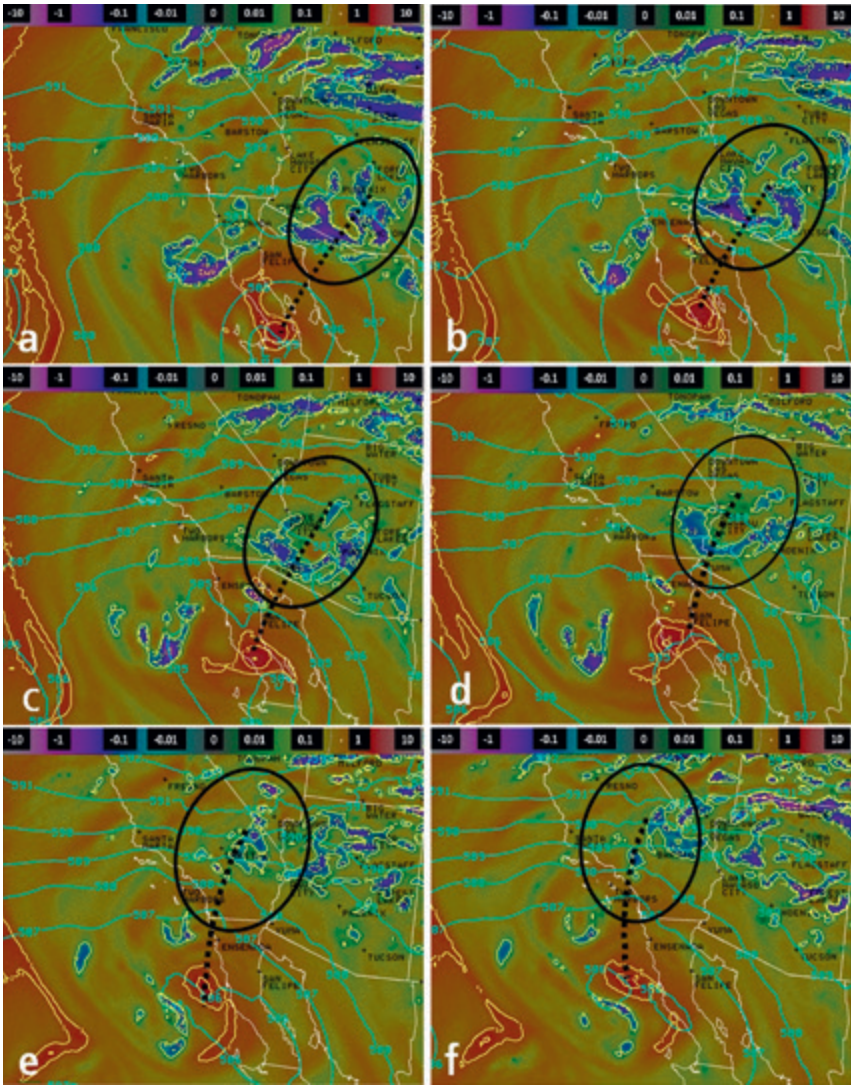

Fig. 6. Progression of the 12-km resolution North American Mesoscale model (NAM12) 300-hPa equivalent potential vorticity (EPV) [shaded and yellow contours, in PVU (1×10^{-6} $m^2 Ks^{-1} kg^{-1}$)], along with 500-hPa heights (cyan contours), as the wave moved through Southern California on 21 Jul 2013. Darker blue/purple shading indicates EPV<0. The dashed line indicates an inverted trough, and the ovals indicate a feature rotating around the upper low and moving through Southern California. The first flash flood was reported at about 1100 UTC (0400 PDT) 21 Jul 2013. Multiple areas of flash flooding were reported the following afternoon at around 0000 UTC 22 Jul 2013. Images are the 1800 UTC 20 Jul 2013 NAM forecast valid at (a) 0600 UTC 21 Jul 2013, (b) 0900 UTC 21 Jul 2013, (c) 1200 UTC 21 Jul 2013, (d) 1500 UTC 21 Jul 2013, (e) 2100 UTC 21 Jul 2013, and (f) 0000 UTC 22 Jul 2013.

included radiosonde observations at Yuma (Arizona) and San Diego, as well as about 20 California GPS-Met stations in the 100 km north of the Mexican border. On the afternoon of 18 July, a sounding at Yuma indicated 44 mm of PW, sufficient monsoonal moisture to cause heavy rainfall (considered to be PW exceeding 35 mm in the local area). Meanwhile, PW of 13 mm in the San Diego sounding indicated the moisture had not spread west to the coast. An increase to 25 mm was measured at San Diego in the 0500 PDT 19 July sounding, but no new sounding from Yuma was available. It was expected that the continued outflows from convection to the east and southeast, and moisture surges from the southeast into the deserts and mountains, would increase the low-level moisture and convective potential. Orographic lifting had the potential to cause heavy rainfall as this flow reached the Coast Ranges.

Forecasters were able to use the GPS PW to characterize the moisture distribution and content in the absence of a Yuma sounding. The expanded GPS dataset also provided moisture information at higher spatial and temporal resolutions. For example, as seen in Fig. 7, the PW increase at Durmid Hill, near the Salton Sea, began to accelerate early on 19 July, exceeding the PW at both San Diego and Glamis a few hours later. By 0700 PDT, 45 mm of PW was observed at GPS stations in the deserts near the mountain slopes. The 0800 PDT aviation routine weather report (METAR) data included dewpoint temperatures at three desert locations exceeding 21°C, indicating increased low-level (boundary layer) moisture. The increase was confirmed when a 0900 PDT Yuma sounding eventually arrived, indicating PW of 53 mm. Note that there is a delay of roughly 2 h before a Yuma sounding is visible in forecasters' Advanced Weather Interactive Process-

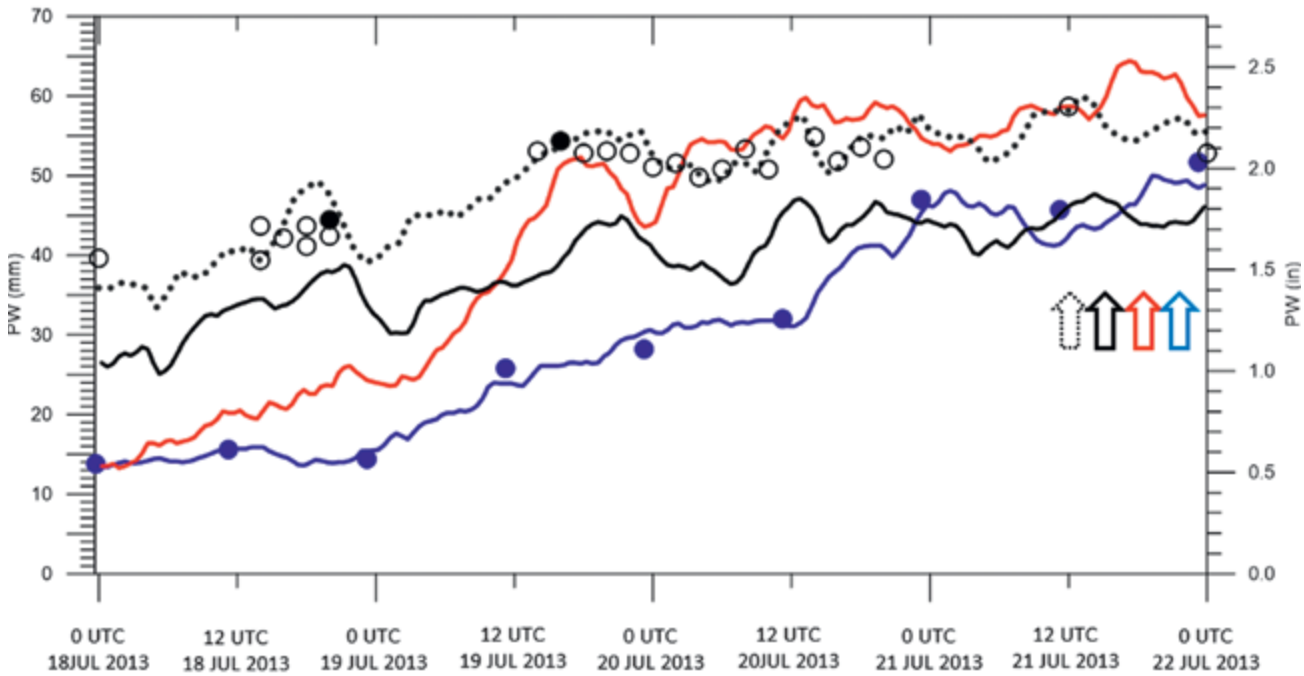

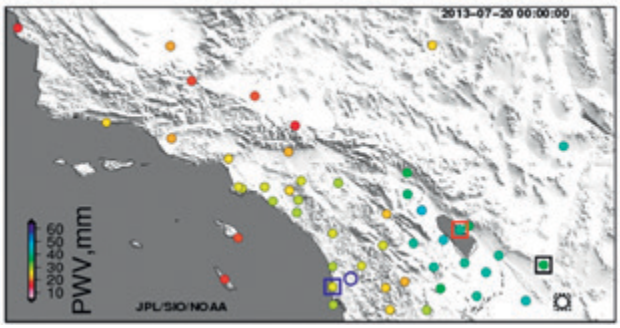

Fig. 7. PW measurements during the evolution of the July event. Circles represent PW (cm) for radiosondes at San Diego, California (blue), and Yuma, Arizona (black). At the U.S. Army Yuma Proving Ground (YPG), radiosondes are launched irregularly in support of the local mission, and many observations only become available to the NWS and WMO retrospectively and with a variable delay. Solid black circles indicate those that were available to forecasters in AWIPS leading up to the flash flood watch and warning described in the text. Open circles represent additional Yuma soundings provided for retrospective insight into the event. Solid traces show GPS PW measurements at San Diego, California (blue), Durmid, California (red), and Glamis, California (black), about 60 km from Yuma. Dotted black trace is PW from a GPS station in Yuma that was not available to the forecasters at the time of this study, but was postprocessed to compare with PW measured by the Yuma radiosondes during the passage of the inverted trough. Arrows indicate the times of passage of the wave illustrated in Fig. 6 at the identified GPS-Met sites. Map locates GPS stations with squares at San Diego (blue), Durmid (red), Glamis (black), and Yuma (dotted black), and radiosondes with circles at San Diego (blue) and Yuma (black). PW in mm at the GPS stations is shown, according to the color scale, at 1700 PDT 19 Jul (0000 UTC 20 Jul).

ing System (AWIPS) terminals. In Fig. 7, we show the two Yuma soundings that were available to the forecasters during this period in solid black; other Yuma soundings are shown as open circles for retrospective context. Animations of the GPS PW during this event, alongside weather model PW, radar reflectivity, and rainfall data, are available as supplemental material.

At 2115 PDT on 19 July 2013, forecasters issued an Area Forecast Discussion (AFD) noting that the upward trend in GPS PW indicated the need for a flash flood watch for the afternoon of 20 July. The watch was issued on the next shift at 0134 PDT on 20 July 2013, about 26 h and 26 min prior to the first report of flash flooding at 0400 PDT on 21 July 2013, which is a significant amount of lead time for this type of event. A flash flood warning was issued at 0343 PDT on 21 July 2013, giving 17 min of lead time between the issuance of the warning and the first report of flash flooding.

As noted by Ivory Small, Science and Operations Officer at the San Diego WFO, "the absence of sounding data at Yuma, AZ, resulted in the GPS-MET PW

Fig. 8. Flooding across Highway 78 in San Diego County, California, 22 Jul 2013. [Photo credit: NOAA]

data being very valuable to the forecaster in order to determine how the moisture distribution and content was changing in Southern California. The high temporal resolution of the GPS-MET PW data . . . eventually led to the issuance of a flash flood watch prior to significant flash flooding in southwest California."

Local storm reports indicated debris flows from recent fire activity, vehicles trapped on a roadway between two flooded locations on Highway 78 (Fig. 8), and bowling ball–sized rocks and 1-m deep flood deposits covering about 24 m of a road in Riverside county.

DISCUSSION OF THE VALUE OF GPS PW TO THE WATCH/WARNING PROCESS. GPS PW gives forecasters confidence about whether a watch or warning is needed, and if so, how soon it will likely be needed and in which area. The GPS-PW data improves the watch/warning process for several reasons, including the high temporal resolution compared with other observations and the rough correlation between high PW and heavy rainfall. In general, if a model indicates an upward PW trend, but the GPS PW does not, forecasters would tend to hold off on the watch and question the model, but if the trend continues or accelerates, the watch would be issued even sooner. Although many factors are considered by forecasters, including wind, stability, orographic lifting, and dynamic conditions related to the upper-level low, flash flood warnings would likely be issued sooner with very high GPS-PW values versus events with "typical" or marginal values of GPS-PW.

GPS PW can also be particularly useful in the case of atmospheric river events, when moisture is concentrated in a band associated with the low-level jet, rain rate is minimally impacted by evaporation, orographically forced ascent is appreciably larger than synoptic ascent, and hydrometeor generation is instantaneous and 100% efficient. In this case, there is a correlation between upslope moisture flux, empirically described by PW and mean wind at ~1 km, and the triggering of heavy precipitation (Alpert 1986; Neiman et al. 2002; Neiman et al. 2009). The empirical relationship between upslope moisture flux and mean wind can be exploited on nowcasting time scales to directly evaluate the change in integrated water vapor as indicating potentially elevated risk of flooding in the regions downslope of the mountains within the forecast area.

FUTURE PLANS. In the 2014 NAM season, several events affecting Southern California caused roadway flooding, stranded hikers and bicyclists, and even one fatality. The products provided by NOAA GPS-Met had comparable impact on forecasts and the watch/warning process. Monitoring the GPS PW dataset has become a routine part of operations at the NWS Oxnard and San Diego WFOs. As discussed above, we also anticipate utility in winter season events involving landfalling atmospheric rivers.

The primary goals of this continuing NASA-sponsored project are to 1) make these tools and techniques available to NWS forecasters, and 2) assess the impact of higher temporal and spatial resolution estimates of PW on local and regional predictions and warnings of heavy precipitation events in flash flood-prone regions of Southern California. Since the initial results are very encouraging, the next steps are to install low-cost micro electro-mechanical systems (MEMS) pressure and temperature sensors at a greater number of real-time GPS sites, to take full advantage of the GPS infrastructure and provide very timely (seconds to a few minutes latency) water vapor estimates at even better spatial and temporal resolution and over a larger area. Ultimately, inclusion in AWIPS will allow enhanced interactive use of the high temporal resolution data.

ACKNOWLEDGMENTS. This research was funded by a NASA AIST-11 NNX09AI67G award to Scripps Institution of Oceanography, and by in-kind support from NOAA's Earth System Research Laboratory and the NOAA Weather Forecasting Offices in San Diego and Oxnard. A portion of this work was carried out at the Jet Propulsion Laboratory, California Institute of Technology, under a contract with NASA. Maps were drawn with the Generic Mapping Tool and matplotlib. San Andreas fault map data are from P. Bird (doi:10.1029/2001GC000252). GPS RINEX data were provided by the NASA MEaSUREs Solid Earth Science ESDR System project through the SOPAC archive and by the UNAVCO Facility with support from the National Science Foundation (NSF) Grant No. EAR-1400901 and NASA under NSF Cooperative Agreement No. EAR-0735156. We thank the editor and three anonymous reviewers for suggestions that greatly improved the paper.

FOR FURTHER READING

Adams, D. K., and A. C. Comrie, 1997: The North American Monsoon. *Bull. Amer. Meteor. Soc.,* **78,** 2197–2213, doi:10.1175/1520-0477(1997)078<2197:TNAM>2.0.CO;2.

Alpert, P., 1986: Mesoscale indexing of the distribution of orographic precipitation over high mountains. *J. Climate Appl. Meteor.,* **25,** 532–545, doi:10.1175/1520-0450(1986)025<0532:MIOTDO>2.0.CO;2.

Arellano, A., C. Castro, Y. Serra, P. Broxton, T. Luong, J. Moker, and S. Silver, cited 2015: Monsoon Weather Discussions 2013. [Available online at http://monsoonwx2013.wordpress.com.]

Bevis, M., S. Businger, T. A. Herring, C. Rocken, R. A. Anthes, and R. H. Ware, 1992: GPS meteorology: Remote sensing of atmospheric water vapor using the Global Positioning System. *J. Geophys. Res.,* **97,** 15 787–15 801, doi:10.1029/92JD01517.

——, ——, S. Chiswell, T. A. Herring, R. A. Anthes, C. Rocken, and R. H. Ware, 1994: GPS meteorology: Mapping zenith wet delays onto precipitable water. *J. Appl. Meteor.,* **33,** 379–386, doi:10.1175/1520-0450(1994)033<0379:GMMZWD>2.0.CO;2.

Bieda, S. W., C. L. Castro, S. L. Mullen, A. C. Comrie, and E. Pytlak, 2009: The relationship of transient upper-level troughs to variability of the North American monsoon system. *J. Climate,* **22,** 4213–4227, doi:10.1175/2009JCLI2487.1.

Böhm, J., A. Niell, P. Tregoning, and H. Schuh, 2006: Global Mapping Function (GMF): A new empirical mapping function based on numerical weather model data. *Geophys. Res. Lett.,* **33,** L07304, doi:10.1029/2005GL025546.

Corbosiero, K. L., M. J. Dickinson, and L. F. Bosart, 2009: The contribution of eastern North Pacific tropical cyclones to the rainfall climatology of the southwest United States. *Mon. Wea. Rev.,* **137,** 2415–2435, doi:10.1175/2009MWR2768.1.

Davis, J. L., T. A. Herring, I. I. Shapiro, A. E. E. Rogers, and G. Elgered, 1985: Geodesy by radio interferometry: Effects of atmospheric modeling errors on estimates of baseline length. *Radio Sci.,* **20,** 1593–1607, doi:10.1029/RS020i006p01593.

Dixon, P. G., 2005: Using sounding data to detect gulf surges during the North American monsoon. *Mon. Wea. Rev.,* **133,** 3047–3052, doi:10.1175/MWR3029.1.

Douglas, M. W., and J. C. Leal, 2003: Summertime surges over the Gulf of California: Aspects of their climatology, mean sounding, and evolution from radiosonde, NCEP reanalysis, and rainfall data. *Wea. Forecasting,* **18,** 55–74, doi:10.1175/1520-0434(2003)018<0055:SSOTGO>2.0.CO;2.

Duan, J., and Coauthors, 1996: GPS meteorology: Direct estimation of the absolute value of precipitable

water. *J. Appl. Meteor.,* **35,** 830–838, doi:10.1175/1520-0450(1996)035<0830:GMDEOT>2.0.CO;2.

Fang, P., M. Bevis, Y. Bock, S. Gutman, and D. Wolfe, 1998: GPS meteorology: Reducing systematic errors in geodetic estimates for zenith delay. *Geophys. Res. Lett.,* **25,** 3583–3586, doi:10.1029/98GL02755.

Favors, J. E., and J. T. Abatzoglou, 2013: Regional surges of monsoonal moisture into the southwestern United States. *Mon. Wea. Rev.,* **141,** 182–191, doi:10.1175/MWR-D-12-00037.1.

Finch, Z. O., and R. H. Johnson, 2010: Observational analysis of an upper-level inverted trough during the 2004 North American Monsoon Experiment. *Mon. Wea. Rev.,* **138,** 3540–3555, doi:10.1175/2010MWR3369.1.

Fuller, R. D., and D. J. Stensrud, 2000: The relationship between tropical easterly waves and surges over the Gulf of California during the North American monsoon. *Mon. Wea. Rev.,* **128,** 2983–2989, doi:10.1175/1520-0493(2000)128<2983:TRBTEW>2.0.CO;2.

Gutman, S. I., S. R. Sahm, S. G. Benjamin, B. E. Schwartz, K. L. Holub, J. Q. Steward, and T. L. Smith, 2004: Rapid retrieval and assimilation of ground based GPS precipitable water observations at the NOAA Forecast Systems Laboratory: Impact on weather forecasts. *J. Meteor. Soc. Japan,* **82,** 351–360, doi:10.2151/jmsj.2004.351.

Higgins, R. W., W. Shi, and C. Hain, 2004: Relationships between Gulf of California moisture surges and precipitation in the southwestern United States. *J. Climate,* **17,** 2983–2997, doi:10.1175/1520-0442(2004)017<2983:RBGOCM>2.0.CO;2.

Kawabata, T., H. Seko, K. Saito, T. Kuroda, K. Tamiya, T. Tsuyuki, Y. Honda, and Y. Wakazuki, 2007: An assimilation and forecasting experiment of the Nerima heavy rainfall with a cloud-resolving nonhydrostatic 4-dimensional variational data assimilation system. *J. Meteor. Soc. Japan,* **85,** 255–276, doi:10.2151/jmsj.85.255.

Ladwig, W., and D. Stensrud, 2009: Relationship between tropical easterly waves and precipitation during the North American monsoon. *J. Climate,* **22,** 258–271, doi:10.1175/2008JCLI2241.1.

Marcus, S., J. Kim, T. Chin, D. Danielson, and J. Laber, 2007: Influence of GPS precipitable water vapor retrievals on quantitative precipitation forecasting in Southern California. *J. Appl. Meteor. Climatol.,* **46,** 1828–1839, doi:10.1175/2007JAMC1502.1.

Means, J. D., 2013: GPS precipitable water as a diagnostic of the North American Monsoon in California and Nevada. *J. Climate,* **26,** 1432–1444, doi:10.1175/JCLI-D-12-00185.1.

Neiman, P. J., F. M. Ralph, A. B. White, D. E. Kingsmill, and P. O. G. Persson, 2002: The statistical relationship between upslope flow and rainfall in California's coastal mountains: Observations during CALJET. *Mon. Wea. Rev.,* **130,** 1468–1492, doi:10.1175/1520-0493(2002)130<1468:TSRBUF>2.0.CO;2.

——, A. B. White, F. M. Ralph, D. J. Gottas, and S. I. Gutman, 2009: A Water vapor flux tool for precipitation forecasting. *Proc. Inst. Civ. Eng.: Water Management,* **162,** 83–94, doi:10.1680/wama.2009.162.2.83.

——, F. M. Ralph, B. J. Moore, M. Hughes, K. M. Mahoney, J. M. Cordeira, and M. D. Dettinger, 2013: The landfall and inland penetration of a flood-producing atmospheric river in Arizona. Part I: Observed synoptic-scale, orographic, and hydrometeorological characteristics. *J. Hydrometeor.,* **14,** 460–484, doi:10.1175/JHM-D-12-0101.1.

Pytlak, E., M. Goering, and A. Bennett, 2005: Upper-tropospheric troughs and their interaction with the North

American Monsoon. *Preprints, 19th Conf. on Hydrology,* San Diego, CA, Amer. Meteor. Soc., JP2.3. [Available online at https://ams.confex.com/ams/pdfpapers/85393.pdf.]

Ralph, F. M., E. Sukovich, D. Reynolds, M. Dettinger, S. Weagle, W. Clark, and P. J. Neiman, 2010: Assessment of extreme quantitative precipitation forecasts and development of regional extreme event thresholds using data from HMT-2006 and COOP Observers. *J. Hydrometeor.,* **11,** 1286–1306, doi:10.1175/2010JHM1232.1.

Schiffer, N. J., and S. W. Nesbitt, 2012: Flow, moisture, and thermodynamic variability associated with Gulf of California surges within the North American Monsoon. *J. Climate,* **25,** 4220–4241, doi:10.1175/JCLI-D-11-00266.1.

Small, I. J., and B. Maxwell, 2014: Early wind forecasting results from the 1.5 KM WRF-ARW in extreme southwestern California. *16th Conf. on Mountain Meteorology,* San Diego, CA, Amer. Meteor. Soc., 3. [Available online at https://ams.confex.com/ams/16MountMet/webprogram/Paper251612.html.]

Smith, T. L., S. G. Benjamin, S. I. Gutman, and S. R. Sahm, 2007: Forecast impact from assimilation of GPS-IPW observations into the Rapid Update Cycle. *Mon. Wea. Rev.,* **135,** 2914–2930, doi:10.1175/MWR3436.1.

Tubbs, A. M., 1972: Summer thunderstorms over Southern California. *Mon. Wea. Rev.,* **100,** 799–807, doi:10.1175/1520-0493(1972)100<0799:STOSC>2.3.CO;2.

White, A., and Coauthors, 2013: A twenty-first-century California observing network for monitoring extreme weather events. *J. Atmos. Oceanic Technol.,* **30,** 1585–1603, doi:10.1175/JTECH-D-12-00217.1.

Whiteman, C. D., 2000: *Mountain Meteorology: Fundamentals and Applications.* Oxford University Press, 355 pp.

Wolfe, D., and S. I. Gutman, 2000: Developing an operational, surface-based, GPS, water vapor observing system for NOAA: Network design and results. *J. Atmos. Oceanic Technol.,* **17,** 426–440, doi:10.1175/1520-0426(2000)017<0426:DAOSBG>2.0.CO;2.

AMS BOOKS: HISTORY • CLIMATE • WEATHER

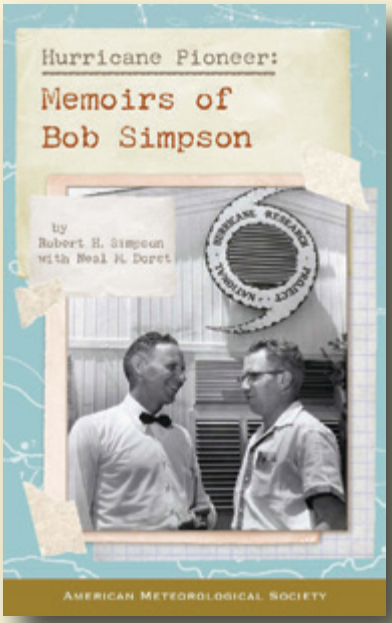

HURRICANE PIONEER

Memoirs of Bob Simpson

Robert H. Simpson with Neal M. Dorst

In 1951, Bob Simpson rode a plane directly into the wall of a hurricane—just one of his many pioneering explorations. This autobiography of the first director of the National Hurricane Research Project and co-creator of the Saffir-Simpson Hurricane Scale starts with childhood remembrance and ends in first-hand account of a revolutionary

© 2014, PAPERBACK
ISBN: 978-1-935704-75-1
LIST $30 MEMBER $20

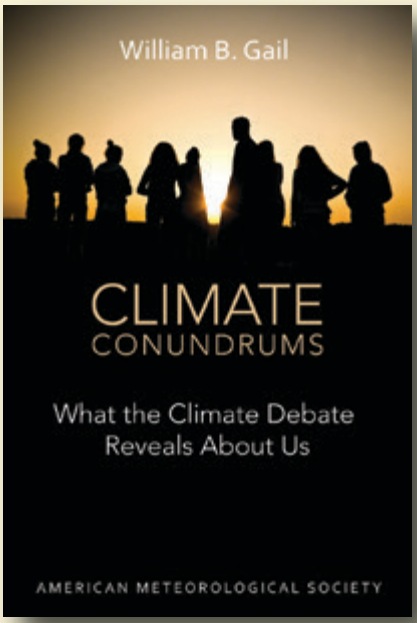

CLIMATE CONUNDRUMS

What the Climate Debate Reveals About Us

William B. Gail

This is a journey through how we think, individually and collectively, derived from the climate change debate. With wit and wisdom, Gail explores several questions: Can we make nature better? Could science and religion reconcile? Insights from such issues can help us better understand who we are and help

© 2014, PAPERBACK
ISBN: 978-1-935704-74-4
LIST $30 MEMBER $20

Browse online at
ametsoc.org/bookstore

FREE SHIPPING
for AMS Members!

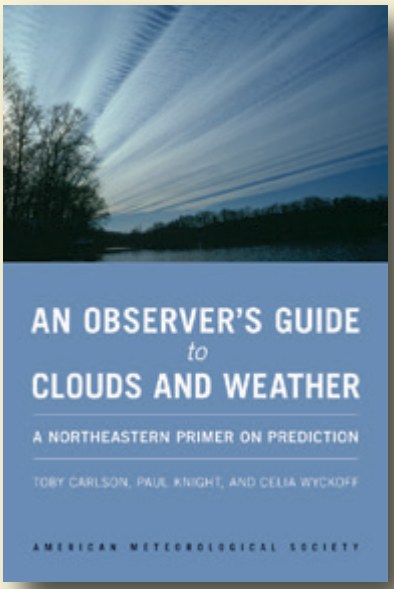

AN OBSERVER'S GUIDE TO CLOUDS AND WEATHER

A Northeast Primer on Prediction

Toby Carlson, Paul Knight, and Celia Wyckoff

With help from Penn State experts, start at the beginning and go deep. This primer for enthusiasts and new students alike will leave you with both refined observation skills and an understanding of the complex science behind the weather: the ingredients for making reliable predictions of your own.

© 2014, PAPERBACK
ISBN: 978-1-935704-58-4
LIST $35 MEMBER $20

AMERICAN METEOROLOGICAL SOCIETY 1919

AMS BOOKS

AMS Books are available to groups and booksellers, and desk copies may be obtained, through our distributor The University of Chicago Press: 1-800-621-2736 or custserv@press.uchicago.edu.

NATURAL GAS PRICES AND THE EXTREME WINTERS OF 2011/12 AND 2013/14

Causes, Indicators, and Interactions

BY CARL J. SCHRECK III, STEPHEN BENNETT, JASON M. CORDEIRA, JAKE CROUCH, JENNY DISSEN, ANDREA L. LANG, DAVID MARGOLIN, ADAM O'SHAY, JARED RENNIE, THOMAS IAN SCHNEIDER, AND MICHAEL J. VENTRICE

Volatility in the natural gas markets can be linked to large temperature variability over the United States in recent winters.

Natural gas is one of the primary sources of energy in the United States. About half of the nation's households use natural gas to heat their homes (U.S. Energy Information Administration 2012). Commodity prices for natural gas become particularly volatile during the peak heating months of December–February, when temperature fluctuations can have large impacts on heating demand. The sensitivity of natural gas markets to weather was unmistakable in the winters of 2011/12 and 2013/14. Unusually warm temperatures in 2011/12 suppressed demand and drove natural gas prices downward, whereas the reverse happened in 2013/14. This study will examine the relationship between weather and natural gas during these two winters. We will use these examples to illustrate how energy meteorologists and traders use weather and climate data to inform their actions in the market.

Natural gas is traded as a commodity on both the Chicago Mercantile Exchange (CME) and the Intercontinental Exchange (ICE). Although numerous natural gas contracts exist, the most common is the Henry Hub natural gas price. Henry Hub is a major pipeline junction in Louisiana, and the quoted price is that of delivery at the hub in terms of dollars per million British thermal units (mmBTU). One mmBTU is equivalent to about 1000 cubic feet (28.3 m^3) of natural gas and is enough to heat an average home for 4 days. The prices quoted in this study will be Henry Hub futures contracts with the earliest delivery date (i.e., the price for delivery in the calendar month following the trade date). Natural gas producers trade futures contracts of Henry Hub natural gas to hedge their risk against market volatility from weather-driven fluctuations in demand. Many traders also speculate in the market to profit from market inefficiencies.

Numerous forces impact the price of natural gas on a variety of different time scales. For example, the advent of high-volume hydraulic fracturing has significantly increased the available supply of natural gas (Turcotte et al. 2014). This increased supply has driven prices downward, although it has been constrained somewhat by the lack of new pipelines to deliver the supply to consumers (Philips 2014). Another external force on the market is the interplay between prices for natural gas and other energy sources (Mjelde and Bessler 2009; Joëts and Mignon 2012; Pettersson et al. 2012). Many electricity companies have the ability to change their production portfolio as seasonal prices fluctuate. The recent drop in natural gas prices has made natural gas more competitive with coal,

oil, and nuclear energy for electricity production. As a result, more utilities are using natural gas to produce electricity and retiring plants that use other fuels (U.S. Energy Information Administration 2012). This "gas for power burn" naturally increases demand for natural gas until the price rises to equilibrium with other fuels.

The largest day-to-day volatility in natural gas prices has been weather-driven demand, which varies by season and region (Linn and Zhu 2004; Mu 2007; Brown and Yücel 2008). The shift toward natural gas as an electricity source has also increased the sensitivity of prices to summer temperatures in the southeastern and south-central United States. However, the greatest weather-related sensitivity still occurs during December–February. During winter, natural gas prices are sensitive to temperatures in the northeastern quadrant of the country roughly bounded by Chicago, Illinois; Boston, Massachusetts; and Atlanta, Georgia (Fig. 1), commonly referred to in the industry as the Midwest–East or the consuming East.

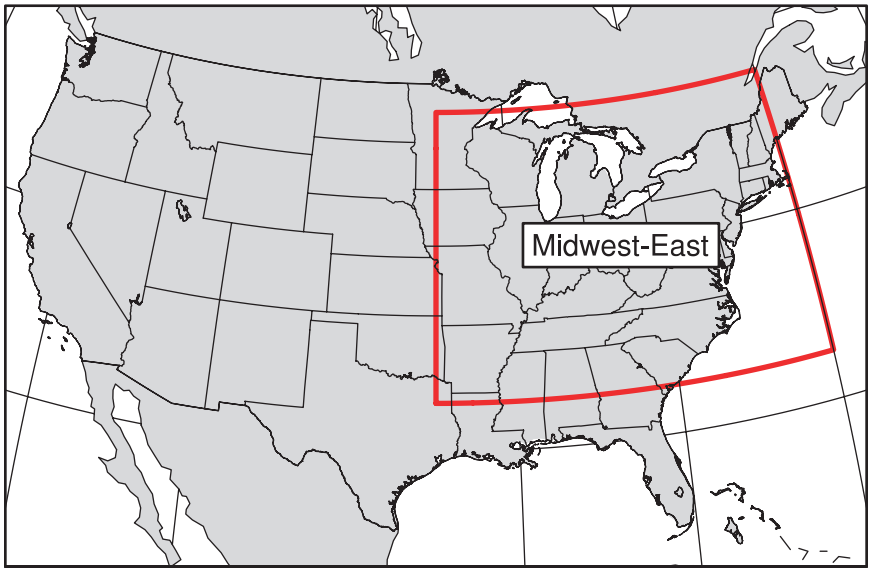

Fig. 1. Outline of the Midwest–East region used in this study to focus on the region where temperatures have the greatest effect on natural gas demand.

Many traders are particularly interested in temperature forecasts at horizons of 2–4 weeks. Monthly futures contracts are naturally forward looking, as they are related to the actual or "spot" price of natural gas weeks or even months later. Weeks 2–4 are also critical time scales for natural gas producers. They can adjust their drilling operations and the prices for natural gas from the wellhead into the pipelines based on the anticipated demand 2–4 weeks later, when that natural gas will be consumed.

Forecasts from global dynamical models play a major role in the natural gas markets. These forecasts are widely available either directly from the forecast centers or through numerous weather vendors (i.e., private companies), so the markets respond quickly to how the forecast temperatures would influence natural gas demand. Large fluctuations in price can happen when the temperature forecast, especially for days 6–15, changes significantly from one model run to the next. The price of natural gas is often most volatile when the 1200 UTC forecast models are released. That is the only model cycle that is disseminated while the markets are open. Traders watch and react as each model run is released: the National Centers for Environmental Prediction (NCEP) Global Forecast System (GFS) at around 1015 eastern standard time (EST), the NCEP Global Ensemble Forecast System (GEFS) at around 1045 EST, and the European Centre

AFFILIATIONS: Schreck, Dissen, and Rennie—Cooperative Institute for Climate and Satellites—North Carolina, North Carolina State University, and NOAA/National Centers for Environmental Information, Asheville, North Carolina; Bennett—EarthRisk Technologies, San Diego, and Verisk Climate, San Francisco, California; Cordeira—Department of Atmospheric Science and Chemistry, Plymouth State University, Plymouth, New Hampshire; Crouch—NOAA/National Centers for Environmental Information, Asheville, North Carolina; Lang—Department of Atmospheric and Environmental Sciences, University at Albany, State University of New York, Albany, New York; Margolin—EarthRisk Technologies, San Diego, California; O'Shay—EarthRisk Technologies, San Diego, California, and Leeward Pointe Capital, Austin, Texas; Schneider—Boston College, Boston, Massachusetts; Ventrice—Weather Service International, Andover, Massachusetts
CORRESPONDING AUTHOR: Carl J. Schreck III, Cooperative Institute for Climate and Satellites—NC, 151 Patton Ave., Asheville, NC 28801
E-mail: cjschrec@ncsu.edu

The abstract for this article can be found in this issue, following the table of contents.

DOI:10.1175/BAMS-D-13-00237.1

In final form 25 November 2014

for Medium-Range Weather Forecasts (ECMWF) deterministic model at around 1400 EST. Speed is crucial to weather vendors that provide these forecasts to traders because prices react as each individual forecast hour is released for a given model. If one vendor can anticipate or distribute those forecasts faster than other sources, then their clients can profit by making their stance in the market before others have access to that information.

Dynamical model forecasts have limited skill beyond 1–2 weeks (Hagedorn et al. 2008; Saha et al. 2006, 2014), but longer-range forecasts are still priced into the market. Savvy traders can profit if they have access to better forecasts because the market will move toward the observed temperatures as the lead-time decreases. Traders often work with energy meteorologists since human forecasts are generally more skillful than those from dynamical models (Roebber and Bosart 1996; Novak et al. 2014). The improvement in skill comes from a combination of forecaster experience and leveraging teleconnections, especially from the tropics and the Arctic. Teleconnections represent low-frequency systems that have life cycles extending beyond the predictive skill of many models (Van Oldenborgh et al. 2003; Saha et al. 2006). Energy meteorologists use the current states of these teleconnections in statistical models or simply examine composite temperature anomalies based on analogous past events. Comparing these composites with the dynamical model forecasts is one way that meteorologists estimate the reliability of those forecasts. A critical component for making these composites or statistical models is having access to datasets like NOAA's climate data records (National Research Council 2004), which are long enough to identify a large sample of past events and also have sufficient homogeneity to ensure data consistency between those events. The primary tropical teleconnections are the El Niño–Southern Oscillation (ENSO) and the Madden–Julian oscillation (MJO). Key Arctic teleconnections include the Arctic Oscillation (AO), the North Atlantic Oscillation (NAO), Eurasian snow cover, and stratospheric temperature and wind anomalies.

ARCTIC TELECONNECTIONS. Two of the leading modes of low-frequency variability in the Northern Hemisphere circulation are the AO and the NAO (Barnston and Livezey 1987). These modes are correlated with each other (Thompson and Wallace 1998; Ambaum et al. 2001), and they are also both positively correlated with Midwest–East temperatures (Higgins et al. 2000, 2002). The AO is related to the strength and orientation of the circumpolar jet. When the AO is positive, the jet is stronger and more zonal, which confines the coldest air to the

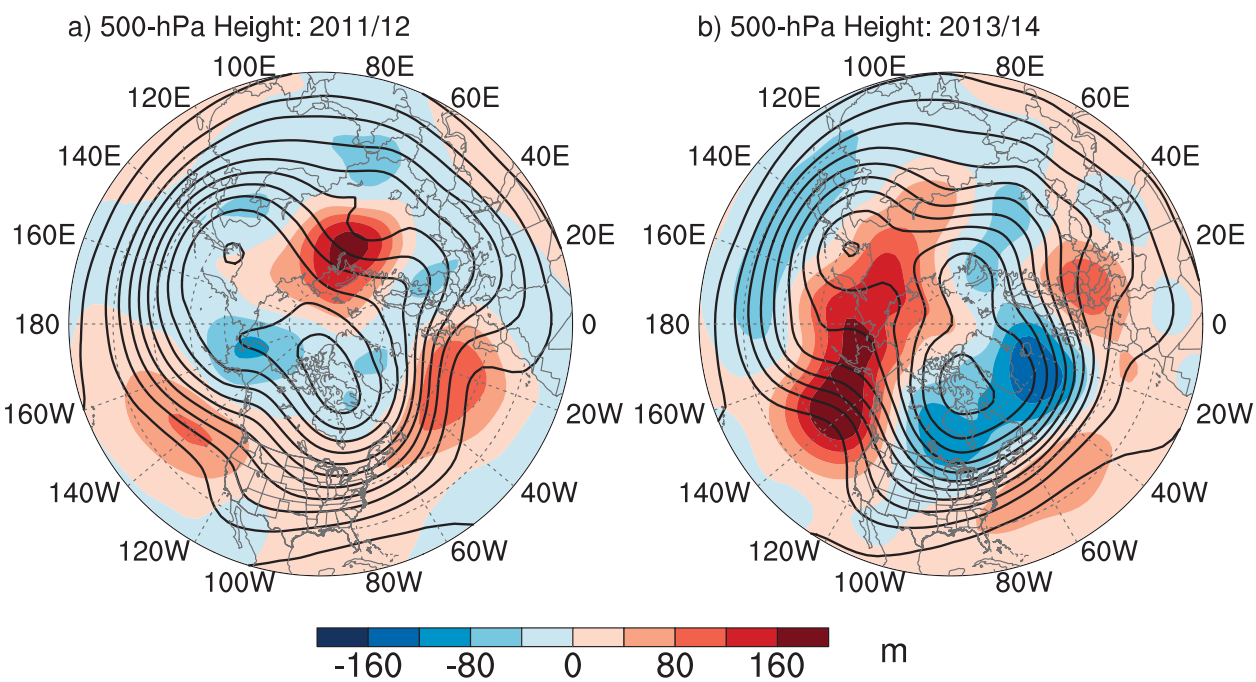

Fig. 2. NCEP–Department of Energy (DOE) Reanalysis-2 (Kanamitsu et al. 2002) 500-hPa geopotential heights (contours) and anomalies relative to 1981–2010 for Dec–Feb (a) 2011/12 and (b) 2013/14. Contours are drawn every 80 m.

Arctic region. Conversely, negative AO is associated with higher-amplitude waves in the jet and generally colder temperatures over the Midwest–East. The NAO is related to the strength and location of the jet and the extratropical storm track over the North Atlantic (Hurrell et al. 2003). Negative AO indicates colder temperatures and more frequent winter storms over the Midwest–East.

Figure 2 shows the mean 500-hPa geopotential heights and anomalies from climatology for December–February 2011/12 and 2013/14. The pattern for 2011/12 was a classic positive AO (Fig. 2a) with negative anomalies near the pole, positive anomalies in the midlatitudes, and a generally zonal flow across the Western Hemisphere. This pattern would be consistent with an extension of the jet over the eastern North Pacific, which limits the opportunities for Arctic intrusions into the United States. Figure 2b shows a very different pattern in 2013/14. Positive anomalies greater than 200 m over the Gulf of Alaska disrupt the eastward extension of the Pacific jet. The ridging associated with these anomalies extended northward all the way to the pole and was associated with enhanced troughing of the central portions of Canada and the United States. The resulting cross-polar flow transported cold Siberian air into the Midwest–East region.

Energy meteorologists often look for ways to forecast changes in the AO and the NAO because of their large impact on Midwest–East temperatures. The stratosphere provides one such source of predictability (Thompson and Wallace 1998; Baldwin and Dunkerton 1999, 2001; Black 2002; Gerber et al. 2012). The stratosphere has a long memory, which makes it useful for long-range forecasting (Newman and Rosenfield 1997; Baldwin et al. 2003; Gerber et al. 2012). Variations in the stratospheric polar vortex can be observed on average 3 weeks before they propagate downward and manifest themselves in the troposphere (Thompson and Wallace 1998; Baldwin and Dunkerton 1999, 2001; Black 2002; Gerber et al. 2012). Accurate representation of the stratosphere also plays a role in the skill of dynamical models (Tripathi et al. 2014). Initialization differences in the stratosphere can affect tropospheric forecasts at leads as short as a few days (Charlton et al. 2004; Jung and Barkmeijer 2006; Gerber et al. 2012). Conversely, improvements to model forecasts of the stratosphere can improve the tropospheric skill for forecasts as long as 3–4 weeks (Roff et al. 2011).

Sudden stratospheric warming (SSW) is a notable exception to the stratosphere's otherwise slow evolution. About every other year, the Northern Hemisphere stratospheric polar vortex abruptly

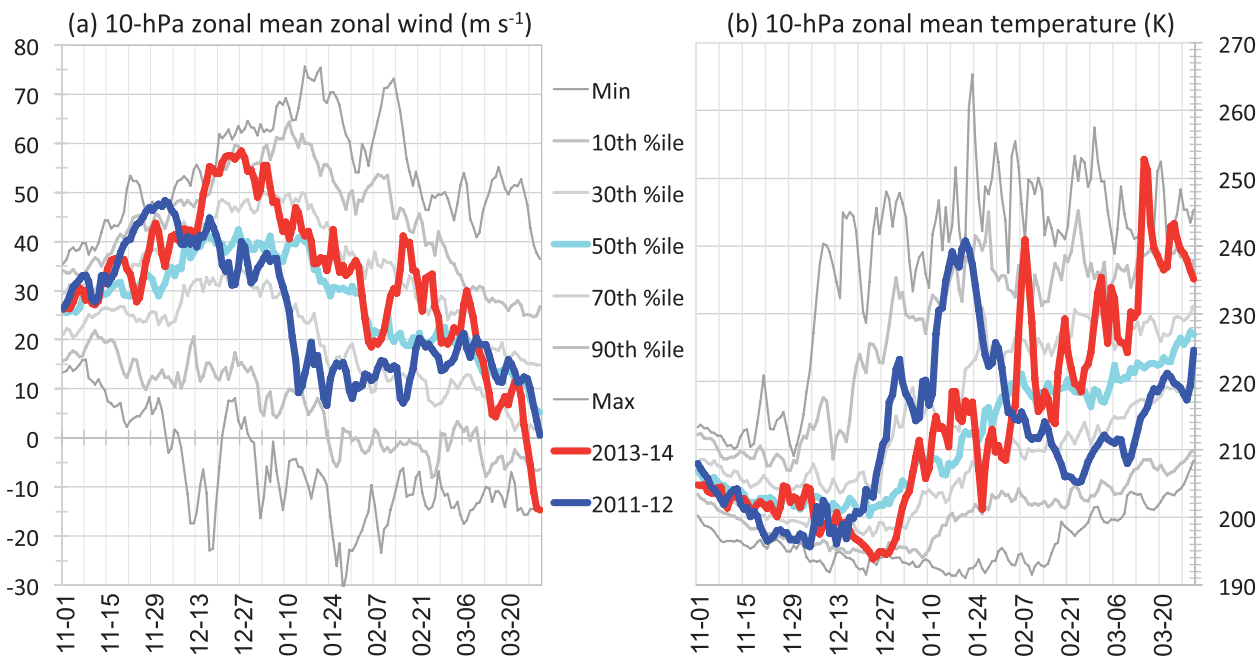

Fig. 3. For the winter (Nov–Mar) of 2011/12 (blue) and 2013/14 (red) along with the minimum, maximum, and 10th, 30th, 50th, 70th, and 90th percentiles for the period covering 1978/79–2013/14, (a) the 10-hPa zonal-mean zonal wind (m s^{-1}) at 60°N and (b) the 10-hPa zonal temperature (K) at 80°N. Data from the National Aeronautics and Space Administration (NASA) Modern-Era Retrospective Analysis for Research and Applications (MERRA; Rienecker et al. 2011).

weakens and the stratosphere dramatically warms (Labitzke 1972; Gerber et al. 2012). These SSWs typically lead to negative AO conditions in the troposphere that can persist for up to 2 months and are associated with persistent cold anomalies over the Midwest–East (Baldwin and Dunkerton 2001; Thompson and Wallace 2001; Thompson et al. 2002).

Figure 3 shows two zonal-mean diagnostics of the stratospheric polar vortex, 10-hPa zonal wind and temperature, during November–March 2011/12 and 2013/14. Both years experienced increases in high-latitude 10-hPa temperatures that coincided with weakening of the 10-hPa westerlies. These warming events did not meet the World Meteorological Organization (WMO) criteria for a major SSW because the zonal-mean circulation never reversed sign from westerly to easterly. However, the stratosphere does not need to experience a major SSW for stratospheric thermal and wind anomalies to impact the tropospheric circulation (Tripathi et al. 2014). For example, the 10-hPa zonal wind rapidly decelerated from over 35 to less than 10 m s^{-1} during the first week of January 2012. Consistent with previous studies (Thompson and Wallace 1998; Baldwin and Dunkerton 1999, 2001; Black 2002; Gerber et al. 2012), this stratospheric warming was associated with a shift in the tropospheric AO index from +2.2 in December 2011 to −0.2 in January 2012 (Fig. 8c).

Despite the zonal-mean similarities in 2011/12 and 2013/14 (Fig. 3), the two winters exhibited notably

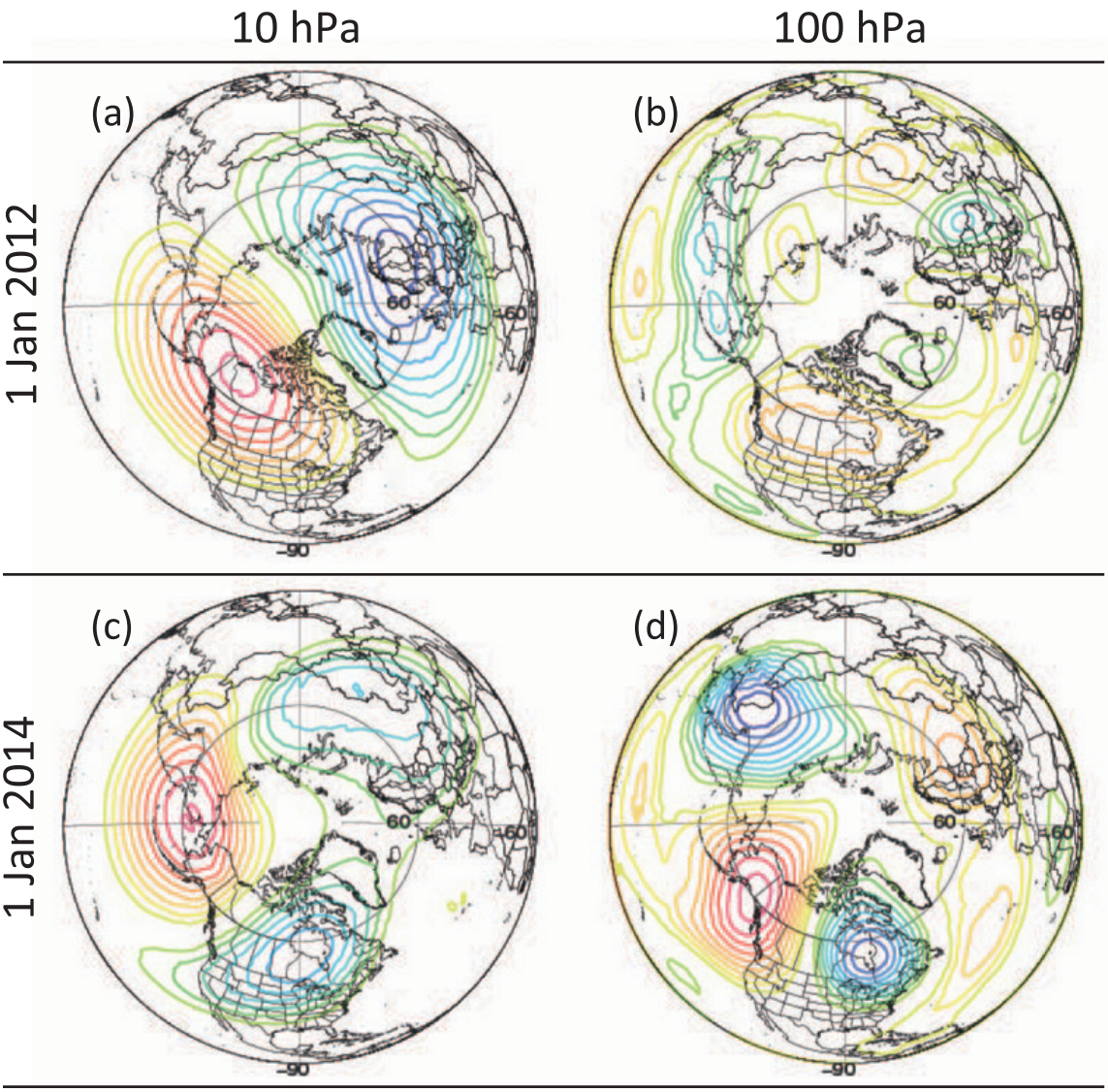

Fig. 4. The departure from GFS analysis zonal-mean geopotential height on 1 Jan 2012 at (a) 10 hPa, every 150 m, and (b) 100 hPa, every 50 m, as well as on 1 Jan 2014 at (c) 10 hPa, every 150 m, and (d) 100 hPa, every 50 m. The 60°N latitude circle represents the characteristic polar vortex edge.

different spatial wave structures in the stratosphere (Fig. 4). The stratospheric pattern was predominantly wavenumber 1 in early January 2012 (Figs. 4a,b), whereas it was closer to wavenumber 2 in January 2014 (Figs. 4c,d). Comparing Figs. 2 and 4 illustrates that anomalous 500-hPa geopotential height anomalies over North America in both winters were connected with similar anomalies in the stratosphere. For example, the anomalous 500-hPa trough over the Midwest–East responsible for the cold winter of 2013/14 (Fig. 2b) extended upward and linked to the wavenumber-2 structure in the stratospheric polar vortex (Figs. 4c,d).

The areal extent of snow cover over Eurasia (Robinson et al. 1993) represents another source of predictability for the AO/NAO. Above-normal Eurasian snow cover in October can lead to a more negative AO/NAO throughout the winter (Cohen and Entekhabi 1999; Cohen et al. 2010; Cohen and Jones 2011; Smith et al. 2011). The enhanced Eurasian snow strengthens the Siberian high, and these anomalies may propagate vertically into the stratosphere where they have more lasting effects on the AO/NAO.

TROPICAL TELECONNECTIONS. ENSO is an important tool for seasonal temperature forecasting. El Niño events are typically associated with warm winter temperatures in the Midwest–East region, whereas La Niña winters are generally cooler than normal (Ropelewski and Halpert 1986; Harrison and Larkin 1998; Higgins et al. 2002; Chiodi and Harrison 2013). The warm signals over North America primarily occur with conventional eastern Pacific warming events and less frequently with central Pacific warming events (Larkin and Harrison 2005; Weng et al. 2009; Chiodi and Harrison 2013).

Just as ENSO is the leading mode of tropical interannual variability, the MJO is the leading mode on intraseasonal time scales. The MJO moves eastward in the tropics with a period of 30–60 days (Zhang 2005), and its tropical convection interacts with circulations around the globe, including weather patterns over North America (Becker et al. 2011; Zhou et al. 2012; Riddle et al. 2013; Johnson and Feldstein 2010; Schreck et al. 2013; Zhang 2013). Dynamical models are only just beginning to tap the long-range predictability of the MJO (Gottschalck et al. 2010; Weaver et al. 2011), so it represents a key opportunity for human forecasts to improve upon those from the models. The MJO's 30–60-day period lends itself to the analog methods that many energy meteorologists use for long-range forecasting. They predict the evolution of the MJO on Wheeler and Hendon's (2004) real-time multivariate MJO (RMM) index and then extrapolate Midwest–East temperatures based on composites for each of the RMM's eight phases. Those temperatures tend to be warmer in the 6–10 days following phases 3–5 and cooler following phase 8 (Zhou et al. 2012; Schreck et al. 2013). The RMM index can be sensitive to higher-frequency equatorial waves (Roundy et al. 2009), so forecasters often complement the index by examining Hovmöller diagrams

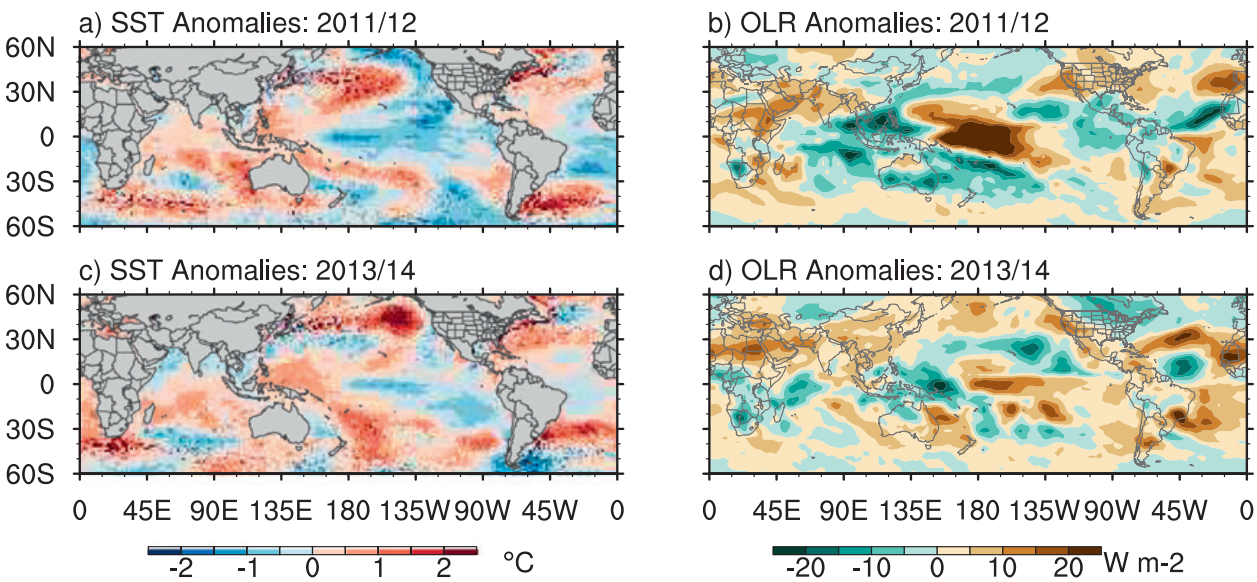

Fig. 5. Dec–Feb anomalies relative to 1981–2010 of (a),(c) optimum interpolation (OI) SST (Reynolds et al. 2007; Reynolds 2009; Banzon and Reynolds 2013) and (b),(d) High Resolution Infrared Radiation Sounder (HIRS) OLR (Lee et al. 2007) for (top) 2011/12 and (bottom) 2013/14.

of daily OLR anomalies (Wheeler and Weickmann 2001; Liebmann and Smith 1996; Lee 2014).

Figure 5 shows global maps of sea surface temperatures (SSTs; Reynolds et al. 2007; Reynolds 2009; Banzon and Reynolds 2013) and outgoing longwave radiation (OLR; Lee et al. 2007), two fields that energy meteorologists use to identify tropical forcing for Midwest–East temperatures. They are particularly concerned with the SST patterns over the tropical Pacific, which define the characteristics of the ENSO state more than any single index (e.g., Fig. 8a) (Trenberth 1997). OLR is similarly important for identifying variability in tropical convection, which acts as a bridge between the SSTs and Midwest–East temperatures (Chiodi and Harrison 2013).

The winters of 2011/12 and 2013/14 both featured cooler-than-normal SSTs in the equatorial central Pacific coincident with positive OLR anomalies that indicate atmospheric subsidence (Fig. 5). These features were stronger in 2011/12 and extended farther into the western Pacific. The enhanced convection near the South China Sea in 2011/12 and the accompanying upper-tropospheric outflow could have played a role in the extended Pacific jet seen in Fig. 2a (Kiladis and Weickmann 1992; Matthews et al. 2004; Johnson and Feldstein 2010). Similarly, the enhanced convection in the western Pacific during 2013/14 was consistent with the more amplified flow that winter.

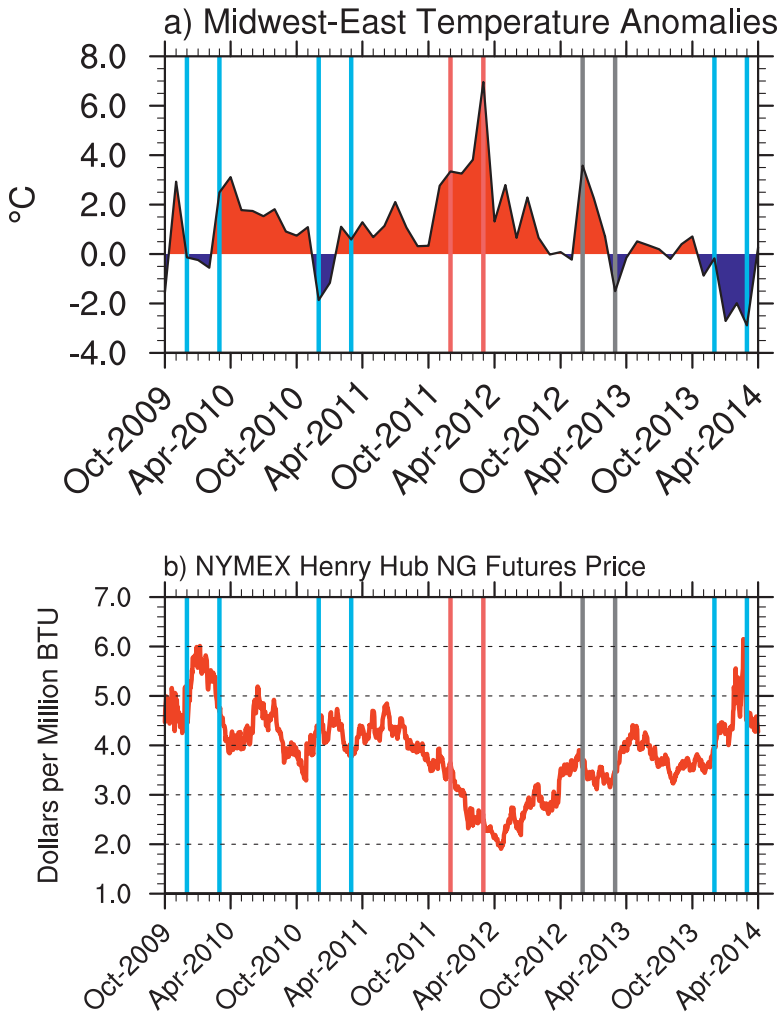

Fig. 6. Time series of (a) monthly temperature anomalies relative to 1981–2010 averaged over the Midwest–East region and (b) daily Henry Hub natural gas futures prices. Vertical lines denote Dec–Feb seasons that were cold (blue), warm (red), or neutral (gray).

Another unique feature in 2013/14 was the unusually warm (>2.5°C) SST anomalies in the Gulf of Alaska (Fig. 5c). These SSTs were more than 1.0°C warmer than any previously experienced in that region during December–February since the satellite record began in 1981/82. Previous studies have generally concluded that North Pacific SST anomalies are driven largely by the local atmospheric circulation (Davis 1976; Cayan 1992; Liu et al. 2006). However, the SST anomalies can in turn affect the atmospheric circulation by forcing a Pacific–North America (PNA) like pattern and an enhanced ridge over the Gulf of Alaska similar to that seen in Fig. 2b (Peng and Whitaker 1999; Liu et al. 2006; Frankignoul and Sennéchael 2007).

FLUCTUATING TEMPERATURES, SUPPLY, AND DEMAND. *Warmth and surpluses in 2011/12.* Figure 6 shows the evolution of Midwest–East temperature anomalies and the Henry Hub natural gas futures price since 2009. The temperature data in this study originate from a subset of the Global Historical Climatology Network-Daily (GHCN-D) dataset (Menne et al. 2012), which is currently used in the National Oceanic and Atmospheric Administration/National Centers for Environmental Information (NOAA/NCEI) climate division dataset (Vose et al. 2014). For most of 2009–11, prices fluctuated steadily around \$3.00–\$5.00 mmBTU^{-1} (Fig. 6b). They had fallen precipitously since their record high

of $13.58 mmBTU^{-1} on 3 July 2008 as a result of the combination of increased supply from high-volume hydraulic fracturing in the Marcellus Shale and a generally weak macroeconomy. During the 2011/12, natural gas prices fell steadily from $4.85 mmBTU^{-1} on 8 June 2011 to an 11-yr low of $1.91 mmBTU^{-1} on 19 April 2012. This drop of 61% in 10 months included an unusually warm winter that squelched demand (Fig. 6b). Midwest–East temperatures were 3.5°C above the 1981–2010 normal for December–February, culminating in an unprecedented anomaly of +7.0°C during March 2012.

Figure 7a shows the distribution of temperature anomalies relative to their twentieth-century climatology by state for December–February 2011/12. Every state had above-normal temperatures, and 2011/12 was the third warmest December–February nationwide in 119 years of records (Vose et al. 2014). More than 20 states from Montana to Maine had one of their 10 warmest winters on record. The largest temperature anomalies were concentrated in the Midwest and northeastern United States, which explains the large impact of this warmth on natural gas prices.

Figure 8 shows the evolution of some of the key teleconnection indices in recent years. Winter 2011/12 demonstrated the limitations of using ENSO for seasonal forecasting. La Niña during 2011/12 (Figs. 5a and 8a) would have suggested cooler Midwest–East temperatures, but instead those temperatures were exceptionally warm. This disconnect from the expected La Niña impacts suggests that higher-latitude signals may have overwhelmed the ENSO signal. Eurasian snow cover was below normal until November (Fig. 8b), which may have played a role in the positive AO/NAO (Figs. 8c,d) and subsequent warm Midwest–East temperatures that winter. Interestingly, Midwest–East temperatures remained above normal even after the SSW in January 2012 (Fig. 3) and the subsequent switch to negative AO (Fig. 8c).

Figure 9 shows the annual cycle of natural gas storage for the last 20 years. Storage increases during the summer months and then that stored gas is consumed during the winter. Reserves of natural gas were already above normal in June of 2011 (red line). Natural gas production has been

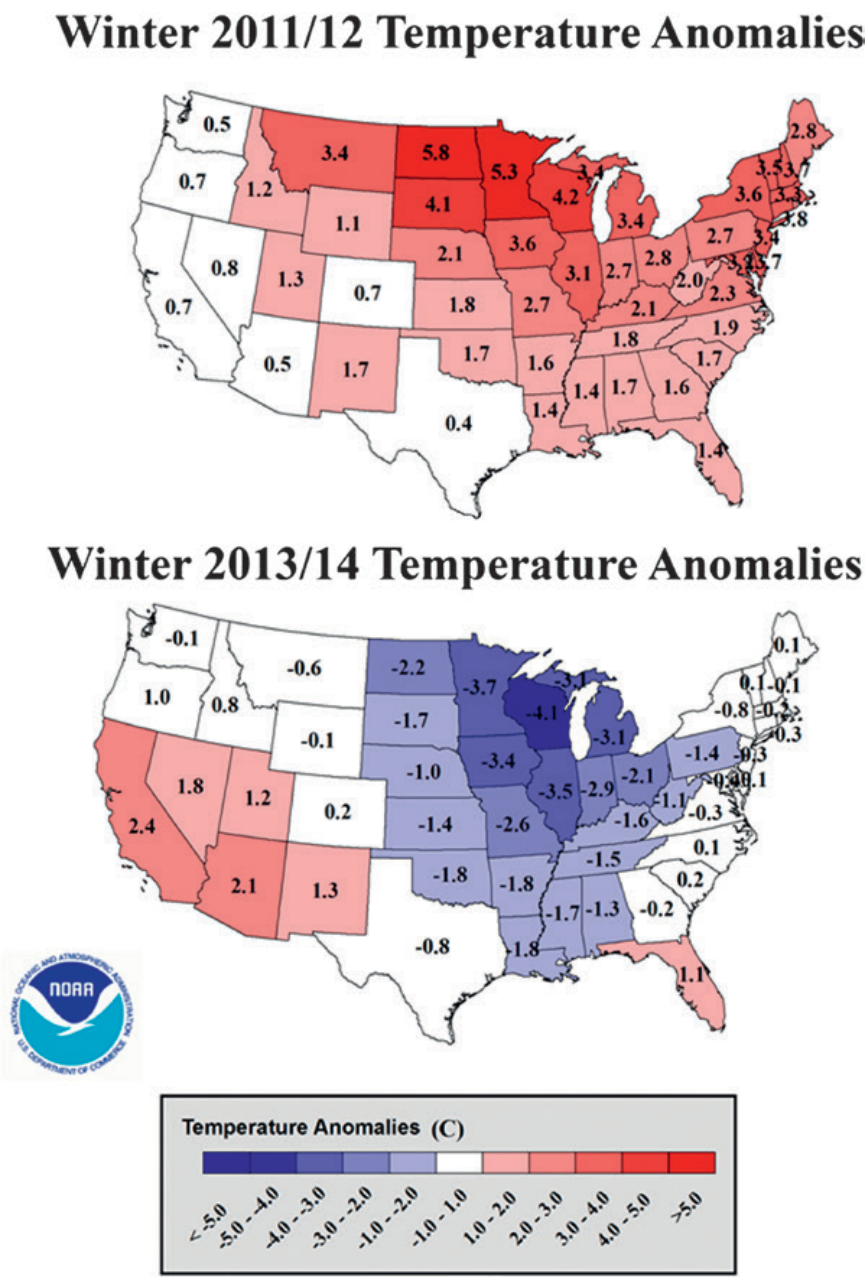

Fig. 7. Statewide Dec–Feb temperature anomalies from their twentieth-century averages for (a) 2011/12 and (b) 2013/14.

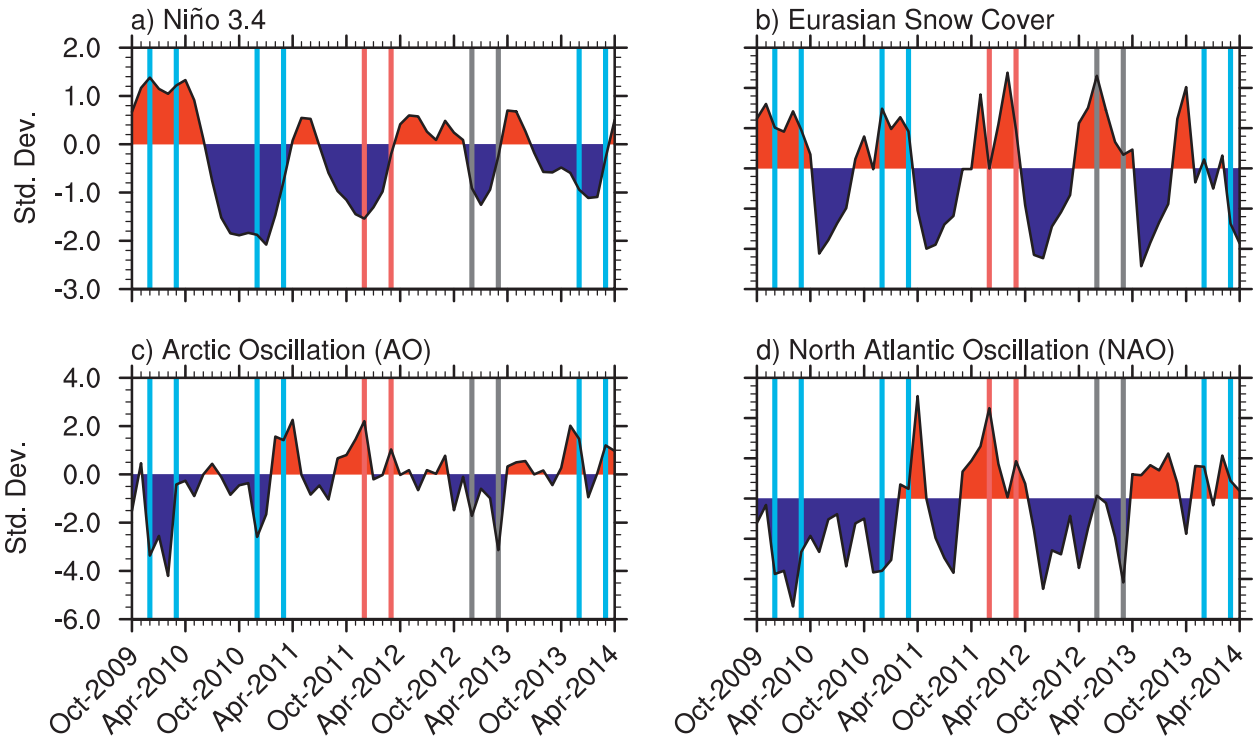

Fig. 8. Monthly standardized anomalies relative to 1981–2010 of the (a) Niño-3.4, (b) Eurasian snow cover, (c) AO, and (d) NAO. Vertical lines are as in Fig. 6.

steadily increasing in recent years with the advent of high-volume hydraulic fracturing in the Marcellus Shale (Turcotte et al. 2014). Producers further increased supply in 2011 to prepare for the possibility of another cold winter with above-normal demand, as in the years 2009/10 and 2010/11. Instead, the extreme warmth suppressed demand in 2011/12. Natural gas storage attained record seasonal levels from December 2011 through April 2012, which pushed prices downward.

Unusual heat and sensitivity in March 2012. March 2012 was exceptional both for its temperatures over the United States and their impacts on the natural gas markets. March is usually a time when energy traders pay less attention to the weather. Temperatures are generally milder during early spring (Arguez et al. 2012), so it is a relative lull in heating and cooling demand. Many power plants use early spring for maintenance, and these maintenance schedules dominate the supply and demand balances. Since humans drive these schedules, traders have less clarity in the market fundamentals and many of them will limit their exposure during this season. However, the warmth in March 2012 was so extreme that even the minimal amount of heating demand typically associated with the month did not materialize. The natural gas markets continued to plunge downward, eventually reaching an 11-yr low of \$1.91 mmBTU^{-1} on 19 April.

The contiguous United States was 4.95°C above its twentieth-century average for March 2012 (3.2 standard deviations above normal). It was the largest positive anomaly for any month since records began in 1895. During the course of the month, over 15,000 warm temperature records were broken at the station level. Numerous stations even had daily minimum (nighttime) temperatures that exceeded the previous daily maximum (daytime) temperature records for the same date. Figure 10 shows the temperature anomalies by state for March 2012. Except for the Pacific coast, every state was above their twentieth-century mean, and 31 states experienced their warmest March on record. The warmth was particularly strong in the Midwest–East region where 10 states were at least 8°C above normal.

A high-amplitude MJO event played a major role in this warmth (Dole et al. 2014). Figure 11a shows the evolution of the RMM index during this event that developed in early February 2012 and continued throughout March (Gottschalck et al. 2013). The first half of March was spent in phases 3–5, which favor warmer Midwest–East temperatures. Schreck et al. (2013) recently showed that the MJO's impacts on North American temperatures depend in part on the preexisting extratropical circulation. To diagnose these effects, they developed the multivariate Pacific–North America (MVP) index (Fig. 11b). When

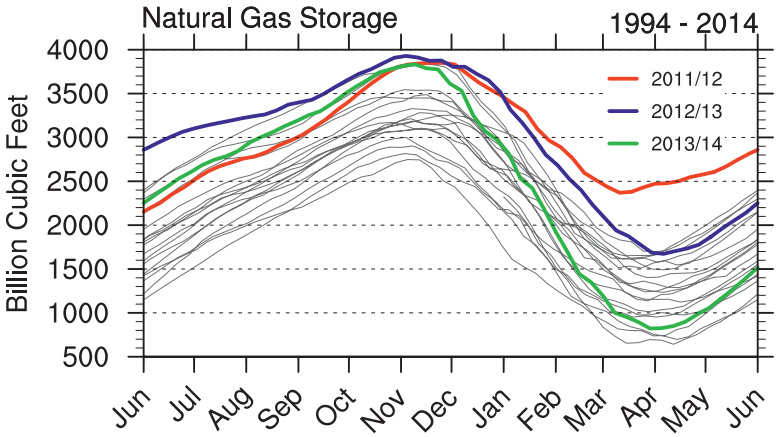

Fig. 9. Seasonal cycle of weekly natural gas in underground storage for each year from 1994/95 to 2013/14.

this index is negative, as it was during most of March 2012, the MJO has an even larger warming effect on Midwest–East temperatures. Figure 11 suggests that both the tropics and extratropics were well positioned to yield the extreme warmth that was observed in March 2012, as discussed in greater detail by Dole et al. (2014).

Cold and depletion in 2013/14. Natural gas prices remained volatile but gradually recovered during 2012 and 2013 as temperatures remained closer to normal and the surplus gas was consumed (Figs. 6 and 9). However, the winter of 2013/14 sent another shock to the markets. Temperatures were 1.6°C below their twentieth-century normal for Midwest–East in December–February. The coldest temperatures were focused on the Midwest (Fig. 7b), with seven states having 1 of their 10 coldest winter seasons. Wisconsin bore the brunt of the cold. The statewide average temperature for December–February 2013/14 was 4.0°C below the twentieth-century average. It was the coldest winter for Wisconsin since 1978/79 and the fifth coldest on record. In addition to the cold temperatures, New York, New York; Philadelphia, Pennsylvania; Chicago; and Boston all had 1 of their 10 snowiest winters on record, with Detroit, Michigan, breaking its December–February snowfall record.

ENSO was neutral in 2013/14 (Fig. 8a), which limited the skill of forecasts going into the season. Eurasian snow cover was above normal in September and October (Fig. 8b), which would favor a negative AO/NAO and cold Midwest–East temperatures. The cold temperatures materialized (Fig. 6a) even though the negative AO/NAO did not (Fig. 8c,d). The widespread cold in 2013/14 drove up natural gas prices and exhausted the surpluses of storage (Figs. 6b and 9). Natural gas storage plummeted from the fifth highest in the 21-yr record in November 2013 to fourth lowest in April 2014 (Fig. 9). Concerns about potential natural gas shortages (Friedman 2014) drove the Henry Hub futures price up 141% from \$3.45 mmBTU^{-1} on 4 November 2013 to \$6.15 mmBTU^{-1} on 19 February 2014, the highest price since before the macroeconomic crash in 2008.

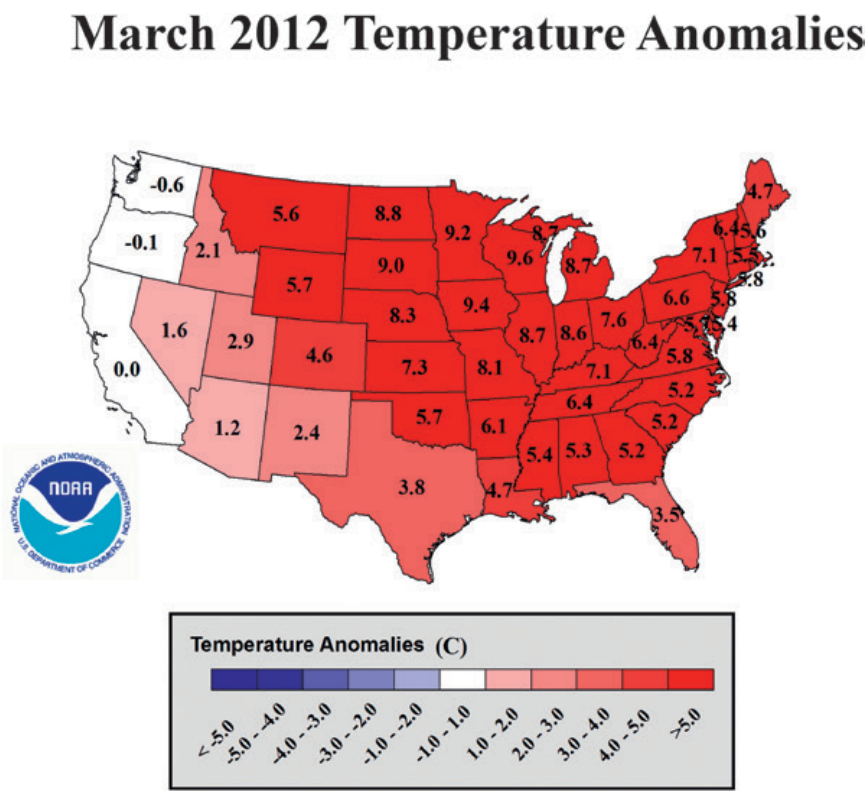

Fig. 10. As in Fig. 7, but for Mar 2012.

Markets and models. One example of the market's reaction to the models happened on Tuesday, 31 December 2013. While the markets were closed over the previous weekend, the ECMWF ensemble trended substantially warmer in its 11–15-day forecasts. Figure 12 shows changes of more than 10°F (5.6°C) for portions of the Midwest–East region compared with the previous forecast. The market remained stable on Monday as the GFS continued to predict a colder solution. However, the 1200 UTC GFS forecast from Tuesday, 31 December, demonstrated a shift toward warmer temperatures (not shown) similar to the one observed in the ECMWF forecasts a few days earlier (Fig. 12). This prompted the larger weather vendors, including Weather Services International (WSI) and EarthSat, to issue warmer outlooks. This consensus on a warmer forecast for week 2 triggered a selloff. Natural gas futures contracts for February (NGG4) declined from an opening of \$4.43 to \$4.23 mmBTU^{-1} at closing, resulting in a 4.4% loss in a single day (Malik 2013). If a trader had foreknowledge that the forecast would continue trending warmer, they could have sold their natural gas holdings ahead of this decline.

The warmer forecast was accurate, with warmer temperatures suppressing demand during an otherwise cold winter in 2013/14. The shift toward warmer forecasts coincided with a sharp increase in wave propagation upward into the stratosphere (not shown). Resolving this upward surge in wave activity may have improved the models' initialization of the stratospheric circulation and enabled them to identify this warmer solution (Charlton et al. 2004; Jung and Barkmeijer 2006; Roff et al. 2011; Gerber et al. 2012).

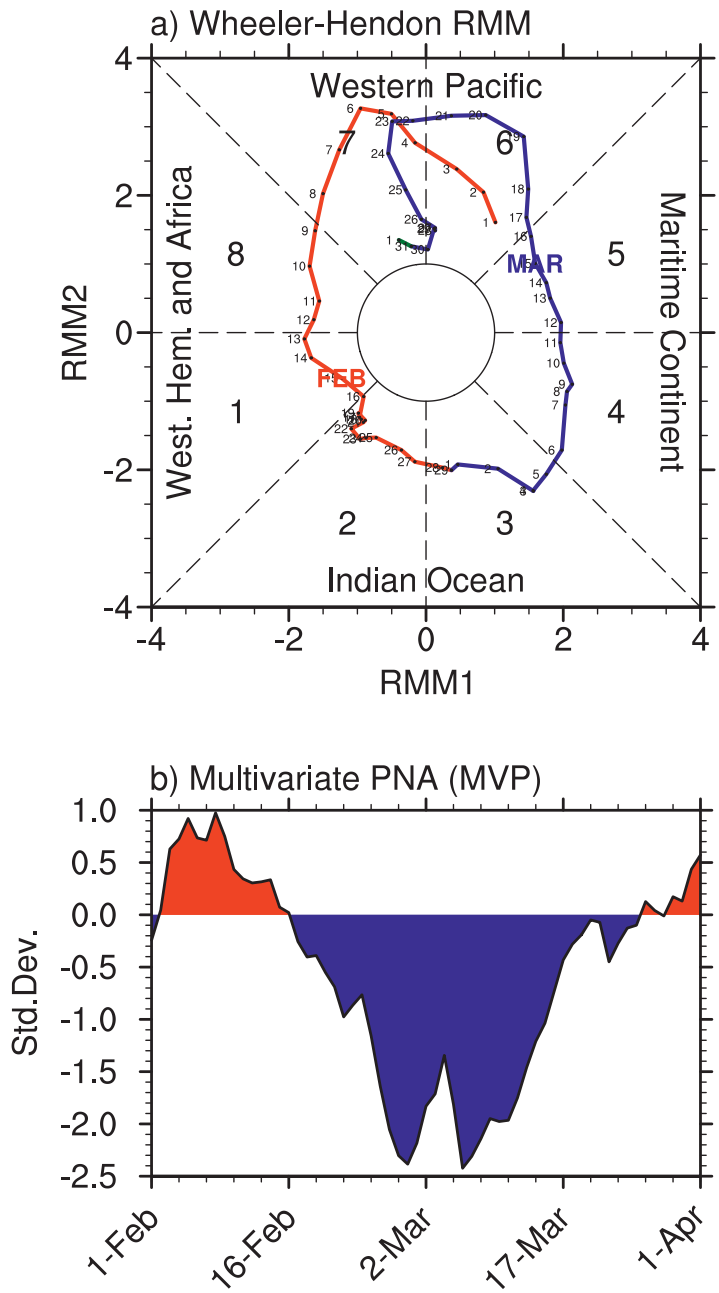

Fig. 11. (a) The Wheeler and Hendon (2004) RMM index and (b) MVP index for Feb–Mar 2012.

SUMMARY. This study used the extreme winters of 2011/12 and 2013/14 to examine the use of weather and climate data in the natural gas markets. While natural gas prices fluctuate with variations in both supply and demand, the events presented here were driven largely by demand related to temperatures over the northeastern quadrant of the United States (Midwest–East; Fig. 1). These linkages were apparent as prices fell during the extremely warm winter of 2011/12 and then rose again during the cold winter of 2013/14.

Energy companies trade monthly futures contracts to hedge their risk against these weather-driven fluctuations, as well as to speculate and increase their overall profitability. Everyone in the market has roughly equal access to guidance from dynamical models, so the market reacts strongly to changes in these forecasts. Traders look to energy meteorologists and weather vendors to provide them with long-range temperature forecasts that can improve upon

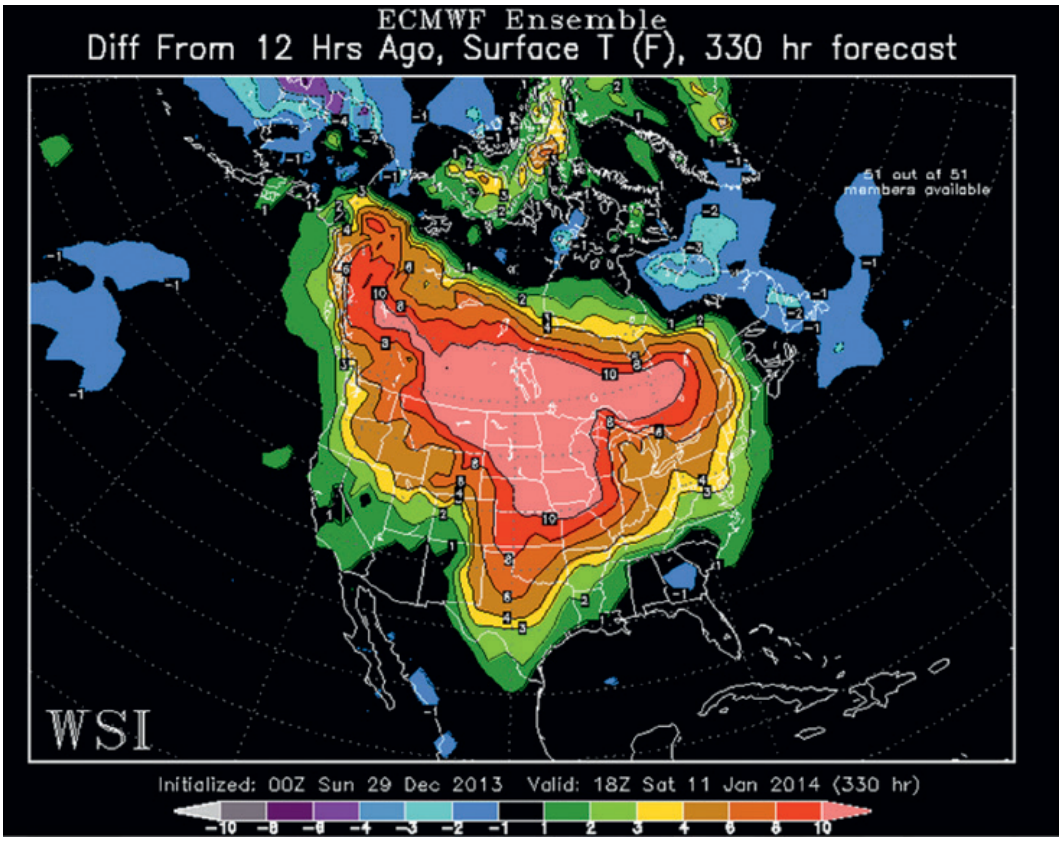

Fig. 12. Difference in forecast surface temperatures valid at 1800 UTC 11 Jan 2014 between ECWMF ensemble runs initialized at 0000 UTC 29 Dec and 1200 UTC 28 Dec 2013.

the models. These forecasts often rely on historical analogs based on teleconnection indices in the tropics and the Arctic. In this study, we examined how the markets and those teleconnections evolved during 2011/12 and 2013/14.

Winter 2011/12 was exceptionally warm (Fig. 7a), which suppressed natural gas demand. Combined with increased natural gas production, the lack of demand led to record surpluses in natural gas storage (Fig. 9) and sharp declines in prices (Fig. 6b). The warmth in 2011/12 was consistent with a classic positive AO pattern (Fig. 2a). That pattern was dominated by zonal flow around the Northern Hemisphere and an elongated Pacific jet that minimized the opportunities for cold-air outbreaks into the United States. The stratospheric vortex broke down in the first week of January 2012 (Fig. 3a), linked to a weakening of the positive AO (Fig. 8c). The warmth in the Midwest–East continued and even intensified in association with intraseasonal and synoptic-scale features, including an unusually strong MJO (Fig. 11) (Dole et al. 2014). As a result, March 2012 was the most anomalously warm month on record for the United States since 1895. Natural gas prices are usually more stable during March, but this extreme anomaly drove prices down to an 11-yr low.

Winter 2013/14 presented a sharp contrast to 2011/12, as Midwest–East temperatures were anomalously cold (Fig. 7b). The resulting demand consumed the remaining surplus of natural gas inventory (Fig. 9) and drove prices upward (Fig. 6b). The cold in 2013/14 emanated from a Northern Hemisphere pattern dominated by anomalous ridging over the Gulf of Alaska (Fig. 2b). The ridge extended all the way to the pole and transported cold air from Siberia to North America. This ridge and the downstream trough over North America were both vertically deep features that were linked with a wavenumber-2 pattern in the stratospheric polar vortex (Figs. 2b and 4c,d). The resulting cold temperatures quickly led natural gas prices upward to their highest levels in 6 yr (Figs. 6b and 9).

The fluctuations in natural gas prices during the extreme winters of 2011/12 and 2013/14 underscore the susceptibility of our economy to ever-changing weather patterns. Continuing improvements to long-range forecasts will increase the efficiency of our energy markets. Ongoing advancements in numerical

weather prediction are an obvious avenue for such improvements. Another would be developing new analog methods to harness the increasing number of long-term homogenized satellite climate data records (National Research Council 2004). Both pathways would enable energy companies to plan and adapt more quickly to future extremes.

ACKNOWLEDGMENTS. This study was inspired by the Executive Forum on Business and Climate supported by the Cooperative Institute for Climate and Satellites—North Carolina (CICS—NC) and NOAA's National Centers for Environmental Information in June 2013. The manuscript benefited significantly from the comments of two anonymous reviewers. Schreck received support for this research from NOAA's Climate Data Record (CDR) program through CICS–NC under Cooperative Agreement NA14NES432003. Natural gas prices and storage data were provided by the Energy Information Administration. Niño-3.4, AO, and NAO are calculated by NOAA/CPC and obtained from NOAA/ESRL/PSD. Eurasian snow cover was obtained from the Rutgers Snow Lab.

REFERENCES

Ambaum, M. H. P., B. J. Hoskins, and D. B. Stephenson, 2001: Arctic Oscillation or North Atlantic Oscillation? *J. Climate,* **14,** 3495–3507, doi:10.1175/1520-0442(2001)014<3495:AOONAO>2.0.CO;2.

Arguez, A., I. Durre, S. Applequist, R. S. Vose, M. F. Squires, X. Yin, R. R. Heim, and T. W. Owen, 2012: NOAA's 1981–2010 U.S. climate normals: An overview. *Bull. Amer. Meteor. Soc.,* **93,** 1687–1697, doi:10.1175/BAMS-D-11-00197.1.

Baldwin, M. P., and T. J. Dunkerton, 1999: Propagation of the Arctic Oscillation from the stratosphere to the troposphere. *J. Geophys. Res.,* **104,** 30 937–30 946, doi:10.1029/1999JD900445.

——, and ——, 2001: Stratospheric harbingers of anomalous weather regimes. *Science,* **294,** 581–584, doi:10.1126/science.1063315.

——, D. B. Stephenson, D. W. J. Thompson, T. J. Dunkerton, A. J. Charlton, and A. O'Neill, 2003: Stratospheric memory and skill of extended-range weather forecasts. *Science,* **301,** 636–640, doi:10.1126/science.1087143.

Banzon, V. F., and R. W. Reynolds, 2013: Use of WindSat to extend a microwave-based daily optimum interpolation sea surface temperature time series. *J. Climate,* **26,** 2557–2562, doi:10.1175/JCLI-D-12-00628.1.

Barnston, A. G., and R. E. Livezey, 1987: Classification, seasonality and persistence of low-frequency atmospheric circulation patterns. *Mon. Wea. Rev.,* **115,** 1083–1126, doi:10.1175/1520-0493(1987)115<1083:CSAPOL>2.0.CO;2.

Becker, E. J., E. H. Berbery, and R. W. Higgins, 2011: Modulation of cold-season U.S. daily precipitation by the Madden–Julian oscillation. *J. Climate,* **24,** 5157–5166, doi:10.1175/2011JCLI4018.1.

Black, R. X., 2002: Stratospheric forcing of surface climate in the Arctic Oscillation. *J. Climate,* **15,** 268–277, doi:10.1175/1520-0442(2002)015<0268:SFOSCI>2.0.CO;2.

Brown, S. P. A., and M. K. Yücel, 2008: What drives natural gas prices? *Energy J.,* **29,** 45–60.

Cayan, D. R., 1992: Latent and sensible heat flux anomalies over the northern oceans: Driving the sea surface temperature. *J. Phys. Oceanogr.,* **22,** 859–881, doi:10.1175/1520-0485(1992)022<0859:LASHFA>2.0.CO;2.

Charlton, A. J., A. O'neill, W. A. Lahoz, and A. C. Massacand, 2004: Sensitivity of tropospheric forecasts to stratospheric initial conditions. *Quart. J. Roy. Meteor. Soc.,* **130,** 1771–1792, doi:10.1256/qj.03.167.

Chiodi, A. M., and D. E. Harrison, 2013: El Niño impacts on seasonal U.S. atmospheric circulation, temperature, and precipitation anomalies: The OLR-event perspective. *J. Climate,* **26,** 822–837, doi:10.1175/JCLI-D-12-00097.1.

Cohen, J., and D. Entekhabi, 1999: Eurasian snow cover variability and Northern Hemisphere climate predictability. *Geophys. Res. Lett.,* **26,** 345–348, doi:10.1029/1998GL900321.

——, and J. Jones, 2011: A new index for more accurate winter predictions. *Geophys. Res. Lett.,* **38,** L21701, doi:10.1029/2011GL049626.

——, J. Foster, M. Barlow, K. Saito, and J. Jones, 2010: Winter 2009–2010: A case study of an extreme Arctic Oscillation event. *Geophys. Res. Lett.,* **37,** L17707, doi:10.1029/2010GL044256.

Davis, R. E., 1976: Predictability of sea surface temperature and sea level pressure anomalies over the North Pacific Ocean. *J. Phys. Oceanogr.,* **6,** 249–266, doi:10.1175/1520-0485(1976)006<0249:POSSTA>2.0.CO;2.

Dole, R., and Coauthors, 2014: The making of an extreme event: Putting the pieces together. *Bull. Amer. Meteor. Soc.,* **95,** 427–440, doi:10.1175/BAMS-D-12-00069.1.

Frankignoul, C., and N. Sennéchael, 2007: Observed influence of North Pacific SST anomalies on the atmospheric circulation. *J. Climate,* **20,** 592–606, doi:10.1175/JCLI4021.1.

Friedman, N., 2014: Natural gas soars as stockpiles drop. *Wall Street Journal,* 13 February, accessed 30 May 2014. [Available online at http://online.wsj.com

/news/articles/SB10001424052702304888404579380732212718914.]

Gerber, E. P., and Coauthors, 2012: Assessing and understanding the impact of stratospheric dynamics and variability on the Earth system. *Bull. Amer. Meteor. Soc.,* **93,** 845–859, doi:10.1175/BAMS-D-11-00145.1.

Gottschalck, J., and Coauthors, 2010: A framework for assessing operational Madden–Julian oscillation forecasts: A CLIVAR MJO Working Group project. *Bull. Amer. Meteor. Soc.,* **91,** 1247–1258, doi:10.1175/2010BAMS2816.1.

——, P. E. Roundy, C. J. Schreck III, A. Vintzileos, and C. Zhang, 2013: Large-scale atmospheric and oceanic conditions during the 2011–12 DYNAMO field campaign. *Mon. Wea. Rev.,* **141,** 4173–4196, doi:10.1175/MWR-D-13-00022.1.

Hagedorn, R., T. M. Hamill, and J. S. Whitaker, 2008: Probabilistic forecast calibration using ECMWF and GFS ensemble reforecasts. Part I: Two-meter temperatures. *Mon. Wea. Rev.,* **136,** 2608–2619, doi:10.1175/2007MWR2410.1.

Harrison, D. E., and N. K. Larkin, 1998: Seasonal U.S. temperature and precipitation anomalies associated with El Niño: Historical results and comparison with 1997-98. *Geophys. Res. Lett.,* **25,** 3959–3962, doi:10.1029/1998GL900061.

Higgins, R. W., A. Leetmaa, Y. Xue, and A. Barnston, 2000: Dominant factors influencing the seasonal predictability of U.S. precipitation and surface air temperature. *J. Climate,* **13,** 3994–4017, doi:10.1175/1520-0442(2000)013<3994:DFITSP>2.0.CO;2.

——, ——, and V. E. Kousky, 2002: Relationships between climate variability and winter temperature extremes in the United States. *J. Climate,* **15,** 1555–1572, doi:10.1175/1520-0442(2002)015<1555:RBCVAW>2.0.CO;2.

Hurrell, J. W., Y. Kushnir, G. Ottersen, and M. Visbeck, 2003: An overview of the North Atlantic oscillation. *The North Atlantic Oscillation: Climatic Significance and Environmental Impact*, J. W. Hurrell et al., Amer. Geophys. Union, 1–35.

Joëts, M., and V. Mignon, 2012: On the link between forward energy prices: A nonlinear panel cointegration approach. *Energy Econ.,* **34,** 1170–1175, doi:10.1016/j.eneco.2011.10.019.

Johnson, N. C., and S. B. Feldstein, 2010: The continuum of North Pacific sea level pressure patterns: Intraseasonal, interannual, and interdecadal variability. *J. Climate,* **23,** 851–867, doi:10.1175/2009JCLI3099.1.

Jung, T., and J. Barkmeijer, 2006: Sensitivity of the tropospheric circulation to changes in the strength of the stratospheric polar vortex. *Mon. Wea. Rev.,* **134,** 2191–2207, doi:10.1175/MWR3178.1.

Kanamitsu, M., W. Ebisuzaki, J. Woollen, S.-K. Yang, J. J. Hnilo, M. Fiorino, and G. L. Potter, 2002: NCEP–DOE AMIP-II Reanalysis (R-2). *Bull. Amer. Meteor. Soc.,* **83,** 1631–1643, doi:10.1175/BAMS-83-11-1631.

Kiladis, G. N., and K. M. Weickmann, 1992: Circulation anomalies associated with tropical convection during northern winter. *Mon. Wea. Rev.,* **120,** 1900–1923, doi:10.1175/1520-0493(1992)120<1900:CAAWTC>2.0.CO;2.

Labitzke, K., 1972: Temperature changes in the mesosphere and stratosphere connected with circulation changes in winter. *J. Atmos. Sci.,* **29,** 756–766, doi:10.1175/1520-0469(1972)029<0756:TCITMA>2.0.CO;2.

Larkin, N. K., and D. E. Harrison, 2005: On the definition of El Niño and associated seasonal average U.S. weather anomalies. *Geophys. Res. Lett.,* **32,** L13705, doi:10.1029/2005GL022738.

Lee, H.-T., 2014: Climate Algorithm Theoretical Basis Document (C-ATBD): Outgoing longwave radiation (OLR) - Daily. Climate Data Record Program Rep. CDRP-ATBD-0526, NOAA/NCDC, 46 pp. [Available online at http://www1.ncdc.noaa.gov/pub/data/sds/cdr/CDRs/Outgoing%20Longwave%20Radiation%20-%20Daily/AlgorithmDescription.pdf.]

——, A. Gruber, R. G. Ellingson, and I. Laszlo, 2007: Development of the HIRS outgoing longwave radiation climate dataset. *J. Atmos. Oceanic Technol.,* **24,** 2029–2047, doi:10.1175/2007JTECHA989.1.

Liebmann, B., and C. A. Smith, 1996: Description of a complete (interpolated) outgoing longwave radiation dataset. *Bull. Amer. Meteor. Soc.,* **77,** 1275–1277.

Linn, S. C., and Z. Zhu, 2004: Natural gas prices and the gas storage report: Public news and volatility in energy futures markets. *J. Futures Mark.,* **24,** 283–313, doi:10.1002/fut.10115.

Liu, Q., N. Wen, and Z. Liu, 2006: An observational study of the impact of the North Pacific SST on the atmosphere. *Geophys. Res. Lett.,* **33,** L18611, doi:10.1029/2006GL026082.

Malik, N. S., 2013: Natural gas trims biggest annual gain since 2005 as cold eases. Bloomberg.com, accessed 30 May 2014. [Available online at www.bloomberg.com/news/2013-12-31/natural-gas-rises-heads-for-biggest-annual-increase-since-2005.html.]

Matthews, A. J., B. J. Hoskins, and M. Masutani, 2004: The global response to tropical heating in the Madden–Julian oscillation during the northern winter. *Quart. J. Roy. Meteor. Soc.,* **130,** 1991–2011, doi:10.1256/qj.02.123.

Menne, M. J., I. Durre, R. S. Vose, B. E. Gleason, and T. G. Houston, 2012: An overview of the Global Historical Climatology Network-Daily database. *J. Atmos. Oceanic Technol.,* **29,** 897–910, doi:10.1175/JTECH-D-11-00103.1.

Mjelde, J. W., and D. A. Bessler, 2009: Market integration among electricity markets and their major fuel source markets. *Energy Econ.,* **31,** 482–491, doi:10.1016/j.eneco.2009.02.002.

Mu, X., 2007: Weather, storage, and natural gas price dynamics: Fundamentals and volatility. *Energy Econ.,* **29,** 46–63, doi:10.1016/j.eneco.2006.04.003.

National Research Council, 2004: *Climate Data Records from Environmental Satellites: Interim Report.* National Academies Press, 150 pp.

Newman, P. A., and J. E. Rosenfield, 1997: Stratospheric thermal damping times. *Geophys. Res. Lett.,* **24,** 433–436, doi:10.1029/96GL03720.

Novak, D. R., C. Bailey, K. F. Brill, P. Burke, W. A. Hogsett, R. Rausch, and M. Schichtel, 2014: Precipitation and temperature forecast performance at the Weather Prediction Center. *Wea. Forecasting,* **29,** 489–504, doi:10.1175/WAF-D-13-00066.1.

Peng, S., and J. S. Whitaker, 1999: Mechanisms determining the atmospheric response to midlatitude SST anomalies. *J. Climate,* **12,** 1393–1408, doi:10.1175/1520-0442(1999)012<1393:MDTART>2.0.CO;2.

Pettersson, F., P. Söderholm, and R. Lundmark, 2012: Fuel switching and climate and energy policies in the European power generation sector: A generalized Leontief model. *Energy Econ.,* **34,** 1064–1073, doi:10.1016/j.eneco.2011.09.001.

Philips, M., 2014: Northeast's record natural gas prices due to pipeline dearth. *BusinessWeek,* 6 February, accessed 6 November 2014. [Available online at www.businessweek.com/articles/2014-02-06/northeasts-record-natural-gas-prices-due-to-pipeline-dearth.]

Reynolds, R. W., 2009: What's new in version 2. NOAA/NCDC Tech. Note, 10 pp. [Available online at www.ncdc.noaa.gov/sites/default/files/attachments/Reynolds2009_oisst_daily_v02r00_version2-features.pdf.]

——, T. M. Smith, C. Liu, D. B. Chelton, K. S. Casey, and M. G. Schlax, 2007: Daily high-resolution-blended analyses for sea surface temperature. *J. Climate,* **20,** 5473–5496, doi:10.1175/2007JCLI1824.1.

Riddle, E. E., M. B. Stoner, N. C. Johnson, M. L. L'Heureux, D. C. Collins, and S. B. Feldstein, 2013: The impact of the MJO on clusters of wintertime circulation anomalies over the North American region. *Climate Dyn.,* **40,** 1749–1766, doi:10.1007/s00382-012-1493-y.

Rienecker, M. M., and Coauthors, 2011: MERRA: NASA's Modern-Era Retrospective Analysis for Research and Applications. *J. Climate,* **24,** 3624–3648, doi:10.1175/JCLI-D-11-00015.1.

Robinson, D. A., K. F. Dewey, and R. R. Heim, 1993: Global snow cover monitoring: An update. *Bull. Amer. Meteor. Soc.,* **74,** 1689–1696, doi:10.1175/1520-0477(1993)074<1689:GSCMAU>2.0.CO;2.

Roebber, P. J., and L. F. Bosart, 1996: The contributions of education and experience to forecast skill. *Wea. Forecasting,* **11,** 21–40, doi:10.1175/1520-0434(1996)011<0021:TCOEAE>2.0.CO;2.

Roff, G., D. W. J. Thompson, and H. Hendon, 2011: Does increasing model stratospheric resolution improve extended-range forecast skill? *Geophys. Res. Lett.,* **38,** L05809, doi:10.1029/2010GL046515.

Ropelewski, C. F., and M. S. Halpert, 1986: North American precipitation and temperature patterns associated with the El Niño/Southern Oscillation (ENSO). *Mon. Wea. Rev.,* **114,** 2352–2362, doi:10.1175/1520-0493(1986)114<2352:NAPATP>2.0.CO;2.

Roundy, P. E., C. J. Schreck, and M. A. Janiga, 2009: Contributions of convectively coupled equatorial Rossby waves and Kelvin waves to the real-time multivariate MJO indices. *Mon. Wea. Rev.,* **137,** 469–478, doi:10.1175/2008MWR2595.1.

Saha, S., and Coauthors, 2006: The NCEP Climate Forecast System. *J. Climate,* **19,** 3483–3517, doi:10.1175/JCLI3812.1.

——, and Coauthors, 2014: The NCEP Climate Forecast System version 2. *J. Climate,* **27,** 2185–2208, doi:10.1175/JCLI-D-12-00823.1.

Schreck, C. J., J. M. Cordeira, and D. Margolin, 2013: Which MJO events affect North American temperatures? *Mon. Wea. Rev.,* **141,** 3840–3850, doi:10.1175/MWR-D-13-00118.1.

Smith, K. L., P. J. Kushner, and J. Cohen, 2011: The role of linear interference in northern annular mode variability associated with Eurasian snow cover extent. *J. Climate,* **24,** 6185–6202, doi:10.1175/JCLI-D-11-00055.1.

Thompson, D. W. J., and J. M. Wallace, 1998: The Arctic oscillation signature in the wintertime geopotential height and temperature fields. *Geophys. Res. Lett.,* **25,** 1297–1300, doi:10.1029/98GL00950.

——, and ——, 2001: Regional climate impacts of the Northern Hemisphere annular mode. *Science,* **293,** 85–89, doi:10.1126/science.1058958.

——, M. P. Baldwin, and J. M. Wallace, 2002: Stratospheric connection to Northern Hemisphere wintertime weather: Implications for prediction. *J. Climate,* **15,**

1421–1428, doi:10.1175/1520-0442(2002)015<1421:SCTNHW>2.0.CO;2.

Trenberth, K. E., 1997: The definition of El Niño. *Bull. Amer. Meteor. Soc.,* **78,** 2771–2777, doi:10.1175/1520-0477(1997)078<2771:TDOENO>2.0.CO;2.

Tripathi, O. P., and Coauthors, 2014: The predictability of the extratropical stratosphere on monthly timescales and its impact on the skill of tropospheric forecasts. *Quart. J. Roy. Meteor. Soc.,* **141,** 987–1003 doi:10.1002/qj.2432.

Turcotte, D. L., E. M. Moores, and J. B. Rundle, 2014: Super fracking. *Phys. Today,* **67,** 34–39, doi:10.1063/PT.3.2480.

U.S. Energy Information Administration, 2012: Annual energy review 2011. DOE/EIA-0384(2011), 370 pp. [Available online at www.eia.gov/totalenergy/data/annual/pdf/aer.pdf.]

Van Oldenborgh, G. J., M. A. Balmaseda, L. Ferranti, T. N. Stockdale, and D. L. T. Anderson, 2003: Did the ECMWF seasonal forecast model outperform statistical ENSO forecast models over the last 15 years? *J. Climate,* **18,** 3240–3249, doi:10.1175/JCLI3420.1.

Vose, R. S., and Coauthors, 2014: Improved historical temperature and precipitation time series for U.S. climate divisions. *J. Appl. Meteor. Climatol.,* **53,** 1232–1251, doi:10.1175/JAMC-D-13-0248.1.

Weaver, S. J., W. Wang, M. Chen, and A. Kumar, 2011: Representation of MJO variability in the NCEP Climate Forecast System. *J. Climate,* **24,** 4676–4694, doi:10.1175/2011JCLI4188.1.

Weng, H., S. K. Behera, and T. Yamagata, 2009: Anomalous winter climate conditions in the Pacific Rim during recent El Niño Modoki and El Niño events. *Climate Dyn.,* **32,** 663–674, doi:10.1007/s00382-008-0394-6.

Wheeler, M., and K. M. Weickmann, 2001: Real-time monitoring and prediction of modes of coherent synoptic to intraseasonal tropical variability. *Mon. Wea. Rev.,* **129,** 2677–2694, doi:10.1175/1520-0493(2001)129<2677:RTMAPO>2.0.CO;2.

——, and H. H. Hendon, 2004: An all-season real-time multivariate MJO index: Development of an index for monitoring and prediction. *Mon. Wea. Rev.,* **132,** 1917–1932, doi:10.1175/1520-0493(2004)132<1917:AARMMI>2.0.CO;2.

Zhang, C., 2005: Madden-Julian oscillation. *Rev. Geophys.,* **43,** RG2003, doi:10.1029/2004RG000158.

——, 2013: Madden–Julian oscillation: Bridging weather and climate. *Bull. Amer. Meteor. Soc.,* **94,** 1849–1870, doi:10.1175/BAMS-D-12-00026.1.

Zhou, S., M. L'Heureux, S. Weaver, and A. Kumar, 2012: A composite study of the MJO influence on the surface air temperature and precipitation over the continental United States. *Climate Dyn.,* **38,** 1459–1471, doi:10.1007/s00382-011-1001-9.

SEASONAL FORECASTING OF GLOBAL HYDROLOGIC EXTREMES

System Development and Evaluation over GEWEX Basins

BY XING YUAN, JOSHUA K. ROUNDY, ERIC F. WOOD, AND JUSTIN SHEFFIELD

A multimodel global hydrologic forecasting system that provides hydroclimate prediction services is evaluated to understand the predictability of seasonal hydrologic extremes over global major river basins.

Persistent hydrologic extreme events such as droughts and wet spells (rainfall anomalies with long durations) have devastating impacts on the human and natural systems and have caused total economic losses of about hundreds of billions of dollars in the United States (Smith and Katz 2013) and around the world (Below et al. 2007). Their occurrences are associated with anomalous atmospheric moisture transport that may be linked to variations of large-scale climate phenomena—for example, El Niño–Southern Oscillation (ENSO), Pacific decadal oscillation (PDO), and Atlantic multidecadal oscillation (AMO)—through ocean–atmosphere teleconnections (Cayan et al. 1999; Hoerling and Kumar 2003; McCabe et al. 2004). Their severities and durations are also influenced by land–atmosphere coupling that can enhance existing extremes (Hong and Kalnay 2000; Schubert et al. 2004). They may be further exacerbated by anthropogenic climate change (Diffenbaugh et al. 2013) and human water consumption (Barnett et al. 2008; Wada et al. 2013).

According to the latest Intergovernmental Panel on Climate Change (IPCC) report, agricultural and hydrological droughts are projected to increase in intensity and duration in presently dry regions by the end of this century under a business-as-usual scenario [representative concentration pathway (RCP) 8.5 scenario], while heavy rainfall events are very likely to increase over most of the midlatitude landmasses and wet tropical regions (IPCC 2013). Such changes impose an increasing risk of hydrologic extremes in the future. Improving understanding of the processes that lead to extremes and establishing operational predictive capabilities that can provide skillful and reliable forecasting of the frequency and intensity of extreme events on regional to global scales are therefore science imperatives of the World

AFFILIATIONS: YUAN—Department of Civil and Environmental Engineering, Princeton University, Princeton, New Jersey, and RCE-TEA, Institute of Atmospheric Physics, Chinese Academy of Sciences, Beijing, China; ROUNDY, WOOD, AND SHEFFIELD—Department of Civil and Environmental Engineering, Princeton University, Princeton, New Jersey
CORRESPONDING AUTHOR: Xing Yuan, RCE-TEA, Institute of Atmospheric Physics, Chinese Academy of Sciences, Huayanli No. 40, Qijiahuozi, Chaoyang District, Beijing 100029, China
E-mail: yuanxing@tea.ac.cn

The abstract for this article can be found in this issue, following the table of contents.
DOI:10.1175/BAMS-D-14-00003.1

A supplement to this article is available online (DOI:10.1175/BAMS-D-14-00003.2)

In final form 4 December 2014

Climate Research Programme (WCRP) and are being considered as WCRP grand challenges (Karoly 2012; Giorgi et al. 2012).

As a core project of the WCRP, the Global Energy and Water Cycle Experiment (GEWEX; Morel 2001; www.gewex.org) is responsible for facilitating research on quantifying, understanding, and predicting global and regional energy and water variations and extremes through improved observations and modeling of the land, atmosphere, and their interactions, thereby providing the scientific underpinnings of climate services. One of three major research foci of GEWEX is to demonstrate skill in predicting changes in water resources on time scales up to seasonal and annual as an integral part of the climate system [in particular at the regional scale through Regional Hydroclimate Projects (RHP); Coughlan and Avissar 1996; Raschke et al. 1998; Stewart et al. 1998; GEWEX 2012]. Therefore, predicting hydrologic extremes at seasonal scales and investigating their predictability over global major river basins in an integrated hydroclimate forecasting system will help address the WCRP grand challenges and GEWEX RHP research focus.

Seasonal predictability originates primarily from tropical oceans via sea surface temperature (SST) anomalies. The SST anomaly over the tropical Pacific Ocean (i.e., ENSO) has global impacts (Shukla 1998; Goddard et al. 2001), the SST anomaly over the tropical Atlantic Ocean plays a role on the hydroclimate of the Sahel region (Camberlin et al. 2001), and the Indian Ocean dipole (Saji et al. 1999) can contribute to the predictability over Australia, Africa, and southern Asia, somewhat independently from ENSO (Zhao and Hendon 2009; Doblas-Reyes et al. 2013). Other sources of seasonal predictability could come from stratospheric condition (Ineson and Scaife 2009), soil moisture anomaly (Koster et al. 2011), and snow cover (Douville 2010), although these impacts are regional as compared with ENSO. With gradual improvements in observational data assimilation, computing resources that facilitate high-resolution numerical simulations, and the understanding of atmosphere–ocean–land physical processes that account for major seasonal predictability (e.g., ENSO), coupled atmosphere–ocean–land general circulation models (CGCMs) are now widely used for seasonal climate predictions (Weisheimer et al. 2009; Barnston et al. 2012; Kirtman et al. 2014). They have also shown improvement in predictive skill over the past decade, especially for large-scale climate features such as ENSO (Barnston et al. 2012) and the North Atlantic Oscillation (NAO; Scaife et al. 2014).

However, owing to deficiencies in land surface hydrologic parameterizations and/or land surface initializations of CGCMs, the hydrologic forecast products (e.g., soil moisture, runoff) from global seasonal prediction models cannot be directly used for applications. A typical solution is to bias correct the meteorological forecasts from the CGCMs and then drive advanced hydrologic models with refined initial land surface hydrologic conditions to produce seasonal hydrologic forecasts and extreme predictions (Wood et al. 2002; Luo and Wood 2007, 2008; Li et al. 2009; Mo et al. 2012; Yuan and Wood 2012a; Sinha and Sankarasubramanian 2013; Yuan et al. 2013a,b; Mo and Lettenmaier 2014b; Shukla et al. 2014). We refer to this as the CGCM-Hydrology forecasting approach.

Nevertheless, to our knowledge, most CGCM-Hydrology seasonal forecasting studies focus on the soil moisture and/or streamflow prediction over a single basin or continent, usually with a single CGCM (Luo and Wood 2008; Mo et al. 2012; Yuan et al. 2013b; Shukla et al. 2014), while a comprehensive investigation of predictability of global hydrologic extremes in a multi-CGCM framework has not been examined. The multi-CGCM framework not only provides a more reliable assessment of hydrologic predictability but also offers an opportunity to help quantify the uncertainty. Another limitation of previous studies is that most of them assess the forecast skill for extreme indices that blend extreme conditions with normal conditions (Quan et al. 2012; Yoon et al. 2012; Sohn et al. 2013) while ignoring the analysis of hydrologic predictability specifically for individual hydrologic extreme events—for example, the predictive skill for drought onset (Yuan and Wood 2013). Last, theoretical estimates of global hydrologic predictability indicate that initial hydrological conditions provide much of the potential hydrological predictability (Shukla et al. 2013; van Dijk et al. 2013; Yossef et al. 2013), depending on the location and season, but this has yet to be evaluated in terms of actual predictability within the CGCM-Hydrology framework.

This article presents the development and validation of a global seasonal hydrologic forecasting system that is based on multiple CGCMs participating in the North American Multimodel Ensemble (NMME) project (Kirtman et al. 2014) and the Variable Infiltration Capacity (VIC; Liang et al. 1996) land surface hydrologic model. An analysis of droughts and wet spells is carried out over global major river basins, and the CGCM-Hydrology approach is evaluated against the traditional ensemble streamflow prediction (ESP; Twedt et al. 1977) approach, which resamples from the historic record to provide an ensemble of

meteorological forcings and relies on the persistence in initial land conditions to provide forecast skill. The association of the extreme event onset with antecedent oceanic and land conditions is discussed, based on the joint distribution of the forecast and observation.

THE POTENTIAL OF USING NMME FOR HYDROLOGIC APPLICATIONS OVER THE GEWEX HYDROCLIMATE PROJECT BASINS. During the past four years, the Climate Forecast System, version 2 (CFSv2; Saha et al. 2014), developed by the National Oceanic and Atmospheric Administration (NOAA)'s National Centers for Environmental Prediction (NCEP) has been widely used for hydrologic applications (Yuan et al. 2011; Mo et al. 2012; Quan et al. 2012; Yoon et al. 2012; Yuan and Wood 2012a; Dirmeyer 2013; Yuan et al. 2013b,a; Kumar et al. 2013; Lang et al. 2014; Sheffield et al. 2014; Shukla et al. 2014; Tian et al. 2014). Within the NMME, CFSv2 has been shown to be the most reliable model for seasonal forecasting of global drought onset (Yuan and Wood 2013). But in terms of global gridded analyses, several studies find that combining CFSv2 with other climate forecast models can increase the predictive skill of precipitation (Yuan et al. 2011; Yuan and Wood 2012b; Becker et al. 2014; Kirtman et al. 2014), including extremes (Yuan and Wood 2013).

Here, we target our analysis on major global river basins that are the focus of the GEWEX RHP. Figure 1 shows the continuous ranked probability skill score (CRPSS; Wilks 2011; see appendix for details) for the seasonal mean, basin average precipitation, predicted by CFSv2 and NMME, using all hindcasts started at the beginning of each calendar month during 1982–2009. CFSv2 has 24 ensemble members, while NMME has 71 ensemble members, in total, from six climate models that are producing real-time seasonal climate forecasts. The six models are the National Center for Atmospheric Research (NCAR) Community Climate System Model, version 3 (CCSM3); Geophysical Fluid Dynamics Laboratory Climate Model, version 2.2 (GFDL CM2.2); National Aeronautics and Space Administration (NASA) Goddard Earth Observing System Model, version 5 (GEOS-5); NCEP CFSv2; Canadian Meteorological Centre (CMC) Third Generation Canadian Coupled Global Climate Model (CanCM3); and CMC CanCM4 [see Kirtman et al. (2014) for ensemble information and full references]. Figure 1 shows that NMME has higher probabilistic predictive skill than CFSv2 over 70% of the river basins selected in this study and has comparable skill to CFSv2 for the remaining basins. In particular, obvious improvement can be found over the Amazon and Parana basins in South America, the Colorado

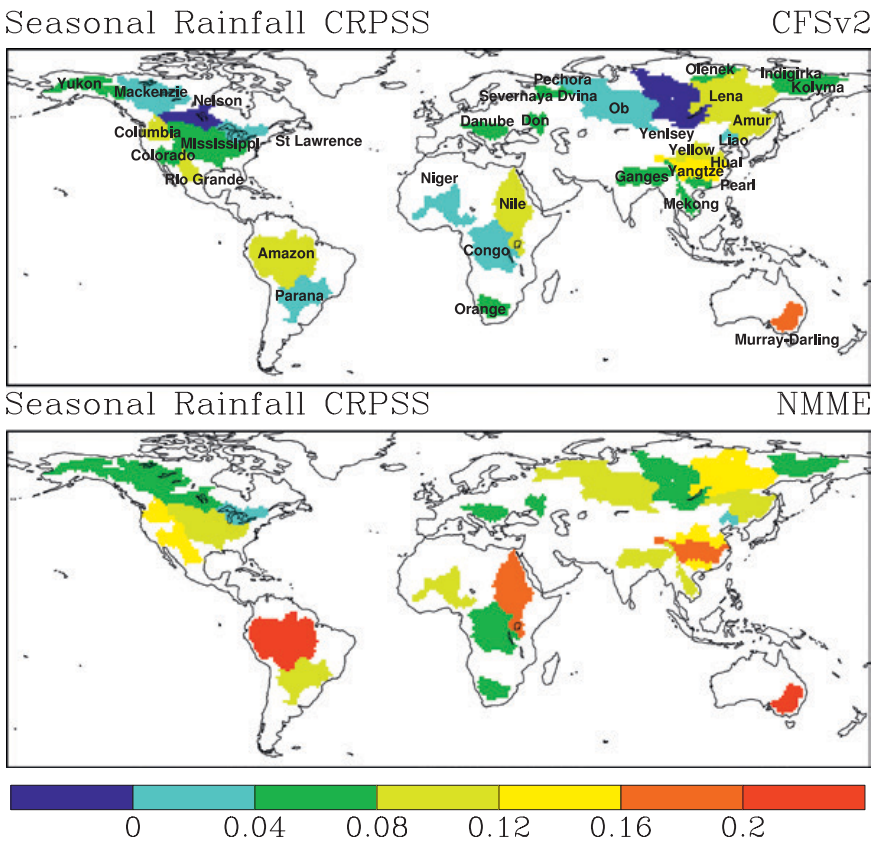

Fig. 1. CRPSS for basin-averaged, seasonal mean precipitation (0.5-month lead) from CFSv2 and NMME. The six NMME models are NCAR CCSM3, GFDL CM2.2, NASA GEOS-5, NCEP CFSv2, CMC CanCM3, and CMC CanCM4 [see Kirtman et al. (2014) for ensemble information and full references]. The statistics are based on the hindcasts started in each calendar month during 1982–2009, and the reference is climatological forecast. A value of CRPSS=0.2, for example, indicates that the probabilistic forecast error is 20% less than the climatological forecast error.

basin in North America, the Nile and Niger basins in Africa, the Yangtze and Pearl basins in China, and several high-latitude basins in Eurasia. Figure S1 [find this and more information online (http://dx.doi.org/10.1175/BAMS-D-14-00003.2)] shows the statistics for each season, suggesting that the improvement from CFSv2 to NMME is not necessarily limited to the dry/low flow periods, such as the Yangtze, Pearl, Mekong (East Asia), and Niger (West Africa) basins during June–August (JJA) and the Orange basin (South Africa) and Murray–Darling basin (Australia) during December–February (DJF), where the NMME shows improvement against CFSv2 in their corresponding wet seasons. The improvement over low latitudes originates from better representation of oceanic forcings in other NMME models (Kirtman et al. 2014), while at high latitudes the improvement may be related to the enhancement in reliability from the multimodel ensemble (Yuan and Wood 2013) or a better description of cold season processes. In fact, Fig. 1 in Yuan and Wood (2013) shows that several NMME models (e.g., GFDL CM2.2 and CMC CanCM4) have higher drought onset detectability than the CFSv2 over high latitudes, but the underlying physical reasons for the improvement are unclear. Further diagnosis is needed on the estimation of solid precipitation and the representation of cryospheric processes (e.g., snow and/or frozen soil).

The improvement of NMME against CFSv2 in basin precipitation prediction [more examples can be found in Kirtman et al. (2014)] provides an opportunity to advance the hydrologic forecast over most GEWEX RHP basins. However, the initial condition also has a strong control on the seasonal hydrologic predictability (Shukla et al. 2013; van Dijk et al. 2013), and its spatiotemporal variation can result in quite different hydrologic predictability as compared with the predictability of precipitation. Therefore, this article focuses on a comparison between NMME-based and ESP-based forecasts of hydrologic extremes and explores to what extent the meteorological forecasts from state-of-the-art climate forecast models can improve the hydrologic forecasts relative to the traditional approach that only relies on the information from hydrologic initial conditions.

PRINCETON'S GLOBAL SEASONAL HYDROLOGIC FORECAST SYSTEM. The global system draws from a legacy of national and continental systems (Luo and Wood 2007; Sheffield et al. 2014) developed by the Terrestrial Hydrology group at Princeton University. Its U.S. Drought Monitoring and Forecast System (Luo and Wood 2007; Yuan et al. 2013b) operates over the conterminous United States (CONUS) at 1/8° resolution and utilizes climate predictions from NCEP's CFSv2 and observations from phase 2 of the North American Land Data Assimilation System (NLDAS-2; Xia et al. 2012a). The system has been transitioned to the NCEP Environmental Modeling Center (EMC) for operational drought prediction (www.emc.ncep.noaa.gov/mmb/nldas/forecast/TSM/perc/). Recently, a continental system for African flood and drought monitoring and

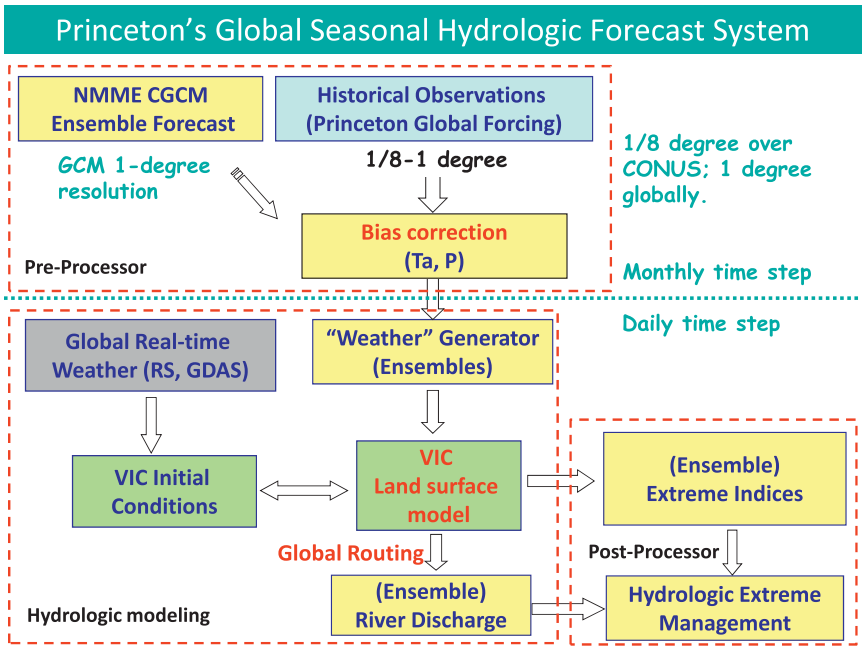

Fig. 2. Schematic view of Princeton's Global Seasonal Hydrologic Forecast System. The system consists of three parts: 1) a preprocessor that bias corrects meteorological ensemble forecasts from global seasonal climate forecast models; 2) VIC land surface hydrologic model calibrated over global major river basins, with a global routing model; and 3) a postprocessor that removes the probabilistic bias of streamflow forecasts and translates hydrologic states to extreme indices. RS = Remote Sensing. GDAS = Global Data Assimilation System.

forecasting (Sheffield et al. 2014; Yuan et al. 2013a) has been developed and installed at regional centers in sub-Saharan Africa.

The central part of a hydrologic forecast system is the land surface hydrologic model. As shown in Fig. 2, the hydrologic modeling part of the global system consists of the VIC land surface model and a global routing model. The VIC model (Liang et al. 1996), version 4.0.5, is used to predict soil moisture and runoff in this study. It is a semidistributed, grid-based hydrologic model with a mosaic representation of land cover and soil water storage capacity. The global routing model utilizes topographic data to derive flow velocity and direction and translates runoff from the VIC grid cells to the river network and routes the flows to the oceans or internal basins, therefore estimating streamflow globally. This first-order approximation of river routing allows for a globally continuous estimate of streamflow that is extremely computationally efficient and therefore can be utilized for both hydrologic monitoring and ensemble forecasting. The VIC model is calibrated over major river basins with 1° global resolution, using monthly streamflow data from Global Runoff Data Centre (GRDC) as compiled by Dai et al. (2009). The streamflow gauge locations and drainage areas for the basins and length of the records are listed in Table S1 (online supplemental material). The calibration is done using the shuffled complex evolution algorithm (Duan et al. 1994) based on long-term (1952–81) global historical model simulations forced by meteorological data from the Princeton Global Meteorological Forcing dataset (PGF; Sheffield et al. 2006). Except for some basins with heavy water resources management such as the Yellow and Murray–Darling basins, the Nash–Sutcliffe efficiency coefficients for the VIC monthly streamflow simulation vary between 0.6 and 0.9 for the calibration period (1952–81) and 0.5 and 0.8 for the validation period (1982–2006).

A preprocessor component bias corrects the monthly precipitation and temperature hindcasts from each NMME ensemble member using a simple quantile-mapping method (Wood et al. 2002) in a cross-validation mode (leaving the target year out for the climatological distribution). For each calendar month and each NMME model, all hindcasts during 1982–2009 (excluding the target year) with all ensemble members for the target month are used to construct cumulative distribution functions (CDFs) of the forecasts. The 62-yr (1948–2010 excluding the target year) PGF observations in that calendar month are used to construct CDFs of the observations. Both CDFs of forecasts and observations are then transformed to normal probability space through quantile mapping (Wood et al. 2002). Both individual members and NMME multimodel ensemble mean in the normal space are then transformed back to the original space using normal observations as the reference distribution. Finally, the bias-corrected individual members are adjusted according to the bias-corrected NMME multimodel ensemble mean to increase the sharpness (Yuan and Wood 2013). This differs from Princeton's CONUS forecast system, which uses a Bayesian merging method to correct bias (Luo and Wood 2008; Yuan et al. 2013b). The reason is that it is difficult to obtain stable weights for different climate models that can outperform the arithmetic mean from a short sample of hindcast data (Doblas-Reyes et al. 2005; Yuan and Wood 2012b), especially for extremes. The bias-corrected forecasts are temporally downscaled to a daily time step by sampling from the historic PGF dataset and rescaling to match the monthly forecasts ("weather" generator). The daily meteorological forecasts are used to force the VIC model and the river routing model to produce soil moisture and streamflow forecasts, based on initial conditions taken from the historical offline simulation. The postprocessor removes the probabilistic bias (Yuan and Wood 2012a) in the soil moisture and streamflow forecasts and calculates extreme indices based on percentile thresholds.

EVALUATION OF HYDROLOGIC HINDCASTS. The hydrologic hindcasts start from the first day of each calendar month during 1982–2009 and run out to six months, with 71 members for NMME VIC. These are compared with hindcasts based on ESP, which samples random 6-month sequences of daily meteorological data from the PGF dataset that are used to force VIC, to give 20 ensemble members for ESP VIC.

For each calendar month, the monthly soil moisture and streamflow are converted into percentiles. Droughts are then defined as monthly soil moisture or streamflow percentiles that are less than 20%, while wet spells are for those larger than 80%. The validation data for soil moisture and streamflow are from the VIC historical simulation.

Figure 3 shows the hit rate of 3-month soil moisture (agricultural) drought from ESP VIC and NMME VIC hindcasts at different lead times over the hindcast period (1982–2009). The hit rate is the fraction of actual events that are predicted (the detectability; see appendix for details). The initial hydrologic conditions (as shown by the ESP VIC results) have a strong control on agricultural drought over the Northern

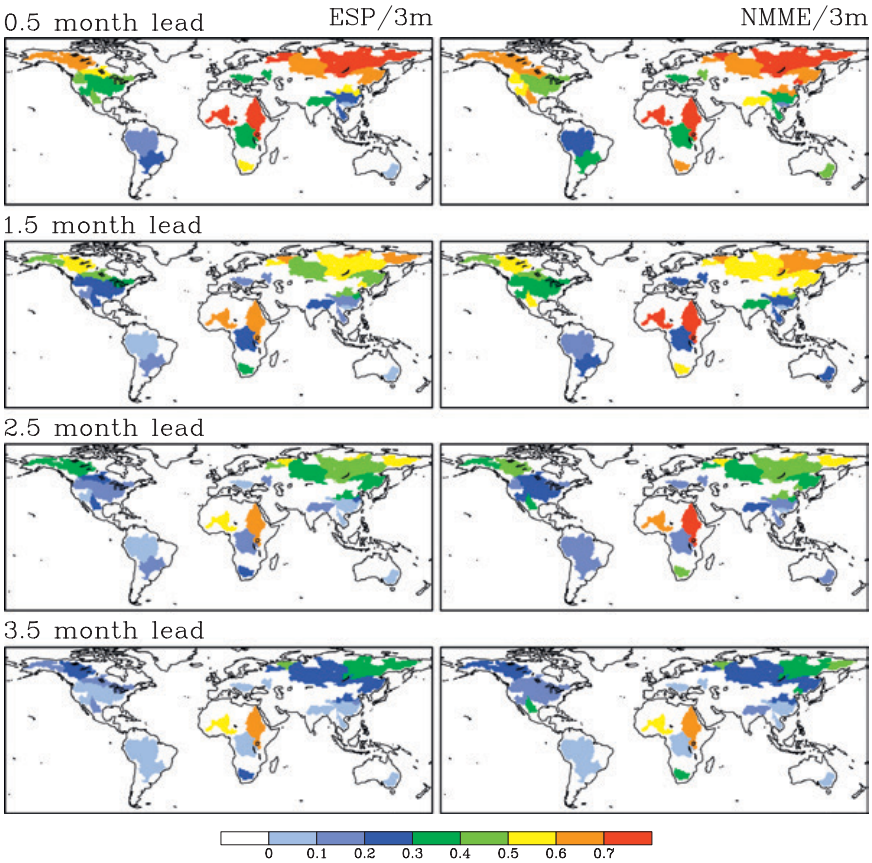

Fig. 3. Hit rate for 3-month drought at different forecast leads during the hindcast period (1982–2009). Statistics are calculated using ensemble median soil moisture from all 1° grid cells within each basin. A hit rate of 0.7, for example, indicates that 70% of 3-month drought in the hindcast period can be detected by the forecast system.

Hemisphere, high-latitude basins, and two of the African basins (Fig. 3, left column). The detectability is not negligible (e.g., >0.2) even in some midlatitude basins at short leads. For example, more than 30% of agricultural droughts over the Mississippi basin can be detected by ESP VIC one season ahead (Fig. 3, top-left panel), and the detectability can be as high as 50% during the dry season (Fig. S2, top-left panel). Unlike the precipitation forecast (Fig. 1), NMME VIC's agricultural drought detectability is not necessarily limited to ENSO-affected regions and is actually a compromise between climatic and hydrologic predictability. For instance, NMME has high precipitation predictive skill over the Amazon basin (Fig. 1) because of the ENSO influence, but NMME VIC has low agricultural drought detectability because of lower predictability from the initial hydrologic conditions (Fig. 3). In contrast, NMME VIC has high detectability over high-latitude basins where the influence of initial condition is strong (Fig. 3), regardless of the low precipitation predictive skill (Fig. 1). As a result, NMME VIC improves drought detectability compared to ESP VIC over basins with moderate control from both remote large-scale oceanic conditions and local initial hydrologic conditions, which are mostly located in midlatitude areas (e.g., Mississippi and Yangtze). For those midlatitude basins, NMME VIC has consistently higher detectability than ESP VIC throughout different seasons, although both methods have higher detectability during dry seasons than during wet seasons (Fig. S2). Similar results can be found for wet spells (not shown), but in general wet spells are less detectable than droughts because of less influence from the initial condition and lower skill in precipitation prediction.

Hit rate (detectability) is one aspect of forecast quality. However, as indicated by Yuan and Wood (2013), the models with high meteorological drought hit rates usually have high false alarm ratios (the fraction of "yes" forecasts that turn out to be wrong; see the appendix for details). Therefore, a balanced index, the equitable threat score (ETS; Wilks 2011; see appendix) that considers both the hit rate and the false alarm ratio is used to quantify the contribution of NMME beyond ESP for the predictive skill of soil moisture extremes. Figure 4 shows the maximum forecast leads for which NMME VIC has significantly ($p < 0.05$) higher ETS than ESP VIC for the prediction of droughts and wet spells. The Student's t test is used here, and samples come from ETS for each grid cell within the basin. For droughts that last for at least 1–2 months, NMME VIC prediction is significantly better than ESP VIC up to 3–6 months over the basins with short soil moisture memory, such as tropical and midlatitude basins (Figs. 4a,b). For the basins with long soil moisture memory, NMME VIC outperforms ESP VIC only if the NMME has high predictive skill for the

precipitation (CRPSS > 0.1; Fig. 1), such as the Nile basin in Africa. For the Niger basin in West Africa with long soil moisture memory, NMME only has moderate precipitation predictive skill (Fig. 1), and so NMME VIC does not have significantly higher ETS than ESP VIC (Figs. 4a,b). For 3-month droughts, NMME VIC also has significantly higher ETS than ESP VIC up to 2–3 months for more than 40% of the basins.

The differences for wet spells (Figs. 4d–f) are much smaller than for droughts, which are expected because of lower skill of the climate models in predicting wet conditions. Similar to drought, the differences between NMME VIC and ESP VIC usually decrease with an increase of the wet spell duration. Some of the exceptions to this are the Columbia and Colorado basins in North America, and the Murray–Darling in Australia, where NMME's advantage emerges as the duration increases.

The results of maximum forecast leads for individual seasons are shown in Fig. S3. Because of the insufficient number of samples for the 2- and 3-month droughts or wet spells, only the results for 1-month duration are plotted. Regardless of the season, NMME VIC drought prediction is significantly better than ESP VIC up to six months over the Mississippi basin. Even for the wet spells, the NMME VIC prediction has significantly higher skill than ESP VIC up to 4–5 months over the Mississippi during wet seasons [March–May (MAM) and JJA].

Given that several seasonal forecast systems based on CFSv1 or CFSv2 have been developed over the United States (Luo and Wood 2008; Mo et al. 2012; Yuan et al. 2013b), Fig. S4 compares the NNME/VIC system with the CFSv2/VIC for drought prediction. Note that CFSv2/VIC in this study has the same resolution as NMME VIC (i.e., 1°), which is coarser than previous studies. Actually a high-resolution (1/8°) NMME VIC system is currently being developed at Princeton University by following the work of Yuan et al. (2013b). Similar to Fig. 4, Fig. S4 shows the maximum forecast leads when CFSv2/VIC is used as the reference forecast. There is no significant difference over the Columbia basin. The NMME VIC prediction is significantly better than CFSv2/VIC up to two months over the Colorado basin for 1- and 2-month droughts and over the Mississippi basin for 2-month droughts.

The streamflow forecasts at the outlet of each basin are also assessed. Figure 5 shows the CRPSS of monthly streamflow predicted by NMME VIC, using ESP VIC as the reference forecast, and Fig. S5 shows the results for different seasons. NMME VIC is generally more skillful than ESP VIC over most regimes. However, the biggest improvement does not necessarily occur in the first month of the forecast (e.g., Amazon, Yangtze, and Murry–Darling). Again, this is another example of the compromise between predictive skill derived from the climate forcing and the initial hydrological conditions. The effects of initial condition on streamflow over these large basins are expected to be larger than the effects on grid-scale runoff because of the memory from upstream areas. This sometimes results in a negligible difference between NMME and ESP skill for the streamflow forecast at the beginning of the forecast, despite that the precipitation predictive skill of NMME is significantly higher than ESP at short leads.

Figure 6 shows the probabilistic forecast quality for low, normal, and high flow conditions, using hindcast samples from all basins. ESP VIC has reliable

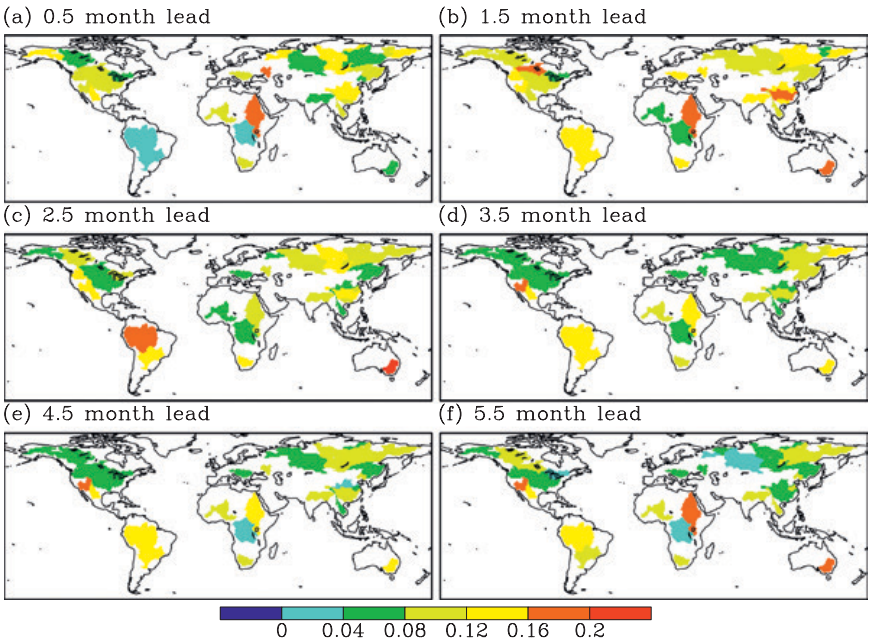

Fig. 4. Maximum forecast lead time (months) that NMMEVIC ensemble median has significantly ($p < 0.05$) higher *ETS* than ESP VIC for the prediction of soil moisture droughts and wet spells during the hindcast period (1982–2009).

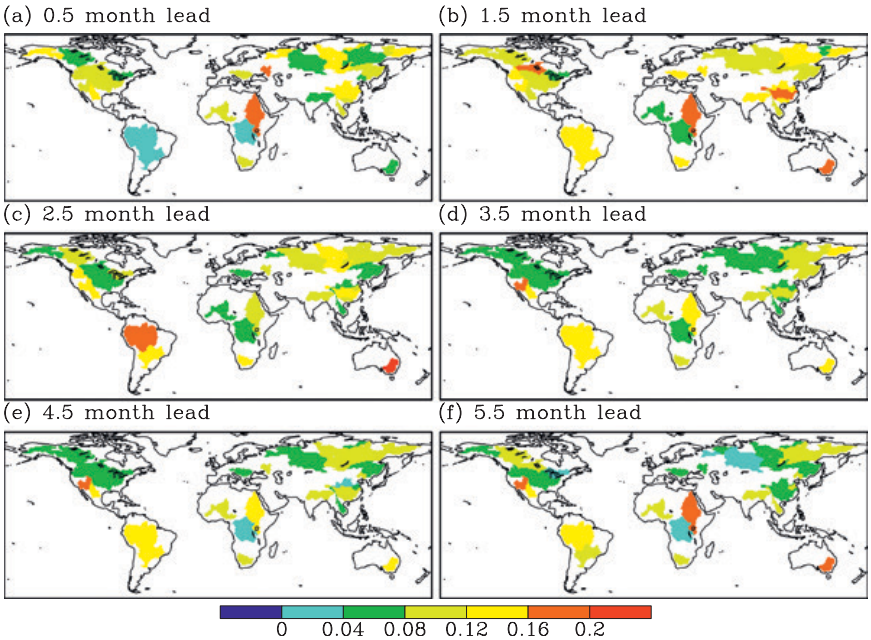

Fig. 5. CRPSS for monthly streamflow predicted by NMME VIC at the outlets of each basin during the hindcast period (1982–2009). The reference forecast is ESP VIC, and VIC offline simulated streamflow is used as validation data. A value of CRPSS=0.2, for example, indicates that the probabilistic streamflow forecast error for NMME VIC is 20% less than the forecast error for ESP VIC.

predictions (results fall along the diagonal lines) for hydrologic droughts and wet spells (red and blue lines, respectively) at 0.5-month lead, but it becomes overconfident as the forecast proceeds. Although the ESP forcings (climatological precipitation and temperature) are very reliable, they are not necessarily reliable for predicting hydrologic extremes. This is especially true for forecasts that start with anomalously dry or wet initial conditions, for which the ensemble of historical forcings tend to bring the hydrological states to neutral conditions, thus degrading the reliability for extremes. In contrast, NMME VIC maintains the reliability for drought and wet conditions much better, even out to 5.5-month lead. Similar to the 2-m temperature forecasts illustrated in Kirtman et al. (2014), the reliability for neutral streamflow conditions is more difficult to maintain for longer forecast lead times (Fig. 6, gray lines).

REAL-TIME FORECASTING OF THE 2012 CENTRAL U.S. DROUGHT. The 2012 summertime drought over the central United States was the most severe seasonal drought in the past 100 years (Hoerling et al. 2014). Most seasonal climate forecast models including CFSv2 failed to predict well the meteorological drought (Kumar et al. 2013; Hoerling et al. 2014). However, some NMME models such as GFDL CM2.2 did capture the 2012 drought (Kam et al. 2014). Kirtman et al. (2014) also showed that a NMME-based 6-month standardized precipitation index that blends antecedent observations with the seasonal forecasts had some skill for the 2012 drought. Here we test the capability of the NMME-based hydrologic forecast system in predicting the 2012 agricultural drought as an extension of the previous results for meteorological drought forecasts (Hoerling et al. 2014; Kirtman et al. 2014).

The approximate "real-time" forecast is done by bias correcting the NMME climate forcings for 2012 using all hindcast data during 1982–2009, which differs from the cross-validation mode of leaving out the target year during the hindcast period. Real-time observational data are used to run the VIC model up to the start of the forecast to produce the initial conditions. The real-time observational data are taken from the Climate Prediction Center (CPC) Unified Gauge-Based Analysis for precipitation (Chen et al. 2008) and the Climate Forecast System Reanalysis (CFSR; Saha et al. 2010) for other meteorological variables. These are used to extend the PGF data after 2010 and are adjusted to match the monthly climatology (1948–2010) of PGF through quantile mapping. The bias-corrected data are then used to force the VIC model from 2011 to 2012 to generate the initial conditions as well as reference soil moisture data to evaluate the forecasts. Note that an operational real-time forecast would be subject to biases in the real-time meteorological forcings that are likely to be high in regions with sparse gauge networks.

Figure 7 shows the 6-month soil moisture drought area forecasts for 20 ESP VIC members and 71 NMME VIC members initialized on two dates: February 2012 and June 2012. Before the drought onset, ESP VIC has some skill in the first two months (February and March forecast in Fig. 7a). After March, almost all ESP VIC ensemble members underestimate the drought area during 2012, especially during the summer when the drought is quite severe. The NMME VIC grand ensemble encompasses the evolution of the

reference drought area (solid black line) quite well (Fig. 7b), and the ensemble mean (blue line) is also much closer to the reference drought area than ESP VIC. Nevertheless, the ensemble mean of NMME VIC shows an earlier drought recovery than the reference data, which indicates the difficulty of predicting drought recovery.

Besides evaluating the 2012 drought forecast with the VIC offline simulation, we also compared the forecast with two satellite-based estimates of the drought: the multidecadal (1979–2013) essential climate variable for soil moisture (ECV_SM) dataset that homogenizes and merges six microwave-based satellite soil moisture retrievals (Liu et al. 2011; Dorigo et al. 2015) and the 11-yr (2003–13) Gravity Recovery and Climate Experiment (GRACE) terrestrial water storage dataset (Wahr et al. 2004). Figure 7 shows that the ECV_SM (dashed black lines) matches the VIC offline simulation (solid black lines) quite well before the drought onset, but they diverge slightly as the drought emerges. This difference can be attributed in part to the representative depth of the satellite soil moisture retrieval, which is for a very thin surface layer (~1 cm) due to the frequency of the sensors, and to the larger errors in more densely vegetated regions for the retrieval. The GRACE data (plus symbols) have larger seasonal variations and show a larger drought area than both the VIC simulation and the ECV_SM, because it represents changes in total water storage that includes surface water bodies (e.g., lakes and reservoirs) and groundwater, which are not represented by other datasets. Additionally, GRACE has a short climatology (11 years) that contributes to a larger uncertainty in its seasonal climatology from which the percentiles are estimated. Nonetheless, the satellite data provide useful information for validating the hydrologic forecasts, especially if their corresponding time scales and uncertainties are well understood.

OCEANIC AND LAND PRECURSORS FOR HYDROLOGIC EXTREMES. Because of chaotic nature of the atmosphere, seasonal prediction relies heavily on the memory imparted by both the ocean and land, as do the predictions of hydrologic extremes. For instance, ENSO is recognized as the largest source of seasonal predictability, and tropical SST anomalies not only alter the Walker circulation and convection in the tropics because of the positive feedbacks between SSTs and wind (Walker and Bliss 1932; Smith et al. 2012) but also affect the climate in midlatitudes through Rossby wave trains (Hoskins and Karoly 1981; Trenberth and Caron 2000). To investigate the impact of ENSO on hydrologic prediction over the GEWEX basins, differences in composite soil moisture percentiles between selected El Niño and La Niña years (i.e., average soil moisture percentiles in El Niño years minus those in La Niña years) during 1982–2009 are shown in Fig. 8. The selected years are according to Smith et al. (2012), which are classified by using a detrended 100-yr SST time series. NMME VIC reproduces the ENSO influence on soil moisture during wintertime very well (Figs. 8a,b) but underestimates its impact over the North American monsoon and East Asian

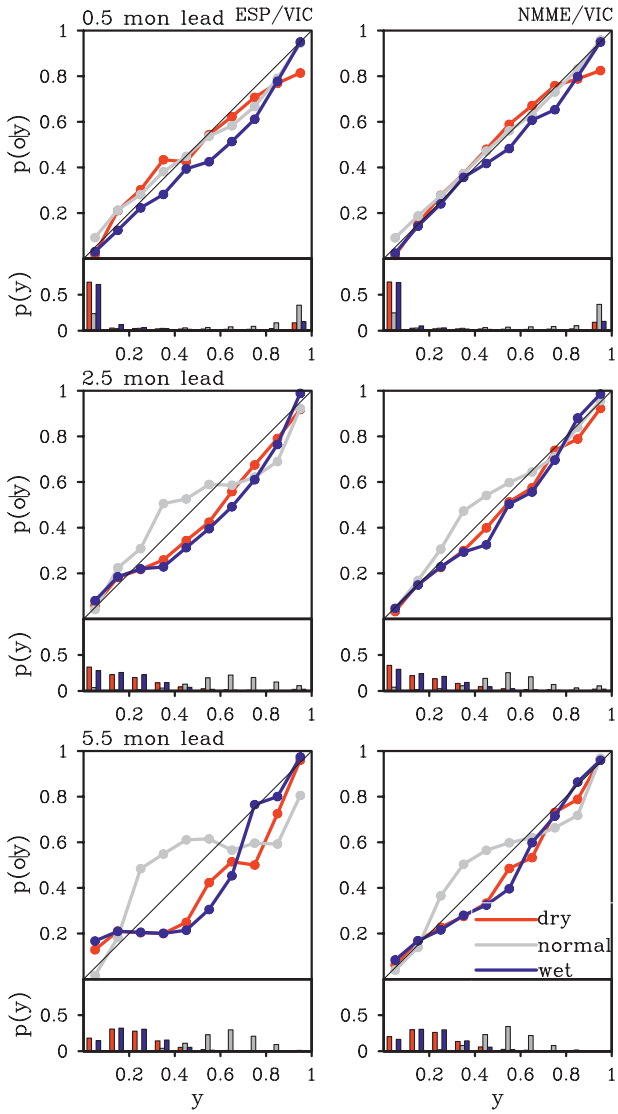

Fig. 6. Reliability diagram for monthly streamflow percentiles predicted by (left) ESP VIC and (right) NMME VIC throughout global major river basins during the hindcast period (1982–2009). Red, gray, and blue are for dry (<20%), normal, and wet (>80%) conditions, respectively. Here p(y) is forecast probability with probabilistic forecast value y, and p(o|y) is the observed probability conditional on the forecast value.

monsoon regions during summertime (Figs. 8e,f). In general, the responses of seasonal soil moisture to ENSO are roughly captured by the CGCM-Hydrology forecast system. There are moderate differences for the summertime composite among individual models: GFDL CM2.2 and two Canadian models are better over North American basins, while NCEP CFSv2 is better over East Asian basins (not shown).

Besides ENSO, the initial soil moisture is also thought to influence both the potential and actual subseasonal to seasonal climate predictability via land–atmosphere coupling (Koster et al. 2004, 2006, 2010). However, the association of oceanic and land precursors with model performance for individual hydrologic extreme events at the global scale is still unclear. Here we investigate the ENSO and soil moisture associations based on the joint distribution of the forecast and observation for the onsets of droughts and wet spells. We would like to answer the following question: What are the probability distributions of antecedent oceanic and land conditions for hit cases (observed extreme events that are captured by the models) and for false alarms (forecasted extreme events that do not occur in the observation)? The onset events of droughts or wet spells are defined as three continuous months when the soil moisture percentile is consistently below 20% or above 80%, respectively.

Figure 9 shows the spatial frequency of conditional mean, antecedent Niño-3.4 SST absolute anomaly and the initial soil moisture percentiles calculated over the GEWEX basins. For example, the green lines (from six NMME models) in Fig. 9a represent the frequency distributions of seasonal mean Niño-3.4 SST (three months before the onset of extreme events) averaged over those forecast events where the models issue a soil moisture drought onset forecast (fcst = T) but drought does not occur in the observation (obs = F), where T and F represent that drought occurs or does not occur, respectively, either for the forecast (fcst) or observation (obs). Red and blue curves are for detected and missed events, respectively. The higher peaks of the blue curves (fcst = T) compared to those of the green and red curves (fcst = F) around small SST anomaly values indicate that climate models have a higher chance of missing the agricultural drought onset when the antecedent SST anomaly is smaller (Fig. 9a). As the SST anomaly increases, climate models have a higher chance of issuing a drought forecast than missing a drought (i.e., the red and green curves show higher frequency than the blue curves), but there is also a higher chance of a false alarm (green curves). This is similar to the meteorological drought analysis in Yuan and Wood (2013). The association for the wet spell onset forecast (Fig. 9b) is similar to the drought onset, but different models have moderate differences

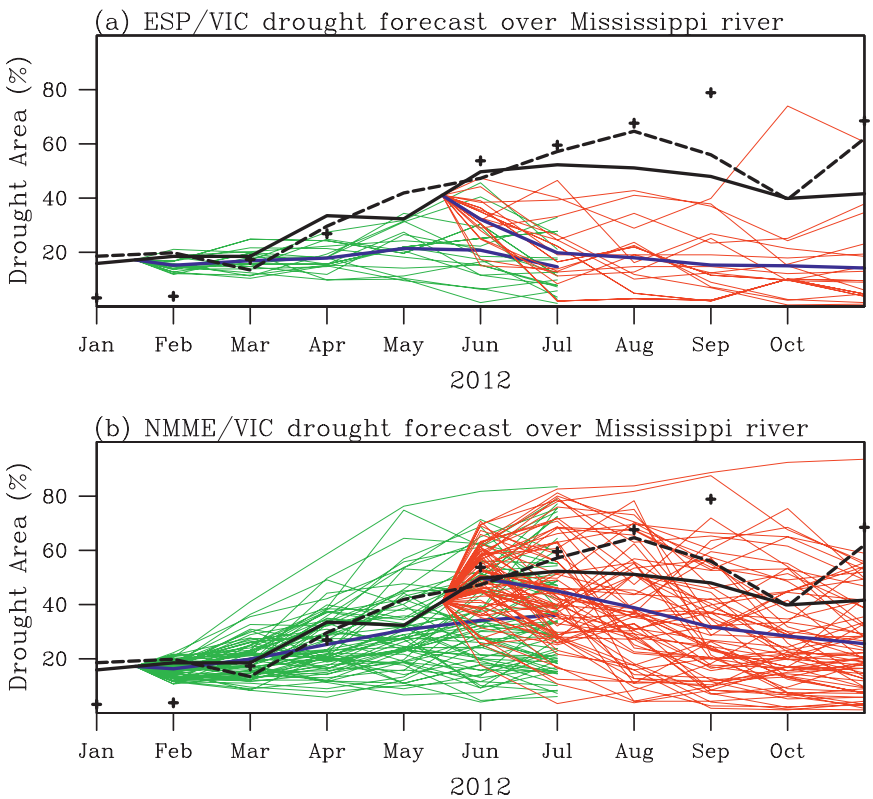

Fig. 7. Real-time seasonal forecasting of the 2012 drought over the Mississippi River basin with ESP VIC and NMME VIC. The drought area is quantified using soil moisture percentiles. Solid black lines represent the VIC offline simulations, dashed black lines are from the ECV-merged satellite soil moisture retrievals, plus symbols are for the GRACE terrestrial water storage anomalies (data for May and Oct are missing), blue lines are the ensemble means of the forecasts, and the green and red lines are for individual ensemble members.

for the false alarms (green curves).

This asymmetric performance for predicting soil moisture droughts and wet spells is more obvious in the analysis of land precursors (Figs. 9c,d). The spread of initial soil moisture percentiles for model-predicted drought events (red and green curves, Fig. 9c) is smaller than that for wet spell events (Fig. 9d), suggesting that there is less dependence of wet spell onset forecast on the initial land conditions than for the drought onset. In fact, as the drought occurs, initial soil moisture memory (anomaly) could persist for a period of time, while when a wet spell occurs, an individual rainfall event can sometimes erase all soil moisture memory. This interacts with the atmospheric asymmetry mentioned above and amplifies the difference between dry and wet conditions. Figures 9c,d also demonstrate that the missed drought (wet spell) events (blue curves) are associated with higher (lower) initial soil moisture (i.e., less information from the land precursor). Therefore, some droughts and wet spells occur without clear SST and soil moisture precursors (e.g., the 2012 central U.S. drought), and they are the most difficult to predict at seasonal time scales. The differences in the red and green curves in Figs. 9c,d are larger than those in Figs. 9a,b, suggesting that the oceanic precursor facilitates a higher probability that the climate models issue an extreme forecast (although it is sometimes difficult to determine whether the forecast is correct or a false alarm), while the land precursor will reduce the probability of false alarms.

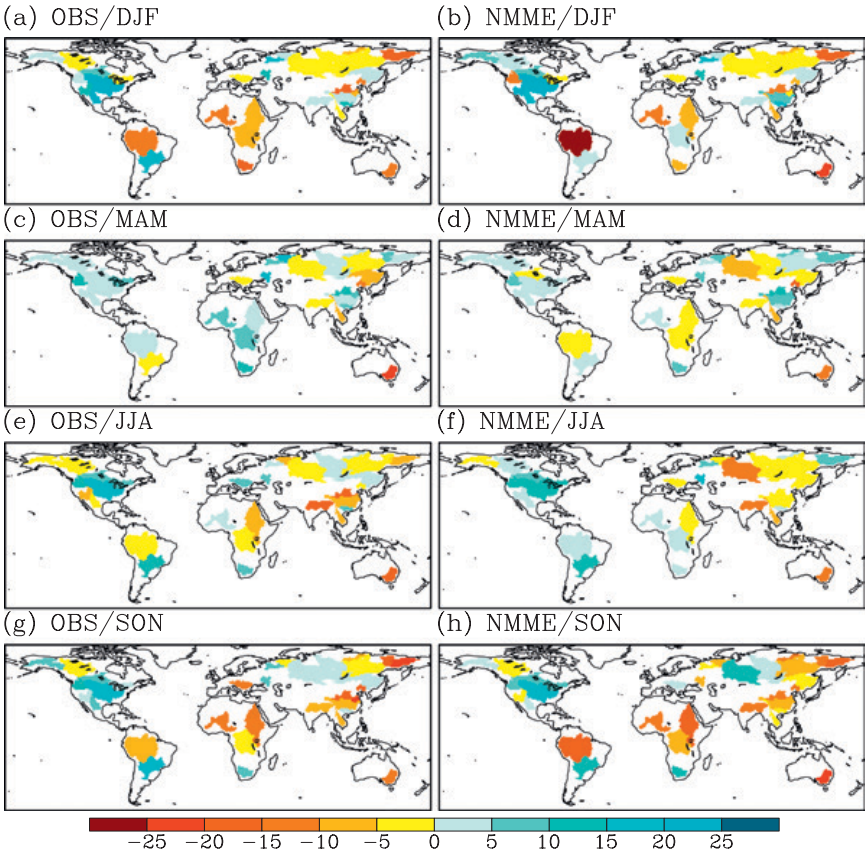

Fig. 8. Composite differences in offline simulated (OBS) and model-predicted (NMME, 0.5-month lead) soil moisture percentiles between positive and negative phases of ENSO for different seasons. Gridpoint soil moisture percentiles are averaged to basin scale before composite analysis. During the hindcast period (1982–2009), positive ENSO years are 1982, 1986, 1991, 1997, and 2009 and negative ENSO years are 1984, 1988, 1999, and 2007.

BEYOND THE NORTH AMERICAN MULTIMODEL ENSEMBLE. Phase 2 of the NMME project (Kirtman et al. 2014) will provide higher-temporal-resolution datasets (e.g., three hourly) with more variables besides precipitation, 2-m surface air temperature, and SST. This will enable a more comprehensive diagnostic study that can provide feedback to model development. Nevertheless, in terms of applications (e.g., hydrologic forecasts), there are other concerns. As pointed out by Yuan and Wood (2012b), six of the seven original NMME models (without the two Canadian models) use the ocean model developed at GFDL, which to some extent may result in similarity or overconfidence in the seasonal climate forecasts. While combining those seven models does not gain much predictability in terms of a deterministic forecast, skill can be increased by including European models, which are considered to be more independently developed (Yuan and Wood 2012b).

To explore this, we briefly evaluate the benefit of combining the NMME models with those in the Climate-System Historical Forecast Project (CHFP; Kirtman and Pirani 2009). Figure 10 shows the CRPSS for basin-averaged, May–July (MJJ) mean precipitation predicted by NMME and

NMME+CHFP. Because of data availability during 1982–2009, the CHFP models used here only include the European Centre for Medium-Range Weather Forecasts (ECMWF) Seasonal Forecast System 4 (S4; Molteni et al. 2011; Dutra et al. 2013), two models from Japan [Meteorological Research Institute Coupled Atmosphere–Ocean General Circulation Model, version 3 (MRI-CGCM3) and Model for Interdisciplinary Research on Climate, version 5 (MIROC5)], one model from Germany [Max Planck Institute Earth System Model (MPI-ESM)], and one from Australia [Predictive Ocean Atmosphere Model for Australia (POAMA-2)]. Figure 10 shows that including CHFP does not improve the MJJ precipitation prediction over the basins in North America (except for Columbia, but MJJ is a transition season between the snow-dominated winter and mostly dry summer), suggesting that the NMME is the best multimodel ensemble in predicting hydroclimate over North America. Nevertheless, improvement over the basins in East Asia and Australia is not negligible (CRPSS difference larger than 0.05) in basins such as the Yangtze, Mekong, Ganges, and Murray–Darling. Therefore, increasing the number of international models (and presumably the level of international collaboration) may be necessary to advance hydrological forecasting at the global scale.

An alternative multimodel ensemble is the ensemble of multiple land surface hydrologic models. In fact, work over the past decade has shown that hydrological models, even when forced with identical atmospheric boundary conditions, can produce results that are substantially different (Dirmeyer et al. 2004; Mitchell et al. 2004; Duan et al. 2007; Wang et al. 2009; Xia et al. 2012b). Recently, Mo and Lettenmaier (2014a) have reported the challenge of applying hydrologic models in monitoring the droughts with different severity categories, and Nijssen et al. (2014) have developed a prototype global drought information system based on multiple land surface models. These studies suggest that augmenting the NMME-based multimodel hydrologic forecasting system with multiple land surface models would enhance its capability in handling the hydrologic extremes with different severity levels.

CONCLUDING REMARKS. A global seasonal hydrologic forecasting system based on the NMME climate forecast models and VIC land surface hydrologic model has been established, and its performance against the traditional ESP forecast approach in predicting droughts and wet spells is assessed over the GEWEX RHP basins for a 28-yr hydrologic hindcast experiment and a "real time" case study. The ESP forecast skill relies on the information from the initial hydrological conditions, and so the comparison between the output of the NMME VIC and ESP VIC provides an opportunity to quantify the origin of hydrological predictability from the ocean and land states.

NMME VIC improves drought detectability against ESP VIC mostly over midlatitude basins where the controls of both remote large-scale oceanic states and local initial hydrological conditions are moderate. It is found that NMME VIC has significantly ($p < 0.05$) higher ETS values than ESP VIC up to 3–6 months over basins with short soil moisture memory. In terms

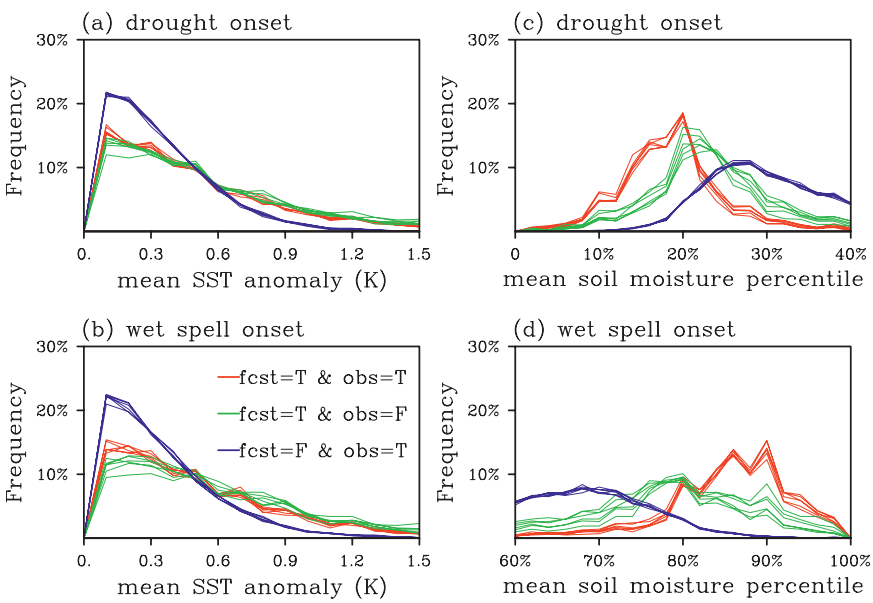

Fig. 9. Frequency distributions of (a),(b) absolute anomaly of antecedent seasonal mean Niño-3.4 SST and (c),(d) initial soil moisture percentile conditional on the joint distribution of forecast and observation for soil moisture drought and wet spell onset events over GEWEX basins. SST absolute anomaly and soil moisture percentile are averaged among all drought/wet events for each grid cell, and spatial frequency is then calculated using averaged values from all grid cells within GEWEX basins.

of the streamflow forecasts, the NMME VIC is superior to ESP VIC for accuracy and reliability, and the biggest improvement does not necessarily occur in the first month of the forecast. A real-time forecasting of the 2012 central U.S. drought shows that none of the ESP VIC ensemble members is able to forecast the drought onset; however, the NMME VIC grand ensemble covers the evolution of drought area quite well, with an ensemble mean closer to the reference data. The association of the onsets of extreme hydrologic events with oceanic and land precursors is also investigated on the basis of the joint distribution of the forecast and observation. Climate models have a higher probability of missing the onset of hydrologic extremes when the antecedent SST anomaly is smaller. Larger SST anomalies offer a higher probability for the models to issue a forecast for extremes but also bring higher probability of issuing a false alarm. The probability of such a false alarm can be reduced if there is a large anomaly in land surface conditions.

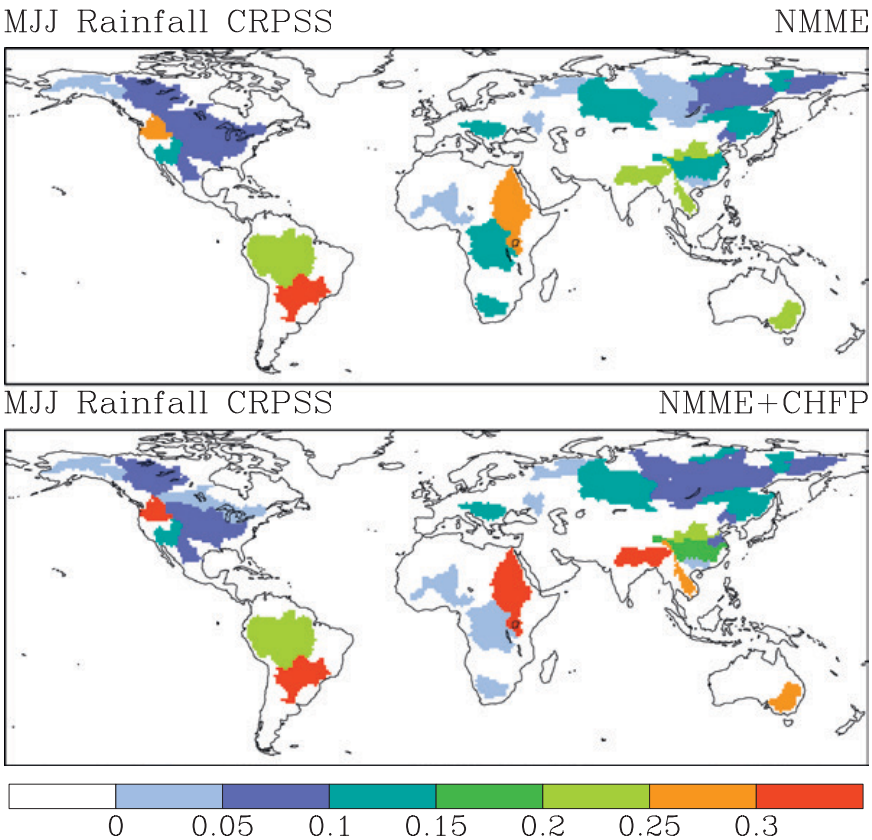

Fig. 10. CRPSS for basin-averaged MJJ mean precipitation (0.5-month lead) from NMME and those combined with CHFP models. The statistics are based on the hindcasts started in each May during 1982–2009, and the reference is climatological forecast.

Overall, the global hydrologic forecast system established in this study shows encouraging performance when compared with the ESP approach for predicting hydrologic extremes, such as higher detectability for historical soil moisture droughts, more reliable streamflow ensemble forecasts for low or high flow conditions, and better prediction for the 2012 North American extreme drought in a real-time forecast mode. The system also shows the potential for successfully utilizing climate models to advance GEWEX RHP. A website is being established to make real-time hydrological forecasts available, drawing from the existing Princeton CONUS and African monitoring and seasonal forecast websites (http://hydrology.princeton.edu/forecast; http://hydrology.princeton.edu/adfm). Linking the real-time forecasting of soil moisture and streamflow with impact models for predicting reservoir inflow, crop yield, and wild fire, etc. will amplify the usefulness of the system. Therefore, the NMME VIC system can serve as a prototype system for the Global Framework for Climate Services (GFCS), both in providing hydroclimate information services and in contributing to the science underpinning the prediction and predictability of the terrestrial hydrologic systems, including droughts and wet spells.

However, initial tests also indicate that the superiority of climate model-based streamflow forecasts tend to diminish when using the observed streamflow data for validation. There are a number of reasons for this, which include the often poor representation of water resources management (e.g., reservoir operation, irrigation) in land surface models and inadequate process parameterization in the hydrological models. Examples of the latter include surface–subsurface interactions; regional to continental surface water transportation (river routing); insufficient parameters for soil and vegetation properties; and inadequate hydrologic model, which includes calibration that requires either statistical postprocessing (e.g., Yuan and Wood 2012a; Ye et al. 2014), or an ensemble of multiple land surface hydrologic models, and/or

model improvements, especially for simulating water resources managements (Jaranilla-Sanchez et al. 2011; Wang et al. 2012). Uncertainties in the observed forcings (e.g., precipitation) can also be significant over basins with sparse in situ observations, which may be a nontrivial problem when implementing a hydrologic forecast system globally.

With the planned release of higher-temporal-resolution NMME datasets (phase 2) with more variables besides monthly precipitation, 2-m temperature, and SST that will also include land surface conditions as well as pressure level atmospheric variables, there will be opportunities to diagnose more completely individual model performance that influence seasonal extreme predictability (e.g., stationary waves, land–atmosphere coupling) and provide feedback to model development. Furthermore, the benefit of incorporating climate models from international centers for improving hydrological predictability globally calls for an international ensemble seasonal prediction system.

ACKNOWLEDGMENTS. The research was supported by the NOAA Climate Program Office through Grants NA10OAR4310246 and NA12OAR4310090. The first author also acknowledges the Thousand Talents Program for Distinguished Young Scholars. We thank the International Research Institute for Climate and Society (IRI) for making the NMME forecast information available. We thank three anonymous reviewers for their comments, Antje Weisheimer for providing the link to the CHFP data, and Ming Pan for introducing the ECV_SM data. We acknowledge WCRP CLIVAR WGSIP and CIMA for the CHFP data and acknowledge PICSciE OIT at Princeton University for the supercomputing support.

APPENDIX: HIT RATE, FALSE ALARM RATIO, ETS, AND CRPSS. The nonprobabilistic forecasts for discrete predictands (e.g., a drought event) can be verified by several measures that are based on a 2 × 2 contingency table. Taking the drought event forecast as an example, define a as the number of events when drought occurs in both the forecast and observation, b for when drought occurs in the forecast but not in the observation, c for when drought occurs in the observation but not in the forecast, and d for when drought does not occur in either the forecast or observation. Then, the hit rate is

$$\frac{a}{a+c}, \tag{A1}$$

where it is also called the probability of detection. The false alarm ratio is

$$\frac{b}{a+b}, \tag{A2}$$

where it is fraction of "drought" forecasts that turn out to be false. The ETS is

$$\frac{a-a_{\mathrm{ref}}}{a-a_{\mathrm{ref}}+b+c}, \tag{A3}$$

where $a_{ref} = (a+b)(a+c)/(a+b+c+d)$.

The probabilistic forecasts for continuous predictands (e.g., precipitation) can be verified through the *CRPSS*. First, the *CRPS* is defined as

$$\mathrm{CRPS} = \int_{-\infty}^{+\infty} [F(y) - F_o(y)]^2\, dy, \tag{A4}$$

where $F(y)$ is the CDF of the forecast with a predictand value of y and $F_o(y)$ is the CDF of the observation and

$$F_o(y) = \begin{cases} 0, & y < observed \quad value \\ 1, & y \geq observed \quad value \end{cases}. \tag{A5}$$

Then, the CRPSS is defined as

$$\mathrm{CRPSS} = 1 - \frac{\mathrm{CRPS}}{\mathrm{CRPS}_{\mathrm{ref}}}, \tag{A6}$$

where $\mathrm{CRPS}_{\mathrm{ref}}$ is the CRPS from the reference forecast (e.g., the climatological forecast used in this study). So, a value of CRPSS = 0.2, for example, indicates that the probabilistic forecast error is 20% less than the climatological forecast error.

REFERENCES

Barnett, T. P., and Coauthors, 2008: Human-induced changes in the hydrology of the western United States. *Science,* **319,** 1080–1083, doi:10.1126/science.1152538.

Barnston, A. G., M. K. Tippett, M. L. L'Heureux, S. Li, and D. G. DeWitt, 2012: Skill of real-time seasonal ENSO model predictions during 2002–11: Is our capability increasing? *Bull. Amer. Meteor. Soc.,* **93,** 631–651, doi:10.1175/BAMS-D-11-00111.1.

Becker, E., H. Van den Dool, and Q. Zhang, 2014: Predictability and forecast skill in NMME. *J. Climate,* **27,** 5891–5906, doi:10.1175/JCLI-D-13-00597.1.

Below, R., E. Grover-Kopec, and M. Dilley, 2007: Documenting drought-related disasters: A global reassessment. *J. Environ. Dev.,* **16,** 328–344, doi:10.1177/1070496507306222.

Camberlin, P., S. Janicot, and I. Poccard, 2001: Seasonality and atmospheric dynamics of the teleconnection between African rainfall and tropical sea-surface temperature: Atlantic vs. ENSO. *Int. J. Climatol.,* **21,** 973–1005, doi:10.1002/joc.673.

Cayan, D. R., K. T. Redmond, and L. G. Riddle, 1999: ENSO and hydrologic extremes in the western United States. *J. Climate,* **12,** 2881–2893, doi:10.1175/1520-0442(1999)012<2881:EAHEIT>2.0.CO;2.

Chen, M., W. Shi, P. Xie, V. B. S. Silva, V. E. Kousky, R. W. Higgins, and J. E. Janowiak, 2008: Assessing objective techniques for gauge-based analyses of global daily precipitation. *J. Geophys. Res.,* **113,** D04110, doi:10.1029/2007JD009132.

Coughlan, M., and R. Avissar, 1996: The Global Energy and Water Cycle Experiment (GEWEX) Continental-Scale International Project (GCIP): An overview. *J. Geophys. Res.,* **101,** 7139–7147, doi:10.1029/96JD00125.

Dai, A., T. Qian, K. E. Trenberth, and J. D. Milliman, 2009: Changes in continental freshwater discharge from 1948 to 2004. *J. Climate,* **22,** 2773–2791, doi:10.1175/2008JCLI2592.1.

Diffenbaugh, N. S., M. Scherer, and M. Ashfaq, 2013: Response of snow-dependent hydrologic extremes to continued global warming. *Nat. Climate Change,* **3,** 379–384, doi:10.1038/nclimate1732.

Dirmeyer, P. A., 2013: Characteristics of the water cycle and land–atmosphere interactions from a comprehensive reforecast and reanalysis data set: CFSv2. *Climate Dyn.,* **41,** 1083–1097, doi:10.1007/s00382-013-1866-x.

——, Z. Guo, and X. Gao, 2004: Comparison, validation, and transferability of eight multiyear global soil wetness products. *J. Hydrometeor.,* **5,** 1011–1033, doi:10.1175/JHM-388.1.

Doblas-Reyes, F. J., R. Hagedorn, and T. N. Palmer, 2005: The rationale behind the success of multimodel ensembles in seasonal forecasting—II. Calibration and combination. *Tellus,* **57A,** 234–252, doi:10.1111/j.1600-0870.2005.00104.x.

——, J. García-Serrano, F. Lienert, A. P. Biescas, and L. R. L. Rodrigues, 2013: Seasonal climate predictability and forecasting: Status and prospects. *Wiley Interdiscip. Rev.: Climate Change,* **4,** 245–268, doi:10.1002/wcc.217.

Dorigo, W. A., and Coauthors, 2015: Evaluation of the ESA CCI soil moisture product using ground-based observations. *Remote Sens. Environ.,* **162,** 380–395, doi:10.1016/j.rse.2014.07.023.

Douville, H., 2010: Relative contributions of soil and snow hydrology to seasonal climate predictability: A pilot study. *Climate Dyn.,* **34,** 797–818, doi:10.1007/s00382-008-0508-1.

Duan, Q., S. Sorooshian, and V. K. Gupta, 1994: Optimal use of SCE-UA global optimization method for calibrating watershed models. *J. Hydrol.,* **158,** 265–284, doi:10.1016/0022-1694(94)90057-4.

——, N. K. Ajami, X. Gao, and S. Sorooshian, 2007: Multi-model ensemble hydrologic prediction using Bayesian model averaging. *Adv. Water Resour.,* **30,** 1371–1386, doi:10.1016/j.advwatres.2006.11.014.

Dutra, E., F. D. Giuseppe, F. Wetterhall, and F. Pappenberger, 2013: Seasonal forecasts of droughts in African basins using the Standardized Precipitation Index. *Hydrol. Earth Syst. Sci.,* **17,** 2359–2373, doi:10.5194/hess-17-2359-2013.

Giorgi, F., C. Vera, and F. Semazzi, cited 2012: WCRP Grand Challenges: Regional climate information. [Available online at www.wcrp-climate.org/gc-regionalclimate.]

Goddard, L., S. J. Mason, S. E. Zebiak, C. F. Ropelewski, R. Basher, and M. A. Cane, 2001: Current approaches to seasonal to interannual climate predictions. *Int. J. Climatol.,* **21,** 1111–1152, doi:10.1002/joc.636.

Hoerling, M., and A. Kumar, 2003: The perfect ocean for drought. *Science,* **299,** 691–694, doi:10.1126/science.1079053.

——, J. Eischeid, A. Kumar, R. Leung, A. Mariotti, K. Mo, S. Schubert, and R. Seager, 2014: Causes and predictability of the 2012 Great Plains drought. *Bull. Amer. Meteor. Soc.,* **95,** 269–282, doi:10.1175/BAMS-D-13-00055.1.

Hong, S. Y., and E. Kalnay, 2000: Role of sea surface temperature and soil-moisture feedback in the 1998 Oklahoma–Texas drought. *Nature,* **408,** 842–844, doi:10.1038/35048548.

Hoskins, B. J., and D. Karoly, 1981: The steady linear response of a spherical atmosphere to thermal and orographic forcing. *J. Atmos. Sci.,* **38,** 1179–1196, doi:10.1175/1520-0469(1981)038<1179:TSLROA>2.0.CO;2.

GEWEX, 2012: GEWEX plans for 2013 and beyond. GEWEX Doc. Series 2012-1, 45 pp. [Available online at www.gewex.org/pdfs/GEWEX_IMPERATIVES_final.pdf.]

Ineson, S., and A. A. Scaife, 2009: The role of the stratosphere in the European climate response to El Niño. *Nat. Geosci.,* **2,** 32–36, doi:10.1038/ngeo381.

IPCC, 2013: Summary for policymakers. *Climate Change 2013: The Physical Science Basis,* T. F. Stocker et al., Eds., Cambridge University Press, 1–29.

Jaranilla-Sanchez, P. A., L. Wang, and T. Koike, 2011: Modeling the hydrologic responses of the Pampanga River basin, Philippines: A quantitative approach for identifying droughts. *Water Resour. Res.,* **47,** W03514, doi:10.1029/2010WR009702.

Kam, J., J. Sheffield, X. Yuan, and E. F. Wood, 2014: Did a skillful prediction of sea surface temperatures help or hinder forecasting of the 2012 Midwestern US drought? *Environ. Res. Lett.,* **9,** 034005, doi:10.1088/1748-9326/9/3/034005.

Karoly, D., cited 2012: WCRP Grand Challenges: Science underpinning the prediction and attribution of extreme events. [Available online at www.wcrp-climate.org/index.php/gc-extreme-events.]

Kirtman, B. P., and A. Pirani, 2009: The state of the art of seasonal prediction outcomes and recommendations from the First World Climate Research Program (WCRP) Workshop on Seasonal Prediction. *Bull. Amer. Meteor. Soc.,* **90,** 455–458, doi:10.1175/2008BAMS2707.1.

——, and Coauthors, 2014: The North American Multimodel Ensemble: Phase-1 seasonal-to-interannual prediction; phase-2 toward developing intraseasonal prediction. *Bull. Amer. Meteor. Soc.,* **95,** 585–601, doi:10.1175/BAMS-D-12-00050.1.

Koster, R. D., and Coauthors, 2004: Realistic initialization of land surface states: Impacts on subseasonal forecast skill. *J. Hydrometeor.,* **5,** 1049–1063, doi:10.1175/JHM-387.1.

——, and Coauthors, 2006: GLACE: The Global Land–Atmosphere Coupling Experiment. Part I: Overview. *J. Hydrometeor.,* **7,** 590–610, doi:10.1175/JHM510.1.

——, and Coauthors, 2010: Contribution of land surface initialization to subseasonal forecast skill: First results from a multi-model experiment. *Geophys. Res. Lett.,* **37,** L02402, doi:10.1029/2009GL041677.

——, and Coauthors, 2011: GLACE2: The second phase of the Global Land–Atmosphere Coupling Experiment: Soil moisture contribution to subseasonal forecast skill. *J. Hydrometeor.,* **12,** 805–822, doi:10.1175/2011JHM1365.1.

Kumar, A., M. Chen, M. Hoerling, and J. Eischeid, 2013: Do extreme climate events require extreme forcings? *Geophys. Res. Lett.,* **40,** 3440–3445, doi:10.1002/grl.50657.

Lang, Y., and Coauthors, 2014: Evaluating skill of seasonal precipitation and temperature predictions of NCEP CFSv2 forecasts over 17 hydroclimatic regions in China. *J. Hydrometeor.,* **15,** 1546–1559, doi:10.1175/JHM-D-13-0208.1.

Li, H., L. Luo, E. F. Wood, and J. Schaake, 2009: The role of initial conditions and forcing uncertainties in seasonal hydrologic forecasting. *J. Geophys. Res.,* **114,** D04114, doi:10.1029/2008JD010969.

Liang, X., E. F. Wood, and D. P. Lettenmaier, 1996: Surface soil moisture parameterization of the VIC-2L model: Evaluation and modifications. *Global Planet. Change,* **13,** 195–206, doi:10.1016/0921-8181(95)00046-1.

Liu, Y. Y., R. M. Parinussa, W. A. Dorigo, R. A. M. De Jeu, W. Wagner, A. I. J. M. van Dijk, M. F. McCabe, and J. P. Evans, 2011: Developing an improved soil moisture dataset by blending passive and active microwave satellite-based retrievals. *Hydrol. Earth Syst. Sci.,* **15,** 425–436, doi:10.5194/hess-15-425-2011.

Luo, L., and E. F. Wood, 2007: Monitoring and predicting the 2007 U.S. drought. *Geophys. Res. Lett.,* **34,** L22702, doi:10.1029/2007GL031673.

——, and ——, 2008: Use of Bayesian merging techniques in a multimodel seasonal hydrologic ensemble prediction system for the eastern United States. *J. Hydrometeor.,* **9,** 866–884, doi:10.1175/2008JHM980.1.

McCabe, G. J., M. A. Palecki, and J. L. Betancourt, 2004: Pacific and Atlantic Ocean influences on multidecadal drought frequency in the United States. *Proc. Natl. Acad. Sci. USA,* **101,** 4136–4141, doi:10.1073/pnas.0306738101.

Mitchell, K. E., and Coauthors, 2004: The multi-institution North American Land Data Assimilation System (NLDAS): Utilizing multiple GCIP products and partners in a continental distributed hydrological modeling system. *J. Geophys. Res.,* **109,** D07S90, doi:10.1029/2003JD003823.

Mo, K., and D. P. Lettenmaier, 2014a: Objective drought classification using multiple land surface models. *J. Hydrometeor.,* **15,** 990–1010, doi:10.1175/JHM-D-13-071.1.

——, and ——, 2014b: Hydrologic prediction over the conterminous United States using the National Multi-Model Ensemble. *J. Hydrometeor.,* **15,** 1457–1472, doi:10.1175/JHM-D-13-0197.1.

——, S. Shukla, D. P. Lettenmaier, and L. Chen, 2012: Do Climate Forecast System (CFSv2) forecasts improve seasonal soil moisture prediction? *Geophys. Res. Lett.,* **39,** L23703, doi:10.1029/2012GL053598.

Molteni, F., and Coauthors, 2011: The new ECMWF seasonal forecast system (System 4). ECMWF Tech. Memo. 656, 49 pp. [Available online at www.researchgate.net/profile/Frederic_Vitart/publication/230688826_The_new_ECMWF_seasonal_forecast_system_%28System_4%29/links/0912f51028aa651240000000.pdf.]

Morel, P., 2001: Why GEWEX? The agenda for a global energy and water cycle program. *GEWEX News,* Vol. 11, No. 1, International GEWEX Project Office, Silver Spring, MD, 1–11.

Nijssen, B., and Coauthors, 2014: A prototype global drought information system based on multiple land surface models. *J. Hydrometeor.,* **15,** 1661–1676, doi:10.1175/JHM-D-13-090.1.

Quan, X.-W., M. Hoerling, B. Lyon, A. Kumar, M. Bell, M. Tippett, and H. Wang, 2012: Prospects for dynamical prediction of meteorological drought. *J. Appl. Meteor. Climatol.,* **51,** 1238–1252, doi:10.1175/JAMC-D-11-0194.1.

Raschke, E., and Coauthors, 1998: The Baltic Sea Experiment BALTEX: A brief overview and some selected results of the authors. *Surv. Geophys.,* **19,** 1–22, doi:10.1023/A:1006567924820.

Saha, S., and Coauthors, 2010: The NCEP Climate Forecast System Reanalysis. *Bull. Amer. Meteor. Soc.,* **91,** 1015–1057, doi:10.1175/2010BAMS3001.1.

——, and Coauthors, 2014: The NCEP Climate Forecast System version 2. *J. Climate,* **27,** 2185–2208, doi:10.1175/JCLI-D-12-00823.1.

Saji, N. H., B. N. Goswami, P. N. Vinayachandran, and T. Yamagata, 1999: A dipole mode in the tropical Indian Ocean. *Nature,* **401,** 360–363.

Scaife, A. A., and Coauthors, 2014: Skillful long-range prediction of European and North American winters. *Geophys. Res. Lett.,* **41,** 2514–2519, doi:10.1002/2014GL059637.

Schubert, S., M. Suarez, P. Pegion, R. Koster, and J. Bacmeister, 2004: On the cause of 1930s Dust Bowl. *Science,* **303,** 1855–1859, doi:10.1126/science.1095048.

Sheffield, J., G. Goteti, and E. F. Wood, 2006: Development of a 50-yr high-resolution global dataset of meteorological forcings for land surface modeling. *J. Climate,* **19,** 3088–3111, doi:10.1175/JCLI3790.1.

——, and Coauthors, 2014: A drought monitoring and forecasting system for sub-Sahara African water resources and food security. *Bull. Amer. Meteor. Soc.,* **95,** 861–882, doi:10.1175/BAMS-D-12-00124.1.

Shukla, J., 1998: Predictability in the midst of chaos: A scientific basis for climate forecasting. *Science,* **282,** 728–731, doi:10.1126/science.282.5389.728.

Shukla, S., J. Sheffield, E. F. Wood, and D. P. Lettenmaier, 2013: On the sources of global land surface hydrologic predictability. *Hydrol. Earth Syst. Sci.,* **17,** 2781–2796, doi:10.5194/hess-17-2781-2013.

——, A. McNally, G. Husak, and C. Funk, 2014: A seasonal agricultural drought forecast system for food-insecure regions of East Africa. *Hydrol. Earth Syst. Sci. Discuss.,* **11,** 3049–3081, doi:10.5194/hessd-11-3049-2014.

Sinha, T., and A. Sankarasubramanian, 2013: Role of climate forecasts and initial conditions in developing streamflow and soil moisture forecasts in a rainfall-runoff regime. *Hydrol. Earth Syst. Sci.,* **17,** 721–733, doi:10.5194/hess-17-721-2013.

Smith, A. B., and R. W. Katz, 2013: US billion-dollar weather and climate disasters: Data sources, trends, accuracy and biases. *Nat. Hazards,* **67,** 387–410, doi:10.1007/s11069-013-0566-5.

Smith, D. M., A. A. Scaife, and B. P. Kirtman, 2012: What is the current state of scientific knowledge with regard to seasonal to decadal forecasting. *Environ. Res. Lett.,* **7,** 015602, doi:10.1088/1748-9326/7/1/015602.

Sohn, S.-J., J.-B. Ahn, and C.-Y. Tam, 2013: Six month–lead downscaling prediction of winter to spring drought in South Korea based on a multimodel ensemble. *Geophys. Res. Lett.,* **40,** 579–583, doi:10.1002/grl.50133.

Stewart, R. E., and Coauthors, 1998: The Mackenzie GEWEX Study: The water and energy cycles of a major North American river basin. *Bull. Amer. Meteor. Soc.,* **79,** 2665–2683, doi:10.1175/1520-0477(1998)079<2665:TMGSTW>2.0.CO;2.

Tian, D., C. J. Martinez, and W. D. Graham, 2014: Seasonal prediction of regional reference evapotranspiration based on Climate Forecast System version 2. *J. Hydrometeor.,* **15,** 1166–1188, doi:10.1175/JHM-D-13-087.1.

Trenberth, K. E., and J. M. Caron, 2000: The Southern Oscillation revisited: Sea level pressures, surface temperatures, and precipitation. *J. Climate,* **13,** 4358–4365, doi:10.1175/1520-0442(2000)013<4358:TSORSL>2.0.CO;2.

Twedt, T. M., J. Schaake, and E. L. Peck, 1977: National Weather Service extended streamflow prediction. *Proc. 45th Western Snow Conf.,* Albuquerque, NM, Colorado State University, 52–57.

van Dijk, A. I. J. M., J. L. Peña-Arancibia, E. F. Wood, J. Sheffield, and H. E. Beck, 2013: Global analysis of seasonal streamflow predictability using an ensemble prediction system and observations from 6192 small catchments worldwide. *Water Resour. Res.,* **49,** 2729–2746, doi:10.1002/wrcr.20251.

Wada, Y., L. P. H. van Beek, N. Wanders, and M. F. P. Bierkens, 2013: Human water consumption intensifies hydrological drought worldwide. *Environ. Res. Lett.,* **8,** 034036, doi:10.1088/1748-9326/8/3/034036.

Wahr, J., S. Swenson, V. Zlotnicki, and I. Velicogna, 2004: Time-variable gravity from GRACE: First results. *Geophys. Res. Lett.,* **31,** L11501, doi:10.1029/2004GL019779.

Walker, G. T., and E. W. Bliss, 1932: World weather V. *Mem. Roy. Meteor. Soc.,* **4,** 53–84.

Wang, A., T. J. Bohn, S. P. Mahanama, R. D. Koster, and D. P. Lettenmaier, 2009: Multimodel ensemble reconstruction of drought over the continental United States. *J. Climate,* **22,** 2694–2712, doi:10.1175/2008JCLI2586.1.

Wang, F., L. Wang, H. Zhou, O. C. Saavedra Valeriano, T. Koike, and W. Li, 2012: Ensemble hydrological prediction-based real-time optimization of a multiobjective reservoir during flood season in a semiarid basin with global numerical weather predictions. *Water Resour. Res.,* **48,** W07520, doi:10.1029/2011WR011366.

Weisheimer, A., and Coauthors, 2009: ENSEMBLES: A new multi-model ensemble for seasonal-to-annual predictions—Skill and progress beyond DEMETER in forecasting tropical Pacific SSTs. *Geophys. Res. Lett.,* **36,** L21711, doi:10.1029/2009GL040896.

Wilks, D. S., 2011: *Statistical Methods in the Atmospheric Sciences.* 3rd ed. International Geophysics Series, Vol. 100, Academic Press, 676 pp.

Wood, A. W., E. P. Mauer, A. Kumar, and D. P. Lettenmaier, 2002: Long-range experimental hydrologic forecasting for the eastern United States. *J. Geophys. Res.,* **107,** 4429, doi:10.1029/2001JD000659.

Xia, Y., and Coauthors, 2012a: Continental-scale water and energy flux analysis and validation for the North American Land Data Assimilation System project phase 2 (NLDAS-2): 1. Intercomparison and application of model products. *J. Geophys. Res.,* **117,** D03109, doi:10.1029/2011JD016048.

——, and Coauthors, 2012b: Continental-scale water and energy flux analysis and validation for North American Land Data Assimilation System project phase 2 (NLDAS-2): 2. Validation of model-simulated streamflow. *J. Geophys. Res.,* **117,** D03110, doi:10.1029/2011JD016051.

Ye, A., Q. Duan, X. Yuan, E. F. Wood, and J. Schaake, 2014: Hydrologic post-processing of MOPEX streamflow simulations. *J. Hydrol.,* **508,** 147–156, doi:10.1016/j.jhydrol.2013.10.055.

Yoon, J. H., K. Mo, and E. F. Wood, 2012: Dynamic-model-based seasonal prediction of meteorological drought over the contiguous United States. *J. Hydrometeor.,* **13,** 463–481, doi:10.1175/JHM-D-11-038.1.

Yossef, N. C., H. Winsemius, A. Weerts, R. van Beek, and M. F. P. Bierkens, 2013: Skill of a global seasonal streamflow forecasting system, relative roles of initial conditions and meteorological forcing. *Water Resour. Res.,* **49,** 4687–4699, doi:10.1002/wrcr.20350.

Yuan, X., and E. F. Wood, 2012a: Downscaling precipitation or bias-correcting streamflow? Some implications for coupled general circulation model (CGCM)-based ensemble seasonal hydrologic forecast. *Water Resour. Res.,* **48,** W12519, doi:10.1029/2012WR012256.

——, and ——, 2012b: On the clustering of climate models in ensemble seasonal forecasting. *Geophys. Res. Lett.,* **39,** L18701, doi:10.1029/2012GL052735.

——, and ——, 2013: Multimodel seasonal forecasting of global drought onset. *Geophys. Res. Lett.,* **40,** 4900–4905, doi:10.1002/grl.50949.

——, ——, L. Luo, and M. Pan, 2011: A first look at Climate Forecast System version 2 (CFSv2) for hydrological seasonal prediction. *Geophys. Res. Lett.,* **38,** L13402, doi:10.1029/2011GL047792.

——, ——, N. W. Chaney, J. Sheffield, J. Kam, M. Liang, and K. Guan, 2013a: Probabilistic seasonal forecasting of African drought by dynamical models. *J. Hydrometeor.,* **14,** 1706–1720, doi:10.1175/JHM-D-13-054.1.

——, ——, J. K. Roundy, and M. Pan, 2013b: CFSv2-based seasonal hydroclimatic forecasts over conterminous United States. *J. Climate,* **26,** 4828–4847, doi:10.1175/JCLI-D-12-00683.1.

Zhao, M., and H. H. Hendon, 2009: Representation and prediction of the Indian Ocean dipole in the POAMA seasonal forecast model. *Quart. J. Roy. Meteor. Soc.,* **135,** 337–352, doi:10.1002/qj.370.

DEFINING SUDDEN STRATOSPHERIC WARMINGS

BY AMY H. BUTLER, DIAN J. SEIDEL, STEVEN C. HARDIMAN, NEAL BUTCHART, THOMAS BIRNER, AND AARON MATCH

Six decades after the discovery of sudden stratospheric warmings, their multiple, and somewhat ambiguous, definitions merit scrutiny in light of contemporary research and forecasting challenges and opportunities.

Sudden stratospheric warmings[1] (SSWs) are among the most impressive dynamical events in the physical climate system. Driven by the breaking of planetary waves propagating up from the troposphere, these events involve a large and rapid temperature increase (>30–40 K in a matter of days) in the mid- to upper stratosphere (30–50 km) and, in the most extreme cases, a reversal of the climatological westerly zonal-mean zonal winds associated with the stratospheric polar night jet (e.g., Scherhag 1952; Quiroz 1975; Labitzke 1977; Schoeberl 1978). Figure 1 demonstrates the rapid changes in the stratosphere during these events, which typically manifest in one of two ways (or both[2]): either the vortex is displaced entirely off the pole (Fig. 1a) or the vortex is split into two smaller vortices (Fig. 1b; see also supplement).

Impressive in their own right, SSWs are also important because associated temperature and wind anomalies can descend downward into the troposphere on time scales of weeks to months (e.g., Baldwin and Dunkerton 2001), with significant impacts on Northern Hemisphere wintertime surface climate. The tropospheric response to SSWs closely resembles the negative phase of the North Atlantic Oscillation (NAO), involving an equatorward shift of the North Atlantic storm track; extreme cold air outbreaks in parts of North America, northern Eurasia, and Siberia; and strong warming of Greenland, eastern Canada, and southern Eurasia (e.g., Thompson et al. 2002). Major midwinter SSWs rarely occur in the Southern Hemisphere, largely because of smaller planetary-wave amplitudes (Van Loon et al. 1973), though a notable exception occurred in September 2002 (Allen et al. 2003; see special issue of the *Journal of Atmospheric Sciences*, 2005, Vol. 62, No. 3). SSWs play a major role in Arctic and Antarctic ozone variability (e.g., Schoeberl and Hartmann 1991), and stratospheric transport and chemistry (e.g., Manney et al. 2009). SSWs can also influence the transport of tropospheric CO_2 and pollutants (Jiang et al. 2013), the extension of the El Niño–Southern Oscillation (ENSO) teleconnection into Eurasia (e.g., Ineson and Scaife 2009; Butler et al. 2014b), decadal variability in the North Atlantic Ocean circulation (Reichler

[1] *Stratospheric sudden warming* and *sudden stratospheric warming* have been used interchangeably in the literature. Note, however, that *sudden stratospheric warming* corresponds more closely to the original German *Stratosphärenerwärmung* (Scherhag 1952), where *stratospheric* and *warming* become one word. Clear and unambiguous acronyms may facilitate efforts by organizations such as the American Meteorological Society to maintain acronym reference lists and improve scientific communication (Heideman 2014).

[2] Split vortices are also typically displaced from the pole.

et al. 2012), equatorial tropospheric convective activity (e.g., Kodera 2006), polar tropospheric clouds (Kohma and Sato 2014), and mesospheric dynamics and the breakdown and reformation of the stratopause (e.g., Siskind et al. 2007; Manney et al. 2008).

Scientists have been trying to understand, monitor, and classify SSWs for over 60 years. As with any noteworthy weather or climate phenomena (El Niño–Southern Oscillation, hurricanes, drought, tornadoes, etc.), reaching community agreement on a standard way to define events is an extremely challenging, though useful, endeavor. We believe that improved observations and better understanding of SSWs in recent decades make this an ideal time to reevaluate and/or clarify the standard definition of SSWs and its purpose. To this end, the key objectives of this paper are 1) to describe the historical background and evolution of the SSW definition, demonstrating the lack of an unambiguous current "standard" definition; 2) to examine how differences among a number of proposed definitions can affect the interpretation of observed and simulated SSW frequency, implying a need for a standard definition for certain applications; 3) to argue that for statistical applications that depend on a robust metric of events, such as model intercomparisons of the stratosphere, a standard definition is necessary; and 4) to describe current efforts to gather community input and to suggest possible ways to proceed to update the standard SSW definition.

HISTORY OF SSW DEFINITIONS. Richard Scherhag first observed "explosive warmings in the stratosphere" (which he referred to as the "Berlin phenomenon") in radiosonde measurements in Berlin, Germany, in January/February 1952 (Scherhag 1952, p. 53). Within about a decade, and as part of the International Years of the Quiet Sun (IQSY) 1964–65, the World Meteorological Organization (WMO) Commission for Atmospheric Sciences (CAS; originally called the Commission for Aerology) developed an international SSW monitoring program called STRATALERT, based on available radiosonde and rocketsonde observations. The program, led by Karin Labitzke at the Freie Universität Berlin, involved teams at meteorological centers in Washington, D.C.; Tokyo, Japan; Berlin; and Melbourne, Australia. A major goal was to "aid in the co-ordination of normal and special observations, particularly throughout the Northern Hemisphere, relating to the physical conditions in the 20-90 km height range of the atmosphere" (WMO/IQSY 1964, p. 7) during an SSW, which by that time had been observed only a few times. From these early monitoring efforts, various definitions for SSWs were developed and appeared in the scientific literature over the latter half of the twentieth century (the STRATALERT program continued until 2004). Because some of the references are not readily available, and for historical completeness, we include a detailed table of major references stating SSW definitions in the electronic supplement to this article (http://dx.doi.org/10.1175/BAMS-D-13-00173.2; see Table ES1).

As evident from these references, definitions for SSWs have changed over time. An early definition for major SSWs based on temperature changes (WMO/IQSY 1964) evolved to one using the reversal of the stratospheric zonal-mean zonal wind circulation, the basic concepts of which have endured in some form since the late 1970s. The appeal of a definition based on the zonal circulation originates in work by Charney and Drazin (1961), Matsuno (1971), and others (O'Neill and Taylor 1979; Palmer 1981), who demonstrated that planetary-scale stationary waves cannot propagate into easterly flow. Thus, following a major SSW in which the stratospheric winds reverse from climatological-mean westerly flow to easterly flow, waves can no longer propagate upward above the level of the reversal and so subsequently break at lower and lower levels in the stratosphere, reversing the wind downward from the upper stratosphere to the lower stratosphere. The reversal of the zonal circulation is thus a fundamental characteristic of major SSWs and their associated dynamics.

Because STRATALERT was organized under the WMO CAS, we have searched all meeting reports of those commissions, and of the WMO Executive

AFFILIATIONS: Butler—Cooperative Institute for Research in Environmental Sciences, University of Colorado, and National Oceanic and Atmospheric Administration/Earth System Research Laboratory/Chemical Sciences Division, Boulder, Colorado; Seidel—National Oceanic and Atmospheric Administration/Air Resources Laboratory, College Park, Maryland; Hardiman and Butchart—Met Office Hadley Centre, Exeter, United Kingdom; Birner—Colorado State University, Fort Collins, Colorado; Match—Cornell University, Ithaca, New York
CORRESPONDING AUTHOR: Amy Butler, NOAA/ESRL/CSD, 325 Broadway, Boulder, CO 80305-3337
E-mail: amy.butler@noaa.gov

The abstract for this article can be found in this issue, following the table of contents.
DOI:10.1175/BAMS-D-13-00173.1

A supplement to this article is available online (10.1175/BAMS-D-13-00173.2)

In final form 12 December 2014

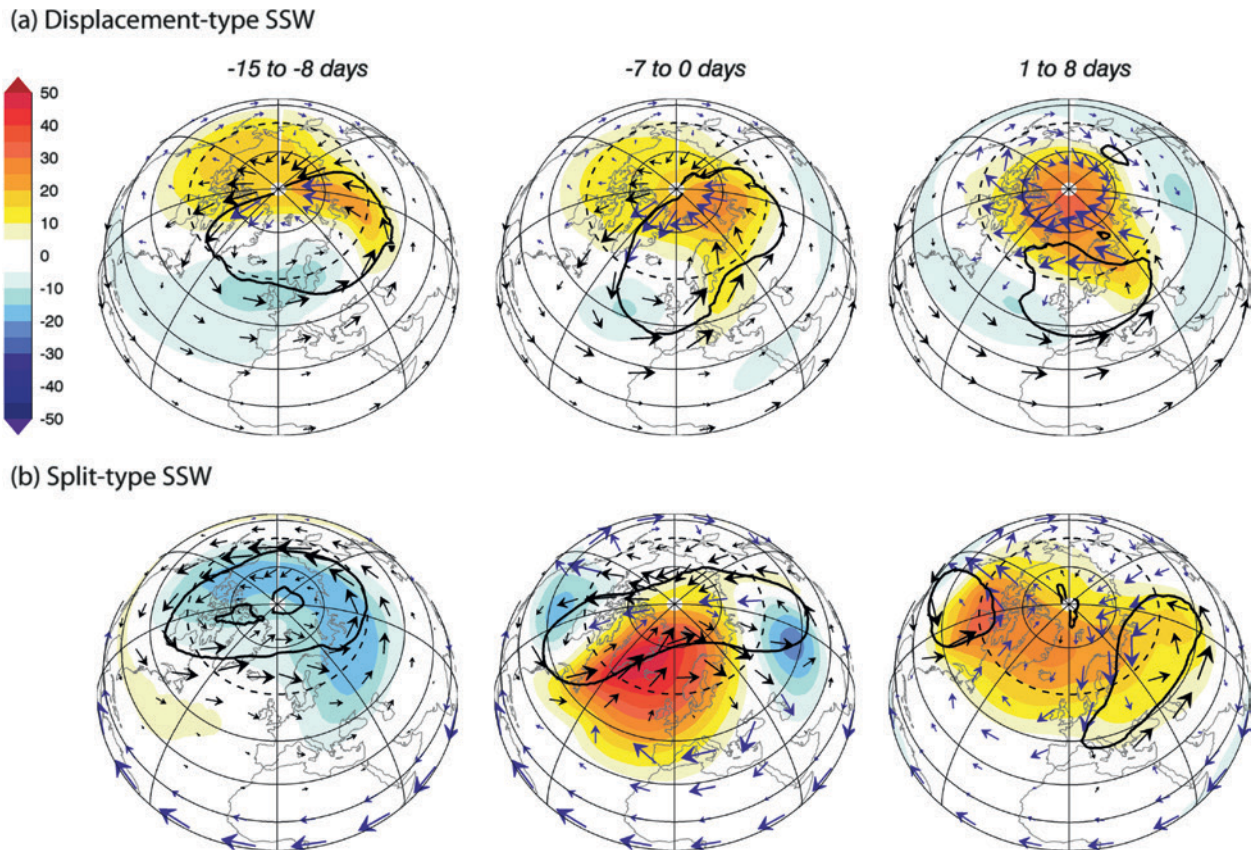

Fig. 1. (a) A displacement-type SSW event on 21 Jan 2006 and (b) a split-type SSW event on 24 Jan 2009, for the average of (left) 8–15 days prior to the event, (middle) 7 days prior to the event, and (right) 1–8 days following the event. ERA-Interim temperature anomalies (based on 1979–2012 climatology) at 10 hPa (K) are shaded. The black solid line marks the 7-PVU contour (1 potential vorticity unit = 10^{-6} K kg^{-1} m^2 s^{-1}) at 10 hPa and indicates the shape of the polar vortex. The arrows indicate the full zonal and meridional wind fields at 10 hPa (arrows with a westerly zonal component are black; arrows with an easterly zonal component are blue). The 60°N latitude line is dashed. A complete movie of these events can be found online (http://dx.doi.org/10.1175/BAMS-D-13-00173.2**).**

Committee and Congress, since the 1950s for language related to the SSW definition. The SSW definition was last formalized by the CAS in 1978, but two reports published that year offer two different interpretations. McInturff (1978, p. 19) (published in January 1978) states that the WMO CAS

> has adopted the following definitions: 1. A stratospheric warming is called minor if a significant temperature increase is observed (i.e., at least 25 degrees in a period of a week or less) at any stratospheric level in any area of the wintertime hemisphere, measured by radiosonde or rocketsonde data and/or indicated by satellite data; and if criteria for major warmings are not met. Less extreme warmings will be referred to as warming pulses. 2. A stratospheric warming can be said to be major if at 10 mb or below the latitudinal mean temperature increases poleward from 60 degrees latitude and an associated circulation reversal is observed (i.e., mean westerly winds poleward of 60° latitude are succeeded by mean easterlies in the same area).

Yet a WMO CAS report (WMO CAS 1978, p. 36, item 9.4.4) published two months later, while stating the same definition for minor SSWs, states: "'major' warmings [occur] with a temperature increase of at least 30 degrees in a week or less at 10 mb or below, or by at least 40 degrees above 10 mb." No criteria about the circulation reversal are mentioned in this WMO CAS report.

These discrepancies between two closely timed early publications are emblematic of the sorts of variations in definitions of SSWs that are pervasive in the literature over the last three decades. While the zonal wind reversal diagnostic (e.g., McInturff 1978) has been the dominant basis for the definition of major SSWs in recent decades, the application of the SSW

Table 1. Nine SSW definitions used in this paper, the details of their calculations, and the average number of major SSWs per year for each definition using 57 winters in NCEP–NCAR (NNR; Jan 1958—Apr 2014) and ERA-40 (Jan 1958–Mar 1989)/ERA-interim (Mar 1989–Apr 2014). Abbreviations for each definition are used in Figs. 2 and 5b.

Definition	Description	SSW per year NNR	SSW per year ERA
Zonal wind and temperature gradient reversal (U&T)	Events occur when the zonal-mean zonal winds at 10 hPa and 60°N fall below 0 m s^{-1} from Nov to Mar. Events that do not also have a meridional temperature gradient reversal (defined as the zonal-mean temperatures averaged from 80° to 90°N minus the temperatures averaged from 60° to 70°N) within ~10 days of the circulation reversal are excluded. Events must return to westerly (>0 m s^{-1}) for at least 20 consecutive days between events. The winds must return to westerly for at least 10 consecutive days prior to 30 Apr (or an event is considered a final warming).	0.58	0.65
Zonal wind reversal at 60°N (CP07)	Events occur when the zonal-mean zonal winds at 10 hPa and 60°N fall below 0 m s^{-1} from Nov to Mar. Events must return to westerly (>0 m s^{-1}) for at least 20 consecutive days between events. The winds must return to westerly for at least 10 consecutive days prior to 30 Apr (or an event is considered a final warming).	0.61	0.65
Zonal wind reversal at 65°N (U65)	Identical to CP07, except using zonal-mean zonal wind at 65°N.	0.77	0.84
Zonal winds averaged from 60° to 90°N (U6090)	Events occur when the zonal-mean zonal winds at 10 hPa, cosine weighted and averaged from 60° to 90°N, fall below 0 m s^{-1} from Nov to Mar. Identical to U60 except using the 60°–90°N averaged zonal-mean zonal wind.	0.81	0.91
Vortex moments* (MOM)	Details can be found in Mitchell et al. (2011) and Seviour et al. (2013). The gridded geopotential height field at 10 hPa is used to find vortex moments: the aspect ratio and centroid latitude. The vortex edge is taken to be the mean value of the Dec–Mar (DJFM) heights at 10 hPa and 60°N. Displacement events occur when the centroid latitude is equatorward of 66°N for 7 days or more. Split events occur when the aspect ratio is greater than 2.4 for 7 days or more. If splits or displacements occur within 30 days of each other, then only the first event qualifies.	0.49	0.68
Polar cap–averaged geopotential height anomalies (ZPOL)	Anomalies of zonal-mean geopotential heights at 10 hPa are found following Gerber et al. (2010). The polar cap anomalies are found by averaging (cosine weighted) anomalies from 60° to 90°N. This (year-round) time series is standardized about the JFM mean (as in Thompson et al. 2002). Events occur when the time series exceed plus three standard deviations. An event that occurs within 60 days after another is excluded.	0.65	0.61
EOF of zonal-mean geopotential height anomalies (EOFZ)	Anomalies of zonal-mean geopotential heights at 10 hPa are found following Gerber et al. (2010). The first EOF is then calculated for anomalies 20°–90°N, after weighting by the square root of the cosine of latitude. The first principal component time series (PC1) is then found by projecting the unweighted original anomaly data onto the first EOF and then standardizing the resulting time series (see Baldwin and Thompson 2009). Events occur when the PC1 index falls below –3 standard deviations (where the negative phase of the EOF is defined by anomalously high heights over the polar cap). An event that occurs within 60 days after another is excluded.	0.65	0.60

Table 1. Continued.			
Definition	**Description**	**SSW per year NNR**	**SSW per year ERA**
EOF of zonal-mean zonal winds (EOFU)	The method for EOFZ (above) is used, but zonal-mean zonal wind anomalies at 50 hPa and 20°–90°N (PC1 < ~3 std dev) are instead analyzed. Similar to Limpasuvan et al. (2004).	0.46	0.49
Temperature changes >40°C in a week or less (TMP)	Zonal-mean temperatures, Nov–Mar, 100–10 hPa, poleward of 60°N. Events occur when any grid cell in this region exceeds a 40°C change in one week. An event that occurs within 60 days after another is excluded.	0.37	0.35

* The SSW dates using the vortex moments definition have been calculated by W. Seviour, Department of Physics, University of Oxford (Seviour et al. 2013), through 2012; dates for 2013–14 have been calculated by A. Butler.

definition varies considerably. Some of these interpretations include the following: using only the 10-hPa level (very common; data at pressures less than 10 hPa are rarely used); using zonal-mean zonal winds at a single latitude (60° or 65° latitude; e.g., Labitzke and Naujokat 2000) rather than zonal winds poleward of 60°; using polar cap–averaged zonal winds poleward of 60° latitude (vs the more stringent requirement that zonal-mean zonal winds reverse at each latitude poleward of 60°); and evaluating minor warmings not by a temperature tendency but rather as those warmings that do not reverse the circulation (e.g., Andrews et al. 1987). This evolutionary history suggests that a true standard definition of SSWs is at best ambiguous and at worst nonexistent.

Additional warming classifications (beyond minor and major) also appear in the literature (e.g., Labitzke 1981; Meriwether and Gerrard 2004). These include Canadian warmings (early winter warmings marked by an eastward shift of the Aleutian high) and final warmings (abrupt, dynamically forced warmings in both hemispheres, after which the winter cyclonic vortex does not recover). But different studies implement these classifications in different ways. For example, some studies (e.g., Charlton and Polvani 2007, hereafter CP07) classify Canadian warmings as major warmings if a circulation reversal occurs, while Labitzke (1977) argues against this based on differences in synoptic development.

The determination of final warmings also varies. Some studies (e.g., CP07; Bancalá et al. 2012) consider some March events to be major midwinter[3] events rather than final warmings if the vortex returns to a westerly state or to a certain amplitude for a certain number of days before the end of winter. Both midwinter and final warmings have important (and often similar) influences on the atmosphere. The frequency of major midwinter SSWs is an important metric of polar stratospheric wintertime variability (final warmings occur every winter, so they do not contribute to the total frequency). The seasonal timing of final warmings each winter is also an important metric of interannual stratospheric variability. What constitutes "midwinter" and how to determine which warmings are final are aspects of current definitions that remain imprecise.

New diagnostics[4] for characterizing SSWs (including minor, major, and final warmings) have been proposed as a result of technological advances and scientific needs. Freie Universität Berlin produced continuous daily stratospheric maps since the late 1950s for STRATALERT activities based largely on radiosonde measurements, which are unique because unlike reanalyses, there are no jumps or irregularities due to model updates, different streams, or upper-boundary effects (Labitzke et al. 2002; Labitzke and Kunze 2005). Like other traditional synoptic analyses, these contain a certain degree of subjectivity. More comprehensive observations from satellites and improved stratospheric model simulations (e.g., Rind et al. 1988; Manzini and Bengtsson 1996; Erlebach et al. 1996; Charlton et al. 2007) have

[3] The adjective *midwinter* in the recent literature has often been used to refer to all, or most, wintertime (November–March) warmings except the final warming—not, as might be assumed, to those warmings occurring only in the middle of winter.

[4] Here, we use *diagnostics* to refer to any technique that may be used to examine particular aspects of SSWs and their evolution; in combination with threshold limits and usage guidelines, diagnostics may form "definitions."

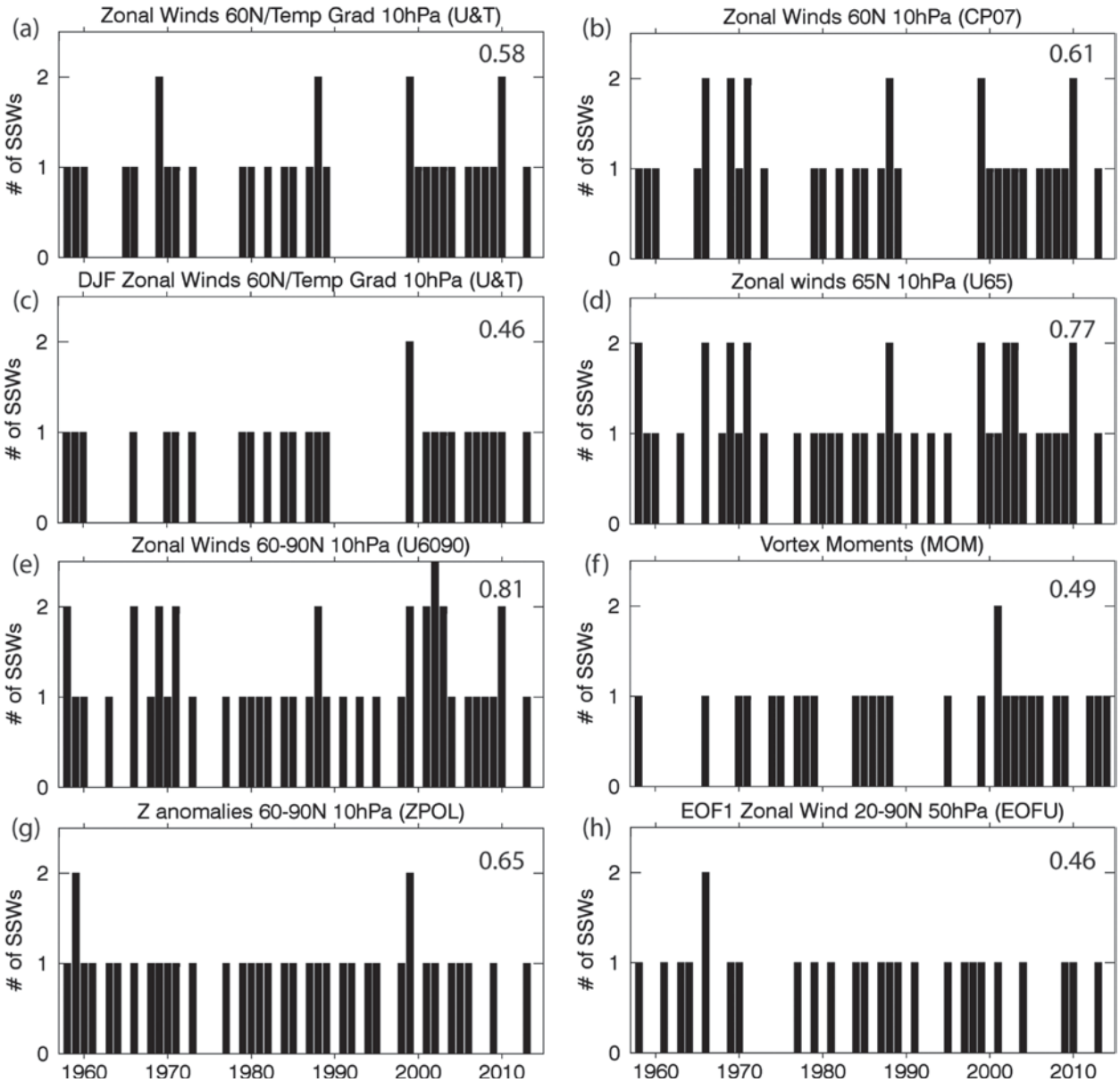

Fig. 2. Time series (using NCEP–NCAR reanalysis from 1958 to 2014) of major midwinter SSWs as defined using seven different definitions (described in Table 1): (a) zonal-mean zonal winds at 60°N and 10 hPa, and a temperature gradient reversal; (b) zonal-mean zonal winds at 60°N and 10 hPa, following guidelines by CP07; (c) as in (a), but for Dec–Feb only; (d) zonal-mean zonal winds at 65°N and 10 hPa; (e) zonal-mean zonal winds at 10 hPa and averaged from 60° to 90°N; (f) vortex moment diagnostics; (g) geopotential height (Z) anomalies averaged from 60° to 90°N at 10 hPa, exceeding three standard deviations of the Jan–Mar (JFM) mean climatology; and (h) the leading EOF of zonal wind anomalies from 20° to 90°N and 50 hPa. The abbreviations correspond to those in Table 1. The average number of SSWs per winter is given in the top-right corner of each panel (corresponding values for ERA-40/ERA-Interim are given in Table 1).

led to an improved understanding of SSWs and their impacts. Diagnostics, many of which are the basis for various SSW definitions (Table 1), include the following:

- Zonal-mean zonal winds at 10 hPa and 60° latitude (Christiansen 2001; CP07)
- Reversal of the meridional zonal-mean temperature gradient poleward of 60° latitude, usually used in combination with a reversal of the zonal-mean zonal winds at or poleward of 60° latitude (e.g., Labitzke 1981; Ayarzagüena et al. 2013)
- Empirical orthogonal functions (EOFs) of a) gridded pressure-level data of either geopotential height

anomalies (Baldwin and Dunkerton 2001; Baldwin 2001) or zonal wind anomalies (Limpasuvan et al. 2004); b) zonal-mean geopotential height anomalies (Baldwin and Thompson 2009; Gerber et al. 2010); and c) vertical profiles of polar cap–averaged temperature (Kuroda and Kodera 2004; Hitchcock and Shepherd 2013; Hitchcock et al. 2013)
- Polar cap–averaged geopotential height anomalies at 10 hPa (e.g., Thompson et al. 2002)
- Tendency of the northern annular mode index at 10 hPa (Martineau and Son 2013), polar cap temperature (Nakagawa and Yamazaki 2006), or the zonal-mean zonal wind at 10 hPa near 60°N (Birner and Albers 2015)
- k-means clustering technique (Coughlin and Gray 2009)
- Vortex geometry, including vortex moments (Waugh and Randel 1999; Matthewman et al. 2009; Hannachi et al. 2011; Mitchell et al. 2011, 2013; Seviour et al. 2013)
- Wavenumber of the disturbed vortex (Johnson et al. 1969; O'Neill and Taylor 1979)
- Supervised learning approach/neural networks (Blume et al. 2012)

Each diagnostic has unique characteristics; for example, EOFs of stratospheric height anomalies may be more strongly coupled to the troposphere compared to zonal-mean zonal winds (Baldwin and Thompson 2009), and vortex moment diagnostics are more physically linked to potential vorticity dynamics. Diagnostics that capture stratosphere–troposphere coupling are appealing from the perspective of physical understanding and potential societal impacts, as are those that provide a simple metric of SSW occurrence for climate model intercomparison and validation.

One of the most commonly used SSW definitions (pertaining to major midwinter SSWs) in the recent literature is based on the diagnostic of zonal-mean zonal wind at 60° latitude and 10 hPa and is described in detail by CP07. The CP07 definition is likely popular because of its simplicity (one variable at one latitude and pressure level) and because it includes detailed implementation guidelines pertaining to a) the separation of closely timed events[5] (i.e., if the zonal-mean zonal wind reverses twice within a short period of time, are those events considered separate and independent?), b) exclusion of final warmings, and c) identification of split-type events. In recent years, this definition has commonly (but mistakenly) been cited as "the WMO definition." However, it lacks the meridional temperature gradient reversal requirement and the consideration of zonal winds poleward of 60° latitude in the McInturff (1978) definition. Moreover, the CP07 definition clearly distinguishes between late midwinter and final warmings, requiring zonal-mean zonal winds to return to westerly for at least 10 days prior to 30 April to be classified as a major midwinter event. As demonstrated in the next section, these distinctions matter.

SENSITIVITY OF SSW CLASSIFICATION TO THE DEFINITION. If identification of major midwinter SSWs were not sensitive to definition, then the differences in the literature would be moot. But this is not the case because of the highly variable nature of SSW events and of wintertime stratospheric dynamics. Figure 2 shows the number of major SSWs per year for seven different definitions described in Table 1, applied to the National Centers for Environmental Prediction–National Center for Atmospheric Research (NCEP–NCAR) reanalysis (Kalnay et al. 1996) from 1958 to 2014 (Fig. 2c is the same as Fig. 2a, but for December–February events only). The average number of major SSWs per winter for this 57-yr period range from 0.46 to 0.81 per winter among the seven definitions, and the dates of major SSWs for each definition differ substantially (see also Table ES2). In fact, of the 26–46 SSWs identified in each definition, only 13 SSWs are identified by all seven definitions using NCEP–NCAR reanalysis data. Using different reanalyses (or six-hourly winds rather than daily-averaged winds, or data on a coarser horizontal grid) produces slightly different results. Tables 1 and ES2 compare the number of major SSWs per winter in NCEP–NCAR and in the 40-yr European Centre for Medium-Range Weather Forecasts (ECMWF) Re-Analysis (ERA-40)[6] (Uppala et al. 2005)/ERA-Interim (Dee et al. 2011) from 1958 to 2014[7] and demonstrate that certain definitions are more sensitive to differences between reanalysis products than others.

Some definitions show noticeably more decadal variability than others. For example, the definitions

[5] Note the corrected guidelines in the corrigendum to Charlton and Polvani (2007).

[6] We employ the NCEP–NCAR and ERA-40 reanalyses here because they extend prior to 1979, and thus they allow better statistics of SSW events. Many of these events have been independently verified in prior studies. However, these reanalysis datasets may poorly represent polar stratospheric processes (e.g., Manney et al. 2003) and may be poorly constrained prior to 1979 when satellite observations became abundant.

[7] Here ERA-40 is used from 1958 to 1 March 1989, and ERA-Interim thereafter, following the justification for combining the datasets in Blume et al. (2012).

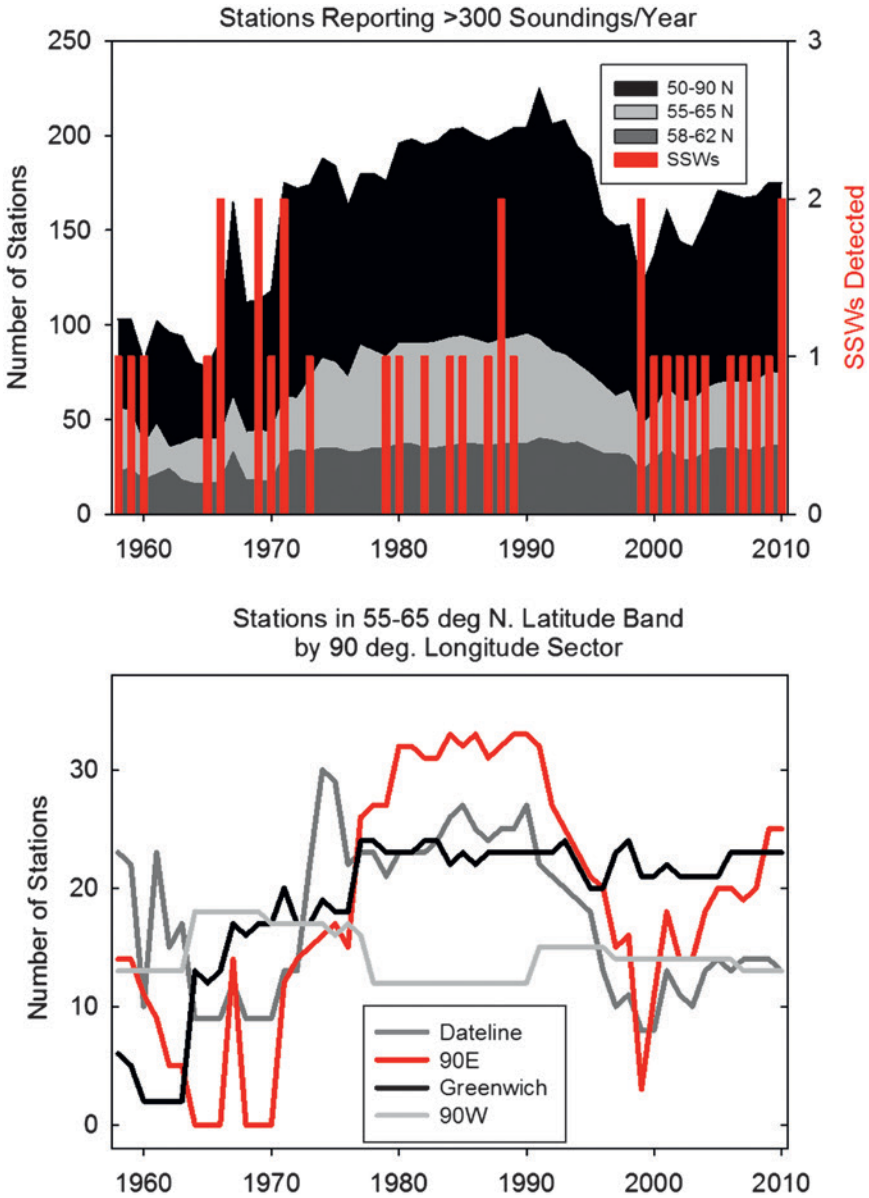

Fig. 3. (top) The number of radiosonde stations reporting >300 soundings per year in different latitude bands, from 1958 to 2010. Red bars indicate the occurrence of SSWs (from Fig. 2b, the CP07 method). (bottom) The number of stations reporting in the 55°–65°N latitude band as a function of longitude quadrant (centered on the given longitude).

based on zonal-mean zonal winds at 60°N yield no major warmings during most of the 1990s, when other definitions, including one based on zonal-mean zonal wind reversal at 65°N, show two to five major SSWs during that decade (Fig. 2). Why do these differences—among the definitions and over time—exist? One contributing factor may be changes in the observations assimilated into reanalyses. Definitions based on one latitude or region may be more sensitive to this than definitions based on larger domains. This explanation appears possible in light of changes in the Northern Hemisphere radiosonde network (Fig. 3). The number of regularly reporting radiosonde stations in the region 50°–90°N increased from the 1960s to the 1980s, but then it dramatically decreased in the 1990s in association with the collapse of the Union of Soviet Socialist Republics (USSR; ~45°–135°E) and parts of its meteorological networks. The timing of the largest reduction in radiosonde observations from 55° to 65°N (which is especially noteworthy in the region of the former USSR; not shown) roughly coincides with the period when few major SSWs are detected using the zonal-mean zonal wind reversal at 60°N. We find it worth noting that the definition most dependent on this particular latitude detects the fewest major SSWs during a decade that experienced the greatest loss of measurements there.

Arguably, assimilation of satellite data into the reanalysis products used to calculate SSW events here should somewhat mitigate the sampling inhomogeneities in radiosonde observations. Moreover, major SSW events are still detected in the early 2000s despite reduced numbers of radiosonde stations. The mid-1990s are known to have been particularly cold years in the Arctic stratosphere (e.g., Pawson and Naujokat 1999), which argues against invoking sampling issues to explain the lack of detected SSWs in the 1990s. On the other hand, the fact that the zonal-mean zonal wind diagnostic at 65°N rather than 60°N does detect major SSWs in the 1990s suggests sensitivity to this particular latitude.

This begs the question: Is 60° latitude a reasonable choice for defining SSWs, particularly now that

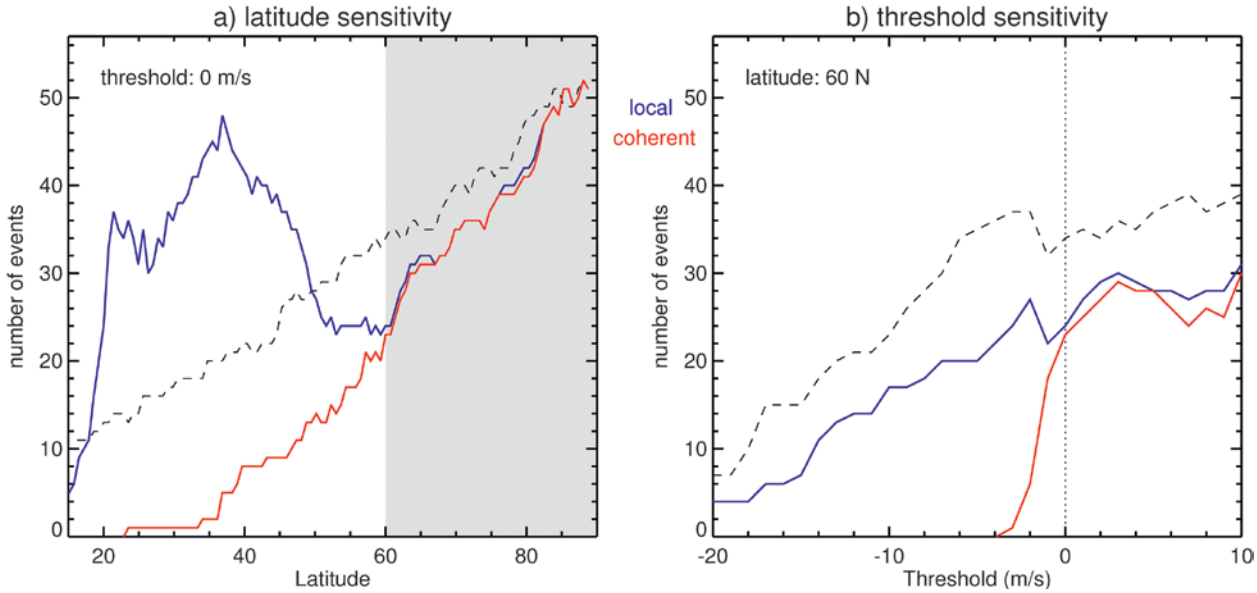

Fig. 4. (a) The number of SSWs (during 1979–2012, in ERA-Interim) as a function of latitude where the zonal wind reverses from westerly to easterly (0 m s^{-1} critical threshold). (b) The number of SSWs as a function of critical threshold (i.e., the wind speed below which a warming is considered to occur), for zonal wind at 60°N. "Local" events (blue) occur when the zonal winds at one particular latitude fall below the critical threshold. "Coherent" reversals (red) occur when the zonal winds at every latitude poleward of the given latitude also fall below the critical threshold within 20 days. "Averaged" reversals (black dashed) occur when the zonal winds averaged from a particular latitude to 90°N fall below the critical threshold. Note: no temperature gradient criterion is applied here, Nov–Mar zonal winds are used, and we follow the CP07 criteria for separation of events and determination of final warmings.

near-global satellite measurements are available? Does this latitude represent some key physical feature of stratospheric circulation? Or does it make sense to choose a more poleward latitude, average over a larger latitude region, or (more stringently) require a reversal of the zonal winds everywhere poleward of a particular latitude? Figure 4a shows the dependence of major SSW frequency on the latitude of circulation reversal. When major SSWs are diagnosed using the reversal of the zonal-mean zonal winds at one latitude only (local reversal, blue line), the number of major SSWs (1979–2012) minimizes if that latitude is between 50° and 60°N. To understand this result, we also consider the number of major SSWs that occur if instead the zonal winds everywhere poleward of a particular latitude must also reverse direction (coherent reversals, red line). Poleward of 60°N, the local and coherent reversal requirements yield nearly identical numbers of SSWs; anywhere in this region, if the wind reverses from westerly to easterly at one latitude, it is also almost certain that the wind is reversing everywhere poleward of that latitude. Equatorward of 60°N, however, the number of coherent reversals continues to decrease while the number of local reversals increases. This bifurcation can be explained by noting that these latitudes mark the surf zone (McIntyre and Palmer 1984), where breaking waves can drive local reversals in the stratospheric circulation, which is not associated with coherent polar vortex dynamics. Thus, 60°N is near the average edge of the coherent polar vortex.

A more subtle aspect of the definitions based on zonal-mean zonal wind diagnostics also affects SSW identification. If one interprets the McInturff (1978) definition, for example, as meaning that the zonal-mean zonal winds everywhere poleward of 60°N must coherently reverse from westerly to easterly, then Fig. 4a suggests that using just 60°N will yield essentially the same events. On the other hand, if one interprets this definition as meaning that the zonal-mean zonal winds averaged from 60° to 90°N must reverse (black dashed line), then about 30% more events will be detected compared to using 60°N only (or coherent reversals from 60°N). Defining the reversals near 65°N rather than 60°N reduces that difference to about 10%, thus minimizing the effect of the different interpretation.

The stratosphere experiences low-frequency variability on interannual and decadal time scales, as well as long-term trends, due to both natural variability like the solar cycle (e.g., Labitzke et al. 2006) and anthropogenic change (e.g., Butchart et al. 2000; Scaife et al. 2005). It is possible then that the polar vortex edge also varies, so that during some years or decades 60°N may be within the surf zone and therefore not

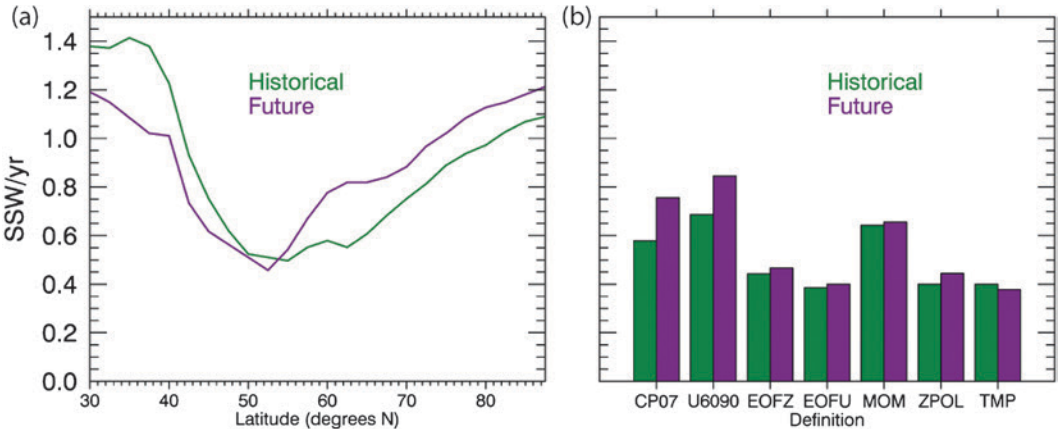

Fig. 5. (a) Average number of SSWs per year using the CP07 zonal wind definition (local reversals) evaluated at different latitudes, for the historical simulation (1860–2005, green) and the climate change simulation (2006–99, purple) in HadGEM2-CCS. (b) Average number of SSWs per year for seven different definitions (described in Table 1), for the historical and climate change simulations.

a suitable place at which to evaluate SSWs. Using historical (1860–2005) and future [2006–99; representative concentration pathway 8.5 (RCP8.5)] climate simulations from the Hadley Centre Global Environment Model, version 2—Carbon Cycle Stratosphere (HadGEM2-CCS) model (Hardiman et al. 2012; Osprey et al. 2013), we consider the frequency of major SSWs using the zonal-mean zonal wind reversal definition at a particular latitude (Fig. 5a). We find that a) in the historical simulation, the separation between the surf zone and the coherent vortex zone resembles the observations (Fig. 4a); and b) in the future simulation, the frequency of major SSWs detected using the zonal wind reversal at a particular latitude increases at every latitude poleward of ~55°N, and that there is a slight equatorward shift in the region experiencing a minimum of reversals between the surf and coherent zones. In other words, whereas 60°N is historically at the edge of the polar vortex, this model simulation suggests 60°N will be well within the coherent vortex in a future climate.

SSW classification is also sensitive to the threshold used to determine an extreme event. In some cases, like EOF-based definitions, the threshold (usually two or three standard deviations) is not dynamical but statistical. For definitions based on zonal wind reversal, the threshold is the speed to which the zonal winds must decelerate. From a dynamical perspective, an appealing threshold represents the wind speed below which waves cannot propagate, leading to wave breaking and descent of the circulation anomalies. In linear planetary-wave theory (Charney and Drazin 1961) and critical-layer theory (Matsuno 1971), stationary planetary waves (i.e., waves with zero phase speed) cannot propagate into easterly winds, and the current threshold of 0 m s^{-1} seems an obvious choice. One question to consider, particularly for impact or stratosphere–tropospheric coupling studies, is whether the dynamical impacts following a wind deceleration to 1–5 m s^{-1} (or some other nonzero value, i.e., minor warmings) are essentially equivalent to the impacts of a complete wind reversal. Figure 4b also suggests that the major SSW frequency is (perhaps surprisingly) not highly sensitive to the critical threshold (for threshold values between 0 and 10 m s^{-1}). Nonetheless, for a standard definition, which by construction requires some threshold criteria, the 0 m s^{-1} threshold seems justifiable based on dynamical arguments.

Finally, certain SSW definitions can be sensitive to changes in the background climatology of the polar wintertime stratosphere. In Fig. 5b, we consider the average number of major SSWs per year, using seven different definitions from Table 1, for historical and future climate simulations from the HadGEM2-CCS model. Whereas the definition using zonal-mean zonal wind at 60°N (CP07), or the polar cap–averaged winds (U6090), shows a significant (at the 90% confidence level) increase in major SSWs in the future, other definitions like those using EOF-based diagnostics show insignificant changes. This result is in agreement with other modeling studies (McLandress and Shepherd 2009; Bell et al. 2010) that indicate an increased major SSW frequency in future climate using the zonal-mean zonal wind reversal criteria, though this result appears to be model dependent (Mitchell et al. 2012; Ayarzagüena et al. 2013). McLandress and Shepherd (2009) also note that the increase in major SSW frequency occurs only for definitions based on zonal wind diagnostics but not for definitions based on anomalies relative to

the contemporaneous climatology. They argue that simulated weaker climatological westerly winds in the polar wintertime stratosphere allow variations in the zonal wind to fall below the 0 m s^{-1} critical threshold more easily, so the increase in major SSW frequency for those definitions may be at least partially due to changes in the climatological state rather than changes in polar wintertime stratospheric variability.

Two perspectives are prevalent regarding the effect of changes in climatology on the SSW definition (e.g., Mitchell et al. 2012). One viewpoint maintains that using the absolute sign change of the stratospheric winds as a measure of major SSW frequency can be interpreted as a change in stratospheric variability, but that it may actually only reflect changes in the climatological state of the vortex; therefore, long-term changes in climatology need to be considered (an analogous example is the adaptation by the National Oceanic and Atmospheric Administration of the ENSO definition to update sea surface temperature climatologies, to account for warming that might erroneously suggest that warm El Niño events are increasing; L'Heureux et al. 2013). The alternative viewpoint is that even if more major SSWs occur only because the thresholds are easier to meet in a weaker westerly climatology, that the stratospheric zonal circulation is still reversing, which has real dynamical implications following the events.

This issue of a variable background state may be relevant even on shorter interannual to decadal time scales. For example, the Northern Hemisphere stratospheric polar vortex was particularly strong during the 1990s (Shindell et al. 1999; Pawson and Naujokat 1999; Manney et al. 2005). Though it is possible that the polar vortex winds were stronger because there were fewer SSWs, it is also conceivable that SSW definitions based on zonal wind diagnostics, particularly at a single latitude like 60°N, might have been less likely to meet the threshold value of 0 m s^{-1} during an extended period of stronger-than-normal westerly flow (particularly because other SSW definitions detect major events during this decade; Fig. 2). Another example may be modeling studies that find fewer major SSWs in models with an overly strong climatological polar vortex using zonal-mean zonal wind diagnostics (Charlton et al. 2007).

We have demonstrated that major SSW identification can be quite sensitive to the definition used and its interpretation and implementation. Aside from latitude and wind speed threshold, results are also sensitive to the pressure level (altitude) considered, the climatology chosen for definitions involving anomalies, and the climatological-mean state of the stratosphere itself and its low-frequency variability.

RECOMMENDATIONS AND OPPORTUNITIES. Is a "standard" SSW definition necessary? The analysis above suggests that it would be impossible to find a single definition to serve every purpose or describe every event perfectly. We believe that the primary purpose of a standard SSW definition should be to characterize polar stratospheric wintertime variability; examining other aspects, like the stratosphere–troposphere coupling of these events, arguably requires different diagnostics. Some applications, like forecasting SSWs, may benefit from a standard definition for the sake of consistency across international operating centers, but they also require further detailed diagnosis for each event.

A standard definition is useful primarily for statistical applications, such as the robust assessment and intercomparison of major SSW frequency in observational datasets and historical/future climate simulations, and between different model generations. For example, Fig. 5b shows the large differences in SSW frequencies for different definitions when applied to historical and future climate simulations. A standard definition allows for consistency across observational and modeling studies. Without consistency, it is difficult to evaluate which models reasonably represent polar stratospheric wintertime variability. Other analyses that depend on the frequency (i.e., statistics) of major SSWs should also use a standard definition for consistency. It should be noted that while a standard definition should be able to detect the vast majority of major SSWs, more detailed diagnostics may be needed to determine a complete set of historical SSWs.

If the community agrees that a standard definition is useful and that the purpose of the standard definition is to characterize wintertime stratospheric variability, then the next step is to consider details of the definition. What qualities are desirable in a standard definition? Our analysis suggests these three characteristics:

- Simplicity: Easily calculated and applicable to reanalyses and model output, both retrospectively and in real time (operationally)
- Relevance: Serves primarily as a metric of polar stratospheric variability, rather than a metric of associated phenomena such as stratosphere–troposphere coupling
- Robustness: Not highly sensitive to details, such as an exact latitude, background climatology,

threshold wind speed, spatial extent, or pressure level

It has been over 35 years since the WMO offered a definition of SSWs, during which time many more SSWs have been observed. We suggest the time is ripe for improvements and updates. A clear reference for the original WMO definition is lacking, and how the definition should be applied is vague, resulting in different interpretations and inconsistent identification and classification of SSWs. We believe a new definition should include, at a minimum, guidelines for determining a) the independence of closely timed events; b) the classification of split-type versus displacement-type events; and c) precise distinctions among major, minor, final, and Canadian SSWs.

In addition to these new guidelines, we propose several options as a starting point for updating the SSW definition.

1) Among the definitions surveyed here, the CP07 definition provides a strong basis for a definition of major SSWs because of its simplicity and relevance. However, it lacks robustness. Using a latitudinal average of zonal winds rather than one particular latitude, or using 65°N instead of 60°N, may decrease sensitivity to changes in the vortex edge.
2) The McInturff (1978) definition, including the temperature gradient criterion, could be clarified and enhanced to address current ambiguities (e.g., How closely timed do the temperature gradient and zonal wind reversals need to occur for major SSWs? During which months? How do we separate closely timed events?). An advantage to this technique is that this definition has a strong historical basis and familiarity; a disadvantage is that more data are required (both temperature and zonal wind), which can be computationally expensive when considering large model intercomparisons.
3) Further consideration could also be given to developing a new kind of stratospheric index, along which a continuum of stratospheric events could be defined, including minor warmings and polar vortex intensification (Limpasuvan et al. 2005). Research would be needed to develop such an index, but it could allow the user to choose the threshold at which extreme events occur in a particular analysis, and it may have a broader application. Still, we argue in this case it would be useful to have a "standard threshold" for major SSWs or for major vortex intensification events to ensure a consistent metric of polar stratospheric variability.
4) We also think it worthwhile and timely to reflect on the name sudden stratospheric warming and whether this terminology is the most useful in light of the fact that major SSWs are now identified primarily on the basis of a circulation reversal, rather than some unspecified measure of a sudden temperature increase. While the historical context (SSWs were first observed in temperature data; e.g., Scherhag 1952) and the need for continuity are important and valid reasons for the maintaining the term sudden stratospheric warming, wording that focuses on circulation rather than the temperature change, and thus more accurately reflects to the public what is being defined, should be considered.

Under the auspices of the World Climate Research Programme's core project on Stratosphere–Troposphere Processes and their Role in Climate (SPARC), efforts are underway to gather community ideas and to develop consensus on an updated standard SSW definition. An initial meeting was held during the SPARC General Assembly in Queenstown, New Zealand, in January 2014 to discuss a timeline and process for gathering input (Butler et al. 2014a). Three additional townhall discussions were held in 2015 (at the American Meteorological Society Annual Meeting, the European Geophysical Union General Assembly, and the Asia Oceania Geosciences Society Annual Meeting) to gather community feedback. The input from these forums will be compiled into a recommendation for an updated standard definition, to be finalized at the SPARC Dynamic Variability (DynVar) meeting in June 2016, prior to submitting recommendations to the WMO. Anyone who is interested can join the e-mail LISTSERV (visit https://sites.google.com/site/stratosphericwarmings/ and following the links therein). Ideas are welcome from anyone who may use the SSW definition for research and operational purposes.

The challenges in understanding the SSW definition and its history, applications, and interpretations are not unique. Other standard definitions face or will face reevaluation in light of new and improved observations, modeling capabilities, and understanding of physical processes. Community involvement and discussion will be essential in determining state-of-the-art definitions for these phenomena to enable improved understanding of past and future climate.

ACKNOWLEDGMENTS. AHB and DJS were supported by the Climate Observations and Monitoring

Program, National Oceanic and Atmospheric Administration, U.S. Department of Commerce. The views expressed herein are those of the authors and do not necessarily reflect the views of NOAA. NB and SCH were supported by the Joint DECC/Defra Met Office Hadley Centre Climate Programme (GA01101), and TB was supported by the NSF Climate Dynamics Program. We thank D. Mitchell and W. Seviour for providing code to calculate vortex moments and the central dates for SSWs using this definition, and D. Mitchell and E. Gerber for their help leading community efforts and providing valuable input. We thank U. Langematz and K. Krüger for their help with understanding and interpreting major references for the WMO SSW definition, the historical role of the Freie Universität Berlin, and the interpretation and application of the WMO definition today. We thank L.M. Polvani and A. Charlton-Perez for their useful feedback, and Melissa Free (NOAA) and the internal reviewers at the Met Office for their helpful reviews of early drafts of this paper. *BAMS* Editor M. Alexander; reviewers U. Langematz, G. Manney, and B. Naujokat; and two anonymous colleagues provided constructive and insightful comments. We thank J. Thomas at the NOAA library for the quick assistance in locating archaic references.

REFERENCES

Allen, D. R., R. M. Bevilacqua, G. E. Nedoluha, C. E. Randall, and G. L. Manney, 2003: Unusual stratospheric transport and mixing during the 2002 Antarctic winter. *Geophys. Res. Lett.,* **30,** 1599, doi:10.1029/2003GL017117.

Andrews, D. G., J. R. Holton, and C. B. Leovy, 1987: *Middle Atmosphere Dynamics.* Academic Press, 489 pp.

Ayarzagüena, B., U. Langematz, S. Meul, S. Oberländer, J. Abalichin, and A. Kubin, 2013: The role of climate change and ozone recovery for the future timing of major stratospheric warmings. *Geophys. Res. Lett.,* **40,** 2460–2465, doi:10.1002/grl.50477.

Baldwin, M. P., 2001: Annular modes in global daily surface pressure. *Geophys. Res. Lett.,* **28,** 4115–4118, doi:10.1029/2001GL013564.

——, and T. J. Dunkerton, 2001: Stratospheric harbingers of anomalous weather regimes. *Science,* **294,** 581–584, doi:10.1126/science.1063315.

——, and D. W. J. Thompson, 2009: A critical comparison of stratosphere–troposphere coupling indices. *Quart. J. Roy. Meteor. Soc.,* **135,** 1661–1672, doi:10.1002/qj.479.

Bancalá, S., K. Krüger, and M. Giorgetta, 2012: The preconditioning of major sudden stratospheric warmings. *J. Geophys. Res.,* **117,** D04101, doi:10.1029/2011JD016769.

Bell, C. J., L. J. Gray, and J. Kettleborough, 2010: Changes in Northern Hemisphere stratospheric variability under increased CO_2 concentrations. *Quart. J. Roy. Meteor. Soc.,* **136,** 1181–1190, doi:10.1002/qj.633.

Birner, T., and J. R. Albers, 2015: Sudden stratospheric warmings and anomalous upward wave activity flux. 18th Conf. on Middle Atmosphere, Phoenix, AZ, Amer. Meteor. Soc., 8.4. [Available online at https://ams.confex.com/ams/95Annual/webprogram/Paper269391.html.]

Blume, C., K. Matthes, and I. Horenko, 2012: Supervised learning approaches to classify sudden stratospheric warming events. *J. Atmos. Sci.,* **69,** 1824–1840, doi:10.1175/JAS-D-11-0194.1.

Butchart, N., J. Austin, J. R. Knight, A. A. Scaife, and M. L. Gallani, 2000: The response of the stratospheric climate to projected changes in the concentrations of well-mixed greenhouse gases from 1992 to 2051. *J. Climate,* **13,** 2142–2159, doi:10.1175/1520-0442(2000)013<2142:TROTSC>2.0.CO;2.

Butler, A. H., E. P. Gerber, D. Mitchell, and W. J. M. Seviour, 2014a: New efforts in developing a standard definition for sudden stratospheric warmings. *SPARC Newsletter,* No. 43, World Climate Research Programme SPARC Office, Zurich, Switzerland, 23–24.

——, L. M. Polvani, and C. Deser, 2014b: Separating the stratospheric and tropospheric pathways of El Niño–Southern Oscillation teleconnections. *Environ. Res. Lett.,* **9,** 024014, doi:10.1088/1748-9326/9/2/024014.

Charlton, A. J., and L. M. Polvani, 2007: A new look at stratospheric sudden warmings. Part I: Climatology and modeling benchmarks. *J. Climate,* **20,** 449–469, doi:10.1175/JCLI3996.1.

——, and Coauthors, 2007: A new look at stratospheric sudden warmings. Part II: Evaluation of numerical model simulations. *J. Climate,* **20,** 470–488, doi:10.1175/JCLI3994.1.

Charney, J. G., and P. G. Drazin, 1961: Propagation of planetary-scale disturbances from the lower into the upper atmosphere. *J. Geophys. Res.,* **66,** 83–109, doi:10.1029/JZ066i001p00083.

Christiansen, B., 2001: Downward propagation of zonal mean zonal wind anomalies from the stratosphere to the troposphere: Model and reanalysis. *J. Geophys. Res.,* **106,** 27 307–27 322, doi:10.1029/2000JD000214.

Coughlin, K., and L. J. Gray, 2009: A continuum of sudden stratospheric warmings. *J. Atmos. Sci.,* **66,** 531–540, doi:10.1175/2008JAS2792.1.

Dee, D. P., and Coauthors, 2011: The ERA-Interim reanalysis: Configuration and performance of the data assimilation system. *Quart. J. Roy. Meteor. Soc.,* **137,** 553–597, doi:10.1002/qj.828.

Erlebach, P., U. Langematz, and S. Pawson, 1996: Simulations of stratospheric sudden warmings in the Berlin troposphere–stratosphere–mesosphere GCM. *Ann. Geophys.,* **14,** 443–463, doi:10.1007/s00585-996-0443-6.

Gerber, E. P., and Coauthors, 2010: Stratosphere-troposphere coupling and annular mode variability in chemistry-climate models. *J. Geophys. Res.,* **115,** D00M06, doi:10.1029/2009JD013770.

Hannachi, A., D. Mitchell, L. Gray, and A. Charlton-Perez, 2011: On the use of geometric moments to examine the continuum of sudden stratospheric warmings. *J. Atmos. Sci.,* **68,** 657–674, doi:10.1175/2010JAS3585.1.

Hardiman, S. C., N. Butchart, T. J. Hinton, S. M. Osprey, and L. J. Gray, 2012: The effect of a well-resolved stratosphere on surface climate: Differences between CMIP5 simulations with high and low top versions of the Met Office climate model. *J. Climate,* **25,** 7083–7099, doi:10.1175/JCLI-D-11-00579.1.

Heideman, K. F., 2014: Editorial. *J. Atmos. Sci.,* **71,** 4397, doi:10.1175/2014JAS1111.1.

Hitchcock, P., and T. G. Shepherd, 2013: Zonal-mean dynamics of extended recoveries from stratospheric sudden warmings. *J. Atmos. Sci.,* **70,** 688–707, doi:10.1175/JAS-D-12-0111.1.

——, ——, and G. L. Manney, 2013: Statistical characterization of Arctic polar-night jet oscillation events. *J. Climate,* **26,** 2096–2116, doi:10.1175/JCLI-D-12-00202.1.

Ineson, S., and A. A. Scaife, 2009: The role of the stratosphere in the European climate response to El Niño. *Nat. Geosci.,* **2,** 32–36, doi:10.1038/ngeo381.

Jiang, X., J. Wang, E. T. Olsen, T. Pagano, L. L. Chen, and Y. L. Yung, 2013: Influence of stratospheric sudden warming on AIRS midtropospheric CO_2. *J. Atmos. Sci.,* **70,** 2566–2573, doi:10.1175/JAS-D-13-064.1.

Johnson, K. W., A. J. Miller, and M. Gelman, 1969: Proposed indices characterizing stratospheric circulation and temperature fields. *Mon. Wea. Rev.,* **97,** 565–570, doi:10.1175/1520-0493(1969)097<0565:PICSCA>2.3.CO;2.

Kalnay, E., and Coauthors, 1996: The NCEP/NCAR 40-Year Reanalysis Project. *Bull. Amer. Meteor. Soc.,* **77,** 437–471, doi:10.1175/1520-0477(1996)077<0437:TNYRP>2.0.CO;2.

Kodera, K., 2006: Influence of stratospheric sudden warming on the equatorial troposphere. *Geophys. Res. Lett.,* **33,** L06804, doi:10.1029/2005GL024510.

Kohma, M., and K. Sato, 2014: Variability of upper tropospheric clouds in the polar region during stratospheric sudden warmings. *J. Geophys. Res. Atmos.,* **119,** 10 100–10 113, doi:10.1002/2014JD021746.

Kuroda, Y., and K. Kodera, 2004: Role of the Polar-night Jet Oscillation on the formation of the Arctic Oscillation in the Northern Hemisphere winter. *J. Geophys. Res.,* **109,** D11112, doi:10.1029/2003JD004123.

Labitzke, K., 1977: Interannual variability of the winter stratosphere in the Northern Hemisphere. *Mon. Wea. Rev.,* **105,** 762–770, doi:10.1175/1520-0493(1977)105<0762:IVOTWS>2.0.CO;2.

——, 1981: Stratospheric-mesospheric midwinter disturbances: A summary of observed characteristics. *J. Geophys. Res.,* **86,** 9665–9678, doi:10.1029/JC086iC10p09665.

——, and B. Naujokat, 2000: The lower Arctic stratosphere in winter since 1952. *SPARC Newsletter,* No. 15, World Climate Research Programme SPARC Office, Zurich, Switzerland, 11–14.

——, and M. Kunze, 2005: Stratospheric temperatures over the Arctic: Comparison of three data sets. *Meteor. Z.,* **14,** 65–74, doi:10.1127/0941-2948/2005/0014-0065.

——, and Coauthors, 2002: The Berlin Stratospheric Data Series. Meteorological Institute, Free University Berlin, CD-ROM.

——, M. Kunze, and S. Brönnimann, 2006: Sunspots, the QBO and the stratosphere in the North Polar Region—20 years later. *Meteor. Z.,* **15,** 355–363, doi:10.1127/0941-2948/2006/0136.

L'Heureux, M. L., D. C. Collins, and Z.-Z. Hu, 2013: Linear trends in sea surface temperature of the tropical Pacific Ocean and implications for the El Niño-Southern Oscillation. *Climate Dyn.,* **40,** 1223–1236, doi:10.1007/s00382-012-1331-2.

Limpasuvan, V., D. W. J. Thompson, and D. L. Hartmann, 2004: The life cycle of the Northern Hemisphere sudden stratospheric warmings. *J. Climate,* **17,** 2584–2596, doi:10.1175/1520-0442(2004)017<2584:TLCOTN>2.0.CO;2.

——, D. L. Hartmann, D. W. J. Thompson, K. Jeev, and Y. L. Yung, 2005: Stratosphere-troposphere evolution during polar vortex intensification. *J. Geophys. Res.,* **110,** D24101, doi:10.1029/2005JD006302.

Manney, G. L., J. L. Sabutis, S. Pawson, M. L. Santee, B. Naujokat, R. Swinbank, M. E. Gelman, and W. Ebisuzaki, 2003: Lower stratospheric temperature differences between meteorological analyses in two cold Arctic winters and their impact on polar processing studies. *J. Geophys. Res.,* **108,** 8328, doi:10.1029/2001JD001149.

——, K. Krüger, J. L. Sabutis, S. A. Sena, and S. Pawson, 2005: The remarkable 2003–2004 winter and other recent warm winters in the Arctic stratosphere since the late 1990s. *J. Geophys. Res.,* **110,** doi:10.1029/2004JD005367.

——, and Coauthors, 2008: The evolution of the stratopause during the 2006 major warming: Satellite data and assimilated meteorological analyses. *J. Geophys. Res.,* **113,** D11115, doi:10.1029/2007JD009097.

——, and Coauthors, 2009: Aura Microwave Limb Sounder observations of dynamics and transport during the record-breaking 2009 Arctic stratospheric major warming. *Geophys. Res. Lett.,* **36,** L12815, doi:10.1029/2009GL038586.

Manzini, E., and L. Bengtsson, 1996: Stratospheric climate and variability from a general circulation model and observations. *Climate Dyn.,* **12,** 615–639, doi:10.1007/BF00216270.

Martineau, P., and S.-W. Son, 2013: Planetary-scale wave activity as a source of varying tropospheric response to stratospheric sudden warming events: A case study. *J. Geophys. Res. Atmos.,* **118,** 10 994–11 006, doi:10.1002/jgrd.50871.

Matsuno, T., 1971: A dynamical model of the stratospheric sudden warming. *J. Atmos. Sci.,* **28,** 1479–1494, doi:10.1175/1520-0469(1971)028<1479:ADMOTS>2.0.CO;2.

Matthewman, N. J., J. G. Esler, A. J. Charlton-Perez, and L. M. Polvani, 2009: A new look at stratospheric sudden warmings. Part III: Polar vortex evolution and vertical structure. *J. Climate,* **22,** 1566–1585, doi:10.1175/2008JCLI2365.1.

McInturff, R. M., Ed., 1978: Stratospheric warmings: Synoptic, dynamic and general-circulation aspects. NASA Reference Publ. NASA-RP-1017, 174 pp. [Available online at http://ntrs.nasa.gov/archive/nasa/casi.ntrs.nasa.gov/19780010687.pdf.]

McIntyre, M. E., and T. N. Palmer, 1984: The 'surf zone' in the stratosphere. *J. Atmos. Terr. Phys.,* **46,** 825–849, doi:10.1016/0021-9169(84)90063-1.

McLandress, C., and T. G. Shepherd, 2009: Impact of climate change on stratospheric sudden warmings as simulated by the Canadian Middle Atmosphere Model. *J. Climate,* **22,** 5449–5463, doi:10.1175/2009JCLI3069.1.

Meriwether, J. W., and A. J. Gerrard, 2004: Mesosphere inversion layers and stratosphere temperature enhancements. *Rev. Geophys.,* **42,** RG3003, doi:10.1029/2003RG000133.

Mitchell, D. M., A. J. Charlton-Perez, and L. J. Gray, 2011: Characterizing the variability and extremes of the stratospheric polar vortices using 2D moment analysis. *J. Atmos. Sci.,* **68,** 1194–1213, doi:10.1175/2010JAS3555.1.

——, and Coauthors, 2012: The nature of Arctic polar vortices in chemistry–climate models. *Quart. J. Roy. Meteor. Soc.,* **138,** 1681–1691, doi:10.1002/qj.1909.

——, L. J. Gray, J. Anstey, M. P. Baldwin, and A. J. Charlton-Perez, 2013: The influence of stratospheric vortex displacements and splits on surface climate. *J. Climate,* **26,** 2668–2682, doi:10.1175/JCLI-D-12-00030.1.

Nakagawa, K. I., and K. Yamazaki, 2006: What kind of stratospheric sudden warming propagates to the troposphere? *Geophys. Res. Lett.,* **33,** L04801, doi:10.1029/2005GL024784.

O'Neill, A., and B. F. Taylor, 1979: A study of the major stratospheric warming of 1976/77. *Quart. J. Roy. Meteor. Soc.,* **105,** 71–92, doi:10.1002/qj.49710544306.

Osprey, S. M., L. J. Gray, S. C. Hardiman, N. Butchart, and T. J. Hinton, 2013: Stratospheric variability in twentieth-century CMIP5 simulations of the Met Office climate model: High top versus low top. *J. Climate,* **26,** 1595–1606, doi:10.1175/JCLI-D-12-00147.1.

Palmer, T. N., 1981: Diagnostic study of a wavenumber-2 stratospheric sudden warming in a transformed Eulerian-mean formalism. *J. Atmos. Sci.,* **38,** 844–855, doi:10.1175/1520-0469(1981)038<0844:DSOAWS>2.0.CO;2.

Pawson, S., and B. Naujokat, 1999: The cold winters of the middle 1990s in the northern lower stratosphere. *J. Geophys. Res.,* **104,** 14 209–14 222, doi:10.1029/1999JD900211.

Quiroz, R., 1975: Stratospheric evolution of sudden warmings in 1969–74 determined from measured infrared radiation fields. *J. Atmos. Sci.,* **32,** 211–224, doi:10.1175/1520-0469(1975)032<0211:TSEOSW>2.0.CO;2.

Reichler, T., J. Kim, E. Manzini, and J. Kröger, 2012: A stratospheric connection to Atlantic climate variability. *Nat. Geosci.,* **5,** 783–787, doi:10.1038/ngeo1586.

Rind, D., R. Suozzo, and N. K. Balachandran, 1988: The GISS Global Climate-Middle Atmosphere Model. Part II: Model variability due to interactions between planetary waves, the mean circulation and gravity wave drag. *J. Atmos. Sci.,* **45,** 371–386, doi:10.1175/1520-0469(1988)045<0371:TGGCMA>2.0.CO;2.

Scaife, A. A., J. R. Knight, G. K. Vallis, and C. K. Folland, 2005: A stratospheric influence on the winter NAO and North Atlantic surface climate. *Geophys. Res. Lett.,* **32,** L18715, doi:10.1029/2005GL023226.

Scherhag, R., 1952: Die explosionsartigen Stratosphärenerwärmungen des Spätwinter 1951/1952 (The explosive warmings in the stratosphere of the late winter 1951/1952). *Ber. Dtsch. Wetterdienstes U.S. Zone,* **38,** 51–63.

Schoeberl, M. R., 1978: Stratospheric warmings: Observations and theory. *Rev. Geophys.,* **16,** 521–538, doi:10.1029/RG016i004p00521.

——, and D. L. Hartmann, 1991: The dynamics of the stratospheric polar vortex and its relation to springtime ozone depletions. *Science,* **251,** 46–52, doi:10.1126/science.251.4989.46.

Seviour, W. J. M., D. M. Mitchell, and L. J. Gray, 2013: A practical method to identify displaced and split stratospheric polar vortex events. *Geophys. Res. Lett.,* **40,** 5268–5273, doi:10.1002/grl.50927.

Shindell, D. T., R. L. Miller, G. A. Schmidt, and L. Pandolfo, 1999: Simulation of recent northern winter climate trends by greenhouse-gas forcing. *Nature,* **399,** 452–455, doi:10.1038/20905.

Siskind, D. E., S. D. Eckermann, L. Coy, J. P. McCormack, and C. E. Randall, 2007: On recent interannual variability of the Arctic winter mesosphere: Implications for tracer descent. *Geophys. Res. Lett.,* **34,** L09806, doi:10.1029/2007GL029293.

Thompson, D. W. J., M. P. Baldwin, and J. M. Wallace, 2002: Stratospheric connection to Northern Hemisphere wintertime weather: Implications for prediction. *J. Climate,* **15,** 1421–1428, doi:10.1175/1520-0442(2002)015<1421:SCTNHW>2.0.CO;2.

Uppala, S. M., and Coauthors, 2005: The ERA-40 Re-Analysis. *Quart. J. Roy. Meteor. Soc.,* **131,** 2961–3012, doi:10.1256/qj.04.176.

Van Loon, H., R. L. Jenne, and K. Labitzke, 1973: Zonal harmonic standing waves. *J. Geophys. Res.,* **78,** 4463–4471, doi:10.1029/JC078i021p04463.

Waugh, D. W., and W. J. Randel, 1999: Climatology of Arctic and Antarctic polar vortices using elliptical diagnostics. *J. Atmos. Sci.,* **56,** 1594–1613, doi:10.1175/1520-0469(1999)056<1594:COAAAP>2.0.CO;2.

WMO CAS, 1978: Abridged final report of the seventh session, Manila, 27 February–10 March 1978. Secretariat of the WMO Rep. WMO-509, 113 pp.

WMO/IQSY, 1964: International Years of the Quiet Sun (IQSY), 1964–1965: Alert messages with special references to stratwarms. Secretariat of the WMO WMO/IQSY Rep. 6, 19 pp. + 3 appendices.

REVISITING THE 26.5°C SEA SURFACE TEMPERATURE THRESHOLD FOR TROPICAL CYCLONE DEVELOPMENT

BY RON MCTAGGART-COWAN, EMILY L. DAVIES, JONATHAN G. FAIRMAN JR., THOMAS J. GALARNEAU JR., AND DAVID M. SCHULTZ

A measure of tropospheric depth and bulk convective stability replaces the traditional sea surface temperature–based threshold as a necessary ingredient for tropical cyclogenesis from baroclinic precursors.

The development of a tropical cyclone is the net result of numerous processes that promote the growth of a weak perturbation into an intense self-sustaining circulation. A list of five necessary ingredients is typically used to assess the favorability of an environment for tropical cyclogenesis: high sea surface temperature (SST), a steep vertical temperature gradient (reduced stability), high lower-tropospheric relative humidity, low wind shear, and a nonzero Coriolis force (Palmén 1948; Riehl 1954; Miller 1958; Gray 1968; Lee et al. 1989; DeMaria et al. 2001). We focus here on the SST element of this list.

Since the statement by Palmén (1948, p. 31) that "hurricanes can be formed only in the oceanic regions outside the vicinity of the Equator where the surface water has a temperature above 26–27°C," a 26.5°C threshold for tropical cyclogenesis has become so well established that it appears in many current textbooks (Wallace and Hobbs 2006; Williams 2009; Ahrens 2009; Laing and Evans 2011; Ackerman and Knox 2015) and review articles [Galvin (2008), rounding up to 27°C]. However, the precise value of the SST threshold has been a matter of debate since its inception.

The value of 26.5°C is conveniently the closest half-degree Celsius to 80°F, a fact thought to have contributed to its selection [Sadler (1964, p. 352), based on Palmén (1956)]. This threshold was found to be globally applicable by Gray (1968) despite being developed based on experience in the Gulf of Mexico, and the western North Atlantic and western North Pacific basins; however, alternative values based on early observational studies include 26.1° (Fisher 1958) and 26.8°C (Wendland 1977). More recently, Dare and McBride (2011) present a global climatology of SSTs associated with tropical cyclogenesis, finding that almost 7% of formations occur over waters whose temperature at the time of formation lies below the 26.5°C threshold. They propose an adjustment of this value to 25.5°C, such that only 1.4% of developments occur over subthreshold SSTs. However, Dare and McBride (2011) also find that 26.5°C is a reasonable threshold when the SST is averaged over the 2-day period leading up to storm formation.

Tropical cyclone development over the relatively cold waters of the northeastern North Atlantic Ocean is found by Mauk and Hobgood (2012) to be associated with the presence of baroclinicity in the storm

environment, consistent with the increasing recognition of the potential importance of baroclinic processes in tropical cyclogenesis (Bosart and Bartlo 1991; Bosart and Lackmann 1995; Davis and Bosart 2004; McTaggart-Cowan et al. 2008, 2013; Evans and Guishard 2009; Guishard et al. 2009). The majority of low-SST formations documented by Mauk and Hobgood (2012) are classified as strong tropical transitions, a development pathway characterized by the presence of a well-defined extratropical precursor that evolves into a warm-core system through the vertical redistribution of mass and momentum by sustained convection (Davis and Bosart 2003, 2004). Considering both the weak and strong forms of tropical transition (TT), McTaggart-Cowan et al. (2013) find that 16% of all tropical cyclones develop from baroclinic precursors.

In this study, we investigate the significant differences that exist between environments associated with tropical cyclogenesis over waters on either side of the 26.5°C threshold. The presence of upper-level baroclinic disturbances during low-SST formation events motivates a development pathway–specific analysis of the relevance of an SST-based threshold for cyclogenesis. For pathways involving the TT of a precursor baroclinic disturbance, a 22.5°C maximum threshold of the coupling index (computed as the difference between upper- and lower-level equivalent potential temperatures) is preferable to the SST threshold in terms of both effectiveness and physical relevance to the problem at hand. The addition of such an element to the list of ingredients required for tropical cyclogenesis will help to refine our understanding of, and improve our ability to, predict this important class of development events.

AFFILIATIONS: McTaggart-Cowan—Numerical Weather Prediction Research Section, Environment Canada, Dorval, Quebec, Canada; Davies—School of Earth, Atmospheric and Environmental Sciences, University of Manchester, Manchester, United Kingdom; Fairman and Schultz—Centre for Atmospheric Science, School of Earth, Atmospheric and Environmental Sciences, University of Manchester, Manchester, United Kingdom; Galarneau—Department of Atmospheric Sciences, University of Arizona, Tucson, Arizona
CORRESPONDING AUTHOR: David Schultz, Centre for Atmospheric Science, School of Earth, Atmospheric and Environmental Sciences, University of Manchester, Simon Building, Oxford Road, Manchester M13 9PL, United Kingdom
E-mail: david.schultz@manchester.ac.uk

The abstract for this article can be found in this issue, following the table of contents.
DOI:10.1175/BAMS-D-13-00254.1

A supplement to this article is available online (DOI:10.1175/BAMS-D-13-00254.2)

In final form 4 November 2014

DATA AND METHODS. This study employs four global datasets that cover a common 25-yr period from 1989 to 2013: tropical cyclone best tracks, high-resolution SST, atmospheric analyses, and cyclone development pathway classifications. A total of 1,757 tropical cyclones are included across all basins, thus allowing for the development of robust statistics even for relatively rare events. As a result, the term *significant* will be used hereafter in the strict statistical sense to indicate the rejection of the null hypothesis at the 99% confidence level.

All tropical cyclone tracking information used in this study is derived from the International Best Track Archive for Climate Stewardship (IBTrACS), version 4, revision 5 (Knapp et al. 2010). The subset of best track data from the World Meteorological Organization's Regional Specialized Meteorological Centers is used to determine storm location and estimated intensity. The tropical storm wind speed threshold for the North Atlantic basin [35 kt (18 m s^{-1})] is used to determine the development time of the cyclone.[1] This definition focuses on the point at which the precursor vortex becomes a self-sustaining circulation (Laing and Evans 2011) and is consistent with the definition adopted by Dare and McBride (2011). The study thereby concentrates on the early intensification stage of developing storms rather than on precursor tropical depressions that may or may not intensify. Of the 2,125 tropical cyclones in the 1989–2013 dataset, 2,026 reach the 35-kt threshold after a median of 30 h of precursor tracking. An analogous investigation performed using a development-time definition of the first IBTrACS entry shows limited sensitivity as described in the "Sensitivity to development-time definition" section of the supplement. Additionally, any storm with an initial intensity estimate greater than or equal to 35 kt in the best track record is rejected from further analysis because the early intensification stage is deemed to have been missed. This criterion eliminates a further 269 storms, leaving a total of 1,757 storms for this study (83% of the original dataset). In the "Sensitivity

[1] In the western North Pacific basin, the Koba et al. (1991) pressure–wind relationship is used to estimate the initial intensity because wind speeds below 35 kt are not reported in the Japan Meteorological Agency best track (Knapp et al. 2013).

to initial intensity restriction" section of the supplement, this condition is shown to be effective at eliminating invalid IBTrACS entries without noticeably affecting results. Dare and McBride (2011) consider only formations that occur equatorward of 35°, a condition that is not applied here in recognition of the fact that TT can occur at a relatively high latitude. However, consistent with Dare and McBride (2011), storms classified as either *subtropical* or *extratropical* in the best track archive are not considered in this investigation in order to eliminate nontropical systems from the dataset.

The Reynolds et al. (2007) SST dataset, available daily with a 0.25° grid spacing, is employed throughout this study. The analyzed state is interpolated linearly for each storm to the formation time derived from the best track record. A pair of definitions of development SST is evaluated by Dare and McBride (2011): the point SST at formation time at the storm center and the maximum SST over the previous 48 h along the precursor track. In this study, we instead adopt a storm-centered area-averaging approach over a 2° radius in order to obtain a representative SST on the storm scale without introducing a potential bias from storms with short preformation tracks. A comparison of the different development SST definitions (Fig. 1) shows that the choice of technique has predictable impacts on the development SST distribution: the Dare and McBride (2011) backtracking increases the SST value by definition, while the use of area averaging reduces the sensitivity of the estimate.

Throughout this study, the atmospheric state is represented by the European Centre for Medium-Range Weather Forecasts interim reanalysis (Dee et al. 2011), archived at 6-hourly intervals on a 1.5° grid. These analyses are used to compute quantities on the dynamic tropopause, here defined as the 2-PVU surface [1 potential vorticity unit (PVU) = 10^{-6} K m^2 kg^{-1} s^{-1}], in order to assess the structure of the upper boundary of the troposphere (Morgan and Nielsen-Gammon 1998). Low values of dynamic tropopause pressure are indicative of the elevated tropopause typical of the tropical environment, higher values are consistent with cold upper-level troughs, and sharp gradients between these extremes represent the upper-level fronts along which lie the subtropical and midlatitude jets.

The tropical cyclone development pathway climatology developed by McTaggart-Cowan et al. (2013) is used to determine the formation characteristics of storms in this study. McTaggart-Cowan et al. (2013) use a linear discriminant analysis (Friedman 1989) to assign each tropical cyclone to one of five categories depending on a pair of metrics: lower-level thickness asymmetry (*Th*) and upper-level quasigeostrophic forcing for ascent (*Q*). For the purposes of the current study, the TT categories (*weak TT* and *strong TT*) are considered independently, whereas the remaining pathways (*nonbaroclinic*, *low-level baroclinic*, and *trough induced*) are combined into a *non-TT* group (Table 1).[2] The study thereby remains focused on the TT pathways in which the ingredients required for low-SST tropical cyclogenesis are found to reside. The metric-based divisions between the development pathways are shown in Fig. 2, from which it is evident that the bulk of events fall into the *non-TT* category (Table 1). An important distinction between

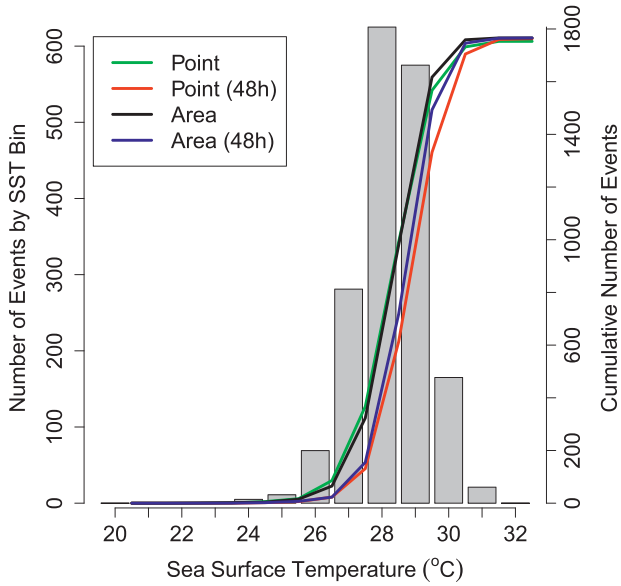

Fig. 1. Distribution of storm-centered 2° area-average SST at tropical cyclone development time (gray bars plotted against the left-hand axis, corresponding to the "Area" entry in the legend). The cumulative distribution functions for four different representations of SST are plotted against the right-hand axis, with line colors as indicated in the legend. The "Point" and "Point (48h)" definitions follow "SST" and "SST48" of Dare and McBride (2011), respectively. The Area and "Area (48h)" represent analogous descriptions that incorporate 2° area averaging, with the results of the study qualitatively insensitive to reasonable changes in the averaging radius. The Area cumulative distribution function corresponds to the histogram plotted in gray bars. Binning is performed at 1°C intervals centered on integer SST values between the 20° and 34°C extrema of the dataset: the 26°C bin therefore contains all events that occur over waters between 25.5° and 26.5°C.

[2] Development pathway category names are typeset in italics to avoid confusion with similar phrases in the text that do not refer specifically to the classification scheme.

the investigation of McTaggart-Cowan et al. (2013) and the current study is that the former did not evaluate the likelihood of tropical cyclogenesis. It focused instead on the development pathway that would be followed if development were to occur. In the current study, these pathway classifications underpin the conditional application of a modified thermodynamic limit for tropical cyclogenesis, precisely to assess the probability of tropical cyclone development.

TROPICAL CYCLONE FORMATION ENVIRONMENTS. Given the large amount of energy required to create and sustain a tropical cyclone, high SSTs are expected to dominate the development distribution as shown in Fig. 1. Without a warm sea surface and oceanic mixed layer, most nascent tropical disturbances are unable to extract the surface enthalpy fluxes required to support active convection and to promote the development of a self-sustaining circulation (Emanuel 1986, 1989; Black et al. 2007; Zhang et al. 2008). However, the long left tail of the development SST distribution leads to a slow ramp-up (sustained shallow slope) in the cumulative distribution function and indicates that in a minority of cases, a tropical cyclone is able to develop without the benefit of such a plentiful source of energy.

A total of 70 tropical cyclones form in regions with 2° area-averaged SSTs below the 26.5°C threshold: roughly 4% of the 1,757 storms considered in this study. These will be called "cold events" to distinguish them from the "warm events" that occur over waters with SSTs greater than 26.5°C. Dare and McBride (2011) characterize 5%–7% of formations as cold events for a similar definition of cyclogenesis. The discrepancy between these percentage estimates is primarily a result of the differing definitions of SST as evidenced by the comparison of the cumulative distribution functions in Fig. 1. Adopting the point SST definition of Dare and McBride (2011) yields an estimate of 6%; however, the area-mean definition will be used in this study because of its relevance to the storm-scale circulation and its reduced sensitivity to small-scale spatial SST variability.

Although the global average of about three cold formation events per year (70 such developments occur in this 25-yr climatology) represents a small component of the overall tropical cyclogenesis rate of 80–90 per year (Emanuel 1991), this subset of events is of particular interest because it appears to challenge the conventional description of the physics of tropical cyclone development. Moreover, the fact that these storms tend to form at relatively high latitudes, combined with their prevalence in the northern North Atlantic basin (Fig. 3), makes them a particular threat to populations and infrastructure not accustomed to, or designed for, the impacts of tropical cyclones.

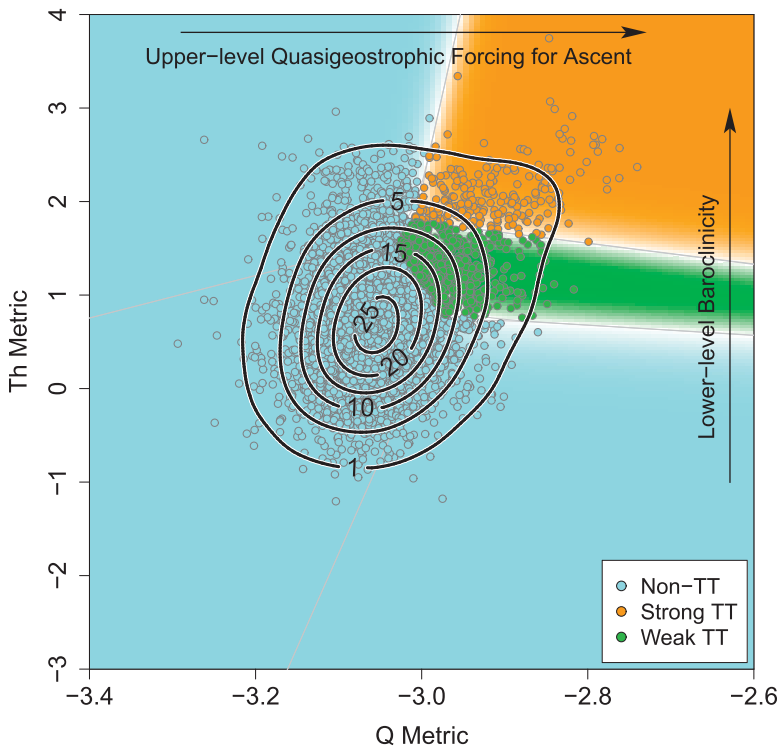

Fig. 2. Classification schematic for the development pathway climatology described by McTaggart-Cowan et al. (2013) and synthesized here into three categories from the original five as described in the "Data and methods" section. The axes of the classification space are the *Q* and *Th* metrics that relate to environmental upper-level quasigeostrophic forcing for ascent and lower-level baroclinicity, respectively (section 2a of McTaggart-Cowan et al. 2013). Background colors follow the legend and represent the classification for each position on the plane. Annotations are used to ease interpretation of the dimensions. Development events for the 1948–2010 period are plotted and classified for reference (points), along with the corresponding kernel density estimate [contours; a continuous function that represents the underlying distribution of TC developments across metric space (Duong 2007)].

Table 1. Summary description of the tropical cyclogenesis development pathways used in this study, based on the classifications of McTaggart-Cowan et al. (2013). The original *nonbaroclinic*, *low-level baroclinic*, and *trough-induced* categories are listed individually as subpathways of the combined *non-TT* group, with their percentage contribution to *non-TT* developments identified in parentheses in the second column.

Pathway name	Subpathway (% contribution)	Description	Occurrence (%)
Non-TT		No superposition of upper- and lower-level baroclinic disturbances	83
	Nonbaroclinic (85%)	No appreciable baroclinic influences	
	Low-level baroclinic (6%)	Strong lower-level thremal gradients without an upper-level disturbance	
	Trough induced (9%)	Upper-level disturbance without appreciable lower-level thermal gradients	
Weak TT		Upper-level disturbance with moderate lower-level thermal gradients	14
Strong TT		Upper-level disturbance with strong lower-level thermal gradients	3

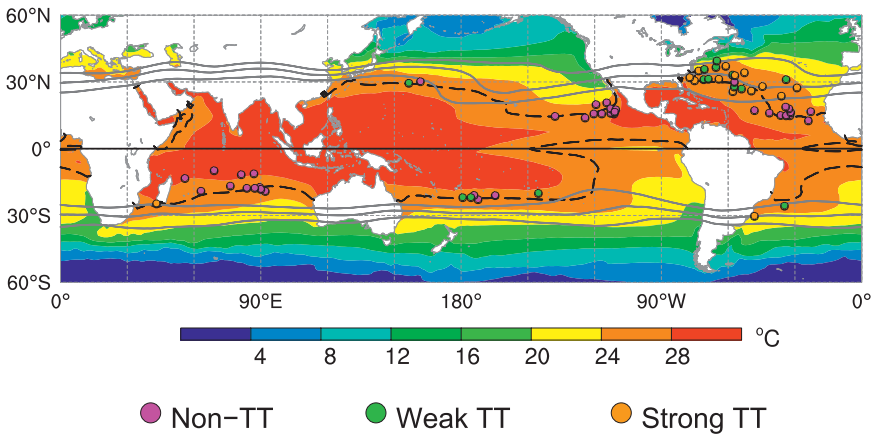

Fig. 3. Formation locations of cold events between 1989 and 2013. The seasonal-mean SST is plotted in the background using colors as indicated on the color bar, with the 26.5°C isotherm highlighted with a thin dashed line for reference. The "season" is defined as the summer and fall for each hemisphere, corresponding to Jun–Nov in the Northern Hemisphere and Dec–May in the Southern Hemisphere. A black line at the equator divides the separate climatologies. The seasonal-mean positions of the 150-, 175-, and 200-hPa isobars on the dynamic tropopause are shown by gray lines, with the lower-pressure isopleths positioned equatorward of their higher-pressure counterparts. The symbol for each tropical cyclone formation location is plotted according to the storm development pathway as indicated in the plot legend (Table 1).

Investigations of individual low-SST formation events such as the 2004 South Atlantic Tropical Cyclone Catarina (Pezza and Simmonds 2005; McTaggart-Cowan et al. 2006) generally emphasize the role of upper-level baroclinic features in the development process. In their small-sample climatology for the northeastern North Atlantic basin, Mauk and Hobgood (2012) show that the environments in which these storms develop are generally characterized by large vertical wind shears and low equilibrium levels (the altitude at which a parcel ascending from lower levels becomes neutrally buoyant). These results suggest that important differences should exist between the environments of warm- and cold-SST formation events.

The distribution of mean dynamic tropopause pressure in the environment surrounding the developing tropical cyclone is significantly different between warm and cold tropical cyclone formation events (Fig. 4). The mean tropopause pressure for cold events is 140 hPa, 25 hPa greater than the average for tropical cyclones developing over warmer waters (median values are 128 and 115 hPa, respectively). The shape of the distributions is also noticeably different, with a secondary maximum at 175 hPa in the cold-SST distribution indicative of the existence of a distinct class of formations that occur preferentially in association with reduced tropopause heights.

The physical implications of tropical cyclone formation in an environment with a lowered tropopause stem from the fact that such a background is associated with the presence of a cold upper-level trough. This feature may be of midlatitude origin (Davis and Bosart 2003), or it may have formed at lower latitudes within the tropical upper-tropospheric troughs (Sadler 1975). The presence of cold air aloft reduces bulk tropospheric stability, putting more convective available potential energy at the disposal of the developing disturbance. The reduced static stability also leads to

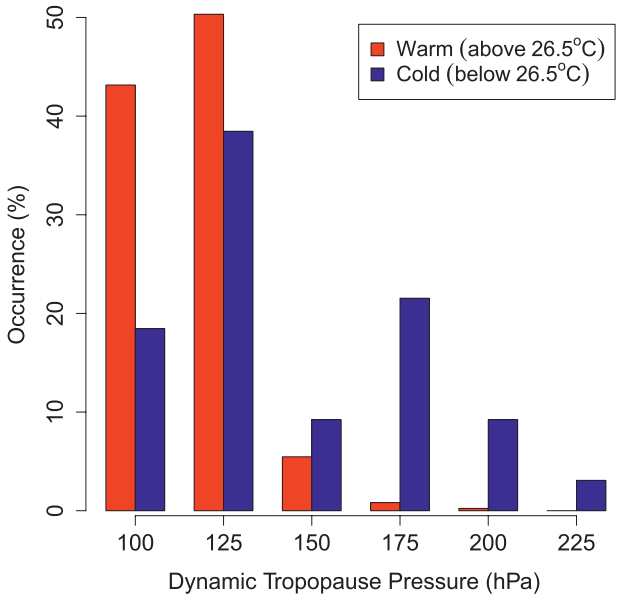

Fig. 4. Probability distribution of the mean dynamic tropopause pressure within 10° of the formation location of the tropical cyclone. Storms are classified as "warm" or "cold" depending on their formation-time SST value and are plotted with red and blue bars, respectively. Binning is performed at 25-hPa intervals centered on the values shown along the abscissa. The 10° radius is used to represent the near-storm environment for consistency with previous studies, and the results of this work are not highly sensitive to reasonable values of this averaging radius.

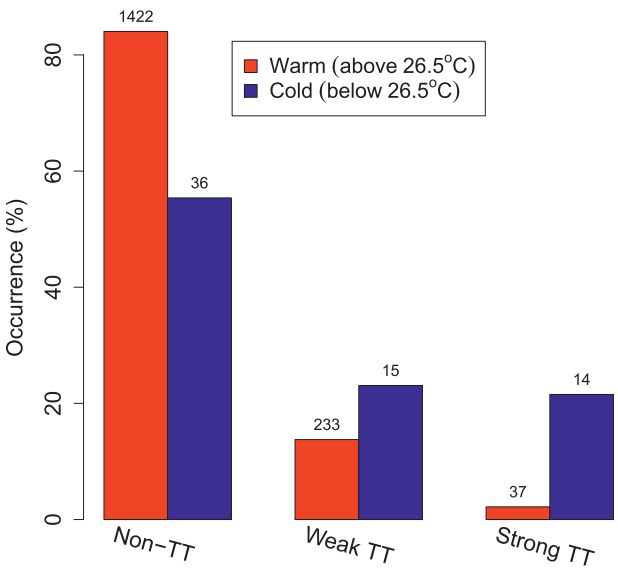

Fig. 5. Frequency of occurrence of warm-SST (red) and cold-SST (blue) tropical cyclogenesis events by development pathway. The number of events in each group is annotated at the top of the bar. A description of the development pathways can be found in Table 1.

an increased Rossby penetration depth, which promotes vertical connections between the upper- and lower-level perturbations (DeMaria 1996), and leads to enhancement of both the developing secondary circulation and the vertical motions resulting from quasigeostrophic forcing for ascent downshear of the upper-level trough (Kelly and Mock 1982).

In light of the apparent relationship between tropopause pressure and development-time SST, and the implications of such an environment for cyclogenesis, a physically based framework is needed for further analysis of these events. Of particular relevance to this study will be the ability of the scheme to identify TT events (Davis and Bosart 2003, 2004), because this development paradigm depends strongly on the presence of a cold trough aloft. Once classifications have been made, the resulting development pathway–specific climatologies can be evaluated to determine whether 26.5°C is a universally applicable threshold, or whether a different quantity yields a more relevant necessary condition for tropical cyclogenesis from baroclinic precursors.

PATHWAY DEPENDENCE OF THE SST THRESHOLD. The TT of an initially baroclinic vortex into a developing tropical cyclone is a distinct form of tropical cyclogenesis (Davis and Bosart 2003, 2004) that accounts for approximately 16% of formations around the globe (McTaggart-Cowan et al. 2013). These events are divided into two groups depending on the strength of the initial lower-level circulation. Developments involving weak extratropical cyclones (WEC) events (Davis and Bosart 2004) are here referred to as *weak TT* events. In these cases, near-surface winds around the precursor are not strong enough to enhance surface fluxes sufficiently to sustain the vortex [less than 10–15 m s^{-1} (Emanuel 1995; Fairall et al. 2003)]. Conversely, the winds associated with an initial disturbance involved in strong extratropical cyclone (SEC) TT [defined as SEC by Davis and Bosart (2004) and *strong TT* here] are capable of triggering wind-induced surface heat exchange to promote the growth of a self-sustaining circulation driven primarily by surface enthalpy fluxes (Emanuel 1986). Despite their differing lower-level intensities, the *weak TT* and *strong TT* development pathways both rely on the cyclogenetic influence of an upper-level trough at the early stages of transition. This dependence suggests that the TT pathways may be particularly well suited to overcoming the detrimental impacts of low SSTs during storm formation.

The *weak TT* and *strong TT* development pathway classifications of McTaggart-Cowan et al. (2013) are

used here to identify this form of development. All other formation events are classified as *non-TT*, a general category in which the baroclinicity of either the upper- or lower-level disturbances is too weak for the storm to follow a TT development pathway (Table 1). The majority of tropical cyclogenesis events in this study follow the *non-TT* pathway (83%), whereas 14% and 3% follow the *weak TT* and *strong TT* pathways, respectively.

The frequency of occurrence of cold events depends on the pathway to tropical cyclogenesis (Fig. 5). Although 84% of warm events follow the *non-TT* pathway, only 55% of cold events resemble this dominant development archetype. Instead, large increases in the relative frequency of *weak TT* and *strong TT* formations are evident. The relative frequency of cold events is highest for the *strong TT* category, in which 27% of events (14/51) occur over waters with area-averaged SST below the 26.5°C threshold.

The relative dominance of the *strong TT* pathway in tropical cyclogenesis over colder waters is also apparent in the cumulative distribution functions (Fig. 6). The slow ramp-up of the *strong TT* pathway over low SSTs, indicative of a left-skewed distribution containing an appreciable number of cold events, provides further evidence that the 26.5°C threshold is not highly applicable to this class of development.[3] The utility of the threshold for storms following the *weak TT* pathway is also questionable, since its curve lies above the dominant *non-TT* class for lower SSTs.

The specification of any SST threshold as a necessary (but not sufficient) condition for tropical cyclone development needs to be based on an "acceptable" level of sensitivity. In the formulation used here, sensitivity refers to the fraction of tropical cyclone formation events that occur over SSTs above the specified threshold. Conversely, the type-II error rate is defined as the complement of sensitivity (1 – sensitivity) to represent the fraction of events that take place on the "wrong" side of the threshold (development over cold SSTs in this case). Because the traditional threshold was defined without any development pathway partitioning, we can deduce the acceptable type-II error rate to be about 4% based on the cumulative distribution functions for the full dataset at 26.5°C (black line in Fig. 6). We round this

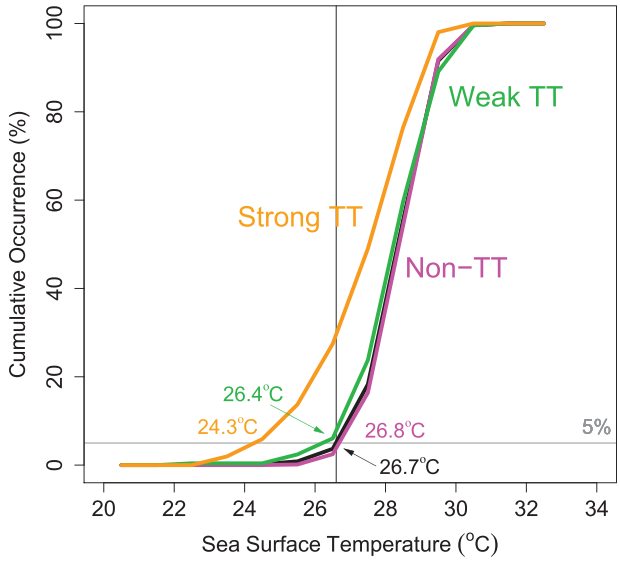

Fig. 6. Pathway-dependent cumulative distribution functions of development SST. Binning is performed at 1°C intervals as described for Fig. 1, and it is plotted using different line colors for individual pathways as labeled (black for the cumulative distribution of all events). The 5th percentile line is plotted in gray, with the values of its intersection point with the cumulative distribution functions annotated in the appropriate color for the pathway. The 26.5°C threshold is identified with a thin vertical line.

value to 5% for consistency with standard confidence intervals and the Dare and McBride (2011) range of 5%–7%. This corresponds to 95% sensitivity for the threshold model, a value that practical use has shown to be acceptable to the community.

The existence of the pathway-dependent sensitivity apparent in Fig. 6 is problematic from the perspective of threshold application. Water temperatures of 26.5°C serve as an effective thermodynamic boundary for *non-TT* formations, yet appear to have relatively little impact on *strong TT* events. Ideally, the threshold would have a consistent meaning for the different development types, expressed as uniform, nonzero[4] type-II error rates. Modifications to the SST threshold for TT developments may be made to achieve the same level of sensitivity (Fig. 6). However, the traditional value would need to be adjusted downward by over 2°C (to 24.3°C) for *strong TT* developments. Such revisions may be considered a first step toward accounting for the

[3] An ideal threshold model would arise from a cumulative distribution function that abruptly transitions from a near-zero subthreshold slope to a steep slope once the threshold is reached.

[4] A threshold with a null type-II error rate (perfect sensitivity) is entirely achievable, but it is likely useless in practice. Consider redefining the SST threshold as 0°C: no tropical cyclone will form below this threshold (0% type-II error rate) but neither will any realistic potential development be excluded by this value.

impact of environmental baroclinicity on tropical cyclogenesis, but they could also be interpreted as an indication that an important element is missing from the description of the thermodynamic factors limiting development.

A THRESHOLD FOR TROPICAL TRANSITION. Given the significant differences in tropopause pressure (Fig. 4) and frequency of TT (Fig. 5) between warm and cold events, a pathway-dependent investigation of the upper-tropospheric state is expected to yield additional insight into the factors acting to facilitate tropical cyclogenesis under low-SST conditions. The pathway-dependent relationships between the pressure of the dynamic tropopause and SST shown in Fig. 7 demonstrate that the environment plays an important role in modulating the sensitivity of the development process to the energy available from the underlying surface. The *weak TT* and *strong TT* pathways both possess significant relationships between tropopause pressure and SST, with cold development events tending to occur in association with stronger troughs aloft.

Distinguishing between the *non-TT* and TT-based pathways also affords an explanation for the bimodal distribution of dynamic tropopause pressure for cold events, centered at 150 hPa in Fig. 4. This value appears to divide cold, near-threshold *non-TT* events occurring under elevated tropopauses (light gray backgrounds in Fig. 7b), from those undergoing *weak TT* and *strong TT* over much lower SSTs in the presence of a trough aloft (dark gray backgrounds in Figs. 4c and 4d). There appears to be an important physical distinction between these subsets of cold development events that is not fully described by SST.

The thermodynamic interpretation of the relationship between tropopause pressure and SST is that the depressed tropopause is potentially colder, and thus it creates an environment in which the bulk column stability is similar to that of the deep tropics despite a lower surface temperature (Emanuel 1986). The deep moist stability is characterized by Mauk and Hobgood (2012) using the equilibrium level and by Emanuel (1986) using a surface–300-hPa lifted index, but here we use the coupling index (Bosart and Lackmann 1995) because of its direct relevance to the baroclinic dynamics that characterize the TT-based development pathways (McTaggart-Cowan et al. 2006, 2010). This quantity is defined as the difference between the dynamic tropopause potential

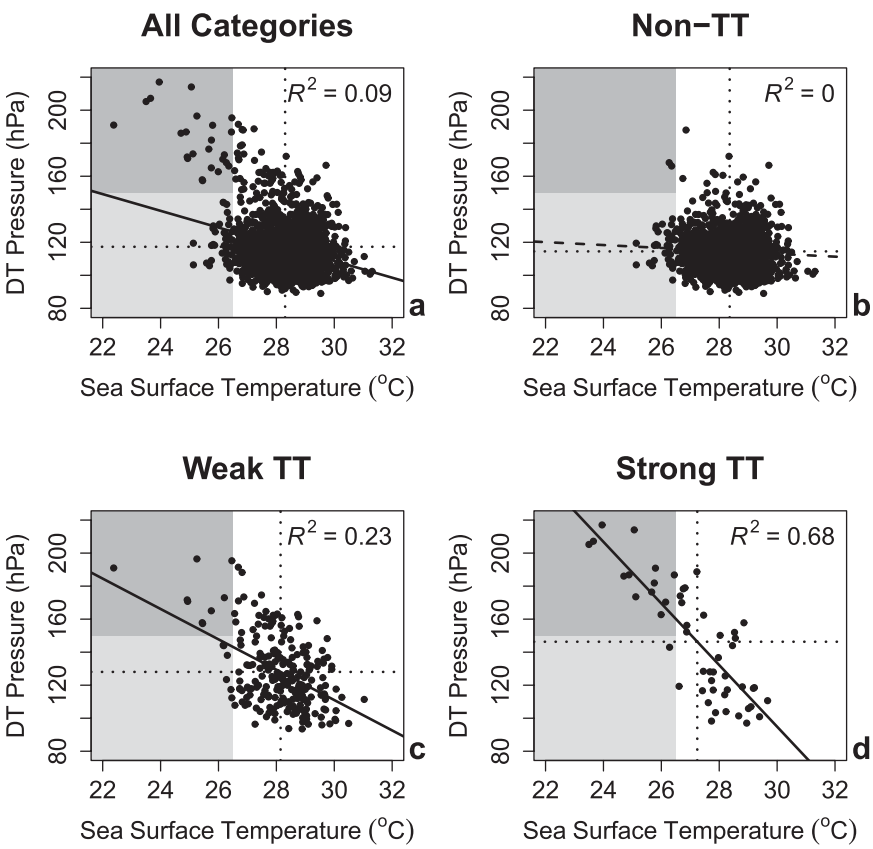

Fig. 7. Pathway-dependent dynamic tropopause pressure, as defined for Fig. 4. Individual panels present development-time SST and tropopause pressure (black dots) for the formation pathway indicated in the plot title. Gray shading appears as a background for SST values below 26.5°C, with light gray for dynamic tropopause pressures above 150 hPa and dark gray for lower tropopauses. The 150-hPa distinction is used because it represents the local minimum in the Fig. 4 distribution for cold events. Horizontal and vertical dotted lines represent the category-mean pressure and SST, respectively. The linear model that best describes the relationship between these quantities is plotted with a solid line if the relationship is significant and with a dashed line for reference if it is not. The square of the correlation coefficient (R^2) is provided in the top-right corner of each panel.

temperature and the 850-hPa equivalent potential temperature. It approximates bulk stability (larger values represent more stable conditions than smaller values), which modulates the degree of interaction between perturbations on the upper and lower boundaries of the free troposphere via the Rossby penetration depth. Because such boundary thermal perturbations can be regarded as potential vorticity anomalies (Bretherton 1966), interactions between these edge waves can promote baroclinic growth in the Eady model (Davies and Bishop 1994), a process highly relevant to TT events. The use of the 850-hPa level rather than the surface in the coupling index formulation is consistent both with the lower free-tropospheric boundary for edge potential temperature perturbations (Hoskins et al. 1985) and with recent modifications to the original undiluted form of the Emanuel (1986) Carnot cycle model. The latter are designed to account for both midlevel entrainment and downdraft-induced moist entropy reductions (Cram et al. 2007; Riemer et al. 2010; Tang and Emanuel 2012).

Recasting the cumulative distribution function in terms of the coupling index instead of SST demonstrates that this quantity is effective at reducing the slow ramp-up of the *strong TT* category by steepening the distribution's slope (cf. Figs. 6 and 8). The sharper onset of development for decreasing coupling index values suggests that a threshold based on this quantity will represent an improvement over the SST condition. Moreover, both TT pathways display similar coupling index distributions as evidenced by their similarity across a broad range of values in Fig. 8, suggesting that a single threshold value should be applicable to TT events in general.

Based on the cumulative distribution functions shown in Fig. 8, a coupling index threshold of 22.5°C is identified as the upper limit for TT. This value is chosen as the point at which the 5th percentile crosses the cumulative distributions, such that the type-II error rate approaches the acceptable 5% value determined from the 26.5°C SST threshold. Errors implied by the use of the 22.5°C coupling index threshold are compared to their SST-based equivalents in Table 2, from which it appears that the former is effective for TT-based developments. The consistency of the type-II error rate across the *weak TT* and *strong TT* pathways, a direct result of their proximity in Fig. 8, is particularly important because it suggests that the threshold is equally applicable across this subrange of formation types. Use of the 22.5°C coupling index maximum for TT-based developments, and the 26.5°C SST minimum for all other events, yields a combined threshold performance that is superior to

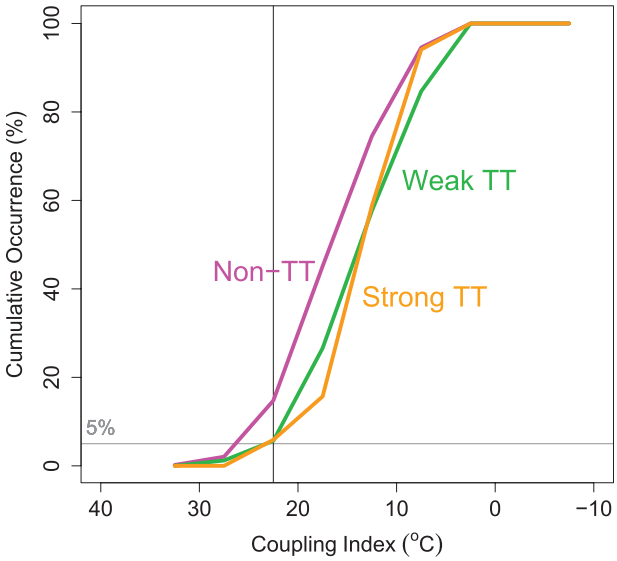

Fig. 8. Pathway-dependent cumulative distribution functions of development-time coupling index in the environment plotted as in Fig. 6, except for coupling index binning performed at 5°C intervals from −10° to 40°C. The 22.5°C threshold is identified with a thin vertical line.

Table 2. Pathway-specific type-II error rates (storm formation on the cold side of the threshold) for the traditional 26.5°C SST threshold (first column) and a 22.5°C coupling index threshold (second column). The combined threshold (third column) uses the criteria corresponding to the values in boldface in the previous two columns to enhance the performance of the ingredients-based tropical cyclogenesis model across the full range of development environments.

	Type-II error rate (%)		
Pathway	**26.5°C SST**	**22.5°C coupling index**	**Combined thresholds**
Non-TT	**2.5**	14.7	2.5
Weak TT	6.0	**5.6**	5.6
Strong TT	27.5	**5.9**	5.9
All	3.7	13.2	3.0

either of these criteria in isolation in terms of both error rate consistency and overall sensitivity (final column of Table 2).

The increase in type-II error rate when the coupling index threshold is applied to *non-TT* events (second column of Table 2) can be understood through an analysis of the coupling index itself. A low coupling index value requires three ingredients: high 850-hPa equivalent potential temperature, a steep tropospheric lapse rate, and a low tropopause (the latter two ingredients imply a low dynamic tropopause potential temperature). Large values of the first two ingredients are unambiguously favorable for all forms of tropical cyclogenesis because they favor the release of latent heat in active convection. The third ingredient, a low tropopause height indicative of an upper-level trough, is a requirement during the initial stages of TT. The trough provides quasigeostrophic forcing for ascent, which enhances the circulation by stretching and brings the midlevels toward saturation, thereby creating a synoptic-scale region favorable for sustained deep moist convection and development of the tropical cyclone vortex. The favorable dynamics and thermodynamics for TT are therefore well described by a low coupling index. However, an elevated tropopause is beneficial to *non-TT* developments because it implies a lower temperature in the outflow layer, a factor that enhances the thermodynamic efficiency of the Carnot cycle that represents the storm energy cycle (Emanuel 1986). With this ingredient favoring a higher coupling index for *non-TT* formations, it is not surprising that these events do not adhere to the same coupling index threshold that applies to *weak TT* and *strong TT* developments. The completion of the TT process is characterized by the replacement of the upper-level trough with an outflow anticyclone, a change that renders the system energetically and morphologically indistinguishable from one that has undergone a *non-TT* form of development. This implies that a direct relationship between the coupling index and TT formation processes exists primarily before and during transformation, the baroclinically influenced portion of the storm life cycle that is incompletely described by SST alone.

The utility of the coupling index is further demonstrated by the relationship between its spatial distribution and the locations of TT events (Fig. 9). Because low values depend on both a cool upper troposphere and a relatively warm boundary layer, a "Goldilocks zone" emerges in the subtropics. It is in this band that midlatitude troughs penetrate sufficiently equatorward to play a role of TT-based development over SSTs that are warm enough to sustain deep convection (Schumacher et al. 2009). For example, the western South Atlantic basin, an area long thought to be devoid of tropical cyclones (Gray 1968), has recently given rise to two possible cold events via TT in an area of reduced coupling index values (Pezza and Simmonds 2005; Evans and Braun 2012; Dias Pinto et al. 2013). Discussion continues about whether such systems constitute tropical or subtropical storms given their high latitude of formation, relatively low underlying SSTs, and initially asymmetric structures; however, even subtropical storms rely largely on surface enthalpy fluxes and reduced tropospheric stability to sustain their circulations (Guishard et al. 2009). Cyclonic features with these characteristics can be found in all oceanic regions from the deep tropics (tropical cyclones) to the high latitudes [the cold-low class of polar lows (Businger and Reed 1989)]. Because these systems rely on similar energetics for their formation and maintenance, they possess similar storm morphologies: radial symmetry, a clear eye, spiral bands, and outflow anticyclone indicative of a warm core (Rasmussen 1979; Ernst and Matson 1983; Rasmussen and Zick 1987; Emanuel and Rotunno 1989; Yanase and Niino 2007).

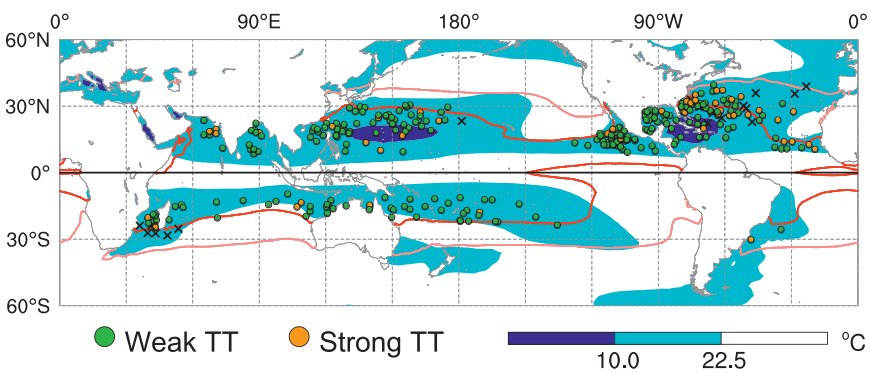

Fig. 9. Climatology of mean coupling index values (plotted according to the color bar) for the summer–fall period in each hemisphere, as for Fig. 3. Also plotted is the formation location of each TT event (dots, color-coded by pathway as shown in the legend) and each subtropical storm (black crisscrosses) in the best track dataset for the period 1989–2013. The seasonal-mean 26.5° and 21°C SST isotherms are plotted with red and salmon lines, respectively.

As a result of these similarities, the area covered by the climatological coupling index threshold (Fig. 9) extends well beyond the tropics into regions where the cold analogs of tropical cyclones form: the Mediterranean Sea (Reale and Atlas 2001; Emanuel 2005; Tous and Romero 2013), the Australian east coast (Qi et al. 2006; Garde et al. 2010; Pezza et al. 2014), the eastern North Atlantic (Shapiro et al. 1987; Føre et al. 2012), and the northern west Pacific (Watanabe and Niino 2014). This expansion is consistent with the physical relevance of the coupling index, but it may be problematic for estimates of tropical cyclone development potential that rely largely on the SST threshold to constrain large values to near-equatorial regions. Following Schumacher et al. (2009), the 21°C SST isotherm is included in Fig. 9 as a potential secondary condition that could be used to limit the poleward extent of the region expected to support the TT-based pathways to tropical cyclogenesis. The application of this condition may be acceptable because it has no effect on the results presented in this study; however, it is arbitrary and error prone because there is no clear physical distinction between these events and their higher-latitude counterparts.

IMPLICATIONS. The pathway-dependent utility of the 26.5°C SST threshold as a thermodynamic limit for tropical cyclogenesis has direct implications for forecasting, because its uniform application may lead to an underestimation of the likelihood of tropical cyclogenesis via TT. This problem is particularly relevant for developments occurring in the subtropics because, although they tend to be less intense than their lower-latitude counterparts, they tend to affect regions not accustomed to the effects of tropical cyclones. Although baroclinic precursors that are candidates for TT are readily identified in satellite imagery (Davis and Bosart 2004), their thermodynamic feasibility is impossible to assess from SST alone. The 22.5°C coupling index threshold provides guidance concerning the possibility of the transition of such systems into tropical cyclones in a manner analogous to the 26.5°C threshold for *non-TT* events.

The applicability of the 22.5°C coupling index threshold extends beyond the TT-based pathways for which it was designed to include the subtropical and hybrid storms in the best track record that meet the selection criteria for this study. Cold events dominate in this development class, with 65% (13/20) of events occurring over waters below 26.5°C. Given the reliance of subtropical storms on sustained convection to trigger moist baroclinic instability (Davis 2010), it is expected that the coupling index will provide an improved estimate of the thermodynamic limits on development. Indeed, the type-II error rate falls to 10% using the 22.5°C coupling index threshold, with all tracked subtropical cyclogenesis events falling within the climatological range of this value (formation locations marked with crosses in Fig. 9). This result is consistent with the expected robustness of the coupling index for the full spectrum of diabatically enhanced cyclones that occur across the global basins.

The use of SST and SST anomalies as predictors in statistical models for seasonal forecasts of tropical cyclone activity is widespread (review provided by Camargo et al. 2007), a consequence of the direct relevance of underlying water temperature to the majority of tropical cyclogenesis events. The addition of a coupling index predictor should enhance the sensitivity of the seasonal guidance to baroclinically influenced systems, thus improving their ability to predict the frequency of occurrence of TT on seasonal time scales. This preliminary introduction of a pathway-dependent predictor in statistical models of tropical cyclogenesis potential represents a first step toward an index that is conditional on the development pathway supported by the storm environment.

On climate time scales, the sensitivity of the coupling index to tropospheric stability makes it well suited to adapt to the nonuniform vertical profiles of temperature trends that affect the validity of SST-based thresholds for convection (Yoshimura et al. 2006; Knutson et al. 2008; Johnson and Xie 2010). Although upper-level warming is expected to offset SST increases in the tropics (Vecchi and Soden 2007; Fu et al. 2011; Vecchi et al. 2013), this constancy in tropospheric stability may not extend into the subtropics (Thorne et al. 2011). The relationship between TT and the coupling index suggests that the climatological prevalence of such events may therefore change as the difference in upper and lower boundary temperatures evolves. Particularly given the apparent poleward expansion of tropical cyclone activity (Kossin et al. 2014), the coupling index may be increasingly useful as an estimator of the impacts of a changing atmospheric state on the thermodynamic limits for tropical cyclone formation in the subtropics.

The traditional 26.5°C SST threshold is of practical use for the majority of tropical cyclogenesis events; however, the presence of a baroclinic precursor can alter the formation process sufficiently to promote development over cooler waters. During such events, a 22.5°C coupling index threshold appears to be a more sensitive and reliable measure of the thermodynamic limits on development. Added to the list of ingredients

required for tropical cyclogenesis, this threshold introduces a conceptually distinct element of direct physical relevance to the important TT subset of storm formation events.

ACKNOWLEDGMENTS. This article arose from the second author's third-year undergraduate dissertation at the University of Manchester. Partial funding for Schultz was provided by the U.K. Natural Environment Research Council (NERC) to the Diabatic Influences on Mesoscale Structures in Extratropical Cyclones (DIAMET) project at the University of Manchester (Grant NE/I005234/1), and partial funding for Fairman was provided by NERC to the Precipitation Structures over Orography (PRESTO) project at the University of Manchester (Grant NE/1024984/1). Partial funding for Galarneau was provided by NOAA/HFIP Grant NA12NWS4680005. Early versions of the study benefited significantly from comments supplied by Drs. John Gyakum, James McTaggart-Cowan, and Ayrton Zadra. The constructive comments of three anonymous reviewers during the peer review process greatly helped to improve the final study.

REFERENCES

Ackerman, S. A., and J. A. Knox, 2015: *Meteorology: Understanding the Atmosphere.* 4th ed. Jones and Bartlett Learning, 575 pp.

Ahrens, C. D., 2009: *Meteorology Today: An Introduction to Weather, Climate, and the Environment.* 9th ed. Cengage Learning, 549 pp.

Black, P. G., and Coauthors, 2007: Air–sea exchange in hurricanes: Synthesis of observations from the Coupled Boundary Layer Air–Sea Transfer Experiment. *Bull. Amer. Meteor. Soc.,* **88,** 357–374, doi:10.1175/BAMS-88-3-357.

Bosart, L. F., and J. A. Bartlo, 1991: Tropical storm formation in a baroclinic environment. *Mon. Wea. Rev.,* **119,** 1979–2013, doi:10.1175/1520-0493(1991)119<1979:TSFIAB>2.0.CO;2.

——, and G. M. Lackmann, 1995: Postlandfall tropical cyclone reintensification in a weakly baroclinic environment: A case study of Hurricane David (September 1979). *Mon. Wea. Rev.,* **123,** 3268–3291, doi:10.1175/1520-0493(1995)123<3268:PTCRIA>2.0.CO;2.

Bretherton, F. P., 1966: Critical layer instability in baroclinic flows. *Quart. J. Roy. Meteor. Soc.,* **92,** 325–334, doi:10.1002/qj.49709239302.

Businger, S., and R. J. Reed, 1989: Cyclogenesis in cold air masses. *Wea. Forecasting,* **4,** 133–156, doi:10.1175/1520-0434(1989)004<0133:CICAM>2.0.CO;2.

Camargo, S. J., A. G. Barnston, P. J. Klotzbach, and C. W. Landsea, 2007: Seasonal tropical cyclone forecasts. *WMO Bull.,* **56,** 297–309.

Cram, T., J. Persing, M. T. Montgomery, and S. Braun, 2007: A Lagrangian trajectory view on transport and mixing processes between the eye, eyewall, and environment using a high-resolution simulation of Hurricane Bonnie (1998). *J. Atmos. Sci.,* **64,** 1835–1856, doi:10.1175/JAS3921.1.

Dare, R. A., and J. L. McBride, 2011: The threshold sea surface temperature condition for tropical cyclogenesis. *J. Climate,* **24,** 4570–4576, doi:10.1175/JCLI-D-10-05006.1.

Davies, H. C., and C. H. Bishop, 1994: Eady edge waves and rapid development. *J. Atmos. Sci.,* **51,** 1930–1946, doi:10.1175/1520-0469(1994)051<1930:EEWARD>2.0.CO;2.

Davis, C. A., 2010: Simulations of subtropical cyclones in a baroclinic channel model. *J. Atmos. Sci.,* **67,** 2871–2892, doi:10.1175/2010JAS3411.1.

——, and L. F. Bosart, 2003: Baroclinically induced tropical cyclogenesis. *Mon. Wea. Rev.,* **131,** 2730–2747, doi:10.1175/1520-0493(2003)131<2730:BITC>2.0.CO;2.

——, and ——, 2004: The TT problem. *Bull. Amer. Meteor. Soc.,* **85,** 1657–1662, doi:10.1175/BAMS-85-11-1657.

Dee, D. P., and Coauthors, 2011: The ERA-Interim reanalysis: Configuration and performance of the data assimilation system. *Quart. J. Roy. Meteor. Soc.,* **137,** 553–597, doi:10.1002/qj.828.

DeMaria, M., 1996: The effect of vertical shear on tropical cyclone intensity change. *J. Atmos. Sci.,* **53,** 2076–2088, doi:10.1175/1520-0469(1996)053<2076:TEOVSO>2.0.CO;2.

——, J. A. Knaff, and B. H. Connell, 2001: A tropical cyclone genesis parameter for the tropical Atlantic. *Wea. Forecasting,* **16,** 219–233, doi:10.1175/1520-0434(2001)016<0219:ATCGPF>2.0.CO;2.

Dias Pinto, J. R., M. S. Reboita, and R. P. da Rocha, 2013: Synoptic and dynamical analysis of subtropical cyclone Anita (2010) and its potential for tropical transition over the South Atlantic Ocean. *J. Geophys. Res. Atmos.,* **118,** 10 870–10 883, doi:10.1002/jgrd.50830.

Duong, T., 2007: ks: Kernel density estimation and kernel discriminant analysis for multivariate data in R. *J. Stat. Software,* **21** (7). [Availble online at www.jstatsoft.org/v21/i07/paper.]

Emanuel, K. A., 1986: An air–sea interaction theory for tropical cyclones. Part I: Steady-state maintenance. *J. Atmos. Sci.,* **43,** 585–605, doi:10.1175/1520-0469(1986)043<0585:AASITF>2.0.CO;2.

——, 1989: The finite-amplitude nature of tropical cyclogenesis. *J. Atmos. Sci.,* **46,** 3431–3456,

doi:10.1175/1520-0469(1989)046<3431:TFANOT>2.0.CO;2.

——, 1991: The theory of hurricanes. *Annu. Rev. Fluid Mech.,* **23,** 179–196, doi:10.1146/annurev.fl.23.010191.001143.

——, 1995: Sensitivity of tropical cyclones to surface exchange coefficients and a revised steady-state model incorporating eye dynamics. *J. Atmos. Sci.,* **52,** 3969–3976, doi:10.1175/1520-0469(1995)052<3969:SOTCTS>2.0.CO;2.

——, 2005: Genesis and maintenance of "Mediterranean hurricanes." *Adv. Geosci.,* **2,** 217–220, doi:10.5194/adgeo-2-217-2005.

——, and R. Rotunno, 1989: Polar lows as arctic hurricanes. *Tellus,* **41A,** 1–17, doi:10.1111/j.1600-0870.1989.tb00362.x.

Ernst, J. A., and M. Matson, 1983: A Mediterranean tropical storm? *Weather,* **38,** 332–337, doi:10.1002/j.1477-8696.1983.tb04818.x.

Evans, J. L., and M. P. Guishard, 2009: Atlantic subtropical storms. Part I: Diagnostic criteria and composite analysis. *Mon. Wea. Rev.,* **137,** 2065–2080, doi:10.1175/2009MWR2468.1.

——, and A. Braun, 2012: A climatology of subtropical cyclones in the South Atlantic. *J. Climate,* **25,** 7328–7340, doi:10.1175/JCLI-D-11-00212.1.

Fairall, C. W., E. F. Bradley, J. E. Hare, A. A. Grachev, and J. B. Edson, 2003: Bulk parameterization of air–sea fluxes: Updates and verification for the COARE algorithm. *J. Climate,* **16,** 571–591, doi:10.1175/1520-0442(2003)016<0571:BPOASF>2.0.CO;2.

Fisher, E. L., 1958: Hurricanes and the sea-surface temperature field. *J. Meteor.,* **15,** 328–333, doi:10.1175/1520-0469(1958)015<0328:HATSST>2.0.CO;2.

Føre, I., J. E. Kristjánsson, E. W. Kolstad, T. J. Bracegridle, O. Saetra, and B. Røsting, 2012: A "hurricane-like" polar low fuelled by sensible heat flux: High-resolution numerical simulations. *Quart. J. Roy. Meteor. Soc.,* **138,** 1308–1324, doi:10.1002/qj.1876.

Friedman, J. H., 1989: Regularized discriminant analysis. *J. Amer. Stat. Assoc.,* **84,** 165–175, doi:10.1080/01621459.1989.10478752.

Fu, Q., S. Manabe, and C. M. Johanson, 2011: On the warming in the tropical upper troposphere: Model versus observations. *Geophys. Res. Lett.,* **38,** l15704, doi:10.1029/2011GL048101.

Galvin, J. F. P., 2008: The weather and climate of the tropics: Part 7—Tropical revolving storms. *Weather,* **63,** 327–333, doi:10.1002/wea.252.

Garde, L. A., A. B. Pezza, and J. A. T. Bye, 2010: Tropical transition of the 2001 Australian Duck. *Mon. Wea. Rev.,* **138,** 2038–2057, doi:10.1175/2009MWR3220.1.

Gray, W., 1968: Global view of the origin of tropical disturbances and storms. *Mon. Wea. Rev.,* **96,** 669–700, doi:10.1175/1520-0493(1968)096<0669:GVOTOO>2.0.CO;2.

Guishard, M. P., J. L. Evans, and R. E. Hart, 2009: Atlantic subtropical storms. Part II: Climatology. *J. Climate,* **22,** 3574–3594, doi:10.1175/2008JCLI2346.1.

Hoskins, B., M. McIntyre, and A. Robertson, 1985: On the use and significance of isentropic potential vorticity maps. *Quart. J. Roy. Meteor. Soc.,* **111,** 877–946, doi:10.1002/qj.49711147002.

Johnson, N. C., and S.-P. Xie, 2010: Changes in the sea surface temperature threshold for tropical convection. *Nat. Geosci.,* **3,** 842–845, doi:10.1038/ngeo1008.

Kelly, W. E., Jr., and D. R. Mock, 1982: A diagnostic study of upper tropospheric cold lows over the western North Pacific. *Mon. Wea. Rev.,* **110,** 471–480, doi:10.1175/1520-0493(1982)110<0471:ADSOUT>2.0.CO;2.

Knapp, K. R., M. C. Kruk, D. H. Levinson, H. J. Diamond, and C. J. Neumann, 2010: The International Best Track Archive for Climate Stewardship (IBTrACS): Unifying tropical cyclone data. *Bull. Amer. Meteor. Soc.,* **91,** 363–376, doi:10.1175/2009BAMS2755.1.

——, J. A. Knaff, C. R. Sampson, G. M. Riggio, and A. D. Schnapp, 2013: A pressure-based analysis of the historical western North Pacific tropical cyclone intensity record. *Mon. Wea. Rev.,* **141,** 2611–2631, doi:10.1175/MWR-D-12-00323.1.

Knutson, T. R., J. J. Sirutis, S. T. Garner, G. A. Vecchi, and I. M. Held, 2008: Simulated reduction in Atlantic hurricane frequency under twenty-first-century warming conditions. *Nat. Geosci.,* **1,** 359–364, doi:10.1038/ngeo202.

Koba, H., T. Hagiwara, S. Osano, and S. Akashi, 1991: Relationships between CI number and minimum sea level pressure/maximum wind speed of tropical cyclones. *Geophys. Mag.,* **44,** 15–25.

Kossin, J. P., K. A. Emanuel, and G. A. Vecchi, 2014: The poleward migration of the location of tropical cyclone maximum intensity. *Nature,* **509,** 349–352, doi:10.1038/nature13278.

Laing, A., and J. L. Evans, 2011: *Introduction to Tropical Meteorology.* 2nd ed. University Corporation for Atmospheric Research. [Available online at www.goes-r.gov/users/comet/tropical/textbook_2nd_edition/index.htm.]

Lee, C. S., R. Edson, and W. M. Gray, 1989: Some large-scale characteristics associated with tropical cyclone development in the north Indian Ocean during FGGE. *Mon. Wea. Rev.,* **117,** 407–426, doi:10.1175/1520-0493(1989)117<0407:SLSCAW>2.0.CO;2.

Mauk, R. G., and J. S. Hobgood, 2012: Tropical cyclone formation in environments with cool SST and high wind shear over the northeastern Atlantic Ocean. *Wea. Forecasting,* **27,** 1433–1447, doi:10.1175/WAF-D-11-00048.1.

McTaggart-Cowan, R., L. F. Bosart, C. A. Davis, E. H. Atallah, J. R. Gyakum, and K. A. Emanuel, 2006: Analysis of Hurricane Catarina (2004). *Mon. Wea. Rev.,* **134,** 3029–3053, doi:10.1175/MWR3330.1.

——, G. D. Deane, L. F. Bosart, C. A. Davis, and T. J. Galarneau Jr., 2008: Climatology of tropical cyclogenesis in the North Atlantic (1948–2004). *Mon. Wea. Rev.,* **136,** 1284–1304, doi:10.1175/2007MWR2245.1.

——, T. J. Galarneau Jr., L. F. Bosart, and J. A. Milbrandt, 2010: Development of an Alpine lee cyclone during MAP D-PHASE. Part I: Case analysis and evaluation of control simulations. *Mon. Wea. Rev.,* **138,** 2281–2307, doi:10.1175/2009MWR3147.1.

——, ——, ——, R. W. Moore, and O. Martius, 2013: A global climatology of baroclinically influenced tropical cyclogenesis. *Mon. Wea. Rev.,* **141,** 1963–1989, doi:10.1175/MWR-D-12-00186.1.

Miller, B. I., 1958: The use of mean layer winds as a hurricane steering mechanism. U.S. National Hurricane Research Project Tech. Rep. 18, 24 pp.

Morgan, M. C., and J. W. Nielsen-Gammon, 1998: Using tropopause maps to diagnose midlatitude weather systems. *Mon. Wea. Rev.,* **126,** 2555–2579, doi:10.1175/1520-0493(1998)126<2555:UTMTDM>2.0.CO;2.

Palmén, E. H., 1948: On the formation and structure of tropical cyclones. *Geophysica,* **3,** 26–38.

——, 1956: Formation and development of tropical cyclones. *Proc. Tropical Cyclone Symp.,* Brisbane, QLD, Australia, Bureau of Meteorology, 213–231.

Pezza, A. B., and I. Simmonds, 2005: The first South Atlantic hurricane: Unprecedented blocking, low shear and climate change. *Geophys. Res. Lett.,* **32,** L15712, doi:10.1029/2005GL023390.

——, L. A. Garde, J. A. P. Veiga, and I. Simmonds, 2014: Large scale features and energetics of the hybrid subtropical low "Duck" over the Tasman Sea. *Climate Dyn.,* **42,** 453–466, doi:10.1007/s00382-013-1688-x.

Qi, L., L. M. Leslie, and M. S. Speer, 2006: Climatology of cyclones over the southwest Pacific: 1992-2001. *Meteor. Atmos. Phys.,* **91,** 201–209, doi:10.1007/s00703-005-0149-4.

Rasmussen, E., 1979: The polar low as an extratropical CISK disturbance. *Quart. J. Roy. Meteor. Soc.,* **105,** 531–549, doi:10.1002/qj.49710544504.

——, and C. Zick, 1987: A subsynoptic vortex over the Mediterranean Sea with some resemblance to polar lows. *Tellus,* **39A,** 408–425, doi:10.1111/j.1600-0870.1987.tb00318.x.

Reale, O., and R. Atlas, 2001: Tropical cyclone–like vortices in the extratropics: Observational evidence and synoptic analysis. *Wea. Forecasting,* **16,** 7–34, doi:10.1175/1520-0434(2001)016<0007:TCLVIT>2.0.CO;2.

Reynolds, R. W., T. M. Smith, C. Liu, D. B. Chelton, K. S. Casey, and M. G. Schlax, 2007: Daily high-resolution-blended analyses for sea surface temperature. *J. Climate,* **20,** 5473–5496, doi:10.1175/2007JCLI1824.1.

Riehl, H. H., 1954: *Tropical Meteorology.* McGraw-Hill, 392 pp.

Riemer, M., M. T. Montgomery, and M. E. Nicholls, 2010: A new paradigm for intensity modification of tropical cyclones: Thermodynamic impact of vertical wind shear on the inflow layer. *Atmos. Chem. Phys.,* **10,** 3163–3188, doi:10.5194/acp-10-3163-2010.

Sadler, J. C., 1964: Tropical cyclones of the eastern North Pacific as revealed by TIROS observations. *J. Appl. Meteor.,* **3,** 347–366, doi:10.1175/1520-0450(1964)003<0347:TCOTEN>2.0.CO;2.

——, 1975: The upper tropospheric circulation over the global tropics. Tech. Rep. UHMET-75-05, Dept. of Meteorology, University of Hawaii, 35 pp.

Schumacher, A. B., M. DeMaria, and J. Knaff, 2009: Objective estimation of the 24-h probability of tropical cyclone formation. *Wea. Forecasting,* **24,** 456–471, doi:10.1175/2008WAF2007109.1.

Shapiro, M. A., L. S. Fedor, and T. Hampel, 1987: Researching aircraft measurements of a polar low over the Norwegian Sea. *Tellus,* **39A,** 272–306, doi:10.1111/j.1600-0870.1987.tb00309.x.

Tang, B., and K. Emanuel, 2012: A ventilation index for tropical cyclones. *Bull. Amer. Meteor. Soc.,* **93,** 1901–1912, doi:10.1175/BAMS-D-11-00165.1.

Thorne, P. W., J. R. Lanzante, T. C. Peterson, D. Seidel, and K. P. Shine, 2011: Tropospheric temperature trends: History of an ongoing controversy. *Wiley Interdiscip. Rev.: Climate Change,* **2,** 66–88, doi:10.1002/wcc.80.

Tous, M., and R. Romero, 2013: Meteorological environments associated with medicane development. *Int. J. Climatol.,* **33,** 1–14, doi:10.1002/joc.3428.

Vecchi, G. A., and B. J. Soden, 2007: Effect of remote sea surface temperature change on tropical cyclone potential intensity. *Nature,* **450,** 1066–1070, doi:10.1038/nature06423.

——, S. Fueglistaler, I. M. Held, T. R. Knutson, and Z. Ming, 2013: Impacts of atmospheric temperature trends on tropical cyclone activity. *J. Climate,* **26,** 3877–3891, doi:10.1175/JCLI-D-12-00503.1.

Wallace, J. M., and P. V. Hobbs, 2006: *Atmospheric Science: An Introductory Survey.* 2nd ed. Academic Press, 483 pp.

Watanabe, S. I., and H. Niino, 2014: Genesis and development mechanisms of a polar mesocyclone over the Japan Sea. *Mon. Wea. Rev.,* **142,** 2248–2270, doi:10.1175/MWR-D-13-00226.1.

Wendland, W. M., 1977: Tropical storm frequencies related to sea surface temperatures. *J. Appl. Meteor.,* **16,** 477–481, doi:10.1175/1520-0450(1977)016<0477:TSFRTS>2.0.CO;2.

Williams, J., 2009: *The AMS Weather Book: The Ultimate Guide to America's Weather.* Amer. Meteor. Soc., 316 pp.

Yanase, W., and H. Niino, 2007: Dependence of polar low development on baroclinicity and physical processes: An idealized high-resolution numerical experiment. *J. Atmos. Sci.,* **64,** 3044–3067, doi:10.1175/JAS4001.1.

Yoshimura, J., M. Sugi, and A. Noda, 2006: Influence of greenhouse warming on tropical cyclone frequency. *J. Meteor. Soc. Japan,* **84,** 405–428, doi:10.2151/jmsj.84.405.

Zhang, X., A. Sorteberg, J. Zhang, R. Gerdes, and J. C. Comiso, 2008: Recent radical shifts of atmospheric circulations and rapid changes in Arctic climate system. *Geophys. Res. Lett.,* **35,** L22701, doi:10.1029/2008GL035607.

AMS BOOKS: SOMETHING FOR EVERYONE

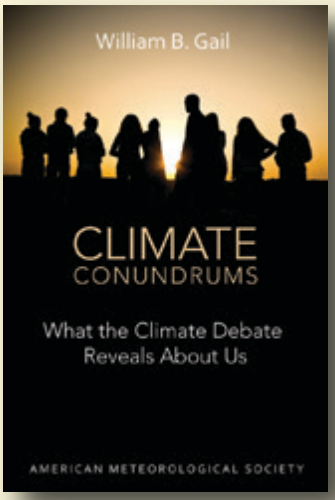

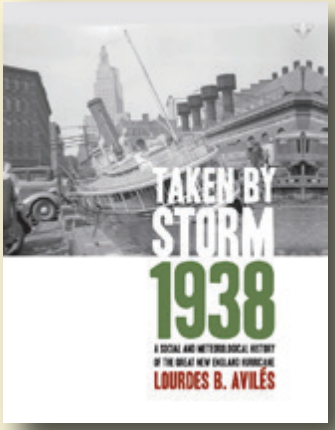

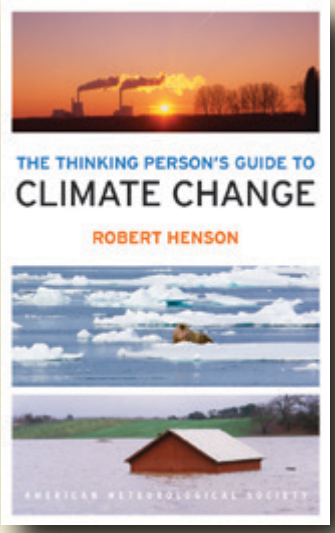

20% OFF your order through 12/31/15 with code BAMS2015
(Does not apply to undergraduate coursebooks.)

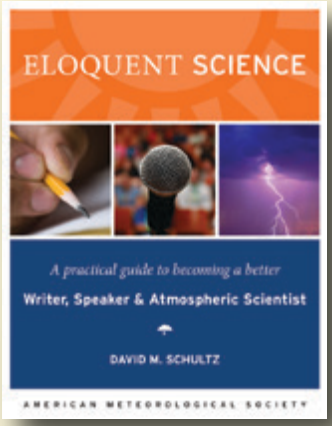

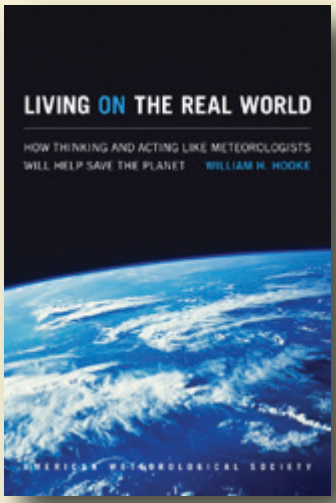

From enthusiasts, to students, to experts

We publish:

- Meteorological reanalysis and storm histories
- Weather, water, and climate coursebooks
- Research monographs for many focused specialties
- Weather and climate images for lecture notes and slides
- References including our bestseller *Eloquent Science*

Members always receive discounts and FREE SHIPPING

www.ametsoc.org/bookstore

AMS BOOKS

SPECIAL
MATERHORN
COLLECTION

THE MATERHORN

Unraveling the Intricacies of Mountain Weather

BY H. J. S. FERNANDO, E. R. PARDYJAK, S. DI SABATINO, F. K. CHOW, S. F. J. DE WEKKER, S. W. HOCH, J. HACKER, J. C. PACE, T. PRATT, Z. PU, W. J. STEENBURGH, C. D. WHITEMAN, Y. WANG, D. ZAJIC, B. BALSLEY,* R. DIMITROVA, G. D. EMMITT, C. W. HIGGINS, J. C. R. HUNT, J. C. KNIEVEL, D. LAWRENCE, Y. LIU, D. F. NADEAU, E. KIT, B. W. BLOMQUIST, P. CONRY, R. S. COPPERSMITH, E. CREEGAN, M. FELTON, A. GRACHEV, N. GUNAWARDENA, C. HANG, C. M. HOCUT, G. HUYNH, M. E. JEGLUM, D. JENSEN, V. KULANDAIVELU, M. LEHNER, L. S. LEO, D. LIBERZON, J. D. MASSEY, K. MCENERNEY, S. PAL, T. PRICE, M. SGHIATTI, Z. SILVER, M. THOMPSON, H. ZHANG, AND T. ZSEDROVITS

Comprehensive, multiscale, and multidisciplinary observations allow scientists to discover novel flow physics, address current deficiencies of predictive models, and improve weather prediction in mountainous terrain.

Through woods and mountain passes
the winds, like anthems, roll.
—Henry Wadsworth Longfellow

For centuries, humans have been both fascinated and awed by mountain weather, and its intriguing aberrancy continues to baffle weather forecasters. For instance, a clear morning on a tranquil mountain slope can swiftly change into violent storms within hours while a nearby valley remains calm. The variability of mountain weather spans a wide swath of space–time scales, contributing to a myriad of phenomena that stymie the predictability of mountain weather. Although isolated mountains are rare, about 20% of Earth's land surface is covered by mountainous areas (Louis 1975). Topography less than 600 m in height (<5% of the atmospheric-scale height) is referred to as hills, but demarcations between different topographic features remain ambiguous. Orographic mosaics that incorporate slopes, valleys, canyons, escarpments, gullies, and buttes (also known as complex terrain) cover about 70% of Earth's land surface (Strobach 1991). The majority of the world's urban areas have emerged in complex terrain because of accompanying water resources. Systematic studies of mountain weather date back to the 1850s, followed by a decline of scientific activity in the early 1900s owing to observational difficulties. A resurgence of research occurred in the midtwentieth century with the advent of aerological networks (Bjerknes et al. 1934) as well as groundbreaking advances of mountain-wave and slope-flow studies (Prandtl 1942; Queney 1948; Long 1953). Vivid applications in areas of urban air pollution (Ellis et al. 2000; Fernando and Weil 2010), dispersion in cities (Allwine et al. 2002), wind energy harvesting (Banta et al. 2013), aviation (Politovich et al. 2011), alpine warfare (Winters et al. 2001), and firefighting (Albini et al. 1982) have burgeoned mountain meteorology, but understanding of flow physics and fidelity of predictions leaves much to be desired. Reviews of relevant past research are found in Taylor et al. (1987), Blumen (1990), Baines (1998), Belcher and Hunt (1998), Whiteman (2000), Wood (2000), Barry (2008), Fernando (2010), and Chow et al. (2013).

Prompted by applications-driven overarching science questions, in 2011 the U.S. Department of Defense (DoD) funded a 5-yr Multidisciplinary University Research Initiative (MURI) aimed at

improving weather prediction in mountainous terrain. Dubbed MATERHORN, this effort involves 11 principal investigators from five academic institutions (see sidebar on "Program synopsis"). Ten additional collaborators have joined the project with an array of research tools [more information can be found online (http://dx.doi.org/10.1175/BAMS-D-12-00023.2) in the supplementary information]. At the outset, the existing barriers to mountain weather forecasting were reviewed and critical science and modeling needs were identified, and based on which, a multifaceted research effort was developed. Commensurate with available resources, the focus was limited to arid/semiarid regions and scales at or smaller than the mesoscale, thus deemphasizing issues such as orographic precipitation and marine pushes. Two extensive field campaigns were conducted within the first 3 years, and their design drew guidance from recent complex-terrain field campaigns such as Vertical Transport and Mixing (VTMX; Doran et al. 2002), Mesoscale Alpine Programme (MAP; Rotach and Zardi 2007), Meteor Crater Experiment (METCRAX; Whiteman et al. 2008), Terrain-Induced Rotor Experiment (T-REX; Grubišić et al. 2008), the Phoenix Air Flow Experiment (PAFEX; Pardyjak et al. 2009), Cold-Air Pooling Experiment (COLPEX; Price et al. 2011), Phoenix Evening Transition Flow Experiment (TRANSFLEX; Fernando et al. 2013), Boundary-Layer Late Afternoon and Sunset Turbulence (BLLAST; Lothon et al. 2014), and Meteo-diffusion (Leo et al. 2015a).

The Granite Mountain Atmospheric Science Testbed of the U.S. Army Dugway Proving Ground (DPG) was selected as the field site. This site has the advantages of a large spatial extent, richness in mountain weather phenomena, interesting climatological regimes, distinct (but few) land-use types, an existing instrumentation network, and unique logistical support. A repertoire of measurement tools were used to observe processes over a wide range of space–time scales, which was augmented by model evaluations and improvements. This paper presents an overview of MATERHORN, starting with an outline of complex-terrain flow processes followed by discussions of critical science gaps, field campaigns, modeling efforts, and preliminary results.

FLOW PROCESSES IN COMPLEX TERRAIN.

Figure 1 schematizes mountain-valley flow processes over a DPG topographic map. Under weak synoptic (wind speed $U_s > 5$ m s^{-1}) conditions dominated by high pressure, the characteristic winds are downslope (katabatic) and downvalley at night (blue arrows) while upslope (anabatic) and upvalley during the day (red), signifying thermal circulation (Whiteman 2000; Fernando 2010; Zardi and Whiteman 2013). Pure slope and valley winds are rare in nature, since they interact among themselves and with synoptic flow. At night, downslope/downvalley winds drain through gaps and canyons (Mayr et al. 2007), separate out from the slopes as intrusions (Lu and Turco 1994), interact with smaller topographic features (Baines 1998), and, as will be discussed later, collide with each other to create spasmodic turbulence episodes. Colder nocturnal air draining down from the slopes accumulates in confined valleys, forming stable cold pools that are weakly turbulent (Whiteman et al. 2008; Monti et al. 2002). Pulsations of katabatic flow at critical internal-wave frequency (Princevac et al. 2008), interleaving intrusions arriving

AFFILIATIONS: Fernando, Di Sabatino, Pratt, Dimitrova, Hunt, Conry, Coppersmith, Hocut, Leo, Liberzon, Mcenerney, Silver, Thompson, and Zsedrovits—University of Notre Dame, Notre Dame, Indiana; Pardyjak, Hoch, Pu, Steenburgh, Whiteman, Gunawardena, Hang, Jeglum, Jensen, Kulandaivelu, Lehner, Massey, Price, and Zhang—University of Utah, Salt Lake City, Utah; Chow—University of California, Berkeley, Berkeley, California; De Wekker, Pal, and Sghiatti—University of Virginia, Charlottesville, Virginia; Hacker—Naval Postgraduate School, Monterey, California, and National Center for Atmospheric Research, Boulder, Colorado; Pace and Zajic—U.S. Army Dugway Proving Ground, Utah; Wang, Creegan, Felton, and Huynh—U.S. Army Research Laboratory, Adelphi, Maryland; Balsley and Lawrence—University of Colorado Boulder, Boulder, Colorado; Emmitt—Simpson Weather Associates, Charlottesville, Virginia; Higgins—Oregon State University, Corvallis, Oregon; Knievel and Liu—National Center for Atmospheric Research, Boulder, Colorado; Nadeau—École Polytechnique de Montréal, Montreal, Quebec, Canada; Kit—University of Notre Dame, Notre Dame, Indiana, and Tel Aviv University, Tel Aviv, Israel; Blomquist and Grachev—University of Notre Dame, Notre Dame, Indiana, and National Oceanic and Atmospheric Administration, Silver Spring, Maryland, and University of Colorado Boulder, Boulder, Colorado
* In memoriam.
CORRESPONDING AUTHOR: Harindra Joseph Fernando, Environmental Fluid Dynamics Laboratories, Department of Civil and Environmental Engineering and Earth Sciences and Department of Aerospace and Mechanical Engineering, 156 Fitzpatrick Hall, University of Notre Dame, Notre Dame, IN 46556-5637
E-mail: hfernand@nd.edu

The abstract for this article can be found in this issue, following the table of contents.

DOI:10.1175/BAMS-D-13-00131.1
A supplement to this article is available online (10.1175/BAMS-D-13-00131.2)

In final form 17 April 2015

PROGRAM SYNOPSIS

The Mountain Terrain Atmospheric Modeling and Observations (MATERHORN) Program was designed to investigate complex-terrain meteorology over a wide range of scales, topographic features, and driving mechanisms by drawing expertise from multiple disciplines and by employing complementary research methodologies. The principal participants are the University of Notre Dame (UND; lead); University of California, Berkeley (UCB); Naval Postgraduate School (NPS); University of Utah (UU); and University of Virginia (UVA).

MATERHORN consists of four components working symbiotically:

- The modeling component (MATERHORN-M) investigates predictability at the mesoscale, in particular, sensitivity (error growth) to initial conditions at various lead times, dependence on boundary conditions and input background properties, as well as merits of different data-assimilation techniques. It also attempts high-resolution simulations with novel modeling and terrain-representation methodologies.
- The experimental component (MATERHORN-X) mainly conducts field measurements at unprecedented spatiotemporal detail by deploying arrays of routine, high-end, and newly developed instrumentation. Laboratory experiments are used for process studies.
- The technology development component (MATERHORN-T) enables currently untenable meteorological observations. The developments include an instrumented UAV, sensors for moisture and fog measurements, and a combined hot-film/sonic anemometer system for probing turbulence down to Kolmogorov scales. Advanced data retrieval and processing algorithms are also attempted.
- The parameterization component (MATERHORN-P) develops high-fidelity physics-based fundamental (quantitative) relationships for complex-terrain processes, which are implemented in mesoscale models followed by model evaluations.

from different topographies (Fernando et al. 2013), and shear layers of flow fanning out from the gaps all contribute to the weakly turbulent state. This differs from very stable boundary layers over flat terrain, where turbulence is highly intermittent in space and time (Mahrt 1999).

As the nocturnal stable boundary layer (SBL) breaks down during the morning transition, paving the way for a daytime convective boundary layer (CBL), a flow reversal occurs from downslope/downvalley to upslope/upvalley. Upslope flow may separate on the slopes in the form of thermal plumes, topped by cumulus clouds (Banta 1984; Hocut et al. 2015). During the evening transition, the signs of heat flux and vertical temperature gradient reverse, convective turbulence collapses, and the downslope/downvalley flow system reemerges. A host of physical processes contribute to morning (Whiteman 1982; Princevac and Fernando 2008) and evening transitions (Hunt et al. 2003; Nadeau et al. 2011). Other flow types include local (micro) circulations driven by thermal and roughness contrasts arising from land-cover inhomogeneities (Jannuzzi 1993; Rife et al. 2002).

Under strong synoptic conditions ($U_s \gg U_t$, where U_t is the characteristic velocity of the thermal circulation), flow is energetic and inertially dominated. When the approach flow is stably stratified (with velocity U and buoyancy frequency N), it responds to the topography (height h) by distorting the flow over horizontal spatial scales on the order of the Rossby deformation radius (Hunt et al. 2004). Ensuing local phenomena are dependent on the Froude number ($\mathrm{Fr} = U/Nh$), with thermal circulation becoming insignificant when $\mathrm{Fr} > 0.5$ (Poulos et al. 2000). Stably stratified mountain wakes consist of lee waves, propagating internal waves, rotors, separated flow, and intriguing vortex structures (Long 1972; Lin et al. 1992; Hunt et al. 2006). If the topography is 3D, the flow above the dividing streamline goes over the mountain while the rest flows around the mountain (Snyder et al. 1985). In 2D cases, the flow below the dividing streamline is blocked upstream, but when there is a gap in the topography the flow can leak through it, depending on Fr and the gap aspect ratio (Baines 1979). At very high Fr, the flow is similar to the neutral case, with shear-layer separation and vortex shedding at the edges of the topography (Brighton 1978).

Daytime heating leads to the CBL development, and when the synoptic condition is such that U_s is of the same order as the Deardorff (1970) convective-scale w_*, the upslope flow on the windward side is reinforced while that on the leeward side is weakened and separated to form recirculation cells (Fernando 2010). Numerical predictions under strong synoptic conditions ($U_s \gg U_t \sim w_*$) tend to be better than those under thermal circulation conditions, but, in general, both could be desired for near-surface predictions (Fernando and Weil 2010). The complexities associated with interacting wakes and shear layers of neighboring mountains, canyon effects, gap flows, and microcirculations are only beginning to be investigated.

CRITICAL SCIENCE NEEDS. Preceding MATERHORN, a workshop entitled "Overcoming Scientific Barriers to Weather Support in Mountainous Terrain" was held in Tempe, Arizona, 1–2 February

2010. Twenty-six invitees representing academia and stakeholders compiled a list of research needs, barriers, and experiences (a report is available from the corresponding author), a subset of which was selected for investigations:

1) the predictability of near-surface wind and temperature in complex terrain remains poor, in part owing to meager understanding of near-surface processes;
2) surface-layer predictions are sensitive to soil moisture and soil properties, which are inputs to the models, yet these key parameters are not accurately measured in field studies to quantify their role;
3) mesoscale models are more prone to forecast error when predicting in complex terrain than over flat terrain, possibly because of the large number of processes exclusive to complex terrain in the subgrid scales;
4) proper assimilation of near-surface observations is useful for improving short-range forecasts;
5) coordinated high-resolution observations from meso- to dissipation scales are needed using dense instrumentation networks, possibly using novel instrumentation, as most past observations have focused on a limited ranges of scales;
6) turbulence closure models and boundary layer parameterizations need to be revisited to help develop better subgrid parameterizations, particularly for the SBL; and
7) there is potential for ultra-high-resolution (<50-m horizontal) simulations using techniques such as the immersed boundary method (IBM).

Considering 1–7, MATERHORN was focused on high-resolution observations, near-surface processes,

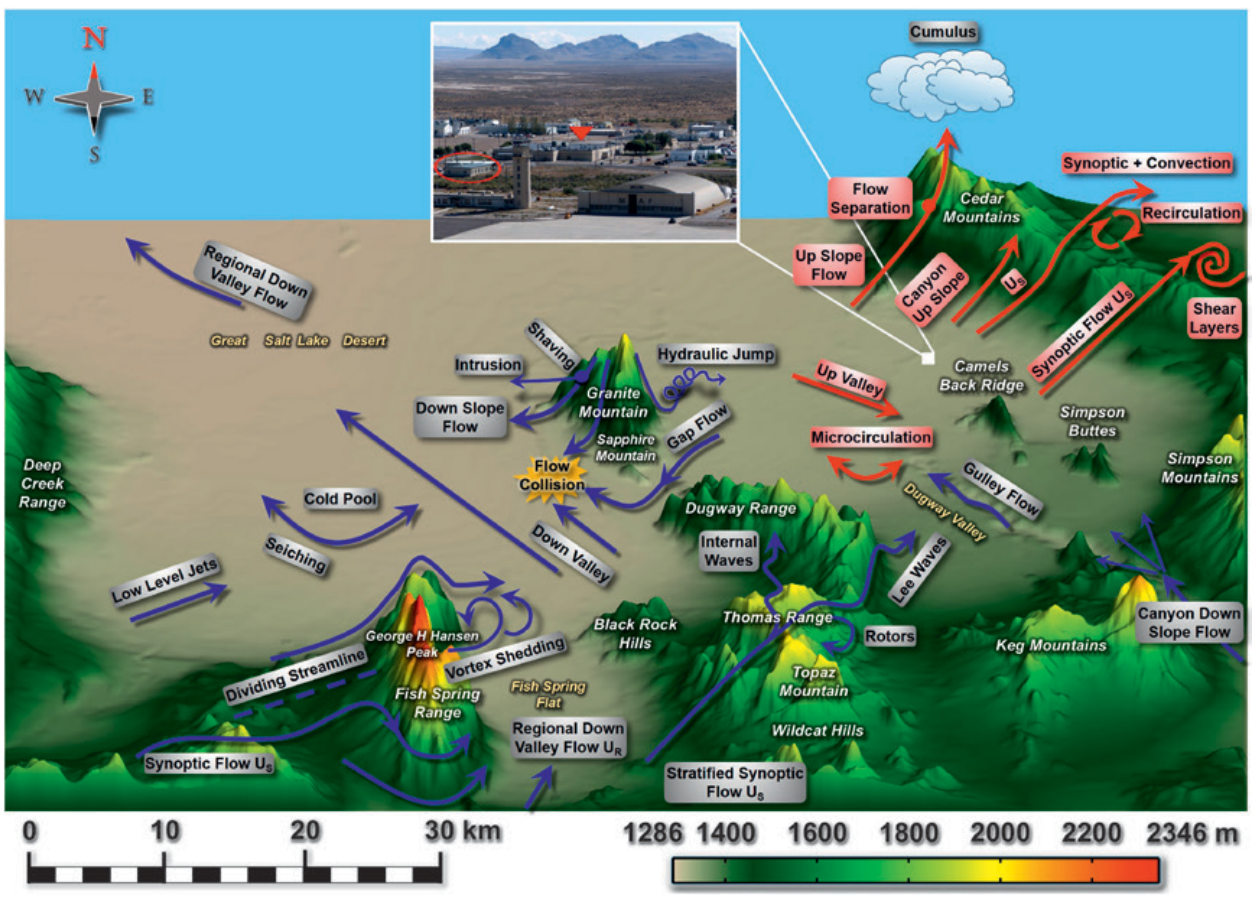

Fig. 1. Physical processes in complex terrain, illustrated on a topographic map of the DPG domain. The spatial and the elevation (shading) scales are shown below. Blue arrows represent nocturnal flows; red arrows represent daytime flows. An arbitrary direction has been used for illustration of synoptic effects (which typically varies from northwest to north to northeast in DPG). Shown in the inset are the control center (red arrow) and Ditto meteorological building (circled) of GMAST.

the role of surface and upper-soil-layer properties, boundary layer parameterizations, data assimilation, and high-resolution (large eddy) simulations (LESs) within mesoscale models.

MATERHORN-X. Two major field campaigns were conducted with high-resolution measurements, focusing on conditions dominated by thermal circulations and strong synoptic forcing. Another smaller study focused on fog formation, which will be a topic of future publications. The field site, equipment, and execution of the first two experiments are discussed next.

Field site. The Granite Mountain Atmospheric Science Testbed (GMAST) is a part of the U.S. Army DPG shown in Fig. 1. DPG is located 137 km southwest of Salt Lake City, Utah, and consists of 3700 km^2 of land in complex terrain with two dominant land-use types: playa and desert shrub. The region is dry with annual precipitation of 197 mm yr^{-1} (WRCC 2014). Within the DPG is a nominally isolated topographic feature, Granite Mountain (GM), 11.8 km in length, 6.1 km at its widest, and peak elevation 0.84 km above the valley floor, which itself is 1.3 km above mean sea level (MSL). The surroundings of the GM are well instrumented for providing meteorological support for weapon systems testing, thus forming GMAST. With DoD-controlled roads, air space, and facilities, it was possible to operate unmanned aerial vehicles (UAV), low-flying manned aircraft, and large smoke-release apparatuses. A special agreement between UND, UU, and DPG allowed access to this highly secured DoD facility on the premise that DPG would also benefit from the findings to improve its own meteorological capabilities. The fall campaign period (25 September–31 October 2012) was characterized by quiescent, dry, fair weather ($U_s < 5$ m s^{-1}) periods dominated by thermal circulation and the spring campaign (1–31 May 2013) by synoptic forcing. A dry experimental run (25–30 August 2012) helped fine-tune the instrument placement and logistics.

Instrumentation and observing locations. The GMAST core (basic) instrumentation consisted of 31 surface atmospheric measurement systems (SAMS), 51 mini-SAMS, and over 100 portable weather instrumentation data systems (PWIDS). SAMS and mini-SAMS are 10-m towers with vane anemometers (RM Young model 05103) at 2 and 10 m above ground level (AGL) to measure wind speed and direction and the temperature T and relative humidity (RH) at 2 m (Fig. 2). They both measure surface pressure and solar radiation, the difference being that mini-SAMS have additional T and RH sensors at 10 m while SAMS measure precipitation and soil temperature. PWIDS are 2-m portable masts on tripods, with a wind monitor and T–RH probes at 2 m. All data from the core instrumentation are transmitted wirelessly to the DPG Meteorology Division (Fig. 1) via a spread spectrum radio.

The core infrastructure was augmented with an extensive suite of investigator-provided and DPG/National Oceanic and Atmospheric Administration (NOAA)/National Center for Atmospheric Research (NCAR)-loaned instrumentation concentrated at six intensive observing sites (IOS; Fig. 3), selected based on science plans and logistical constraints:

A: IOS-Playa was in the Great Salt Lake Desert west of GM; the area is extremely flat, smooth, and mostly devoid of vegetation, with a thin crust of crystalline salt above layers of alkaline sediments (Boettinger 2009). It is characterized by high albedo, low roughness length (see Table ES1), and seasonally changing moisture and albedo (Hang et al. 2015, manuscript submitted to *Bound.-Layer Meteor.*). Studies on the surface energy budget, internal waves, finescale turbulence, skin flows, and the effects of contrasting albedo, roughness, and moisture availability were conducted therein.

B: IOS-Obverse was the footprint where north/northwesterly/northeasterly approach flow impinges on the GM, yielding a range of phenomena such as dividing streamlines, vortex shedding, and wake flows.

C: IOS-WS (west slope) was on the western slope of GM for studies on slope flows and their interaction with synoptic, valley, and canyon flows.

D: IOS-Gap was a flow exchange area covered by sparse desert shrub vegetation between west and east basins. This site covered a small gap and a big gap. (The nominally semienclosed area east of the GM is referred to as the east basin, and the similar confinement to the west of GM is the west basin.)

E: IOS-ES (east slope) was on the eastern slope of GM. Covered by sparse desert shrub vegetation and long grasses, local slope flows played an important role at this site, including flow collisions, critical internal-wave oscillations, and seiching motions.

F: IOS-Sagebrush was located east of the GM and centrally in the main valley. Covered by sparse desert shrub vegetation, it was highly representative of the land cover in DPG. This site was in the

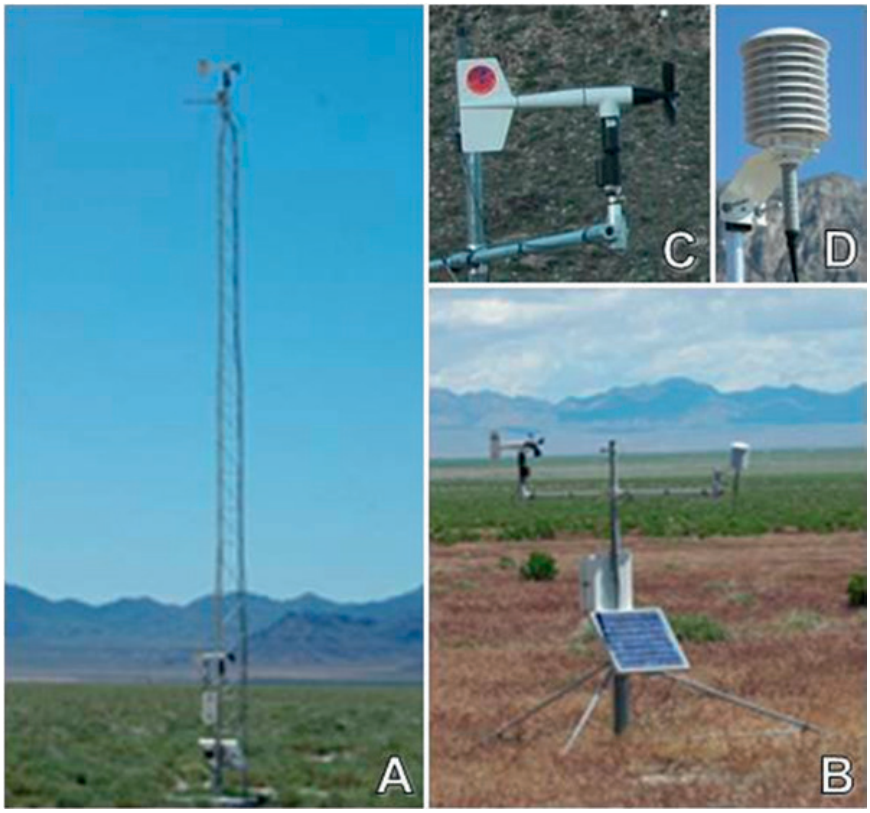

Fig. 2. GMAST core instrumentation: (a) SAMS/mini-Sams, (b) PWIDs, (c) vane anemometer, and (d) HMP45 temperature–relative humidity probe in radiation shield.

path of the nocturnal mesoscale drainage flows over the Dugway Valley and at times was influenced by slope flows from different directions.

The placement of auxiliary instrumentation in IOS was guided by physical intuition and mesoscale model (hindcasting) runs. Photographs of auxiliary instrumentation are shown in Fig. 4, and their specifications are in Table ES2. All IOSs had instrumented towers, at least one 20 m in height, along with a suite of other sensors. Some instruments were relocated and additional instrumentation was brought in periodically as deemed necessary. The towers measured some or all of the following: 1) T, RH, wind velocities, momentum, and sensible heat fluxes (using 3D sonics and fine-wire thermocouples, located at 2, 5, 10, and 20 m and operating at 20 Hz); 2) CO_2 and water vapor concentration (open-path infrared gas analyzers) and fine-structure temperature profiles (~25 thermocouples up to 10 m, with enhanced vertical resolution near the ground); 3) full radiation budget (incoming and outgoing long- and shortwave fluxes at 2–3 m); 4) infrared (IR) surface temperature; and 5) soil heat flux, soil moisture, soil thermal properties, as well as multiple levels of subsurface temperature. Sonic anemometers were also placed at 0.5 m AGL to investigate skin flows, a known phenomenon (Clements et al. 2003) yet unresolved by both numerical models and observations.

The IOS-ES had five heavily instrumented towers [ES-1–ES-5 (see Fig. 3), with ES5 at the foothill], with a total of 30 sonics, Krypton hygrometers, or LI-COR infrared gas analyzers (for eddy covariance, CO_2, water vapor fluxes), 9 HOBO temperature dataloggers, 13 local energy-balance measurement stations (LEMS), and lidars with hemispherical scanners. At times, three lidars were used for virtual tower mode operations (Y. Wang et al. 2014, unpublished manuscript) and on other occasions IOS-ES had tethered-balloon profiling. A fiber optic distributed temperature sensing (DTS) system measured the temperature variation along a 2-km track of the slope at 0.5 and 2 m AGL. The DTS uses the Raman scattering principle for laser light confined within a fiber optic cable to determine the spatially resolved temperature of the cable (Thomas et al. 2012). IOS-ES also housed fine-resolution combo probes developed by MATERHORN-T, an extension of a prototype developed at NCAR. It consisted of in situ calibrated 3D hot films collocated with 3D sonic anemometers that measured turbulence down to Kolmogorov dissipation scales (Kit et al. 2010). A FLIR IR camera facing uphill measured the spatiotemporal distribution of the surface IR temperatures. Smoke releases illuminated by a powerful argon–ion laser as well as by natural light portrayed large-scale flow structures and processes.

The IOS-WS consisted of two towers (WS-1 and WS-2), a SAMS station, eight HOBOs, and a LEMS along the western slope of GM for observing the interactions of synoptic and slope flows as well as contrasting developments of thermal circulations on the east and west slopes. WS-1 and the LEMS were

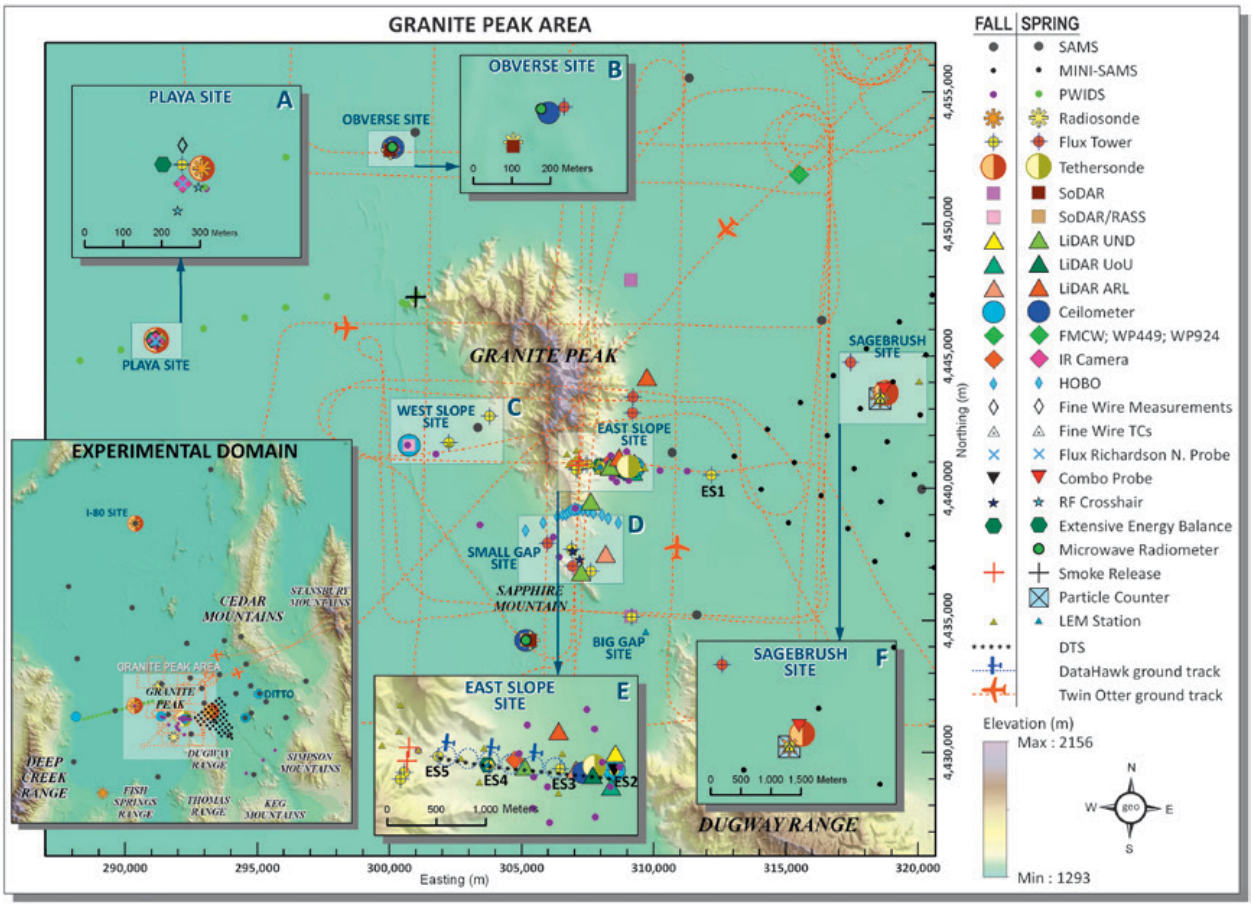

Fig. 3. Instrument placement during fall and spring campaigns. Insets provide details of IOSs as well as the full experimental domain (bottom-left inset). Only the additional instruments deployed (or relocated) for the spring experiment are shown under the "spring" column (courtesy of Dott. Ing. Roberto Perrone).

on the lower portion of the slope approximately 20 m above the Playa floor. The former was a 28-m tower instrumented with six levels of 3D sonics and *T*–RH sensors. During the fall campaign, IOS-WS hosted a sound detection and range/radio acoustic sounding system (SoDAR/RASS) , a ceilometer, and additional PWIDS. The 20-m WS-2 was located farther along the slope with five sonics, a vane anemometer, Krypton hygrometer, 12 thermocouples, and extensive surface energy budget instrumentation.

The IOS-Sagebrush had a 20-m tower equipped with sonics, Campbell infrared gas analyzers, energy-balance equipment, and fine-wire thermocouples. Tethered-balloon soundings were operated at this site synchronous with the Playa sites. Upper-air (radiosonde) soundings were also launched at this site. Additional towers in the spring campaign included a 10-m mast approximately 2 km northwest of the main site with two 3D hot-film combos at two different heights and a 28-m tower with sonics and *T*–RH sensors at five heights.

The IOS-Playa featured unique instrumentation for finescale turbulence, employing a near-surface flux Richardson number (hot wire) probe, complementing the ES-2/Sagebrush combos. Also at IOS-Playa were a high-resolution thermal image velocimetry system (for near-surface temperature and velocity fluctuations), tethered-balloon and radiosonde sounding systems, and a heavily instrumented 20-m tower. In the spring, this site hosted two MATERHORN-T developed radio frequency (RF) measurement systems called RF polarimetric crosshairs. They characterized polarization signatures of signals on a receiving antenna, thus allowing the measurement of the electromagnetic response of emitted polarized radiation caused by environmental changes (Pratt et al. 2014). This instrument measured surface moisture at approximately 1-km scale (i.e., mesoscale grid resolution). For both campaigns, a RF-crosshairs system was deployed at the IOS-Gap. Manual soil moisture observations were also conducted at IOS-Playa during the spring campaign

to characterize soil moisture spatial variability and its role on the energy balance and land–atmosphere moisture exchange (Hang et al. 2015, manuscript submitted to *Bound.-Layer Meteor.*).

The instrumentation at IOS-Gap was suitably distributed over small and large gaps southeast of the GM, at the top of Sapphire Mountain as well as at multiple locations in the proximity. During the spring, a mini-SoDAR, microwave radiometer profiler (MWRP; for vertical profiles of temperature, liquid water content, and humidity up to 10 km), ceilometer, and radiosonde launches were deployed approximately 2.5 km southwest of Sapphire Mountain.

The IOS-Obverse provided approach flow information for the spring campaign, based on a 32-m tower located 400 m northwest of GM with 3D sonics collocated with *T*–RH sensors (2, 4, 6, 8, 16, and 28 m) and an open path CO_2–H_2O analyzer (LiCOR, 28 m). Also included were a MWRP, ceilometer, mini-SoDAR, and frequency-modulated continuous-wave (FM-CW) radar (Eaton et al. 1995) for profiling background thermodynamic structure. PWIDS recorded the local flow close to the GM leading edge. A scanning lidar and three towers along the east side of GM captured the leeside separated flow. At least eight upwind radiosonde launches per intensive observing period (IOP) provided information for data-assimilation studies. Elaborate multiple smoke releases provided information on flow physics related to dividing streamlines, streak lines, and flow separation (Leo et al. 2015b, manuscript submitted to *Bound.-Layer Meteor.*).

Aerial measurements were performed by the (manned) NPS Twin Otter Aircraft with Doppler Wind Lidar (TODWL) as well as unmanned aerial vehicles (UAV) dubbed DataHawk and ND-Flamingo. In the fall campaign, TODWL flights crisscrossed the basin at 2400 m AGL, transecting the GM ridge, while conically scanning the terrain with onboard Doppler lidar to probe the mountain flows (De Wekker et al. 2012). Seven TODWL flights were conducted during IOPs 4–7, collecting data during four afternoons and three mornings. DataHawk flights flew circular Auto-Helix patterns, spiraling from the ground to 700 m AGL and then back down traversing the IOS-ES tower line, thus providing data from elevations that towers could not reach. A series of towers were also placed in a deep canyon close to IOS-ES for a special canyon flow experiment, which included smoke releases.

Some duplicate measurements were recorded at IOS within close proximity to each other, providing an opportunity for intercomparison of instruments and high-resolution spatiotemporal information. Instruments were relocated as needed after preliminary data analysis, but exhaustive time demands on researchers did not leave much room for coeval data analysis.

IOPs and data. Each campaign included 10 IOPs where all instruments were operated in coordination. The core instruments (SAMS, mini-SAMS, PWIDS) and some selected observing platforms, however, were operated continuously. The IOPs were classified according to the synoptic wind speed (Table 1), and the IOP days were chosen a day earlier considering weather briefings by DPG forecasters with input from MATERHORN meteorologists as well as logistical and manpower constraints. The forecasting products employed included DPG's high-resolution Weather Research and Forecasting (WRF) Model–based advanced Four-Dimensional (4DWX) weather modeling system developed by NCAR (Liu et al. 2008), a 30-member 4DWX ensemble, North American Mesoscale (NAM), and Global Forecast System (GFS) model outputs as well as satellite products. A typical IOP lasted 24 h, although a few lasted longer or shorter. The data (~50 TB) are stored on a dedicated server at UND. The data will be released to the scientific community 3 years after the end of each experiment.

MATERHORN-M. The continuing work of MATERHORN-M seeks improvements in both mesoscale and submesoscale predictions. The model choices for the mesoscale are WRF and Coupled Ocean–Atmosphere Mesoscale Prediction System (COAMPS), but the focus hitherto has been on WRF, approaching from multiple angles using complementary efforts. To help instrumentation siting for campaigns, WRF was used to hindcast flow at DPG, which proved to be extremely useful. For example, the original design of IOS-ES assumed strong slope flows from ES-5 to ES-2 towers, and hence the combo (hot film/sonic) probe systems for turbulence (which require approach flow to be within approximately ±30° of the probe direction) were oriented accordingly. The simulations, however, indicated that downslope flows below ES-4 are quickly overshadowed by valley and secondary flows. This suggested reorientation of combos, thus circumventing a costly misperception. During campaigns, real-time WRF forecasts were made at high resolution (~1-km horizontal grid intervals), initialized four times per day (at 0000, 0600, 1800, and 2400 UTC). After the field programs, the forecasts were evaluated against observations, which has been particularly helpful in model performance evaluation and devising improvements (Pu et al. 2014).

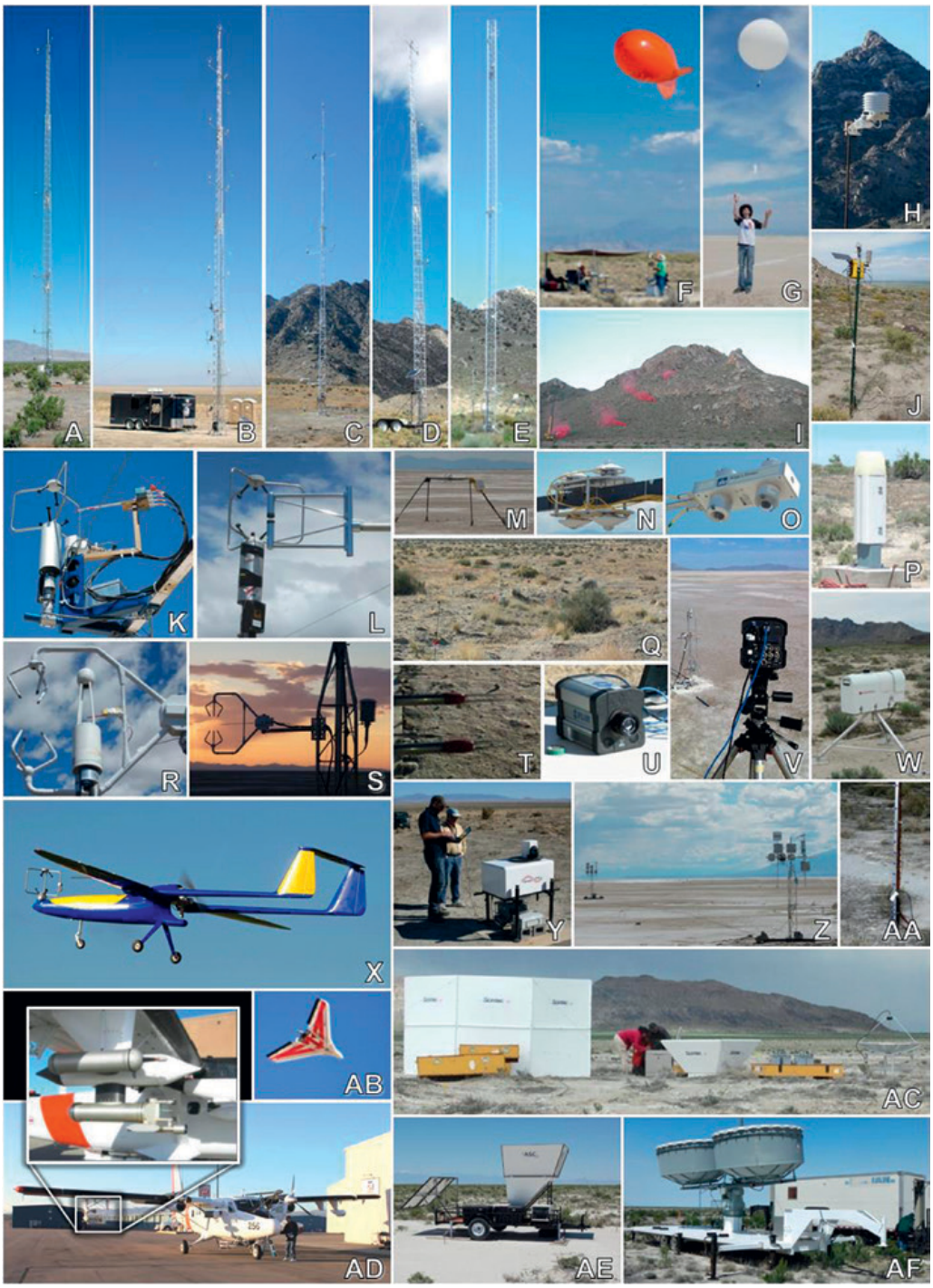

Fig. 4. Salient instruments at DPG: (a) ES-1; (b) ES-2; (c) ES-3; (d) ES-4; (e) ES-5; (f) tethered-balloon soundings; (g) radiosondes; (h) HOBO weather stations; (i) dividing streamline smoke release located on the northwest side of Granite Mountain; (j) LEMS weather stations; (k) 3D hot-film combo probe; (l) Krypton hygrometer; (m) radiation balance observations at IOS-Playa; (n) radiation balance observations at IOS-Sagebrush; (o) net radiometer as the tower-mounted component of the energy budget; (p) ceilometers; (q) distributed temperature sensing system (DTS); (r) infrared gas analyzers; (s) fine-wire thermocouples coupled with 3D sonic anemometers; (t) flux Richardson number hot-wire probe for near-ground measurements; (u) FLIR IR camera; (v) high-resolution near-surface thermal-image velocimetry; (w) microwave radiometer profiler; (x) Flamingo UAV; (y) scanning lidars; (z) RF polarimetric crosshairs surface moisture probes; (aa) array of fine-wire thermocouples, enhanced resolution near the ground; (ab) DataHawk UAV; (ac) SoDAR/RASS; (ad) Twin Otter with wind lidar (TODWL); (ae) mini-SoDARs; and (af) frequency-modulated continuous-wave radar (FM-CW) radar.

A number of studies were conducted to evaluate forecasting and data-assimilation skills of WRF. In one study, the relative performance of a 3D variational data-assimilation method and an ensemble Kalman filter (EnKF) assimilation over complex terrain was evaluated (Pu et al. 2013). In two other studies, the EnKF system developed by NCAR's Data Assimilation Research Testbed (DART; Anderson 2003; Anderson et al. 2009) was applied, assimilating radiosonde and surface observations from both campaigns. Errors in near-surface temperature and wind from WRF simulations in complex-terrain regions were also examined (Zhang et al. 2013; Zhang and Pu 2014). In two related studies, WRF biases due to poorly represented soil properties of DPG (Massey et al. 2014) as well as skills of PBL schemes (R. Dimitrova et al. 2015, manuscript submitted to *Bound.-Layer Meteor.*) were investigated.

Inspired by the rich observational datasets of MATERHORN, another study concerned ensemble sensitivity analysis (ESA) as an alternative to adjoint sensitivity, focusing on quiescent flow at DPG and over the Salt Lake Valley. It particularly dealt with model-based studies on sensor placement configurations to maximize forecast accuracy and to enable the capture of useful dynamical processes (Hacker and Lei 2015), the results of which could be applied to a future experiment that dealt with fog in complex terrain (MATERHORN-Fog). Methods for observing network design are immature at fine scales (e.g., 1–4-km horizontal grid spacing), during weak flows, and over complex terrain. ESA becomes inaccurate when the underlying assumptions of linear dynamics and Gaussian statistics are violated or when the sensitivity cannot be robustly sampled, and hence the limits of applicability of ESA were of interest.

For submesoscales, the emphasis is on the development of the IBM nested in WRF (i.e., for large-eddy simulations), enabling simulations over very steep slopes at very high resolutions (~10 m) using realistic atmospheric forcing. The goal is to achieve fully coupled mesoscale to microscale simulations without the undesirable numerical effects of terrain-following coordinates (Lundquist et al. 2010, 2012). Selecting the optimal transition point between the coordinate systems arguably minimizes model errors. The IBM method involves the use of a ghost-cell IBM that employs a Cartesian grid, where the effect of solid boundaries is realized by adding body forces, allowing the treatment of topography without terrain-following coordinates.

SOME PRELIMINARY FINDINGS. A few noteworthy outcomes of MATERHORN are summarized below, and detailed results are expected to appear in special issues of AMS journals as well as *Boundary-Layer Meteorology* and *Environmental Fluid Mechanics*.

Forecasting challenges. The daily MATERHORN weather briefings often pointed to the difficulties of predicting mountain weather, especially in the DPG region where a rich variety of synoptic and mesoscale systems, fronts, and airmass boundaries influence the weather. Intermountain cyclones and cold fronts are most frequent and intense during the spring, and their evolution is strongly influenced by the upstream Sierra Nevada. Surface pressure troughs and associated low-level confluence (i.e., the Great Basin confluence zone; Steenburgh et al. 2009) that often extend northeastward from the Sierra Nevada to DPG can be accompanied by abrupt transitions in sensible weather and serve as a locus for cyclogenesis or frontogenesis (e.g., Jeglum et al. 2010; West and Steenburgh 2010, 2011). Interactions between synoptic and mesoscale weather systems and the DPG terrain led to hazardous weather at times, unforeseen owing to significant model forecast errors, posing major challenges for operations. For example, during the afternoon hours of spring IOP8, WRF called for a weak trough to move southward through GMAST with moderate (~5 m s^{-1}) northerly to northwesterly surface flow in its wake at 2200 UTC. Instead, this boundary was delayed, developed into a strong cold front, and moved through the GMAST domain with winds of approximately 15 m s^{-1} (Fig. 5), requiring an early termination of the IOP.

As a part of data-assimilation studies, a 1-month-long, 3-hourly continuous data assimilation and forecast cycle was conducted (Zhang and Pu 2014). The results illustrated that the quality of EnKF/WRF analysis is generally reasonable, and the short-range (3 h) forecast errors are comparable to those of NCEP's NAM forecasts for both 10-m wind speed and temperature. Since the latter sets the gold standard for operational forecasts, having EnKF/WRF performance statistically on par with NAM implies that substantial progress has been made with respect to EnKF/WRF; further improvements are continuing. With the data assimilation, the model reproduced reasonable forecasts of various synoptic and local flows, including mountain–valley circulations and frontal passages. The flow features over different land types were also distinguished.

Diurnally varying model biases for temperature and wind velocity were evident, especially in near-surface atmospheric predictions under quiescent

cases, consistent with other published work, indicating model inadequacies (Mass et al. 2002; Cheng and Steenburgh 2005; Hart et al. 2005; Zhang et al. 2013). Flow-dependent errors associated with flow transitions as well as strong synoptic forcing were also evident. Evaluations against synoptic-network and MATERHORN rawinsonde and tethersonde launches, nonetheless, showed that WRF is generally skilled in predicting conditions above the surface layer in complex terrain. Although wind predictions in the SBL were accurate, temperature predictions remained a challenge. Bias and RMSE during the night were approximately 2 and 4 K, respectively (Pu et al. 2014).

Ongoing modeling activities continue to highlight challenges faced by (Army) forecasters at DPG, whose tools include the GMAST observational network and the NCAR 4DWX. The latter employs data assimilation, cycling eight times a day at 1.1-km resolution, and it combines the WRF predictive core with current atmospheric conditions to make detailed predictions for the next several days. Because 4DWX uses WRF as its predictive core, MATERHORN WRF modelers' experiences were similar to DPG's experiences with 4DWX, such as an underpredicted diurnal cycle, biases in the near-surface wind speed, and insufficiently stratified conditions in the shallow SBL. The 30-member multiphysics ensemble version of 4DWX running at DPG mitigates the forecast errors that are rooted in specific physical parameterizations or sources of forcing at the boundaries. As the model–data comparison continues, our hypotheses for model shortcomings continue to unravel, pointing to problems of structure, physics, and parameterizations of WRF while defining avenues for improvements.

Table 1. Classification of IOPs, dates, and types.

IOP classification	Definition (based on 700-hPa wind speed)
Quiescent	<5 m s^{-1}
Moderate	5–10 m s^{-1}
Transitional	Variable, >10 m s^{-1} possible with frontal passages

Fall 2012 IOPs

IOP	Period	Type
0	1400 MDT 25 Sep–1400 MDT 26 Sep	Quiescent
1	1400 MDT 28 Sep–1400 MDT 29 Sep	Quiescent
2	1400 MDT 1 Oct–1400 MDT 2 Oct	Quiescent
3	0200 MDT 3 Oct–0200 MDT 4 Oct	Transitional
4	1400 MDT 6 Oct–1400 MDT 7 Oct	Moderate
5	1400 MDT 9 Oct–1400 MDT 10 Oct	Transitional (quiescent–moderate)
6	0200 MDT 14 Oct–0200 MDT 15 Oct	Quiescent
7	1200 MDT 17 Oct–2000 MDT 17 Oct	Transitional (quiescent–moderate)
8	0500 MDT 18 Oct –1200 MDT 19 Oct	Quiescent
9	1400 MDT 20 Oct –1400 MDT 21 Oct	Moderate

Spring 2013 IOPs

IOP	Period	Type
1	1400 MDT 1 May–1400 MDT 2 May	Transitional (moderate–quiescent)
2	1400 MDT 4 May–1400 MDT 5 May	Moderate
3	0500–1700 MDT 7 May	Moderate
4	1400 MDT 11 May–1400 MDT 12 May	Quiescent
5	1200 MDT 13 May–1200 MDT 14 May	Transitional (moderate–quiescent)
6	1200 MDT 16 May–1200 MDT 17 May	Transitional (moderate–quiescent)
7	1715 MDT 20 May–1400 MDT 21 May	Quiescent
8	1400 MDT 22 May–1400 MDT 23 May	Moderate
9	1000 MDT 25 May–1000 MDT 26 May	Moderate
10	1400 MDT 30 May–1000 MDT 31 May	Moderate

Scale symbiosis. The dense instrumentation permitted both individual- and multiple-scale processes studies. For example, Fig. 6 shows horizontal wind components taken by TODWL at two representative levels, selected from a series of measurements at about 2-km intervals in the horizontal with a vertical resolution of 50 m from about 250 m AGL to 500 m below the aircraft altitude. Note the coexisting flows at multiple scales, with upper-level synoptic flow (macro-β scale; Fig. 6a), near-surface northerly upvalley and upslope flows (meso-γ scale), flow channeling

through the small gap (micro-α scale), and vortex structures (micro-β scale) formed in the mountain wake (Fig. 6b). Yet, flow patterns in the two basins maintained their own unique characteristics; for example, as evidenced later, they have different PBL heights and microcirculation features. WRF 4DWX could predict the overall flow patterns, including the flow distortion by GM, but as expected finer features such as vortex structures and in-canyon flows could not be captured (Fig. 6c).

Surface energy budget and soil property differences. Measurements of individual components of radiation, surface energy budget (SEB), and related variables at three representative locations (IOS-Sagebrush, IOS-Playa, and ES-5) revealed the role of soil thermal property (e.g., thermal conductivity) gradients, which dictate the ground heat flux and hence the soil moisture content (Table ES1). Soil moisture content and its spatial variability were much higher at the IOS-Playa than at the other two sites, thus creating a larger energy sink during the day. This is due to the shallow water table at IOS-Playa (~80 cm from the surface) during the spring compared to the other two sites with much deeper water tables (deeper than 200 cm; Soil Survey Staff 2014). The heat stored in the Playa was released during the night, leading to higher surface temperatures and longwave radiation emissions.

The importance of soil properties was also accentuated by MATERHORN-M (Massey et al. 2014). It is known that the near-surface (2 m) temperature forecasts of WRF over the western United States, as well as by other modeling systems applied to various regions of the world, frequently underpredict the diurnal cycle with a strong nocturnal warm bias (Mass et al. 2002; Hart et al. 2005; Kilpelainen et al. 2012; Ngan et al. 2013; Zhang et al. 2013). Existing hypotheses concerning these forecast errors range from inadequate horizontal or vertical resolution to the inaccurate initialization and parameterization of the boundary layer to the land surface characteristics and processes (e.g., Hanna and Yang 2001; Marshall et al. 2003; Cheng and Steenburgh 2005). Using surface observations, soil observations from the U.S. Department of Agriculture's Soil Climate Analysis Network (SCAN). and SEB collected during the fall campaign, a pronounced nocturnal warm bias was identified over areas with silt loam and sandy loam soils at DPG (Massey et al. 2014). This bias could be traced to errors in the initialization of soil moisture and parameterization of soil thermal conductivity. WRF forecasts of nocturnal surface temperature as well as the predicted ground heat flux, soil thermal conductivity, and near-surface radiative fluxes could be improved by initializing with measured soil moisture and replacing the Johansen (1975) parameterization for soil thermal conductivity in the Noah land surface model with that proposed by McCumber and Pielke (1981) for silt loam and sandy loam soils. We anticipate similar improvements for other arid regions during periods of low soil moisture.

Surface-layer similarity theory. The Monin–Obukhov similarity theory (MOST) has been extensively discussed and evaluated (e.g., Foken 2006), but questions linger on its applicability to complex terrain and morning and/or evening transition periods, as both violate the basic tenets of MOST—that is, stationarity and horizontal homogeneity of the flow. Yet, models continue to use MOST in a local sense, conveniently overlooking its limitations. During the BLLAST campaign in France, Blay-Carreras et al. (2014) observed near-surface countergradient behavior of sensible heat fluxes during the evening transition, when the MOST stability functions also deviated greatly from (neutrally stable) idealized

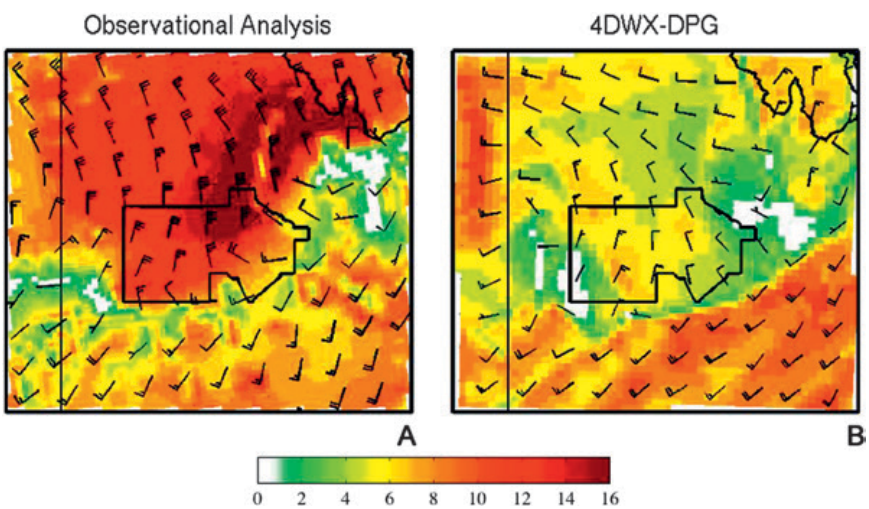

Fig. 5. (a) Analyzed and (b) 14-h WRF 4DWX forecast of 10-m wind speeds at DPG depicted using a color scale (shown below, m s^{-1}) and wind barbs (full and half barb denote 5 and 2.5 m s^{-1}, respectively) at 2200 UTC 22 May 2013, during IOP8.

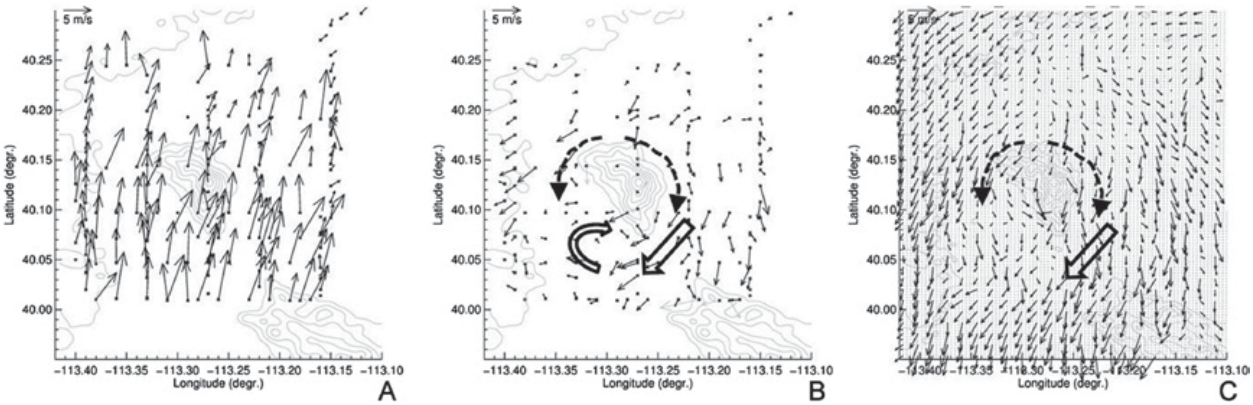

Fig. 6. Example of TODWL data obtained, 9 Oct 2012, during IOP 5, in the afternoon at 3000 m MSL representing (a) upper-level flow at 1750 m MSL, (b) near-surface flow, and (c) 300-m-resolution simulations of near-surface flow for the same time (1700 MDT) using WRF. The arrows indicate recurring surface flow patterns in the afternoon boundary layer around Granite Mountain.

profiles typically used in weather prediction models (Smedman et al. 2007). A similar behavior was also observed during MATERHORN-X at all of the flux sites. An intriguing result, in addition, was the nature of transition over surfaces with very different thermal characteristics (Jensen et al. 2015, manuscript submitted to *Bound.-Layer Meteor.*). Below 5 m, at the vegetated IOS-Sagebrush, the local temperature gradient changed sign after the flux changed sign, while at the Playa site the gradient preceded the flux reversal. At each of the sites, the fluxes at all heights in the lower 20 m appear to change the sign roughly at the same time. Both countergradient situations lead to similar deviations from MOST, but at different times owing to the large thermal storage of the Playa. The abrupt collapse of turbulence observed during evening transition points to the inapplicability of MOST for transition periods (even in a local sense), calling for further studies on the (evening) collapse of convective turbulence under different land-use conditions. The dependence of turbulence collapse on overlying capping inversions (Caughey and Kaimal 1977) and surface characteristics (Cole and Fernando 1998) has been pointed out in previous work, and our database offers opportunities for delving into such intricacies.

Evening transition. The evening transition is rich in interesting physics, depending on the slope, vigor of prior convection, land use, shading, and existing local flows. At the outset, it was hypothesized that the temperature jump across a shadow front (leading edge of a moving shadow created by the obstruction of sunlight by topography), similar to that observed by Nadeau et al. (2013) in the Swiss Alps and Katurji et al. (2013) in Antarctica, would dominate the transitional behavior. Such a behavior was indeed found during a quiescent IOP of the spring field campaign, where transition followed the shadow front down the slope (Lehner et al. 2015). For the fall campaign, however, the data indicated otherwise; that is, two flow transition types (front and cooling slab) discussed and illustrated recently by Fernando et al. (2013) were present at IOS-ES, uncorrelated with the passage of the shadow front. When present, the transition front originated upslope of the observation towers and moved downslope, sequentially switching the wind direction of towers and intensifying turbulence, and these observations have some consistency with the mechanism proposed by Hunt et al. (2003). The DTS measurements of near-surface temperature vividly confirmed the frontal propagation (Fig. 7), where the lower (0.5 m) air layer showed progressive cooling due to the front arrival in consonance with the flow-reversal data of towers. The front had an inclined nose, as evident from the reversal times at different heights (not shown). During slab transitions, winds of all towers reversed simultaneously as if a slab of dense fluid slid down the slope. Both mechanisms were found to exist in approximately equal numbers during quiescent IOPs in the fall.

The investigations of morning transition were focused on physical mechanisms and processes—for example, those proposed by Whiteman (1982) and Princevac and Fernando (2008). The former is based on the growth of CBL within the valley and simultaneous generation of an upslope flow that causes the stable core aloft the CBL to descend; the collusion between the two promotes the breakup of nocturnal stratification. Princevac and Fernando (2008) proposed that intrusions shaving off the upslope flow (see Fig. 1) may entrain into the growing CBL, thus providing an

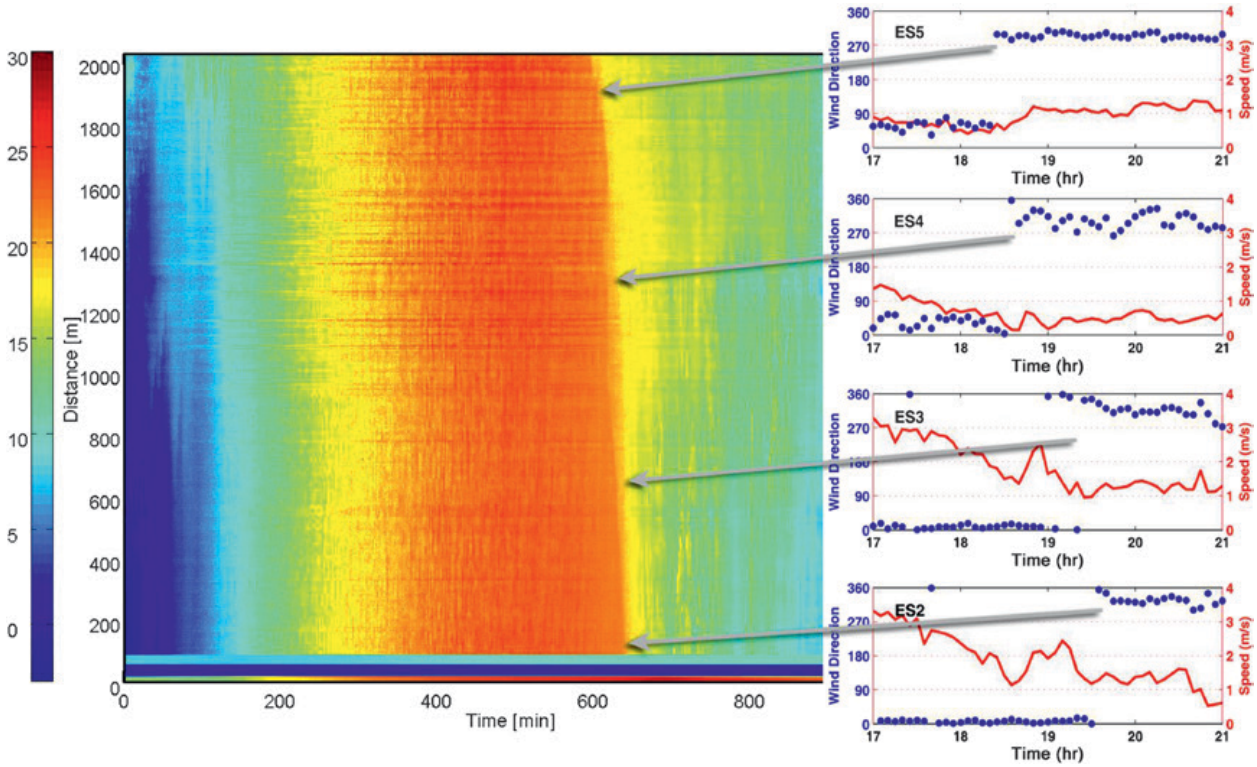

Fig. 7. Near-surface (0.5 m AGL) temperature measurements by DTS installed on the east slope of Granite Mountain on 9 Oct 2012 (IOP 5). DTS spanned a 2-km transect between towers ES-2 and ES-5. The timeline starts at local sunrise, determined using radiation measurements at ES-5 (located about 2000 m on the ordinate in this plot). The wind direction and speed are shown to the right for ES-2–ES-5, and the change of wind direction roughly coincided with the drop of local temperature. There is a progression of temperature drops from ES-5 to ES-2.

additional breakup mechanism. Figure 7 shows that the morning warming at the east slope site first occurs close to the foothills, impeding the flow draining from high to low slopes, and continues down the slope with time. Wind transitions in the presence of slope breaks and spatially inhomogeneous surface warming have not been investigated, and our data repository offers a range of kindred research opportunities.

Flows in the basins. The basinwide stratification is dependent on the spatial distribution of SEB, basin morphology, and large-scale forcing. Tethered-balloon flights in the east and west basins during quiescent IOPs demonstrated the differences of stratification and SBL height. Southeasterly flows originating at the Dugway Valley and the slopes of the Simpson, Keg, and Thomas Mountains travel to the east of GM, while southerly flows on the west of GM originate at the Fish Springs Flat and upstream Snake Valley. The two sides communicate through intermountain (big and small) gaps. Figure 8 shows the measured vertical structure of fully established nocturnal downvalley flow in the basins, where a low-level jet is evident. The IOS-Sagebrush exhibits much cooler surface temperatures and a strong low-level elevated capping inversion that prevents the surface jet from mixing vertically. The larger ground heat flux at IOS-Playa leads to warmer nighttime surface temperatures than at Sagebrush, allowing the nocturnal jet to mix deeper aloft.

The two sites were simulated using WRF, where the modified land surface model of Massey et al. (2014) described earlier was employed but with a different model initialization (GFS) and without soil moisture assimilation. Six default PBL schemes were used, and starkly different predictions were obtained. The predictions based on Yonsei University (YSU) and quasi-normal-scale elimination (QNSE) (default) schemes are shown in Fig. 8, selected considering their performance statistics at 10 m. QNSE was found to perform better for the near-surface temperature (at 2 m) compared to YSU that performed better for the wind speed (at 10 m). Overall, the relative performance of PBL schemes depended on the type of observation and the height range used for statistics [see the caption and R. Dimitrova et al. (2015, manuscript

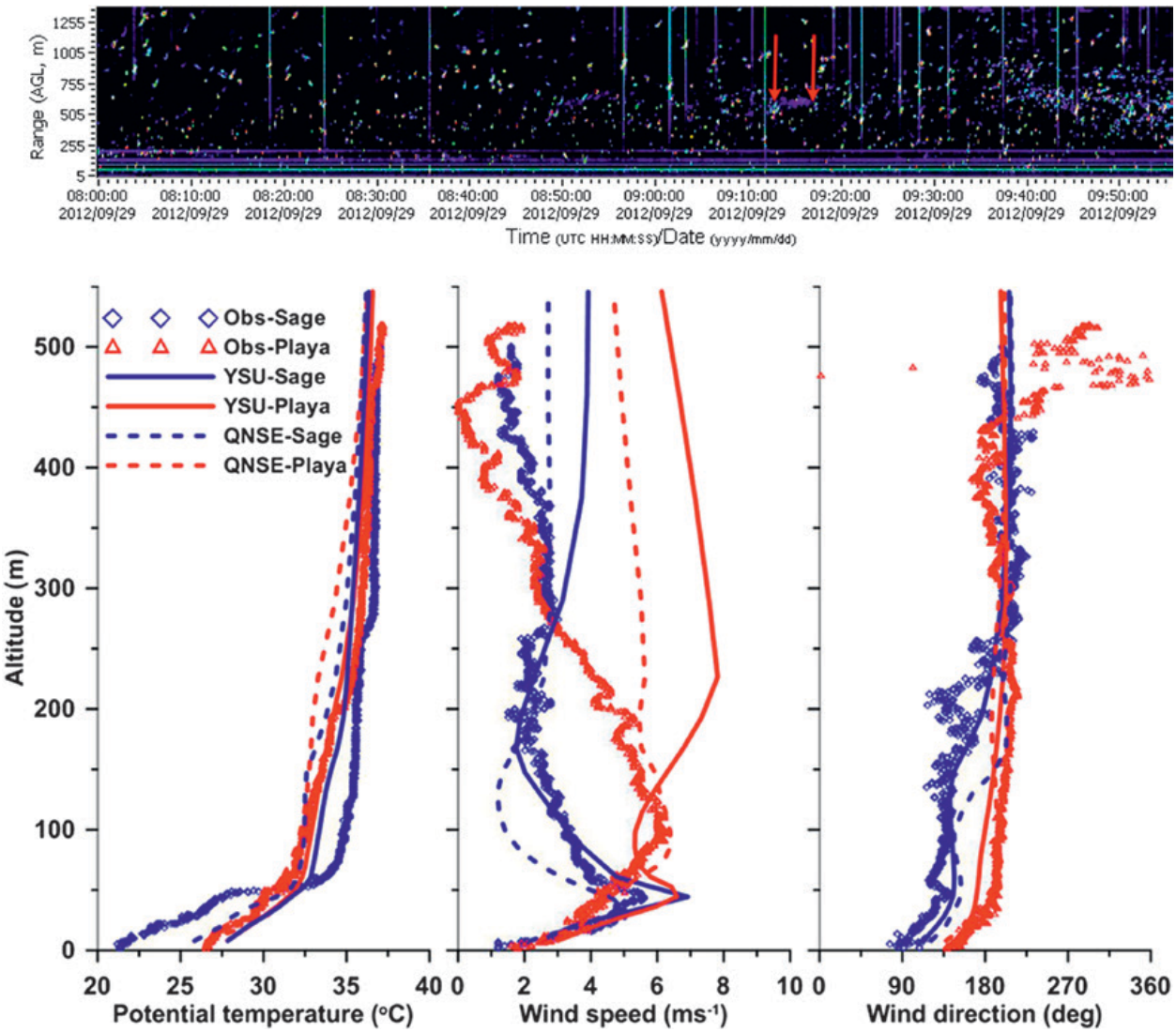

Fig. 8. (bottom) Comparison of the wind and temperature structure of the nocturnal SBL at IOS-Playa and IOS-Sagebrush during IOP1 on 29 Sep 2012. The profiles are compared with WRF (500-m grid size) simulations with two PBL schemes: YSU and QNSE schemes. Tethered-balloon ascent time is 0907–0927 UTC (0307–0327 MDT). Model output is averaged over 0000–0920 UTC (0300–0320 MDT). Six default PBL schemes in WRF were attempted, and two were selected based on overall statistical performance using data at 10 m. For the example shown, YSU provides the best overall performance up to 200 m and QNSE performs better beyond 200 m. (top) Power backscatter signal from FM-CW radar indicates a developing inversion at approximately 500 m during the measurement period (arrows), which was not captured by the simulations.

submitted to *Bound.-Layer Meteor.*)]. In addition, the performance is expected to be sensitive to the basin configuration, since nuances of flow physics therein determine the efficacy of a particular PBL scheme.

A warm bias appeared near the surface, although the predictions of wind speed and direction were satisfactory. The YSU scheme predicted the position but not the magnitude of the Sagebrush jet, while overall disparities for IOS-Playa jet were marked. The wind direction was reasonably well predicted by both schemes over the entire 500-m column measured by tethered balloons. FM-CW radar showed a developing inversion above the approximately 500-m level, just above the ceiling of balloon flights, but this feature was not captured by WRF. Such disparities call for continued improvements of PBL schemes for SBL.

On the other hand, the observed differences of key variables between the east and west basins were reduced during the convective period, facilitated by significant exchange of air between them (i.e., exchange flows) through the big and small gaps (Fig. 6). Nevertheless, some differences were still noticeable.

This is evident from Fig. 9, where concurrent CBL measurements using TODWL and Datahawk UAV are shown for morning flights of fall IOP5, with terrain-following PBL heights derived from the aerosol backscatter profiles. A consistent picture emerges with PBL heights 100–300 m AGL, indicating evolving convective boundary layer with appreciable differences in CBL heights between the basins.

Slope and valley flow interactions. Valley circulations that develop on either side of Granite Mountain during quiescent IOPs are likely to be modulated by differential thermal forcing, for example, owing to the land surface contrast between sparsely vegetated areas to the southeast and the playa to the northwest (Rife et al. 2002). Adding to the complexity is the vacillating interbasin air exchange through the small and big gaps; see Figs. 3 and ES1. Air exchange through the narrow gap increases turbulence and vertical mixing when the flow is fanning out from the gap and when horizontal shear layers develop within the gap periodically.

An interesting valleywide flow interaction phenomenon was observed during quiescent IOPs, when a southeasterly downvalley flow in the Dugway basin merged with southwesterly flow through the big gap. The vorticity that develops during this confluence acted to steer the colder air of the valley flow toward the (relatively warmer) katabatic flow on the eastern slope of GM, leading to collision of two counterflows. A set of small-scale processes (turbulence, instabilities, and intrusions) emerged during collisions, enhancing the local subgrid-scale heat and momentum transfer. The corresponding lidar scans and laser-illuminated smoke visualization along the ES tower line are shown in Figs. 10a,c. Figure ES2 presents a movie of smoke flow visualization. Figure 10b depicts a controlled laboratory experiment designed to mimic the collisions and parameterize observed high turbulent intensities and fluxes (Fig. 10d).

The impact of collisions leads to rapid hydraulic adjustment in the basin flow, prompting the flushing of the basin on the north side while generating basin-scale oscillations (seiching), as evinced by IR imaging. As the colder air that had been pushed up the slope recedes back out into the basin, it is met by a reestablishing valley flow after the collision. This collision cycle repeated numerous times during quiescent evenings (Fig. 10d).

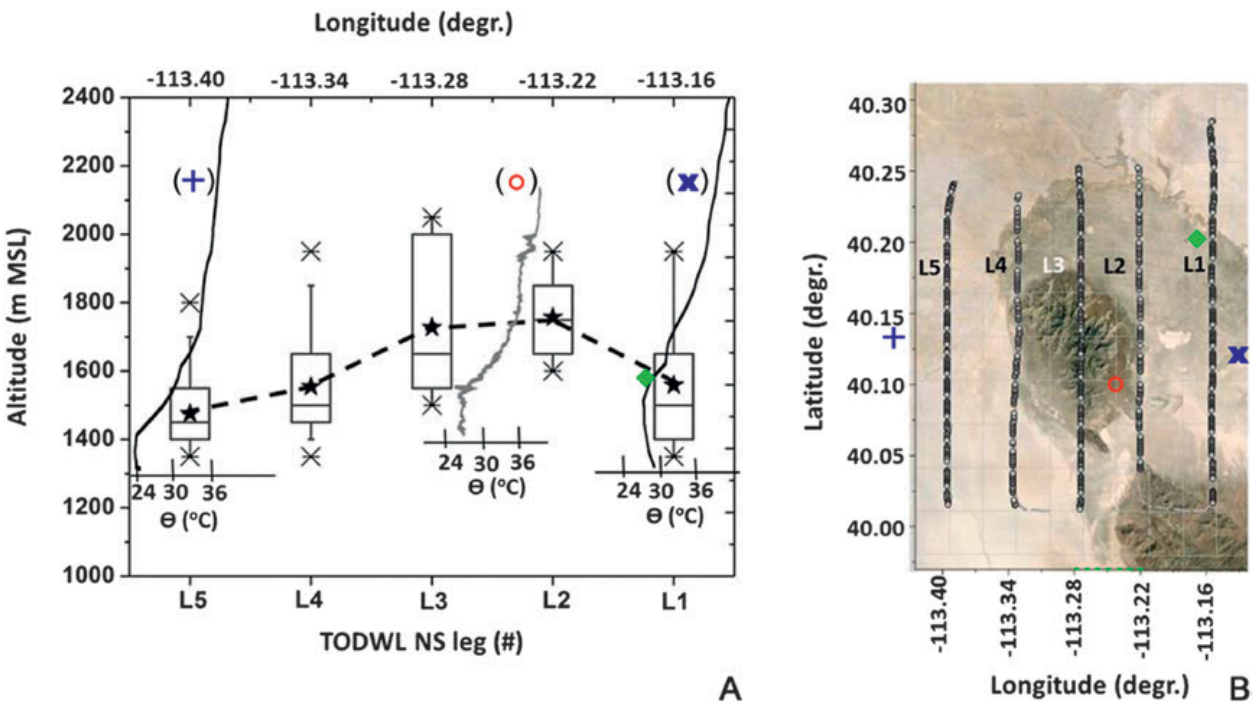

Fig. 9. (a) Box-and-whisker plot of CBL heights derived from aerosol backscatter profiles along the (b) north–south TODWL flight legs. The data were collected during a morning mission between 1012 and 1052 MDT 10 Oct 2012. The horizontal line in the box and the bottom and top lines of the box show the median of the data and the lower and upper quartiles (25% and 75%), respectively. The whiskers show the minimum and maximum values while ∗ is the mean value. Potential temperature profiles from the radiosondes at the Playa (+) and Sagebrush (×) sites, a DATAHAWK UAV (O) profile near the ES-2 tower, and the CBL height based on FM-CW radar (♦) are shown in (a).

Similar flow collisions appeared in other locations that are conducive for opposing flows, as indicated by the decomposition of valley flow into topological structures (Fig. 10e) using the proper orthogonal decomposition (POD) technique (Adrian et al. 2000). In general, collisions appear to be distributed over space and time within the SBL. WRF and other mesoscale models do not account for such spasmodic subgrid heat and/or momentum flux–generating processes, and their incorporation through conditional parameterizations is

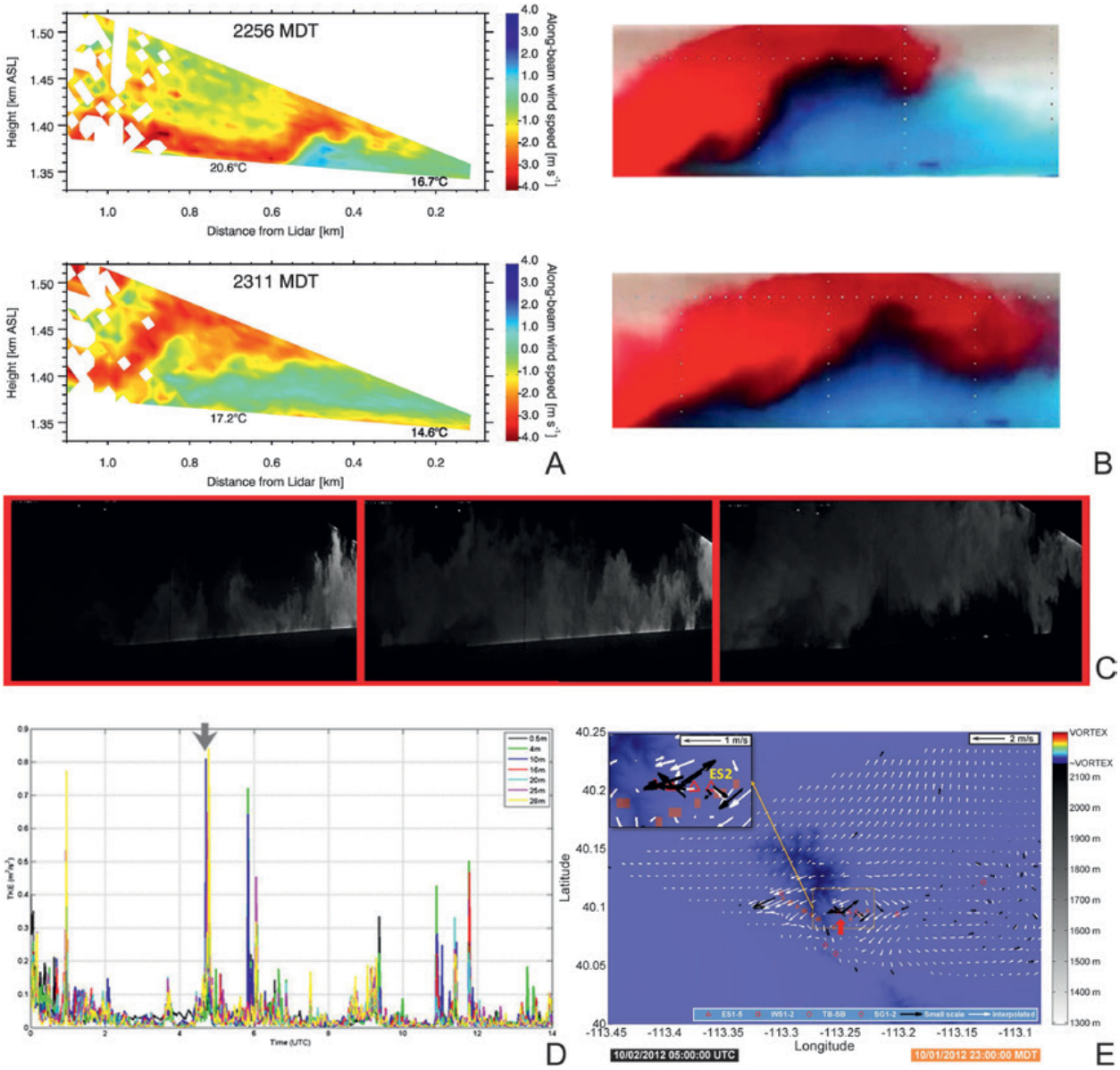

Fig. 10. A collision event during fall IOP2. (a) Lidar scans (located near ES-2) captured the collision between the downslope flow (red) and valley flow (blue), with the latter arriving almost normal to the slope because of its modification by the gap flow. Upon collision, the denser fluid undercuts the lighter fluid. (b) A laboratory experiment on collision of lighter (red) and denser (blue) fluids. Intense small-scale mixing is evident in (a) and (b). (c) A collision captured by smoke visualization on the slope (initially smoke travels to the right, downslope, and denser smoke-free flow undercuts it); the lower limit of beam does not coincide with the ground (see movie in Fig. ES2). (d) Collisions are temporally intermittent and associated with a rapid rise of turbulent kinetic energy (TKE), as evidenced by ES-2 anemometers. Arrow corresponds to the event in (a). (e) Collision events educed using the POD technique. The measured vector field (black) by towers and PWIDS is decomposed to small- and large-scale fields using POD, and the interpolated small-scale field is shown (white). The red arrow shows the collision area in (a), which is rich in smaller scales. Collisions were spatially distributed over the Dugway Valley, as evident from flow convergence and/or stagnation areas.

crucial for modeling of mountain terrain winds. To this end, a comprehensive laboratory experiment is being conducted to develop parameterizations for fluxes associated with the collisions as a function of governing dimensionless variables and delineate conditions for productive (high flux) collisions.

Instrumentation siting for forecast accuracy. The ESA performed to guide the MATERHORN-Fog campaign (successfully conducted in January 2015) provides an example of ESA's utility. It concerned a fog event over the Salt Lake City airport (SLC), an area with frequent wintertime fog affected by complex terrain and the site for MATERHORN-Fog. Perfect-model ensemble data-assimilation experiments using DART and realistic upper-air observing network provided the statistics for ESA. Results showed that water vapor mixing ratios over SLC are sensitive to temperature on the first model layer tens of kilometers away, 6 h prior to verification, and before the onset of fog (Wile et al. 2015). Sensitivity 12 h prior was weaker but led to qualitatively similar results. Temperatures were a predictor of inversion strength in the Salt Lake basin; the ESA linked fog to southerly flow that strengthened inversions. In linearity tests, small perturbations did not lead to the expected forecast change, but larger perturbations did, suggesting that noise can dominate a small perturbation in weak flow conditions. Variations in the ESA as a function of ensemble size confirmed that the sensitivities are more difficult with smaller ensembles when flows are weak (Fig. 11). All of the linear ESA estimates systematically overpredicted the actual response to a perturbation, consistent with sampling error in estimates derived from a finite ensemble. Results from the ESA for fog over SLC motivated theoretical work as well as experiments with a simple model to elucidate the role of both sampling error and a commonly used approximation in ESA (Hacker and Lei 2015). Ensuing results showed that sampling error can be mitigated by reducing regression coefficients according to the expected error in the sensitivities and that the approximation can be easily avoided through a minimum-norm regression. Including full spatial analysis covariance information, and accounting for sampling error, improved the ESA predictions for where observations are most likely to reduce forecast uncertainty.

SUMMARY. MATERHORN is truly a multidisciplinary effort, where a group of physical scientists and engineers collaborate across disciplines to create knowledge and develop tools to help improve weather prediction in mountain terrain (see www.nd.edu/~dynamics/materhorn). It has four components: modeling (M), experimental (X), technology (T), and parameterization (P). From the inception, MATERHORN-M was active, collaborated with stakeholders, and provided useful insights for experimental planning and development of hypotheses. Noticeable forecast improvements for WRF were realized using new land surface parameterizations with improved soil moisture and thermodynamic representations. Ensemble sensitivity runs were conducted and a localization theory was derived. The degree of usefulness of data assimilation was evaluated, and new assimilation techniques are being attempted. The modeling realm is being extended to ultra-high-resolution simulations via immersed boundary methods implemented in WRF.

MATERHORN-X delved into eight orders of spatial scales (10^{-3}–10^{5} m, from Kolmogorov to mesoscales) and five orders of temporal scales (1–10^{5} s). The most extensive are the first two field campaigns conducted in a secure, richly instrumented, complex-terrain test bed (Fernando and Pardyjak 2013), novel results of which were emphasized in this report. MATERHORN-T developed new sensor systems for moisture, fog, and turbulence as well as novel retrieval

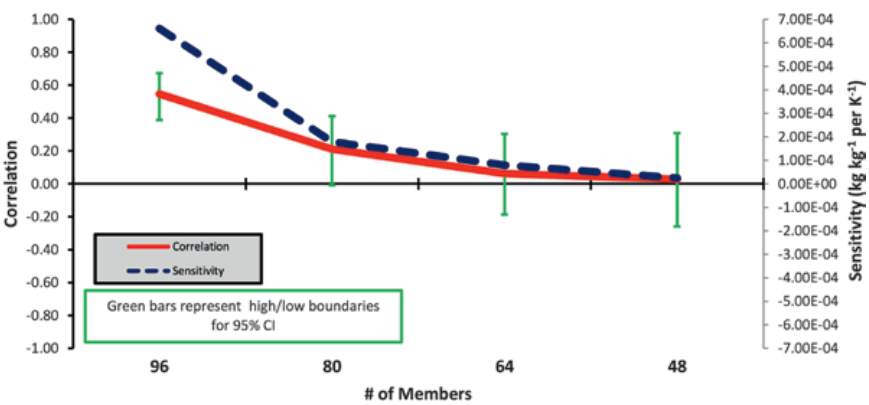

Fig. 11. The 6-h correlation (red) and ensemble sensitivity (blue) vs the number of ensemble members for a single point of positive sensitivities at 39.5°N, 112.9°W. Green bars indicate the 95% confidence interval. Correlations and covariances, underpinning the ensemble sensitivities, are more difficult to detect with smaller ensembles.

algorithms. The data are being extensively used for gaining physical insights, process studies, and model improvements. MATERHORN-P continues to verify existing parameterizations and develop new ones that are being implemented in WRF. The project has entered its data processing and intensive modeling phases at full steam. The overall theoretical, numerical, and technological development efforts as well as the massive dataset collected are expected to help future research in mountain meteorology immensely.

ACKNOWLEDGMENTS. The MATERHORN Program was funded by the Office of Naval Research (MURI) Award N00014-11-1-0709 (Program Officers: Drs. Ronald Ferek and Daniel Eleuterio), with additional funding from the Army Research Office (Program Officers: Gordon Videen and Walter Bach), Air Force Weather Agency, Research Offices of University of Notre Dame and University of Utah, and Wayne and Diana Murdy Family Endowment at Notre Dame. MATERHORN-M gratefully acknowledges the DART team at NCAR, the U.S. Army Test and Evaluation Command, DoD High-Performance Computing Modernization Program (HPCMP), High Performance Computing at UU, Center for Research Computing (CRC), and Engineering and Science Computing (ESC) at UND. The GIS rendition of Fig. 4 was skillfully prepared by Dott. Ing. Roberto Perrone, Territorial Planning Department of Province of Lecce, Italy. Without the invaluable support of Chris Fairall (ESRL/PSD, NOAA), Vanda Grubišić, and Steven Oncley (EOL, NCAR), James Doyle (Naval Research Laboratory), many DPG and U.S. government personnel, domestic, and international visitors, as well as a host of technical staff, the program could not have been a reality. Four referees provided invaluable comments that improved the paper substantially.

REFERENCES

Adrian, R. J., K. T. Christensen, and Z.-C. Liu, 2000: Analysis and interpretation of instantaneous turbulent velocity fields. *Exp. Fluids,* **29,** 275–290, doi:10.1007/s003489900087.

Albini, F. A., D. J. Latham, and R. G. Baughman, 1982: Estimating upslope convective wind speeds for predicting wildland fire behavior. USDA Forest Service Intermountain Forest and Range Experiment Station Research Paper INT-257, 19 pp.

Allwine, K. J., J. H. Shinn, G. E. Streit, K. L. Clawson, and M. Brown, 2002: Overview of URBAN 2000: A multiscale field study of dispersion through an urban environment. *Bull. Amer. Meteor. Soc.,* **83,** 521–536, doi:10.1175/1520-0477(2002)083<0521:OOUAMF>2.3.CO;2.

Anderson, J. L., 2003: A local least squares framework for ensemble filtering. *Mon. Wea. Rev.,* **131,** 634–642, doi:10.1175/1520-0493(2003)131<0634:ALLSFF>2.0.CO;2.

——, T. Hoar, K. Raeder, H. Liu, N. Collins, R. Torn, and A. Avellano, 2009: The Data Assimilation Research Testbed: A community facility. *Bull. Amer. Meteor. Soc.,* **90,** 1283–1296, doi:10.1175/2009BAMS2618.1.

Baines, P. G., 1979: Observations of stratified flow past three-dimensional barriers. *J. Geophys. Res.,* **84,** 7834–7838, doi:10.1029/JC084iC12p07834.

——, 1998: *Topographic Effects in Stratified Flows.* Cambridge University Press, 482 pp.

Banta, R. M., 1984: Daytime boundary-layer evolution over mountainous terrain. Part I: Observations of the dry circulations. *Mon. Wea. Rev.,* **112,** 340–356, doi:10.1175/1520-0493(1984)112<0340:DBLEOM>2.0.CO;2.

——, Y. L. Pichugina, N. D. Kelley, R. M. Hardesty, and W. A. Brewer, 2013: Wind energy meteorology: Insight into wind properties in the turbine-rotor layer of the atmosphere from high-resolution Doppler lidar. *Bull. Amer. Meteor. Soc.,* **94,** 883–902, doi:10.1175/BAMS-D-11-00057.1.

Barry, R. G., 2008: *Mountain Weather and Climate.* 3rd ed. Cambridge University Press, 512 pp.

Belcher, S. E., and J. C. R. Hunt, 1998: Turbulent flow over hills and waves. *Annu. Rev. Fluid Mech.,* **30,** 507–538, doi:10.1146/annurev.fluid.30.1.507.

Bjerknes, and Coauthors, 1934: For mountain observatories. *Bull. Amer. Meteor. Soc.,* **15,** 993–994.

Blay-Carreras, E., E. R. Pardyjak, D. Pino, D. C. Alexander, F. Lohou, and M. Lothon, 2014: Countergradient heat flux observations during the evening transition period. *Atmos. Chem. Phys.,* **14,** 9077–9085, doi:10.5194/acp-14-9077-2014.

Blumen, W., Ed., 1990: *Atmospheric Processes over Complex Terrain. Meteor. Monogr.,* No. 45, Amer. Meteor. Soc., 323 pp.

Boettinger, J. L., 2009: Soils of Utah. Rangeland resources of Utah, Utah State University Extension Cooperative Extension Doc., 46–48. [Available online at https://extension.usu.edu/utahrangelands/files/uploads/RRU_Final.pdf.]

Brighton, P. W. M., 1978: Strongly stratified flow past three-dimensional obstacles. *Quart. J. Roy. Meteor. Soc.,* **104,** 289–307, doi:10.1002/qj.49710444005.

Caughey, S. J., and J. C. Kaimal, 1977: Vertical heat flux in the convective boundary layer. *Quart. J. Roy. Meteor. Soc.,* **103,** 811–815, doi:10.1002/qj.49710343821.

Cheng, W. Y. Y., and W. J. Steenburgh, 2005: Evaluation of surface sensible weather forecasts by the WRF and

the Eta models over the western United States. *Wea. Forecasting,* **20,** 812–821, doi:10.1175/WAF885.1.

Chow, F. K., S. F. J. De Wekker, and B. Snyder, Eds., 2013. *Mountain Weather Research and Forecasting: Recent Progress and Current Challenges.* Springer, 750 pp., doi:10.1007/978-94-007-4098-3.

Clements, C. B., C. D. Whiteman, and J. D. Horel, 2003: Cold-air-pool structure and evolution in a mountain basin: Peter Sinks, Utah. *J. Appl. Meteor.,* **42,** 752–768, doi:10.1175/1520-0450(2003)042<0752:CSAEIA>2.0.CO;2.

Cole, J. S., and H. J. S. Fernando, 1998: Some aspects of the decay of convective turbulence. *Fluid Dyn. Res.,* **23,** 161–176, doi:10.1016/S0169-5983(97)00051-8.

Deardorff, J. W., 1970: Convective velocity and temperature scales for the unstable planetary boundary layer and for Rayleigh convection. *J. Atmos. Sci.,* **27,** 1211–1213, doi:10.1175/1520-0469(1970)027<1211:CVATSF>2.0.CO;2.

De Wekker, S. F. J., K. Godwin, G. D. Emmitt, and S. Greco, 2012: Airborne Doppler lidar of valley flows in complex coastal terrain. *J. Appl. Meteor. Climatol.,* **51,** 1558–1574, doi:10.1175/JAMC-D-10-05034.1.

Doran, J. C., J. D. Fast, and J. Horel, 2002: The VTMX 2000 campaign. *Bull. Amer. Meteor. Soc.,* **83,** 537–551, doi:10.1175/1520-0477(2002)083<0537:TVC>2.3.CO;2.

Eaton, F. D., S. A. McLaughlin, and J. R. Hines, 1995: A new frequency-modulated continuous wave radar for studying planetary boundary layer morphology. *Radio Sci.,* **30,** 75–78, doi:10.1029/94RS01937.

Ellis, A. W., M. L. Hilderbrandt, W. Thomas, and H. J. S. Fernando, 2000: A case study of the climatic mechanisms contributing to the transport of lower atmospheric ozone across metropolitan Phoenix area. *J. Climate Res.,* **15,** 13–31, doi:10.3354/cr015013.

Fernando, H. J. S., 2010: Fluid dynamics of urban atmospheres in complex terrain. *Annu. Rev. Fluid Mech.,* **42,** 365–389, doi:10.1146/annurev-fluid-121108-145459.

——, and J. C. Weil, 2010: Whither the stable boundary layer? A shift in the research agenda. *Bull. Amer. Meteor. Soc.,* **91,** 1475–1484, doi:10.1175/2010BAMS2770.1.

——, and E. R. Pardyjak, 2013: Field studies delve into the intricacies of mountain weather. *Eos, Trans. Amer. Geophys. Union,* **94,** 313–315, doi:10.1002/2013EO360001.

——, B. Verhoef, S. Di Sabatino, L. S. Leo, and S. Park, 2013: The Phoenix Evening Transition Flow Experiment (TRANSFLEX). *Bound.-Layer Meteor.,* **147,** 443–468, doi:10.1007/s10546-012-9795-5.

Foken, T., 2006: 50 years of the Monin–Obukhov similarity theory. *Bound.-Layer Meteor.,* **119,** 431–447, doi:10.1007/s10546-006-9048-6.

Grubišić, V., and Coauthors, 2008: The Terrain-Induced Rotor Experiment: An overview of the field campaign and some highlights of special observations. *Bull. Amer. Meteor. Soc.,* **89,** 1513–1533, doi:10.1175/2008BAMS2487.1.

Hacker, J. P., and L. Lei, 2015: Multivariate ensemble sensitivity with localization. *Mon. Wea. Rev.,* **143,** 2013–2027, doi:10.1175/MWR-D-14-00309.1.

Hanna, S. R., and R. Yang, 2001: Evaluations of mesoscale models' simulations of near-surface winds, temperature gradients, and mixing depths. *J. Appl. Meteor.,* **40,** 1095–1104, doi:10.1175/1520-0450(2001)040<1095:EOMMSO>2.0.CO;2.

Hart, K. A., W. J. Steenburgh, and D. J. Onton, 2005: Model forecast improvements with decreased horizontal grid spacing over finescale intermountain orography during the 2002 Olympic Winter Games. *Wea. Forecasting,* **20,** 558–576, doi:10.1175/WAF865.1.

Hocut, C. M., 2013: Multi-scale flow and turbulence in complex terrain under weak synoptic conditions. Ph.D. dissertation, University of Notre Dame, 163 pp.

——, D. Liberzon, and H. J. S. Fernando, 2015: Separation of upslope flow over a uniform slope. *J. Fluid Mech.,* **775,** 266–287, doi:10.1017/jfm.2015.298.

Hunt, J. C. R., H. J. S. Fernando, and M. Princevac, 2003: Unsteady thermally driven flows on gentle slopes. *J. Atmos. Sci.,* **60,** 2169–2182, doi:10.1175/1520-0469(2003)060<2169:UTDFOG>2.0.CO;2.

——, A. Orr, J. W. Rottman, and R. Capon, 2004: Coriolis effects in mesoscale flows with sharp changes in surface conditions. *Quart. J. Roy. Meteor. Soc.,* **130,** 2703–2731, doi:10.1256/qj.04.14.

——, G. G. Vilenski, and E. R. Johnson, 2006: Stratified separated flow around a mountain with an inversion layer below the mountain top. *J. Fluid Mech.,* **556,** 105–119, doi:10.1017/S0022112006009335.

Jannuzzi, J. A., 1993: The onshore push of marine air into the Pacific Northwest. *Wea. Forecasting,* **8,** 194–203, doi:10.1175/1520-0434(1993)008<0194:TOPOMA>2.0.CO;2.

Jeglum, M. E., W. J. Steenburgh, T. P. Lee, and L. F. Bosart, 2010: Multi-reanalysis climatology of intermountain cyclones. *Mon. Wea. Rev.,* **138,** 4035–4053, doi:10.1175/2010MWR3432.1.

Johansen, O., 1975: Thermal conductivity of soils. Ph.D. thesis, University of Trondheim, 671 pp. [Available from Universitetsbiblioteket i Trondheim, Høgskoleringen 1, 7034 Trondheim, Norway.]

Katurji, M., P. Zawar-Reza, and S. Zhong, 2013: Surface layer response to topographic solar shading in Antarctica's dry valleys. *J. Geophys. Res. Atmos.,* **118,** 12 332–12 344, doi:10.1002/2013JD020530.

Kilpelainen, T., and Coauthors, 2012: Modelling the vertical structure of the atmospheric boundary layer over Arctic fjords in Svalbard. *Quart. J. Roy. Meteor. Soc.,* **138,** 1867–1883, doi:10.1002/qj.1914.

Kit, E., A. Cherkassy, T. Sant, and H. J. S. Fernando, 2010: In situ calibration of hot-film probes using a colocated sonic anemometer: Implementation of a neural network. *J. Atmos. Oceanic Technol.,* **27,** 23–41, doi:10.1175/2009JTECHA1320.1.

Lehner, M., C. D. Whiteman, S. W. Hoch, D. Jensen, E. R. Pardyjak, L. S. Leo, S. Di Sabatino, and H. J. S. Fernando, 2015: A case study of the nocturnal boundary-layer evolution on a slope at the foot of a desert mountain. *J. Appl. Meteor. Climatol.,* **54,** 732–751, doi:10.1175/JAMC-D-14-0223.1.

Leo, L. S., H. J. S. Fernando, and S. Di Sabatino, 2015a: Flow in complex terrain with coastal and urban influence. *J. Environ. Fluid Mech.,* **15,** 349–372, doi:10.1007/s10652-013-9327-y.

Lin, Q., W. R. Lindberg, D. L. Boyer, and H. J. S. Fernando, 1992: Stratified flow past a sphere. *J. Fluid Mech.,* **240,** 315–354, doi:10.1017/S0022112092000119.

Liu, Y., and Coauthors, 2008: The operational mesogamma-scale analysis and forecast system of the U.S. Army Test and Evaluation Command. Part I: Overview of the modeling system, the forecast products, and how the products are used. *J. Appl. Meteor. Climatol.,* **47,** 1077–1092, doi:10.1175/2007JAMC1653.1.

Long, R. R., 1953: Some aspects of the flow of stratified fluids: I. A theoretical investigation. *Tellus,* **5,** 42–58, doi:10.1111/j.2153-3490.1953.tb01035.x.

——, 1972: Finite amplitude disturbances in the flow of inviscid rotating and stratified fluids over obstacles. *Annu. Rev. Fluid Mech.,* **4,** 69–92, doi:10.1146/annurev.fl.04.010172.000441.

Lothon, M., and Coauthors, 2014: The BLLAST field experiment: Boundary-Layer Late Afternoon and Sunset Turbulence. *Atmos. Chem. Phys. Discuss.,* **14,** 10 789–10 852, doi:10.5194/acpd-14-10789-2014.

Louis, H., 1975: Neugefasstes hohendiagramme der Erde. *Math-Naturwisse Klasse,* B. Messerli B. and J. D. Ives, Eds., Bayerische Akademie der Wissenschaften, 305–326.

Lu, R., and R. P. Turco, 1994: Air pollutant transport in a coastal environment. Part I: Two-dimensional simulations of sea-breeze and mountain effects. *J. Atmos. Sci.,* **51,** 2285–2308, doi:10.1175/1520-0469(1994)051<2285:APTIAC>2.0.CO;2.

Lundquist, K. A., F. K. Chow, and J. K. Lundquist, 2010: An immersed boundary method for the Weather and Research Forecasting model. *Mon. Wea. Rev.,* **138,** 796–817, doi:10.1175/2009MWR2990.1.

——, ——, and ——, 2012: An immersed boundary method enabling large-eddy simulations of complex terrain in the WRF model. *Mon. Wea. Rev.,* **140,** 3936–3955, doi:10.1175/MWR-D-11-00311.1.

Mahrt, L., 1999: Stratified atmospheric boundary layers. *Bound.-Layer Meteor.,* **90,** 375–396, doi:10.1023/A:1001765727956.

Marshall, C. H., K. C. Crawford, K. E. Mitchell, and D. J. Stensrud, 2003: The impact of the land surface physics in the operational NCEP Eta Model on simulating the diurnal cycle: Evaluation and testing using Oklahoma Mesonet data. *Wea. Forecasting,* **18,** 748–768, doi:10.1175/1520-0434(2003)018<0748:TIOTLS>2.0.CO;2.

Mass, C. F., D. Ovens, K. Westrick, and B. A. Colle, 2002: Does increasing horizontal resolution produce more skillful forecasts? The results of two years of real-time numerical weather prediction over the Pacific Northwest. *Bull. Amer. Meteor. Soc.,* **83,** 407–430, doi:10.1175/1520-0477(2002)083<0407:DIHRPM>2.3.CO;2.

Massey, J. D., W. J. Steenburgh, S. W. Hoch, and J. C. Knievel, 2014: Sensitivity of near-surface temperature forecasts to soil properties over a sparsely vegetated dryland region. *J. Appl. Meteor. Climatol.,* **53,** 1976–1995, doi:10.1175/JAMC-D-13-0362.1.

Mayr, G. J., and Coauthors, 2007: Gap flows: Results from the Mesoscale Alpine Programme. *Quart. J. Roy. Meteor. Soc.,* **133,** 881–896, doi:10.1002/qj.66.

McCumber, M. C., and R. A. Pielke, 1981: Simulation of the effects of surface fluxes of heat and moisture in a mesoscale numerical model. *J. Geophys. Res.,* **86,** 9929–9938, doi:10.1029/JC086iC10p09929.

Monti, P., H. J. S. Fernando, M. Princevac, W. C. Chan, T. A. Kowalewski, and E. R. Pardyjak, 2002: Observations of flow and turbulence in the nocturnal boundary layer over a slope. *J. Atmos. Sci.,* **59,** 2513–2534, doi:10.1175/1520-0469(2002)059<2513:OOFATI>2.0.CO;2.

Nadeau, D. F., E. R. Pardyjak, C. W. Higgins, H. J. S. Fernando, and M. B. Parlange, 2011: A simple model for the afternoon and early evening decay of convective turbulence over different land surfaces. *Bound.-Layer Meteor.*, **141,** 301–324, doi:10.1007/s10546-011-9645-x.

——, ——, ——, H. Huwald, and M. B. Parlange, 2013: Flow during the evening transition over steep Alpine slopes. *Quart. J. Roy. Meteor. Soc.,* **139,** 607–624, doi:10.1002/qj.1985.

Ngan, F., H. Kim, P. Lee, B. Dornblaser, and K. Al-Wali, 2013: A study on nocturnal surface wind

speed overprediction by the WRF-ARW model in southeastern Texas. *J. Appl. Meteor. Climatol.,* **52,** 2638–2653, doi:10.1175/JAMC-D-13-060.1.

Pardyjak, E., H. J. S. Fernando, J. C. R. Hunt, A. Grachev, and J. Anderson, 2009: Development of nocturnal flow and transport in a wide open valley. *Meteor. Z.,* **18,** 85–100, doi:10.1127/0941-2948/2009/362.

Politovich, M. K., R. K. Goodrich, C. S. Morse, A. Yates, R. Barron, and S. A. Cohn, 2011: The Juneau terrain-induced turbulence alert system. *Bull. Amer. Meteor. Soc.,* **92,** 299–313, doi:10.1175/2010BAMS3024.1.

Poulos, G. S., J. E. Bossert, T. B. McKee, and R. A. Pielke, 2000: The interaction of katabatic flow and mountain waves. Part I: Observations and idealized simulations. *J. Atmos. Sci.,* **57,** 1919–1936, doi:10.1175/1520-0469(2000)057<1919:TIOKFA>2.0.CO;2.

Prandtl, L., 1942: *Strömungslehre* (*Flow Studies*). Vieweg und Sohn, 382 pp.

Pratt, T., Z. Lin, S. DiSabatino, L. Leo, N. Dodson, and J. Mueller, 2014: Towards estimation of soil moisture using RF polarimetric responses with topographical data and electromagnetic scattering models. *18th Joint Conf. on the Applications of Air Pollution Meteorology with the A&WMA,* Atlanta, GA, Amer. Meteor. Soc., 16.1. [Available online at https://ams.confex.com/ams/94Annual/webprogram/Paper235742.html.]

Price, J. D., and Coauthors, 2011: COLPEX: Field and numerical studies over a region of small hills. *Bull. Amer. Meteor. Soc.,* **92,** 1636–1650, doi:10.1175/2011BAMS3032.1.

Princevac, M., and H. J. S. Fernando, 2008: Morning break-up of cold pools in complex terrain. *J. Fluid Mech.,* **616,** 99–109, doi:10.1017/S0022112008004199.

——, J. C. R. Hunt, and H. J. S. Fernando, 2008: Quasi-steady katabatic winds over long slopes in wide valleys. *J. Atmos. Sci.,* **65,** 627–643, doi:10.1175/2007JAS2110.1.

Pu, Z., H. Zhang, and J. A. Anderson, 2013: Ensemble Kalman filter assimilation of near-surface observations over complex terrain: Comparison with 3DVAR for short-range forecasts. *Tellus,* **65A,** 19620, doi:10.3402/tellusa.v65i0.19620.

——, and Coauthors, 2014: Evaluation of the real-time WRF forecasts during the Mountain Terrain Atmospheric Modeling and Observations (MATERHORN) Program: Performance, comparison with observations, and further implications. *18th Joint Conf. on the Applications of Air Pollution Meteorology with the A&WMA,* Atlanta, GA, Amer. Meteor. Soc., 16.2. [Available online at https://ams.confex.com/ams/94Annual/webprogram/Paper240171.html.]

Queney, P., 1948: The problem of airflow over mountains: A summary of theoretical studies. *Bull. Amer. Meteor. Soc.,* **29,** 16–26.

Rife, D. L., T. T. Warner, F. Chen, and E. G. Astling, 2002: Mechanisms for diurnal boundary layer circulations in the great basin desert. *Mon. Wea. Rev.,* **130,** 921–938, doi:10.1175/1520-0493(2002)130<0921:MFDBLC>2.0.CO;2.

Rotach, M. W., and D. Zardi, 2007: On the boundary-layer structure over highly complex terrain: Key findings from MAP. *Quart. J. Roy. Meteor. Soc.,* **133,** 937–948, doi:10.1002/qj.71.

Smedman, A.-S., U. Högström, J. C. R. Hunt, and E. Sahlée, 2007: Heat/mass transfer in the slightly unstable atmospheric surface layer. *Quart. J. Roy. Meteor. Soc.,* **133,** 37–51, doi:10.1002/qj.7.

Snyder, W. H., and Coauthors, 1985: The structure of strongly stratified flow over hills: Dividing-streamline concept. *J. Fluid Mech.,* **152,** 249–288, doi:10.1017/S0022112085000684.

Soil Survey Staff, 2014: Web soil survey. Natural Resources Conservation Service, United States Department of Agriculture, accessed 28 May 2014. [Available online at http://websoilsurvey.nrcs.usda.gov/.]

Steenburgh, W. J., C. R. Neuman, G. L. West, and L. F. Bosart, 2009: Discrete frontal propagation over the Sierra-Cascade Mountains and Intermountain West. *Mon. Wea. Rev.,* **137,** 2000–2020, doi:10.1175/2008MWR2811.1.

Strobach, K., 1991: *Unser Planet Erde: Ursprung und Dynamik.* Gebruder Bornträger, 253 pp.

Taylor, P. A., P. J. Mason, and E. F. Bradley, 1987: Boundary-layer flow over low hills. *Bound.-Layer Meteor.,* **39** (1–2), 107–132, doi:10.1007/BF00121870.

Thomas, C. K., A. M. Kennedy, J. S. Selker, A. Moretti, M. H. Schroth, A. R. Smoot, N. B. Tufillaro, and M. J. Zeeman, 2012: High-resolution fibre-optic temperature sensing: A new tool to study the two-dimensional structure of atmospheric surface layer flow. *Bound.-Layer Meteor.,* **142,** 177–192, doi:10.1007/s10546-011-9672-7.

West, G. L., and W. J. Steenburgh, 2010: Life cycle and mesoscale frontal structure of an intermountain cyclone. *Mon. Wea. Rev.,* **138,** 2528–2545, doi:10.1175/2010MWR3274.1.

——, and ——, 2011: Influences of the Sierra Nevada on intermountain cold-front evolution. *Mon. Wea. Rev.,* **139,** 3184–3207, doi:10.1175/MWR-D-10-05076.1.

Whiteman, C. D., 1982: Breakup of temperature inversions in deep mountain valleys: Part I. Observations. *J. Appl. Meteor.,* **21,** 270–289, doi:10.1175/1520-0450(1982)021<0270:BOTIID>2.0.CO;2.

——, 2000: *Mountain Meteorology: Fundamentals and Applications.* Oxford University Press, 355 pp.

——, and Coauthors, 2008: METCRAX 2006: Meteorological experiment in Arizona's Meteor Crater. *Bull. Amer. Meteor. Soc.,* **89,** 1665–1680, doi:10.1175/2008BAMS2574.1.

Wile, S. M., J. P. Hacker, and K. H. Chilcoat, 2015: The potential utility of high-resolution ensemble sensitivities during weak flow in complex terrain. *Wea. Forecasting,* in press.

Winters, H. A., G. A. Galloway Jr., W. J. Reynolds, and D. W. Rhyne, 2001: *Battling the Elements: Weather and Terrain in the Conduct of War.* The Johns Hopkins University Press, 226 pp.

Wood, N., 2000: Wind flow over complex terrain: A historical perspective and prospect for large-eddy modeling. *Bound.-Layer Meteor.,* **96,** 11–32, doi:10.1023/A:1002017732694.

WRCC, 2014: Western historical climate summaries. Western Regional Climate Center, accessed 15 Sep 2015. [Available online at www.wrcc.dri.edu/Climsum.html.]

Zardi, D., and C. D. Whiteman, 2013: Diurnal mountain wind systems. *Mountain Weather Research and Forecasting,* F. K. Chow, S. F. J. De Wekker, and B. Snyder, Eds., Springer, 35–119.

Zhang, H., and Z. Pu, 2014: Predictability of atmospheric conditions over complex terrain with ensemble Kalman filter data assimilation: Evaluation with observations from MATERHORN field program. *18th Joint Conf. on the Applications of Air Pollution Meteorology with the A&WMA,* Atlanta, GA, Amer. Meteor. Soc., 16.5. [Available online at https://ams.confex.com/ams/94Annual/webprogram/Paper240176.html.]

——, Z. Pu, and X. Zhang, 2013: Examination of errors in near-surface temperature and wind from WRF numerical simulations in regions of complex terrain. *Wea. Forecasting,* **28,** 893–914, doi:10.1175/WAF-D-12-00109.1.

ENSO EXTREMES AND DIVERSITY

Dynamics, Teleconnections, and Impacts

BY AGUS SANTOSO, WENJU CAI, MAT COLLINS, MIKE MCPHADEN, FEI-FEI JIN, ERIC GUILYARDI, GABRIEL VECCHI, DIETMAR DOMMENGET, AND GUOJIAN WANG

Underlying a predictive capability of the El Niño–Southern Oscillation (ENSO) is a grounded understanding of its dynamics. The 1982/83 and 1997/98 "super–El Niño" events pose a challenge to this understanding. The 1997/98 event was dubbed "the climate event of the twentieth century" for its extraordinary magnitude and global-scale destructive effects. Modeling studies over the last 2 years have led to further insights into extreme El Niños and have found that their frequency is projected to increase significantly under greenhouse warming.

ENSO EXTREMES AND DIVERSITY: DYNAMICS, TELECONNECTIONS, AND IMPACTS

WHAT: Sixty leading ENSO experts met to review recent progress in ENSO research and determine the present state of understanding of ENSO in terms of its extreme and diverse behavior and its overarching physical implications.
WHEN: 4–6 February 2015
WHERE: Sydney, New South Wales, Australia

AFFILIATIONS: SANTOSO—ARC Centre of Excellence for Climate System Science and Climate Change Research Centre, University of New South Wales, Sydney, Australia; CAI AND WANG—CSIRO Marine and Atmospheric Research, Aspendale, Victoria, Australia; COLLINS—College of Engineering Mathematics and Physical Sciences, University of Exeter, Exeter, United Kingdom; MCPHADEN—NOAA/Pacific Marine Environmental Laboratory, Seattle, Washington; JIN—Department of Meteorology, SOEST, University of Hawai'i at Mānoa, Honolulu, Hawai; GUILYARDI—NCAS-Climate, University of Reading, Reading, United Kingdom, and Laboratoire d'Océanographie et du Climat: Expérimentation et Approches Numériques (LOCEAN), IRD/UPMC/CNRS/MNHN, Paris, France; VECCHI—NOAA/Geophysical Fluid Dynamics Laboratory, Princeton, New Jersey; DOMMENGET—ARC Centre of Excellence for Climate System Science and School of Earth, Atmosphere and Environment, Monash University, Clayton, Victoria, Australia
* Pacific Marine Environmental Laboratory Contribution No. 4328
CORRESPONDING AUTHOR: Dr. Agus Santoso, Climate Change Research Centre, L4 Mathews Bldg., University of New South Wales, Sydney, NSW 2052, Australia
E-mail: a.santoso@unsw.edu.au

DOI:10.1175/BAMS-D-15-00141.1

In final form 11 May 2015

In boreal spring of 2014, the tropical Pacific was primed for an El Niño, when most forecast agencies such as the National Oceanic and Atmospheric Administration (NOAA) and the Australian Bureau of Meteorology elevated their El Niño probability to more than 60%. A remarkable increase in warm water volume with a series of westerly wind bursts in boreal spring alerted ENSO experts to the possibility of a strong event, one which some thought could be the first extreme El Niño since 1997, generating news headlines worldwide. However, while the equatorial Pacific remained anomalously warm, the expected super–El Niño did not materialize. That failed expectation may, in part, be a reflection of our incomplete knowledge of extreme El Niño and its predictability or perhaps the very nature of the ENSO system itself.

Against this backdrop of progress, uncertainties, and ensuing greenhouse warming, it is timely to ask—what is the current state of understanding of ENSO diversity, extremes, impacts, and teleconnections? It is for this reason that ENSO researchers gathered in Sydney, Australia, earlier this year for a 3-day workshop at the University of New South Wales. The 60 participants consisted of leading ENSO experts,

including 20 postdoctorates and graduate students, who delivered 39 oral and 24 poster presentations, highlighting recent advances and ongoing research to facilitate the discussions of ENSO extremes and diversity. The science presented covered the use of modeling, observations, theories, and paleoreconstructions.

The workshop was opened by a stimulating presentation called "Who Killed the Big 2014 El Niño," which outlined the possible factors that may hold the key to understanding this elusive event. The general perception is that the atmospheric feedback failed to occur, despite the significant ocean subsurface warming, and this appears to be due to various factors such as the cold phase of the interdecadal Pacific oscillation (IPO) or the Pacific decadal oscillation (PDO), an anomalously warm Indian Ocean, and muted westerly wind bursts, among other possibilities. All of these factors reflect the main complexities of ENSO dynamics, which remain today an active topic of investigation. These are outlined below as discussed by several presenters.

ROLE OF THE BACKGROUND STATE ON ENSO VARIABILITY. The mean climate, upon which ENSO evolves, varies on multidecadal time scales, manifesting itself as a global-scale phenomenon in what is commonly known as the IPO or PDO. Disentangling the link between ENSO and IPO has been one challenging research topic as the two are intertwined. Is the IPO an ENSO rectification effect on the mean climate, for instance through ENSO skewness as discussed by a presenter? Or is the IPO an independent mode of low-frequency variability that impacts ENSO? A clear example of this was demonstrated in a presentation that ENSO predictability was weaker during the recent negative IPO phase than during the preceding positive IPO phase. Our current theoretical understanding, as mentioned by a keynote speaker, is that modest changes in the basic state can lead to different types of El Niño emerging during certain epochs. As such, the presence of the IPO would complicate the detection of greenhouse warming effects, as well as other external forcing, on ENSO changes.

PRECURSORS. A positive warm water volume anomaly was mentioned to be a necessary condition for a strong El Niño, as are strong westerly wind anomalies in boreal spring/summer. Warm water volume increase is achieved through downwelling Kelvin waves, often initiated by westerly wind bursts. However, it was shown that the different spatial and temporal characteristics of the wind bursts mean that the effect of the generated waves on El Niño development can be very different. A potential link between variations in the warm pool spatial structure and development of strong El Niño was also suggested. Other precursors of extreme El Niño include specific vacillations in surface pressure in the Southern and Northern Hemispheres, respectively, referred to as the "Southern Hemisphere booster" and the "Pacific meridional mode." Such insights have direct implications for the seasonal prediction of El Niño.

INTERBASIN INTERACTIONS. While ENSO influences air–sea processes outside of the tropical Pacific, those processes in turn affect ENSO evolution. The interactions between climate variability in the Indian (e.g., Indian Ocean dipole), Atlantic, and extratropics (e.g., North Pacific Oscillation) were presented, with apparent impacts on ENSO evolution. The results, which can be model dependent, suggest that understanding ENSO evolution should be approached from a global perspective rather than focusing solely on the tropical Pacific.

COUPLED FEEDBACK PROCESSES. Representing ENSO feedbacks in climate models remains challenging, with biases attributed significantly to inaccuracies in cloud simulation. A presentation showed cloud feedback accounts for a substantial portion of ENSO variability in a climate model. This issue needs to be resolved, not least because the growth of extreme El Niños was suggested to involve convectively nonlinear Bjerknes feedbacks. On a closely related topic, the characteristics of coupled feedback processes were shown to be notably different between eastern and central Pacific ENSO events, contributing to the debate as to whether ENSO exhibits a number of independent modes of variability or whether these are part of an ENSO continuum.

SEASONAL PHASE LOCKING. The explanation for why ENSO amplitude tends to peak in boreal winter is not complete. Yet seasonal phase locking contributes to the nonlinear behavior of ENSO, such as the southward wind shift at the peak of a strong El Niño that leads to the demise of the event and preconditioning for La Niña in the following year. Seasonal feedback between clouds and sea surface temperature (SST) was suggested to be a mechanism for ENSO seasonal phase locking. Other potential contributors include the annual cycle of the warm pool, as well as feedback from Atlantic and Indian Ocean variabilities.

ENSO ASYMMETRY. El Niño and La Niña are not mirror images of one other. El Niño events tend to be of shorter duration and can attain a much larger magnitude than La Niña. Asymmetry underpins the notion of ENSO extremes whose many aspects were extensively discussed, from the characteristics of SST anomaly patterns and the ocean mixed-layer heat budget to the nonlinear response of rainfall to SST anomalies. The role of reversing equatorial Pacific zonal currents coupled with an eastward shift of atmospheric convection in pushing El Niño to extreme amplitudes was also highlighted. This mechanism was also proposed as a possible explanation for the differing skewness of ENSO SST anomalies across models.

The aforementioned factors are an integral component of ENSO dynamics. A better understanding in one will lead to further insights into another. Rapid gain of knowledge has been facilitated by the breadth of data from the latest generation of climate models as part of the Coupled Model Intercomparison Project (CMIP) initiative. Data from the fifth phase of CMIP (CMIP5) were utilized by several presenters. It was shown that although CMIP5 models still have issues in simulating many aspects of ENSO including its extremity, they have some success in seasonal predictions of the 1997/98 event. This is in part because of the good quality observational data used to initialize the models, but the predictive skill is hampered by numerical drifts and model biases.

The challenge in simulating ENSO was highlighted. One presentation showed that atmosphere–ocean dynamics can be very different in an ocean-only model forced by air–sea fluxes than when it is coupled to an atmospheric model, illustrating the complex coupled nature of ENSO. In earlier generations of models, "flux adjustments" were used to more realistically capture the seasonal cycle and minimize drifts. However, flux adjustments are a rather artificial fix to a problem that is inherently complex. A finer model resolution has been generally thought to be the most appropriate solution. A speaker, however, put forth a compelling argument for the use of flux adjustment, which appears to actually have overarching benefits along with increasing resolution. Regardless of these issues, the large diversity, accessibility, and economy of running CMIP models make them desirable for understanding future projections of ENSO. In light of the relatively short instrumental record, paleoreconstructions are also a useful tool. Here, a speaker provided paleo-based evidence that an increase in ENSO variance since the mid-Holocene is outside the range of internal variability, indicating the role of external forcing.

How ENSO responds to greenhouse warming has long been a contentious issue, with disagreement among the models in projecting ENSO's amplitude, typically defined as the magnitude of eastern equatorial Pacific SST anomalies. However, as one speaker showed, CMIP5 models with more realistic balance among the coupled feedback components exhibit a time-varying response in amplitude, in contrast to the less realistic group of models exhibiting a static increase into the future. The time-varying response appears to be driven by surface warming differences between the Indian and Pacific Oceans, which in itself is an interesting feature requiring further investigation. As discussed in other presentations, several recent projection studies have instead utilized more process-based indicators. These include the propagation direction of the SST anomalies and rainfall response to ENSO SST patterns superimposed on the background warming. These studies found an increase in the frequency of events, with unique features seen in the 1982/83 and 1997/98 extreme El Niños, as well as extreme La Niña events.

The workshop featured many presentations on ENSO teleconnections and their impacts, including effects on regional rainfall and interannual variability of atmospheric CO_2 concentrations. Presentations on the atmospheric teleconnections of ENSO include the effect on East Asian rainfall, the effect on Arctic Oscillation via the stratosphere, and the influence of La Niña on the 2010 eastern Australian extreme rainfall via an SST warming trend and interactions with the southern annular mode. There were also presentations on oceanic teleconnections, including the impact of ENSO on Southern Ocean circulation. A paleo-based presentation linked La Niña with ocean heat-wave events off of western Australia, dubbed the Ningaloo Niño, via ocean advection through the Indonesian Throughflow. A marked increase in the occurrence of Ningaloo Niño since the late 1990s was suggested by a speaker as related to the negative IPO, with a possible feedback on ENSO. Another highlight was a talk on the influence of El Niño heat discharge on eastern Pacific tropical cyclones, underscoring the importance of ENSO ocean teleconnections on extreme weather.

The workshop concluded with a discussion on coordinated multimodel experiments proposed for the sixth phase of CMIP (CMIP6) and the opportunities they present for understanding ENSO dynamics. It was agreed that, in addition to all the analysis that will be performed on the many CMIP6 multimodel experiments, some more targeted experiments should be conducted to investigate aspects such as the role of

the pattern of mean SST change in driving uncertainties in rainfall response to ENSO events in the future. Further discussions of the details will be scheduled for future meetings.

This workshop highlighted current issues in ENSO research that are also under the broader research focus of the Climate and Ocean: Variability, Predictability and Change (CLIVAR; www.clivar.org/research-foci/enso) project: robustness of ENSO projections amid model uncertainties and relatively short instrumental records; proper simulation of underlying physical processes (getting ENSO right for the right reasons); ENSO linkage with the background climate (e.g., IPO); characteristics, predictability, and teleconnections of extreme ENSO; mechanisms behind seasonal phase locking, ENSO diversity, and interbasin feedback interactions; and the use of paleoproxies for studying the spatial evolution of ENSO. With the increasing availability of observations, improved models, more elaborate experiments, and more paleoreconstructions, some of these issues will eventually be resolved. The workshop has further highlighted the need to bring together theories, models, observations, and paleoreconstructions to make significant progress and demonstrated that the ENSO research community has the breadth of expertise and enthusiasm to address the challenges that lie ahead.

ACKNOWLEDGMENTS. This workshop was financially supported by CSIRO and the Australian Research Council (ARC) Centre of Excellence for Climate System Science. Logistic support provided by the Climate Change Research Centre and the University of New South Wales is gratefully acknowledged. The authors thank Sarah Ineson, Harry Hendon, Neil Holbrook, and WonMoo Kim for proofreading this article and all participants for contributing to the workshop. Workshop program, abstracts, full report, participants list, and most presentations can be found at www.climatescience.org.au/content/806-enso-workshop-australia-2015. This workshop contributes to the objectives of CLIVAR of the World Climate Research Programme (WCRP) and to the interests of the International Commission on Climate (ICCL) of International Association of Meteorology and Atmospheric Sciences (IAMAS)/International Union of Geodesy and Geophysics (IUGG).

READINGS

BOOK REVIEWS

CLIMATE CHANGED: A PERSONAL JOURNEY THROUGH THE SCIENCE

Philippe Squarzoni, 2014, 480 pp., $24.95, softbound, Abrams ComicArts, ISBN 978-1-41971-255-5

Climate Changed is the story of a journey. The journey is that of the author, Philippe Squarzoni, through the subject of human-caused climate change. Aside from the personal perspective, what really makes this volume stand out is the fact it is a graphic novel. This is the first graphic novel I have ever encountered concerned with this crucial topic.

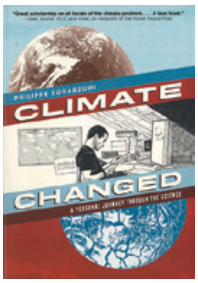

The book's drawings possess a beautiful simplicity that well suit its unflinching narrative. However, I would have appreciated a bit more visual action: the overwhelming majority of the illustrations consist solely of people talking or thinking. While textual conveyance of a significant amount of information is appropriate, with graphic novels visual storytelling is equally necessary. Inclusion of additional dynamic images would have enhanced interest in and understanding of the story. Still, I can't help but welcome the originality of the genre choice.

In regard to the written content, a comprehensive overview of the global warming issue is provided. An intriguing twist is further built in with the integration of real people as characters—mostly a number of international experts in the climate field. The sheer amount of information presented is impressive, ranging from the science behind Earth's climate to the mechanisms of human-caused climate change. Most strikingly, possible repercussions and solutions are intricately described. The contents are also enhanced by extensive use of statistics, graphs, and professional interviews. To me, the greatest narrative strength of *Climate Changed*, however, is its focus on society's values as the ultimate factor behind the climate emergency. This thought-provoking premise seems to offer the most effective route to abatement of and recovery from global warming.

I didn't care for the novel's tendency to occasionally veer into somewhat obscure cinematic references. Although adding a certain philosophical depth to the work, they also distract from the overarching narrative. I wasn't familiar with all the referenced movies and, as a consequence, felt lost at points. Other readers may experience the same issue.

As a whole, though, I do recommend *Climate Changed*. It will be of particular interest to anyone unfamiliar with the subject who wishes to obtain an across-the-board picture of what global warming is about. I also recommend it to everyone who remains skeptical about whether human-caused climate change is occurring. This book will especially appeal to those who don't care for traditional written works.

Climate Changed provides an informative, serious, and sometimes frightening overview of climate change. However, the very starkness of the novel is another point in its favor. There is far too much "literature" out there implying a debate still exists about whether human-caused climate change is even happening. It is encouraging to encounter a book that dispenses with such nonsense and imparts this global catastrophe with the urgency it demands. By focusing upon what the problem is and what can be done about it, *Climate Changed* becomes more than just a good read. It is a worthy contributor to the ongoing struggle to acknowledge and save ourselves from our own mistakes.

—Jennifer Yoshioka

Jennifer Yoshioka is an undergraduate meteorology major at SUNY Oswego in upstate New York.

CLIMATE SHOCK: THE ECONOMIC CONSEQUENCES OF A HOTTER PLANET

Gernot Wagner and Martin L. Weitzman, 2015, 250 pp., $27.95, hardbound, Princeton University Press, ISBN 978-0-691-15947-8

Climate Shock provides a unique perspective on climate change. In many other books on the subject, the focus has been on one of two sides: that climate change is a hoax, or that climate change is the absolute worst phenomenon that Earth has ever experienced and there is no way we will win the battle. This book, on the other hand, fully acknowledges the impacts of climate change but also explains the solutions with optimism. While they may go overboard on times with their optimistic views, the authors do a great job in engaging the reader into recognizing that we can still make a difference—a take on climate change that is lacking in some other climate change books.

Audience. This book appeals to a very wide audience. With its readable prose and at times witty comments, it keeps the attention of its reader, regardless if the reader is your average Joe or a Ph.D. student. Additionally, I believe this book should be read by politicians, businessmen, and others in leadership roles as a wake-up call and tool for enhancing climate policy.

This book is suitable for use in teaching. In fact, I would highly recommend it. I believe students would respond very positively to the writing style of Wagner and Weitzman, which is completely different from that of most textbook authors. This book provides a great overview of the economic perspective of climate change, focusing on the big picture while providing sufficient evidence to back up the authors' claims. I do believe this book would be best suited for a more economics-oriented class, however, as there are some sections that in my opinion would require a basic understanding of economic concepts to fully understand and appreciate.

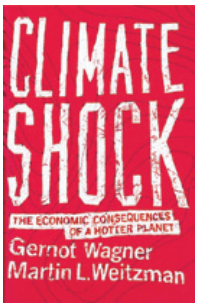

Strengths. I found the authors' introduction to the greenhouse gas problem, using the bathtub metaphor of rate of carbon emissions versus level of carbon in the atmosphere, to be very effective. This seemingly simple concept is misunderstood by many politicians, which the authors bluntly source as the cause of climate policy failures. This concept is carried throughout the book. The authors provide several other metaphors, such as how people buy insurance for a risk that is less than 10% (like a car accident), but don't share the same concern for climate change despite its equal risks. The authors find effective ways like this example to describe difficult concepts, and are successful in connecting with the reader.

NEW PUBLICATIONS

ATMOSPHERIC AEROSOLS

O. Boucher, 2015, 303 pp., $99.00, hardbound, Springer, ISBN 978-94-017-9648-4

This book is geared toward graduate and Ph.D. students and postdoctorates who share a common interest in aerosols and their role in the climate system. After covering atmospheric aerosols, atmospheric radiation, and cloud physics, the book dives into techniques used for in situ and remote-sensing measurements of aerosols as well as data assimilation. It also explores aerosol–radiation interactions, aerosol–cloud interactions, and the many impacts of aerosols on the climate system. Most chapters contain exercises at the end.

THE SUN'S INFLUENCE ON CLIMATE

J. Haigh and P. Cargill, 2015, 207 pp., $93.00, hardbound, Princeton University Press, ISBN 978-0-691-15384-1

This book provides an introduction to the significant relationship between the Earth's climate system and the sun. It highlights the basic properties of the climate system on Earth, the composition and behavior of the sun, and the absorption of solar radiation in the atmosphere. It elucidates the variations in solar activity and how they influence the Earth's environment, and is aimed toward both students and nonspecialists.

ATMOSPHERIC BOUNDARY LAYER: INTEGRATING AIR CHEMISTRY AND LAND INTERACTIONS

J. de Arellano et al., 2015, 265 pp., $48.00, softbound, Cambridge University Press, ISBN 978-1-107-09094-1

Studying the atmospheric boundary layer—the lowest part of the atmosphere in which atmospheric and surface conditions interact in the soil–vegetation–atmosphere system—provides a distinctive opportunity to describe and bring up an extensive range of ideas. Topics covered in this text include surface properties, plant physiology, atmospheric chemistry, and atmospheric dynamics. In addition, CLASS software is available on the book's website that provides hands-on practical exercises and allows students to design their own numerical experiments.

There is also valuable discussion on blame and the free rider effect, geoengineering as a cop-out to not doing anything to reduce carbon emissions, and basic climate terms and milestones, including the Montreal and Kyoto protocols and climate sensitivities. The authors always remind the reader of the main take-home message within each chapter, which is helpful, especially for students.

Unlike other climate change books, *Climate Shock* provides a clear and optimistic solution to the greenhouse gas problem: price carbon emissions as a way to make up for generations of subsidizing it. Another strength is its take on the uncertainties in climate change projections. Unlike some other authors, Wagner and Weitzman stress that the large uncertainties in temperature and other projections are not excuses for inaction. Rather, it's these uncertainties that should be the driver for action—action that should have been taken yesterday as opposed to next year. The authors discuss the problem using a risk-assessment framework and point out the frequently overlooked fact that simply reducing carbon emissions will not solve the problem; reducing emissions to zero is the only way that the atmosphere can naturally rid itself of carbon to pre-Industrial Revolution levels.

On another note, the writing is humorous while maintaining integrity.

Weaknesses. I found *Climate Shock* to be very repetitive. I believe the book could have been 30 pages shorter had the authors not repeated certain facts and concepts. I also found the writing style to be difficult to understand in some sections. It took rereading those sections a few times to fully understand the authors' point. Lastly, it seemed a bit narrow in perspective. There was no discussion on the larger picture of climate change in it being cyclical and not entirely caused by humans. I understand the economic take on the book, but a brief discussion on anthropogenic climate change in relation to other more natural drivers could have been useful.

Illustrations. The book includes several graphs depicting varying carbon emissions and climate sensitivity topics. These graphs helped illustrate the authors' point that there indeed are great uncertainties in projected climate temperatures.

Bottom Line. I recommend this book wholeheartedly. It provides a unique perspective on the climate change issue while remaining optimistic and engaging.

—Stephanie Hoekstra

Stephanie Hoekstra is a Ph.D. candidate at East Carolina University in the Coastal Resources Management Department.

VOLCANISM AND GLOBAL ENVIRONMENTAL CHANGE

A. Schmidt, K. Fristad, and L. Elkins-Tanton, 2015, 324 pp., $120.00, hardbound, Cambridge University Press, ISBN 978-1-107-05837-8

Bringing together present-day observations of volcanism and environmental changes and information from past eruptions preserved in the geologic record, this book delineates the effects of volcanism on the environment. It discusses the origins, features, and timing of volumetrically large volcanic eruptions; methods for assessing gas and tephra release in the modern day and the paleorecord; and the impacts of volcanic gases and aerosols on the environment, from ozone depletion to mass extinctions.

AN INTRODUCTION TO THE GLOBAL CIRCULATION OF THE ATMOSPHERE

D. Randall, 2015, 442 pp., $90.00, hardbound, Princeton University Press, ISBN 978-0-691-14896-0

With the recurring application of isentropic coordinates and implementing the methods of vector calculus, this textbook underlines the jobs of water vapor and clouds, contains thorough coverage of energy flows and transformations, and pays careful regard to scale interactions. It explores considerable historical contributions of important scientists and ends with a debate about how Earth's climate changes are causing global circulation to evolve.

AN INTRODUCTION TO LIGHTNING

V. Cooray, 2015, 386 pp., $80.00, hardbound, Springer, ISBN 978-94-017-8937-0

This book summarizes the essence of physics and effects of lightning in a nontechnical manner and provides a description of the phenomenon of lightning in simple language. Starting with the myths related to lightning, the reader is introduced to the mechanism of lightning flashes and their interactions with humans, human-made systems, and Earth's environment. It is tailored to the needs of university students who plan to study electrical engineering, meteorology, or environmental or basic physics, but is also appropriate for laymen who are interested in knowing more about this phenomenon.

AMS BOOKS

RESEARCH | APPLICATIONS | HISTORY

AMS MEMBERS GET FREE

CLIMATE

The Thinking Person's Guide to Climate Change

ROBERT HENSON

This fully updated and expanded revision of The *Rough Guide to Climate Change* combines years of data with recent research. It is the most comprehensive overview of climate science, acknowledging controversies but standing strong in its stance that the climate is changing—and something needs to be done.

© 2014, PAPERBACK, 520 PAGES,
ISBN: 978-1-935704-73-7
LIST $30 MEMBER $20

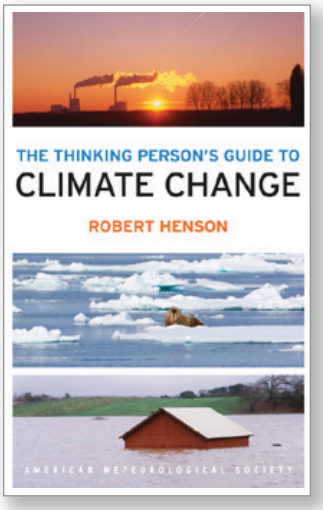

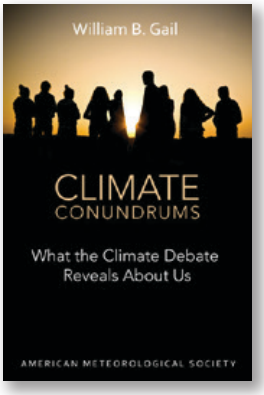

Climate Conundrums:
What the Climate Debate Reveals about Us

WILLIAM B. GAIL

This is a journey through how we think, individually and collectively, about humanity's relationship with nature, and more. Can we make nature better? Could science and religion reconcile? Gail's insights on such issues help us better understand who we are and find a way forward.

© 2014, PAPERBACK, 240 PAGES,
ISBN: 978-1-935704-74-4 LIST $30 MEMBER $20

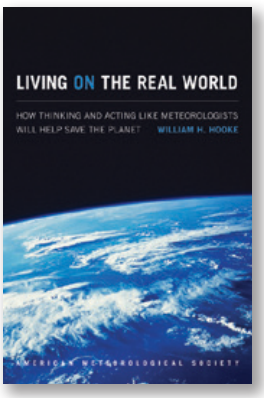

Living on the Real World:
How Thinking and Acting Like Meteorologists Will Help Save the Planet

WILLIAM H. HOOKE

Meteorologists focus on small bits of information while using frequent collaboration to make decisions. With climate change a reality, William H. Hooke suggests we look to the way meteorologists operate as a model for how we can solve the 21st century's most urgent environmental problems.

© 2014, PAPERBACK, 272 PAGES, ISBN 978-1-935704-56-0 LIST $30 MEMBER $22

GUIDES

An Observer's Guide to Clouds and Weather:
A Northeastern Primer on Prediction

TOBY CARLSON, PAUL KNIGHT, AND CELIA WYKOFF

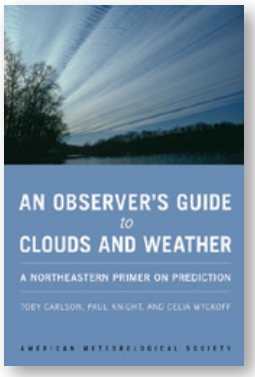

With help from Penn State experts, start at the beginning and go deep. This primer, intended for both serious enthusiasts and new meteorology students, will leave you with both refined observation skills and an understanding of the complex science behind the weather: the ingredients for making reliable predictions of your own. It connects fundamental meteorological concepts with the processes that shape weather patterns, and will make an expert of any dedicated reader.

© 2014, PAPERBACK, 210 PAGES,
ISBN: 978-1-935704-58-4 LIST $30 MEMBER $20

Eloquent Science:
A Practical Guide to Becoming a Better Writer, Speaker, and Atmospheric Scientist

DAVID M. SCHULTZ

The ultimate communications manual for undergraduate and graduate students as well as researchers in the atmospheric sciences and their intersecting disciplines.

© 2009, PAPERBACK, 440 PAGES,
ISBN 978-1-878220-91-2

LIST $45 MEMBER $30

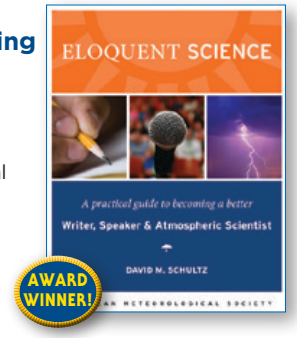

TEXTBOOK

Midlatitude Synoptic Meteorology:
Dynamics, Analysis, and Forecasting

GARY LACKMANN

This textbook links theoretical concepts to modern technology, facilitating meaningful application of concepts, theories, and techniques using real data.

©2011, PAPERBACK, 360 PAGES,
ISBN 978-1-878220-10-3
LIST $100 MEMBER $75 STUDENT MEMB. $65

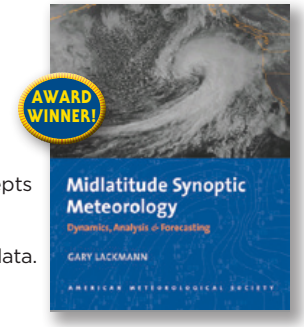

Midlatitude Synoptic Meteorology Teaching CD
More than 1,000 PowerPoint Slides.

© 2013, CD, ISBN 978-1-878220-27-1 LIST $100 MEMBER $75

To order: bookstore.ametsoc.org, 617-226-3998, or use the order form in this magazine

SHIPPING + DISCOUNTS AT BOOKSTORE.AMETSOC.ORG

COMING SOON!

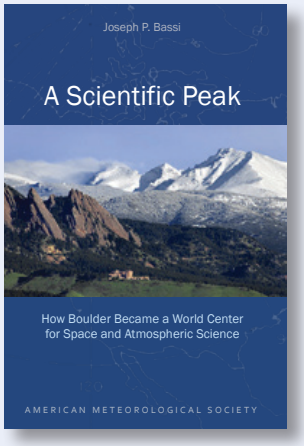

A Scientific Peak:

How Boulder Became a World Center for Space and Atmospheric Science

JOSEPH P. BASSI

How did big science come to Boulder, Colorado? Joe Bassi introduces us to the characters, including Harvard sun–Earth researcher Walter Orr Roberts, and the unexpected brew of politics, passion, and sheer luck that during the Cold War era transformed this "Scientific Siberia" to home of NCAR and NOAA.

METEOROLOGICAL MONOGRAPH SERIES

Synoptic–Dynamic Meteorology and Weather Analysis and Forecasting:

A Tribute to Fred Sanders

EDITED BY LANCE F. BOSART AND HOWARD B. BLUESTEIN

© 2008, HARDCOVER, 440 PAGES, VOL. 33, NO. 55, ISBN 978-1-878220-84-4

LIST $120 MEMBER $80
STUDENT MEM. $60

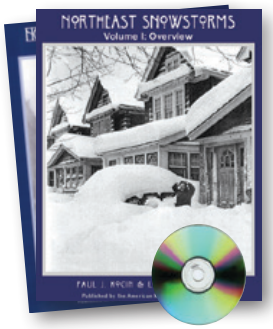

Northeast Snowstorms

(Volume I: Overview, Volume II: The Cases)

PAUL J. KOCIN AND LOUIS W. UCCELLINI

© 2004, TWO HARDCOVER VOLS. PLUS DVD, VOL. 32, NO. 54, ISBN 978-1-878220-64-6

LIST $100 MEMBER $80
STUDENT MEM. $60

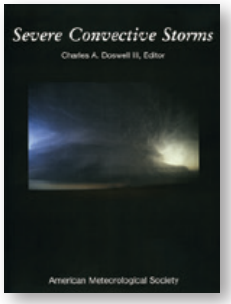

Severe Convective Storms

EDITED BY CHARLES A. DOSWELL III

© 2001, HARDCOVER, 570 PAGES, VOL. 28, NO. 50, ISBN 978-1-878220-41-7

LIST $110 MEMBER $90
STUDENT MEM. $75

Booksellers, groups, or for examination copies:
The University of Chicago Press:
1-800-621-2736 (US & Canada)
773-702-7000 (all others)
custserv@press.uchicago.edu

NOTIFICATION OF NEW AMS TITLES: www.ametsoc.org/JOIN

HISTORY

Taken by Storm, 1938:

A Social and Meteorological History of the Great New England Hurricane

LOURDES B. AVILÉS

The science behind the 1938 Hurricane, which hit New England unannounced, is presented here for the first time along with new data that sheds light on the motivations of the Weather Bureau forecasters. This compelling history successfully weaves science, historical accounts, and social analyses to create a comprehensive picture of the most powerful and devastating hurricane to hit New England to date.

© 2013, HARDCOVER, 288 PAGES, ISBN: 978-1-878220-37-0

LIST $40 MEMBER $30

Father Benito Viñes:

The 19th-Century Life and Contributions of a Cuban Hurricane Observer and Scientist

LUIS E. RAMOS GUADALUPE
TRANSLATED BY OSWALDO GARCIA

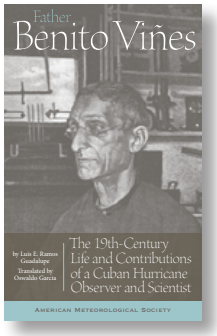

Before Doppler radar and weather broadcasts, Spanish Jesuit Benito Viñes (1837–1893) spent decades observing the skies at Belen Observatory in colonial Cuba. Nicknamed "the Hurricane Priest," Viñes taught the public about the weather and developed the first network of weather observation stations in the Caribbean, groundwork for the hurricane warning systems we use today.

© 2014, PAPERBACK, 172 PAGES
ISBN: 978-1-935704-62-1 LIST $20 MEMBER $16

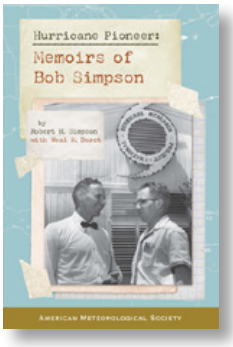

Hurricane Pioneer:

Memoirs of Bob Simpson

ROBERT H. SIMPSON AND NEAL DORST

In 1951, Bob Simpson rode a plane into a hurricane—just one of the many pioneering exploits you'll find in these memoirs. Bob and his wife Joanne are meteorological icons: Bob was the first director of the National Hurricane Research Project and a director of the National Hurricane Center. He helped to create the Saffir–Simpson Hurricane Scale; the public knows well his Categories 1–5. Proceeds from this book help support the AMS's K. Vic Ooyama Scholarship Fund.

© 2015, PAPERBACK, 156 PAGES
ISBN: 978-1-935704-75-1 LIST $25 MEMBER $20

THE AMS POSITIONS ON CLIMATE CHANGE AND ADVOCACY

I was recently reviewing some of the results of the survey of AMS members that was completed about a year ago, reading through the narrative responses to questions about things people liked and did not like about AMS.[1] I was somewhat disheartened that some of the responses showed a misunderstanding and mischaracterization of the Society's approach to science and to policy engagement, especially in the area of climate change. Those responses suggested a perception that AMS is no longer focused on science and, instead, that it has become an advocacy or lobbying organization pushing a specific agenda with respect to climate change. The actual number of such responses was small (a little over a dozen specific comments out of 96 pages of narrative responses), so the data suggest this is far from the majority opinion, but similar comments arise from time to time in other contexts, so I thought it worth addressing again here.

The Society's contribution to the science of climate change has been and continues to be enormous. Much of the cutting-edge climate science research is published in AMS journals and presented at AMS scientific conferences. The AMS position on climate change, based on comprehensive scientific assessment and an open process that included broad input from the community, is expressed in a statement released by the Council in 2012 (see: www2.ametsoc.org/ams/index.cfm/about-ams/ams-statements/statements-of-the-ams-in-force/climate-change/). The Statement on Climate Change recognizes that AMS not only supports the advance of scientific understanding, but also promotes the use of scientific understanding in societal decision making. AMS activities include initiatives that focus on understanding the policy options available for addressing climate change (what they are and the advantages and disadvantages of each). Those activities focus on informing policy options—not advocating particular courses of action—and take advantage of the expertise in the science that our community brings to the table.

In terms of advocacy, the Society takes a very careful approach to its interaction with government agencies and Capitol Hill that is quite different from the more traditional forms of advocacy and lobbying seen in other organizations. I described those differences, which take advantage of the strong scientific expertise the Society brings to issues and results in AMS being viewed as a trusted source of information, a little over a year ago in this column (see the July 2014 *BAMS*, pages 1105–1106). As I noted then, the approach taken by AMS has been very successful in bringing the science of our community to bear on appropriate policy issues across a wide range of topics that include, but are far from limited to, climate change. To be sure, I also noticed in the survey responses a number that urged AMS to become more active in advocacy. Some of those respondents may also not be aware of the careful approach taken on these issues and the effectiveness of that approach.

As I mentioned at the outset of the column, I am disheartened anytime there is misunderstanding of the careful and critical role the Society plays in the advance of the science and its beneficial use. I would be very happy to discuss these issues, or any other ones, with anyone who has concerns about AMS positions or activities. Please feel free to e-mail me at *kseitter@ametsoc.org* or call me on my direct line at 617-226-3901.

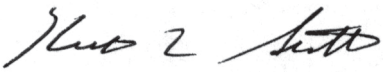

Keith L. Seitter, CCM
Executive Director

[1] A group of volunteers is currently analyzing the complete set of AMS Member Survey responses and preparing that analysis for release in *BAMS* in the near future.

Justin McLay, research meteorologist at the U.S. Naval Research Laboratory (NRL) Marine Meteorology Division, received the Laboratory Scientist of the Quarter award honoring extraordinary service to the Department of Defense (DoD). McLay was given the award for his distinguished accomplishments in leading the "New Rules of Predictability" project and his key role in developing and transitioning the Navy Global Environmental Model (NAVGEM) Ensemble Forecast System (EFS).

McLay is a subject-matter expert in the design and application of atmospheric ensemble predictions, and works on the 6.1 level predictability project and 6.4 level NAVGEM EFS. Providing detailed knowledge of future extreme weather variability and conditions (wind speeds, wave heights, air and sea temperatures, sea ice thickness and extent, and sea level), the ensemble will enable the U.S. Navy and DoD to adapt to future environmental impacts.

Beginning his career in weather science as a certified weather observer for the National Weather Service, McLay worked to obtain a doctorate in atmospheric science from the University of Wisconsin—Madison, where he had received both a bachelor's and master's degree in atmospheric science, in 1997 and 2001, respectively. After receiving

ON-AIR METEOROLOGY

10 QUESTIONS WITH . . .

A new series of profiles celebrating AMS Certified Broadcast Meteorologists and Sealholders

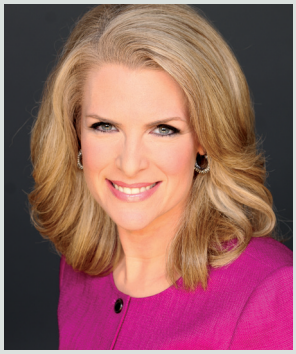

Janice Dean
Fox News Senior Meteorologist

When did you know you wanted to become a meteorologist/broadcaster? I studied journalism and radio/television broadcasting in college back home in Canada, but my interest in weather goes back to my childhood when we had snow piled up to our rooftops during the big Canadian winters. I went on to be a local weather presenter right out of college on the CBC while I was a radio host. Back then, you could do the weather without having the meteorology background. When I was hired at Fox to be their daytime weather person, I decided it was time to go back to school and study the science while working full time.

What do you think the next "big thing" is in weather reporting? Social media is definitely bringing us close to the story in terms of getting real-time pictures and reports. I get a little upset when people put themselves into harm's way to get pictures of tornadoes or extreme weather events (including meteorologists!). I'm probably one of the only broadcast meteorologists who does NOT like to report outside during big weather events. I find it ridiculous to be telling people to stay safe while holding onto a tree or sign post.

How often are you recognized in public? Rarely! We have the best hair and makeup team in the business here at Fox. They are magicians. I come to work with no makeup on with my hair in a ponytail and that's how I leave work. Plus, living in New York, even if people do recognize you, they don't have time to stop and chat. Everyone is on the move.

What is the best thing about what you do? I work at an amazing place with wonderful people, which makes it a joy to come into work. Plus, my kids love to come visit me and play on the green screen. I also love going to visit schools and reading my *Freddy the Frogcaster* books to them. Seeing children talk about weather is fantastic. It's the one thing that every single person experiences. It brings us all together.

his Ph.D. in 2004, he was granted a postdoctoral appointment within the National Research Council (NRC) for a position at NRL-Monterey in the Global Modeling Section of the Atmospheric Dynamics and Prediction Branch.

In 2007, McLay started his federal career at NRL-Monterey and progressed to improve the design of the now retired Navy Operational Global Atmospheric Prediction System EFS through the implementation of locally banded ensemble transform perturbations of the initial state. In March 2015, he led the transition of the U.S. Navy's first operational method for stochastic forcing of the NAVGEM global model, which improves the measurement of forecast uncertainty.

McLay has authored or coauthored 17 journal publications and has led 9 successful technical transitions for the U.S. Navy's NAVGEM global EPS. In April 2015, he received the Alan Berman Annual Research Publication Award for a study of statistical inference applied to model parameter uncertainty. He is currently associate editor for *Monthly Weather Review* and a member of the AMS Weather Analysis and Forecasting Committee. McLay has presented his research at numerous conferences and workshops, including as an invited speaker on the topic of forecast time series behavior at the Developmental Testbed Center, National Center for Atmospheric Research.

How would you define the value of the AMS seal programs? I feel very fortunate to have received my AMS Seal and enjoy getting together with fellow broadcast meteorologists to talk about the business and the future of weather. AMS has been very supportive of my career, my children's books, and opportunities within the community.

What's the biggest weather event you've reported on? Hurricane Sandy was a huge event for us in the Northeast, but I have to say Hurricane Katrina was the biggest weather event I've ever forecasted or witnessed. I remember reading that "doomsday statement" saying this would be the worst-case scenario for New Orleans. I read that warning on-air in front of the green screen while the satellite of the storm swirled behind me and just had this overwhelming feeling of dread. And then I remember the next day when we all thought New Orleans had dodged a bullet…and then the levees broke.

What weather myths do you hear the most? I absolutely can't stand seeing videos of people putting masking tape or electrical tape on their windows as preparation for a hurricane! This is a total waste of time. The windows are still going to break, and the pieces of glass are going to be larger and more dangerous than the smaller little pieces that get shattered. It's better to board up windows. Also, the myth that you should crack open windows to stabilized pressure during hurricanes or tornadoes. The last thing you should be doing is opening your windows during violent wind storms.

What is the strangest/most interesting question you've received as a broadcaster? When I was pregnant, I got an e-mail from someone saying, "When is your baby due?" They couldn't wait for my belly to disappear from the weather map so they could see their hometown that was hidden for nine months.

What's been your most difficult moment on-air? It's the moments when we see massive destruction or hear stories about someone being killed by a severe weather event that are difficult. There have been a few times where I've been moved to tears on television by a visual or a family member or friend talking about losing a loved one due to an extreme weather situation.

Who is your dream mentor? I don't really have a dream mentor. I've always had great real-life mentors like teachers, coworkers, or bosses that have taught me things or given me great advice. I would love to meet Bill Murray one day since I thought he was a genius in *Groundhog Day*.

Janice Dean received the AMS Seal of Approval in 2009. For more information on AMS Certification Programs, go to www.ametsoc.org/amscert/index.html.

Ronald E. Stewart has received the Patterson Distinguished Service Medal for his contributions to Canadian meteorology and his exceptional scientific leadership. The Patterson Distinguished Service Medal, presented since 1954, is considered the preeminent award recognizing outstanding work in meteorology by residents of Canada.

Stewart is a professor in the Department of Environment and Geography at the University of Manitoba. He is a leading expert on winter and summer storms, associated precipitation, and weather and regional climate extremes. He has led numerous Canadian and international research activities addressing the important aspects of meteorology, and has conducted research projects—often involving detailed field measurements—of precipitation and related weather conditions all across Canada.

Stewart's influence on meteorology is also reflected in his more than 126 scientific papers, and he has recently published articles on weather/climate phenomena over every region of Canada, including all the surrounding oceans. He has been on numerous scientific committees and societies and served as president of the Canadian Meteorological and Oceanographic Society. He is a member of the Changing Cold Regions Network, the World Climate Research Program task team on extremes, and the Canadian National Roundtable on Disaster Risk Reduction.

The American Geophysical Union (AGU) announced its 2015 class of Fellows. This honor is given to individual AGU members who have made exceptional scientific contributions and attained acknowledged eminence in the fields of Earth and space sciences. Since the establishment of the AGU Fellows program in 1962, and in accordance with AGU bylaws, no more than 0.1% of the total membership of AGU is recognized annually.

The following AMS members have been elected as 2015 Fellows and will be recognized during a ceremony held during the 2015 AGU Fall Meeting in San Francisco:

- **Jonathan T. Overpeck**, University of Arizona
- **Peter A. Troch**, University of Arizona
- **Robert W. Carlson,** Jet Propulsion Laboratory
- **Sarah T. Gille**, University of California, San Diego
- **Robert Pinkel**, University of California, San Diego
- **Jose-Luis Jimenez**, University of Colorado Boulder
- **Bette L. Otto-Bliesner**, NCAR
- **William J. Randel**, NCAR
- **Michael J. Thompson**, UCAR
- **Allan J. Clarke**, Florida State University
- **Axel Timmermann**, University of Hawaii
- **Praveen Kumar**, University of Illinois at Urbana-Champaign
- **Lorraine A. Remer**, University of Maryland, Baltimore County
- **Amitava Bhattacharjee**, Princeton University
- **Cynthia Rosenzweig**, NASA Goddard Institute for Space Studies
- **Larry D. Travis**, NASA Goddard Institute for Space Studies
- **Roger M. Samelson**, Oregon State University
- **Christopher S. Bretherton**, University of Washington
- **Alex B. Guenther**, Pacific Northwest National Laboratory
- **Philip J. Rasch**, Pacific Northwest National Laboratory
- **Daniel Rosenfeld**, Hebrew University of Jerusalem
- **Martin Visbeck**, GEOMAR Helmholtz Centre for Ocean Research Kiel

The AGU has also announced its 2015 medalists, awardees, and prize recipients. These individuals are recognized for their breakthrough achievements in advancing Earth and space science and their outstanding contributions and service to the scientific community. Their passion, vision, creativity, and leadership have expanded scientific understanding, illuminated new research directions, and made Earth and space science thrilling, immediate, and relevant to audiences beyond as well as within the scientific community. The honorees will be recognized during the Honors Tribute at the 2015 AGU Fall Meeting. The following AMS members were among the 2015 recipients:

- *William Bowie Medal*—**Wilfried H. Brutsaert**, Cornell University

IN MEMORIAM

HAROLD NAGEL
1932–2015

RAY PARSONS
1931–2015

LAURENT PRIMEAU
1924–2015

HARRY VOLKMAN
1926–2015

- *James B. Macelwane Medal*—**Colette L. Heald**, Massachusetts Institute of Technology
- *Maurice Ewing Medal*—**Russ E. Davis**, Scripps Institution of Oceanography
- *Roger Revelle Medal*—**Anne M. Thompson**, NASA Goddard Space Flight Center
- *Ambassador Award*—**Gordon McBean**, University of Western Ontario
- *Charles S. Falkenberg Award*—**Benjamin L. Preston**, Oak Ridge National Laboratory
- *International Award*—**Peter John Webster**, Georgia Institute of Technology
- *Robert C. Cowen Award for Sustained Achievement in Science Journalism*—**Andrew Revkin**, *The New York Times*
- *David Perlman Award for Excellence in Science Journalism—News Award*—**Sandi Doughton**, *The Seattle Times*
- *Climate Communications Prize*—**Richard C. J. Somerville**, Scripps Institution of Oceanography

LIVING ON THE REAL WORLD

[Editor's Note: The following post is adapted from William Hooke's blog, Living on the Real World (www.livingontherealworld.org/). Hooke is the former director of the AMS Policy Program and currently a senior policy fellow.]

Remembering Katrina (and the Human Condition)

Originally posted on August 30, 2015

These past weeks, you've likely found yourself struggling to stay afloat in a storm surge of ten-year Hurricane Katrina remembrance. News/social media outlets have been awash with reflections on the 2005 storm itself, which killed 1,000–2,000 people (yes, the range of estimates is that great), and inflicted $100B of losses in the form of property damage and business disruption. Media coverage has explored the subsequent enhancements to flood-protection infrastructure; recent improvements in weather- and storm-surge warnings; the progress of the recovery with respect to housing, demographics, poverty, education, the economy of the region, and the lives of individual survivors (those who have since returned and those permanently displaced); and much more. No aspect has gone ignored. The narratives have been poignant and gripping.

The Katrina retrospectives come on top of a worldwide tide of recollection. This past month has also marked the 70th anniversary of the end of World War II, including the bombing of Hiroshima and Nagasaki, which killed tens of thousands, and brought a close to a decade of conflict which saw 50–80 million deaths (50%–70% civilian), some 3% of the world's population of the time. And, these days, each week calls to mind centennial reminiscence of particular World War I events, which killed another 15–20 million people over the period 1914–1918.

Statistics such as these impoverish the respective discussions. It is the individual deaths that consecrate the events. Abraham Lincoln famously captured this point in his Gettysburg address, saying about that Civil War battlefield:

> …we can not dedicate, we can not consecrate, we can not hallow this ground. The brave men, living and dead, who struggled here, have consecrated it, far above our poor power to add or detract. The world will little note, nor long remember what we say here, but it can never forget what they did here. It is for us the living, rather, to be dedicated here to the unfinished work which they who fought here have thus far so nobly advanced. It is rather for us to be here dedicated to the great task remaining before us—that from these honored dead we take increased devotion to that cause for which they gave the last full measure of devotion—that we here highly resolve that these dead shall not have died in vain—that this nation, under God, shall have a new birth of freedom—and that government of the people, by the people, for the people, shall not perish from the earth.

Some might wonder, or even take umbrage, with the idea of lumping together those who died from so-called natural disasters with those who died heroically in war, but the reality is that there's no clear dividing line between the two groups. Many who have died in combat were drawn in by degrees—through accident of birth and position and a series of small decisions and a process of

acquiescence—rather than making any dramatic, conscious decision to sacrifice their lives for others or for a cause. And many who die from so-called natural hazards find much the same thing—that it was the last climactic consequence of the poverty and associated assumption of risk imposed on them by life's circumstances and the actions and failures of others as much as any personal shortsightedness of their own making. They had, in effect, been in a war all along.

Back then, Lincoln noted that there was (and is) only one decent way for the living to respond: through renewed and enlarged determination, to avoid any repetition of the tragedies of wars and natural disasters.

As we look around, we see evidence that we're doing a far better job of remembrance than such rededication. Media coverage on Katrina and its aftermath has been thorough and eloquent. Katrina recovery efforts—still underway, and likely to be needed for yet another decade—on occasion provide reasons for cheer. But New Orleans hasn't seen the back of the hurricane threat. Those risks are ongoing—if anything, growing. That is even more true of the hurricane threat to the United States more generally, and truer still of the broader risk exposure—to floods and drought; sea-level rise; earthquakes and volcanism; pandemic; acts of terror; and cyber-vulnerabilities. Disasters, like snowflakes, are all different. Each day we draw 24 hours closer to a diverse range of catastrophes that we'll then add to our growing calls to remembrance.

Often it feels that we're sleepwalking into this problematic future. But there's good news buried in this reality. First, not all future disaster scenarios are hidden from us. Thanks to advances in the geosciences and social sciences we know where many of the vulnerabilities and risks lie. What's more, we don't have to "guess exactly right" when it comes to the next disaster. We can take many measures now to build a generalized resilience to those future events, whatever precise form they may take (much as our immune system provides continuing protection against infections we've survived, and as an autumn flu shot provides added protection not just to the few strains in the serum but to a broader class of viruses). What's more, to enlist in and prosecute the effort to build societal resilience to hazards can be profoundly satisfying. Ask any emergency manager, or NOAA National Weather Service forecaster, or anyone working toward a weather ready-nation or emergency healthcare or business continuity; they'll tell you.

But this doesn't have to be a spectator sport for the rest of us. We actively build societal resilience whenever and however we work to create a more equitable and just society, to provide health care to all, to enhance public education, to create meaningful jobs, to protect habitat and the environment.

And at the core, it's about values. As we respect others, love each other, make opportunity for action and participation available to all, both locally and nationally—in short, as we respond to Lincoln's age-old call for a new birth of freedom—we'll find community-level resilience to hazards arises as a cobenefit. (By contrast, attempt to build hazards resilience while refusing to address or even acknowledge the challenges posed by basic human values, and we'll likely fail at both.)

Are you in?

CERTIFIED BROADCAST METEOROLOGISTS (CBM)

The following individuals were recently granted the Certified Broadcast Meteorologist (CBM) designation. For more information on the AMS CBM program, go to www.ametsoc.org/amscert/index.html#cbm.

681	Eric Burke	2015
682	Alyssa Caroprese	2015
683	Caitlin Roth	2015
684	Michael Page	2015
685	Tyler Eliasen	2015
686	Jacqueline Charles	2015
687	Eric Stone	2015
688	Brittany Bell	2015
689	Jennifer Constantine	2015
690	William J. Karins	2015
691	Thomas Meiners	2015
692	Monica Tassoni	2015
693	Richard Katzfey	2015
694	Bryan Bennett	2015
695	Jessica Quick	2015
696	Heather Waldman	2015
697	Lindsey Anderson	2015
698	Mackenzie Morris	2015

NEW MEMBERS

The Council has approved the election of the following candidates to the grade of **Full Member:**

John Aaron
Ghassan J. Alaka Jr.
Valentina Aquila
Norman E. Avila
Ahmad Bajjey
Rebecca Batchelor
Jennifer L. Beale
Steven T. Beale
Jack Bohl
Jaron M. Breen
Robert G. Brown
Darrin Cartwright
Rebecca M. Chewitt
Brittany A. Dahl
Shannon Darcy
Charlotte A. DeMott
Admassu Kassa Dewol
Tracey A. Dorian
Henrique F. Duarte
Laura Dunlap
Arthur J. Eiserloh, Jr.
Cynthia D. Engholm
Erik M. Esparza
Michael N. Evans
Bernard C. Falco
David Finkelstein
John A. Firth
Kimberly Genareau
Bevan T. Glynn
Grant R. Gray
Houston R. Green
Bryan A. Guarente
Chris Havely
Helen Holt
Leiqiu Hu
Patrick T. Hyland
Matthew R. Igel
Ginger Jeffries
Jason Kaiser
Donald Matthew Lafleur
James Lee
Xinfeng Liang
Robert D. Loper Jr.
Sasha Madronich
Josette E. Marrero
Alyssa A. Matthews
Mary J. Mays
Francis P. McInerney
Tim Miller
Krizia Negron-Hernandez
Liang Ning
Junichi Ninomiya
Satoshi Noda
Stephen Osinski
Wes Peery
Teke Solomon Ramotubei
Adriana Raudzens Bailey
Akkihebbal R. Ravishankara
Kevin Repasky
Gary J. Riley
Ross J. Salawitch
Adaline Schelling
Amanda J. Schroeder
Sergio A. Sejas
Edil A. Sepulveda Carlo
Kay L. Shelton
Jordan T. Sherman
Ravi P. Shukla
Peter J. Speirs
Derek Straub
Sarah Strode
Paul L. Tayler
Meaghan A. Thomas
Katelyn L. Tisch
Russell Todd
Nicholas J. Troiano
Takashi Unuma
Vittorio Villasmunta
Shih-Yu Wang
Shugong Wang
Kaylee A. Wendt
Emily A. Wood
Long Yang
Ke Zhang
Mitch Ziesemer

The Council has approved the election of the following candidate to the grade of **Full Member with Student Privileges:**

Akemi D. Briggs
Federico Di Catarina
Faraz Enayati Ahangar
Pierre Glaize
Darryl D. Halley
David W. Karppala Jr.
Ching-Yin Ke
Charles C. Morris
Albert Oude Nijhuis
Rafael Resendiz
Klint T. Skelly
McKenna W. Stanford
Zhan Su
Akintoye O. Towase
Kristy Weber
Matt C. Wilbanks

The Executive Committee has approved the election of the following candidates to the grade of **Associate Member:**

Michelle Brooks
Roger D. Clark
Bill Edgar
David M. Fischer
Brian K. Fowler
Stephen Giordano
Michael Purpura
Jorge Rivas
John C. Sans
Trevor B. Starner

The Executive Committee has approved the election of the following candidates to the grade of **Associate Member—Precollege Student:**

Zachary R. Burns
Madelyn M. Fosen
Vincent Garibaldi
David M. Judge
Michael A. Knoll
AJ Mastrangelo
David C. Pessin
Kimberly S. J. Walker

The Executive Committee has approved the election of the following candidates to the grade of **Associate MemberK–12 Teacher:**

Edward W. Laverdure
Koa Lavery
Judy Wasserman

NEW MEMBERS

The Executive Committee has approved the election of the following candidates to the grade of **Student Member:**

Marieke Akerboom
Zainab Ali
Scott T. Allen
Samuel E. Arcand
Alvaro Avila
Jeremy Behen
Charles A. Bertram
Kari Bowen
Alexandra L. Brosius
Zachary S. Bruick
Noelle Bryan
Carly Buxton
Matthew A. Campbell
Zachary T. Chabala
Younghyun Cho
Enrique Chon
Kara Cleghorn
Lamar S. Coats
Yair Cohen
Andrea G. Cook
Michael M. Cook
Austin Dickey
Alyson R. Douglas
Colin P. Egerer
Cristiano W. Eichholz
Jeffrey Fitzgerald
Jason P. Flemke
Joseph Fogarty
Rashida D.S Francis
Ryan Gonzalez
Will Hall
Jason R. Halmo
Ali Hamidi
Crystal Harper
Andre Hernandez-Espiet
Josh P. Heyer
Andrew Huang
Bo Huang
Tony O. Hurt
Colby Hyde
Andrew Janiszeski
Hema Joshi
Rachel Joyce
Bryan Kaiser
Joshua S. Kastman
Thomas R.J. Kavanagh
David King
Sidney E. King
Theodore K. Koenig
Nicholas F. Lenssen IV
Guiomar Lopez Fernandez
Holly Mallinson
Wilmarie Marrero Ortiz
Andrew M. McCalmont
Grant McKercher
Ashante McLeod-Perez
Hadjer Moussa
Gail S. Murray
Kelly L. Neely
Shania Nichols
Christian D. Norris
Quinn Pallardy
AnnaNicole Pietrus
Andrew Poppick
Nichole C. Riddle
Anna M. Robertson
Nevin Schaeffer
Stephanie Spera
Allyson Stanton
Justin Stark
Katelyn M. Stringer
Rachel Sussman
Sheng-Lun Tai
Joshua B. Teves
Liyan Tian
Zheming Tong
Simona Trefalt
Tyler Trigg
Shih-Che Tsai
Conner S. Ubert
Stephen VanHoesen
Carlos Roberto Wah Gonzalez
Hannah Wells
Jeffrey A. Wetterlin
Chi Fai Wong
Melissa Wrzesien
Katharine Wunsch
Sungduk Yu
Jayoung Yun
Xiangxiang Zhang
Heather M. Zons
Alec Zuch

Preliminary Program

AMS

American Meteorological Society

96th Annual Meeting

10-14 January 2016

Ernest N. Morial Convention Center
New Orleans, Louisiana

THE 96TH AMS ANNUAL MEETING will be held 10–14 January 2016 at the Ernest N. Morial Convention Center in New Orleans, Louisiana. Mary Cairns is the overall chairperson and Patricia Pu and Heidi Centola are the 2016 Annual Meeting Cochairpersons.

The theme for the 2016 AMS Annual Meeting, "Earth System Science in Service to Society," weaves the many parts of AMS into a common core. Emphasizing the academic and research strength of AMS, the theme also connects that research to the benefits that society gains from our science. AMS merges the physical, chemical, and biological study of the Earth with human-centered "domains of action": 1) observing, 2) analysis and research leading to understanding, 3) modeling and prediction, and 4) social sciences—how people deal with Earth. "Service to Society" explicitly evokes the integrated and complementary government and commercial enterprise that the AMS has done so much to foster over the last decade. The 2016 meeting integrates AMS' proud, nearly 100-year history of making a positive difference in the lives of our citizens by continually communicating the advances of its science research to the public and policy makers. The meeting will also feature numerous town hall meetings, the 16th Presidential Forum, and three special named symposia honoring Marvin Geller, Peter Lamb, and Mario Molina.

The 15th Annual AMS Student Conference and Career Fair, with a theme of "Beyond the Weather: Embracing the Interface of Science and Society," will provide junior and senior undergraduate and first-year graduate students with information for and insights into making effective career decisions.

Daily Weather Briefings will be held during lunch each day beginning on Monday, 11 January, and will be hosted by National Weather Service New Orleans/Baton Rouge Forecast Office.

The AMS Annual Meeting is host to the largest exhibit program anywhere in the atmospheric, oceanic, and related sciences. Exhibitors come from all over the United States and abroad, with over 100 organizations showcasing a wide range of products, publications, and services. The show allows organizations to make major announcements and roll out new products. Demonstrations of new and innovative equipment are given daily. The exhibit schedule is designed to both encourage social interaction and provide an opportunity to look at future trends in equipment, systems, and software.

The Annual Meeting will be preceded by nine short courses, the 15th Annual WeatherFest, a briefing for first-time attendees to the meeting, the 96th Annual Review, New Fellows and Featured Awards, and a Welcome Reception.

CONFERENCES AND SYMPOSIA
MONDAY–THURSDAY, 11–14 JANUARY

- 16th Presidential Forum: Serving Society in Times of Crisis: Past, Present, and Future
- 32nd Conference on Environmental Information Processing Technologies
- 30th Conference on Hydrology
- 28th Conference on Climate Variability and Change
- 25th Symposium on Education
- 23rd Conference on Probability and Statistics in the Atmospheric Sciences
- 22nd Conference on Applied Climatology
- 20th Symposium on Integrated Observing and Assimilation Systems for the Atmosphere, Oceans, and Land Surface (IOAS-AOLS)
- 19th Conference of Atmospheric Science Librarians International
- 19th Joint Conference on the Applications of Air Pollution Meteorology with the A&WMA
- 18th Conference on Atmospheric Chemistry
- 18th Symposium on Meteorological Observation and Instrumentation
- 15th Annual Student Conference—Beyond the Weather: Embracing the Interface of Science and Society
- 14th Conference on Artificial Intelligence Applications to Environmental Science
- 14th History Symposium
- 14th Symposium on the Coastal Environment
- 13th Conference on Space Weather
- 12th Annual Symposium on New Generation Operational Environmental Satellite Systems
- 11th Symposium on Societal Applications: Policy, Research, and Practice
- Ninth Annual CCM Forum
- Eighth Symposium on Aerosol–Cloud–Climate Interactions
- Seventh Conference on Weather, Climate, and the New Energy Economy
- Seventh Symposium on Environment and Health
- Sixth Conference on Transition of Research to Operations: Successes, Plans, and Challenges
- Sixth Symposium on Advances in Modeling and Analysis Using Python
- Fifth Aviation, Range, and Aerospace Meteorology Special Symposium
- Fourth AMS Conference for Early Career Professionals
- Fourth AMS Symposium on the Joint Center for Satellite Data Assimilation (JCSDA)
- Fourth Symposium on Building a Weather-Ready Nation: Enhancing Our Nation's Readiness, Responsiveness, and Resilience to High-Impact Weather Events
- Fourth Symposium on Prediction of the Madden–Julian Oscillation
- Fourth Symposium on the Weather, Water, and Climate Enterprise
- Second Symposium on High Performance Computing for Weather, Water, and Climate
- Special Symposium on Hurricane Katrina: Progress in Leveraging Science, Enhancing Response, and Improving Resilience
- Special Symposium on Seamless Weather and Climate Prediction—Expectations and Limits of Multiscale Predictability
- Special Sessions on U.S.–International Partnerships
- IMPACTS: Major Events and Impacts of 2015
- WeatherFest

COSPONSORS OF THE 95TH ANNUAL MEETING

American Academy of Environmental Engineers and Scientists (AAEES)
American Geosciences Institute (AGI)
American Geophysical Union (AGU)
American Society of Agronomy (ASA)
American Water Resources Association (AWRA)
Atmospheric Science Librarians International (ASLI)
Australian Meteorological and Oceanographic Society (AMOS)
Canadian Meteorological and Oceanographic Society (CMOS)
Crop Science Society of America (CSSA)
Indian Meteorological Society (IMS)
National Weather Association (NWA)
Soil Science Society of America (SSSA)
The Oceanography Society (TOS)
World Meteorological Organization (WMO)

Walter Orr Roberts Lecture
Monday, 11 January, 1:30–2:30 P.M.
The Walter Orr Roberts Lecture will be given in a session sponsored by the 28th Conference on Climate Variability and Change. The lecture will be given by Dr. Venkatachalam Ramaswamy. The title of the lecture is "Understanding the Earth System through Numerical Modeling: Crossing the Disciplinary Frontiers."

Bernhard Haurwitz Memorial Lecture
Tuesday, 12 January, 1:30–2:30 P.M.
The Bernhard Haurwitz Memorial Lecture will be given in a session sponsored by the 28th Conference on Climate Variability and Change. The lecture will be given by Dr. John C. Marshall, Cecil and Ida Green Professor of Oceanography, Massachusetts Institute of Technology, Cambridge, Massachusetts. The title of the lecture is "What's Happening over the Poles?"

Robert E. Horton Lecture
Wednesday, 13 January, 1:30–2:30 P.M.
The Robert E. Horton Lecture will be given in a session sponsored by the 30th Conference on Hydrology. The lecture will be given by Dr. Efi Foufoula-Georgiou, University of Minnesota, Minneapolis, Minnesota. The title of the lecture is "Climate and Humans as Amplifiers of Hydro-Ecologic Change: Science and Policy Implications for Intensively Managed Landscapes."

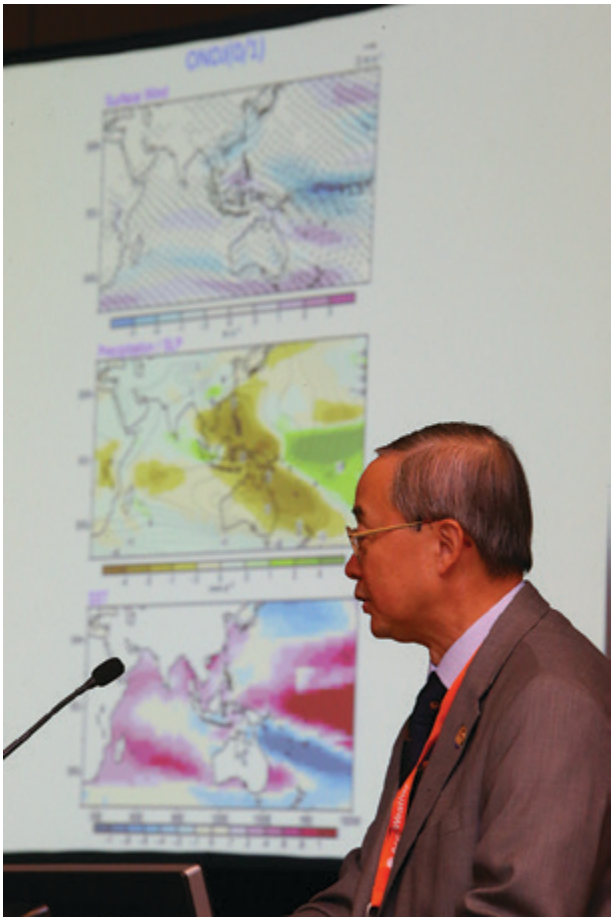

Ngar-Cheung Lau delivering the 2015 Bernhard Haurwitz Memorial Lecture.

SPECIAL SESSIONS/PROGRAMS OF GENERAL INTEREST

16th Presidential Forum: Serving Society in Times of Crisis: Past, Present, and Future
9:00–10:30 A.M., 11 January 2016
This year's Presidential Forum reflects upon the American Meteorological Society (AMS) annual meeting theme of "Earth System Science in Service to Society," which provides participants a better understanding of living through extreme events. Our society continues to experience the effects of more and more extreme events like hurricanes, tornadoes, floods, and drought, some as a result of our changing climate and others as a result of our expanding population. The AMS needs to continue to address lessons learned, and more importantly, identify what future actions it will take to help mitigate the impact of these devastating life-changing events. To highlight this, an outstanding panel of speakers has been invited to address attendees: Admiral Thad Allen, U.S. Coast Guard (ret.), executive vice president Booz Allen Hamilton; Max Mayfield, director, National Oceanic and Atmospheric Administration/National Hurricane Center (ret.); Dr. Kerry Emanuel, Massachusetts Institute of Technology; and Dr. Shirley Laska, professor emerita, and founding past director of the Center for Hazards Assessment, Response and Technology, University of New Orleans. Moderator Maureen McCann, News 13 Orlando, will lead a discussion of the panel's personal experiences during Hurricane Katrina and the Deepwater Horizon oil spill. The panel will also address AMS's current activities that encompass research and forecasting of events and inspire our members to embrace a renewed sense of purpose as they direct our Society in the coming years.

In addition to the Monday Presidential Forum, other related activities to this year's theme include a Presidential Town Hall on Wednesday called "Demystifying Careers in the Atmospheric Sciences," a one-day Special

Symposium on Hurricane Katrina entitled "Progress in Leveraging Science, Enhancing Response, and Improving Resilience," Core Science Talks, and a series of international sessions and joint themed sessions crossing many conferences and symposia.

Core Science Keynotes

The Core Science Keynotes series is an ongoing element of the AMS Annual Meeting. For the AMS 2016 Annual Meeting, the talks are intended to highlight, discipline by discipline, the history, foundational knowledge, and research challenges that drive our field forward as a whole, as well as provide information on career opportunities with the specific or closely related field. Each keynote speaker will summarize the state of current knowledge in their field in a manner accessible to all AMS disciplines. They will also describe future research directions, the challenges in pursuing them, and the expected benefits to both the discipline and to the society's broad science and applications directions including career opportunities within the enterprise. The Core Science Keynotes will be linked as a series in the program so that interested attendees may gain broad exposure to the scientific forefront of work being done in our community and knowledge of other career opportunities by attending several or all of these presentations.

Please reference the Program and Events page of the AMS Annual Meeting Web page for the full listing of talks (http://annual.ametsoc.org/2016/index.cfm/programs-and-events/).

SHORT COURSES/WORKSHOPS

SHORT COURSES

(Please note that there is an additional fee to attend the following Short Courses. The rates are noted in the registration section.)

- **A Beginner's Course to Using Python in Climate and Meteorology**
- **Coastal Surge and Inundation Modeling**
- **Data Management Resource Center**
- **Geostationary Operational Environmental Satellite-R (GOES-R) and Joint Polar Satellite System (JPSS) Meteorological Measurements and Instrumentation**
- **GIS Tutorial for Atmospheric Sciences**
- **Introduction to PyNIO and Related Python Tools for Geoscientific Data Analysis**
- **Meteorological Measurements and Instrumentation**
- **Soil Moisture Data Tutorial**

To view the program from the AMS website (www.ametsoc.org), click on the Annual Meeting logo, then use the "Program and Events" dropdown menu to select "Short Courses."

AMS VOLUNTEER PROJECT

Please join the AMS Committee on Environmental Stewardship to help remove invasive plant species from New Orleans City Park's wetlands and bioretention parking lot. AMS will be working with local landscape architecture firm, Dana Brown & Associates, designers of both of these spaces in City Park.

Volunteers are encouraged to wear outdoor working clothes and shoes that can potentially get muddy. Waterproof shoes are encouraged, as some parts of the wetlands may hold up to an inch of water. Sunscreen may be needed, weather permitting, and all other tools will be provided, including bug spray.

There is a $25 fee per person to participate, which will cover the cost of transportation and snacks. There will be two time slots (with the first and last half-hour for transportation) on Sunday, 10 January:

- 8:30 a.m.–12:30 p.m.
- 12:30–4:30 p.m.

Buses will depart from the Convention Center on Sunday, 10 January. The bus will depart at 8:30 a.m. for the morning session and at 12:30 p.m. for the afternoon session. Interested attendees are invited to sign up for the project when preregistering for the meeting. The deadline for registration for the volunteer project will be *Wednesday, 16 December.*

For information on this event, please contact Christine Keane (ckeane@ametsoc.org). Those participating in this event should plan to meet in the lobby of Hall D, across from the AMS Registration Desk, located on the first level of the convention center at 900 Convention Center Blvd.

AMS NATIONAL OFFICERS

President: Alexander E. MacDonald
President Elect: Frederick H. Carr
Executive Director: Keith L. Seitter
Executive Directors Emeritus: Richard E. Hallgren and Ronald D. McPherson
Secretary–Treasurer: Richard D. Rosen

ANNUAL MEETING OVERALL PROGRAM COMMITTEE

Overall Program Cochairpersons

Mary Cairns
Heidi Centola
Scott Mackaro
Zhaoxia (Patricia) Pu

2016 Annual Meeting Program Chairpersons

Josh Alland
Susan Avery
Kristen Averyt
Lourdes Aviles
Bruce Baker
Joe Bassi
Andrea Bleistein
Barbara Mayes Boustead
Amy Butros
Ken Carey
Kristy Carter
Edmund Chang
Andrew Clifton
Jeff Collett
Gerry Creager
Brian D'Agostino
Kristie Ebi
Kerry Emanuel
Brian Etherton
John Eylander
Jiwen Fan
Eric Fetzer
Genene Fisher
Tanja Fransen
John Furgerson
Dave Gochis
Jie Gong
Sultan Hameed
Steve Hanna
Patrick Harr
Douglas Hilderbrand
Scott Jacobs
Michael Jamilkowski
Dave Jones
Olivia Kellner
Benjamin Kirtman
Kevin Kloesel
Sonia Kreidenweis
Matt Lacke
Valliappa Lakshmanan
Johnny Lin
Sharan Majumdar
Steve Mango
Bob McCoy
Amy McGovern
John McHenry
Gary McWilliams
Daniel Mendoza
Cecilia Miner
Tim Miner
Brian Mischel
Andrew Molthan
Jinny Nathans
Randy Peppler
John Pereira
Nicolas Powell
Pallav Ray
Jared Rennie
Timothy J. Schmit
Carl Schreck
Chris Schultz
Hyodae Seo
Kathy Sherman-Morris
Viviane Silva
Chris Strager
Austin Stanforth
Diane Stanitski
Andre van der Westhuysen
Jennifer Vanos
Jeff Weil
Olga Wilhelmi
Dan Wilks
Klaus Wolter
Jim Yoe
Fuqing Zhang
Renyi Zhang

IN THE EXHIBIT HALLS

POSTERS

All Posters will be located in Hall DE of the Convention Center.

Poster Hall schedule

Day	Sunday	Monday	Tuesday	Wednesday	Thursday
Poster Hall hours	12:00–7:15 A.M. (Student Conference)	8:00 A.M.–4:30 P.M.	8:00 A.M.–6:00 P.M.	8:00 A.M.–6:30 P.M.	8:00 A.M.–12:00 P.M.
Formal Poster viewings	5:45–7:15 P.M. (Student Conference)	2:30–4:00 P.M.	9:45–11:00 A.M.	2:30–4:00 P.M.	9:45–11:00 A.M.

GENERAL INFORMATION

Location of Functions

Annual Meeting registration, scientific sessions, poster sessions, short courses, town hall meetings, special sessions, the Annual Meeting Banquet, the Molina Symposium Dinner, the Lamb Symposium Luncheon, and exhibits will be held in the Ernest N. Morial Convention Center, 900 Convention Center Boulevard, New Orleans, Louisiana 70130 (tel: 504-582-3000). AMS committee meetings and the Geller Symposium Dinner will be held at the Hilton Riverside Hotel, Two Poydras Street, New Orleans, Louisiana, 70130 (tel: 504-561-0500).

Hotels

Attendees are responsible for making their own hotel reservations directly with their hotel of choice. Please refer to the AMS website (www.ametsoc.org) for direct reservation links and phone numbers. Blocks of rooms have been reserved at seven New Orleans hotels with all rooms being at the 2016 government per diem rate of $160.

Reservations will be made on a first-come, first-served basis. Attendees are encouraged to book their reservations at AMS-contracted hotels to help the Society avoid penalties for not filling its hotel block. This will help slow the rate of growth in registration fees. All guaranteed reservations are for the date of arrival only. Attendees who fail to notify the hotel that they are arriving on a different day will lose their room.

Ground Transportation

Airport Shuttle New Orleans is the official shuttle operator at the airport that serves downtown hotels. Shuttle service is available from the Louis Armstrong International Airport to the downtown hotels.

Once travelers depart their plane, they should follow the signs to the baggage claim area on the lower level. Exit the doors located across from Baggage Claim Area 10 onto the loading dock. Look for Airport Shuttle staff, who will help direct travelers to the next available vehicle. Upon arrival, proceed directly to the Airport Shuttle, present e-ticket to the driver, and board the van.

If purchasing ticket(s) at the airport, proceed to the baggage claim area on the ground level. After retrieving any luggage, proceed to one of the Airport Shuttle ticket desks, located across from Baggage Claim Areas 1, 5, 9, 11, and 12.

Service is available on a continuous basis with vans departing approximately every 30 minutes. The price for shared van service for one passenger, round trip, is $38; a one-way trip is $20.

Handicapped-accessible vehicles are available and reserving one in advance is recommended. If wheelchair-accessible service is needed upon arrival, please call the Airport Shuttle reservations department at 866-596-2699 for assistance.

For departure reservations, please call 504-522-3500 no later than 24 hours prior to flight departure time. An advance reservation will ensure a timely departure from the airport. Information on reservations can be found at the Airport Shuttle New Orleans Web site (http://www.airportshuttleneworleans.com/services-rates.html) or by calling 504-522-3500.

CONFERENCE HOTELS

- Hilton Riverside (Headquarters hotel; most AMS committee and side meetings will be held at the Hilton)
- Embassy Suites New Orleans Convention Center
- Marriott Downtown at the Convention Center
- Courtyard New Orleans Downtown Convention Center
- Residence Inn New Orleans Downtown
- Springhill Suites New Orleans Downtown
- Doubletree by Hilton New Orleans

Taxi

Effective 1 Septemer 2015, a cab ride costs $36.00 from the airport to the New Orleans Central Business District (CBD) for one or two persons and $15.00 (per passenger) for three or more passengers. Taxi fare to most hotels near the Convention Center is approximately $33. Pickup is on the lower level, outside the baggage claim area. There may be an additional charge for extra baggage. Taxis are required to offer fares a credit card payment option.

Local Ground Transportation

All hotels are within walking distance of the Convention Center. A shuttle will be available between the Convention Center, the Hilton New Orleans Riverside Hotel (0.7 miles from the Convention Center), and the Doubletree by Hilton New Orleans Hotel (1 mile from the Convention Center) for the convenience of meeting attendees.

CONFERENCE AT A GLANCE

SATURDAY, 9 JANUARY

* Short Course: A Beginner's Course: Using Python in Climate and Meteorology

15th Annual Student Conference

5:30–7:30 P.M.
AMS Career Fair (Student Conference Attendees only)

Green highlighted items are featured events.

Brown highlighted items are programs of general interest.

Blue highlighted items are social events.

Short Courses and workshops are highlighted in burgundy.

***A separate registration fee applies to all short courses and special conferences.**

Coffee Breaks

Monday	10:30–11:00 A.M., La Nouvelle Foyer
	2:30–4:00 P.M., Formal Poster Viewing
Tuesday	9:45–11:00 A.M., Formal Poster Viewing
	3:00–3:30 P.M., Exhibit Hall
Wednesday	10:00–10:30 A.M., Exhibit Hall
	2:30–4:00 P.M., Formal Poster Viewing
Thursday	9:45–11:00 A.M., Formal Poster Viewing
	3:00–3:30 P.M., Levels 2 and 3 Foyers

SUNDAY, 10 JANUARY

* Short Course: A Beginner's Course: Using Python in Climate and Meteorology
* Short Course: Coastal Surge and Inundation Modeling
* Short Course: Data Management Resource Center
* Short Course: Geostationary Operational Environmental Satellite (GOES)-R and Joint Polar Satellite System (JPSS) Meteorological Measurements and Instrumentation Coastal Surge and Inundation Modeling
* Short Course: GIS Tutorial for Atmospheric Sciences
* Short Course: Introduction to PyNIO and Related Python Tools for Geoscientific Data Analysis
* Short Course: Meteorological Measurements and Instrumentation
* Short Course: Soil Moisture Data Tutorial
* Short Course: Ultrascale Visualization Climate Data Analysis Tools

15th Annual Student Conference and Career Fair

Fourth Conference for Early Career Professionals

12:00–4:00 P.M.
15th Annual WeatherFest

3:00–4:00 P.M.
Newcomer's Welcome and Informational Exchange

4:00–5:30 P.M.
96th Annual Review, New Fellows, and Featured Awards

5:00–7:00 P.M.
AMS Career Fair

5:45–7:15 P.M.
Welcome Reception Honoring Newly Elected Fellows and Featured Award Winners

Student Conference Poster Session

7:00–9:00 P.M.
Annual Colour of Weather (CoWx) Networking Reception

7:30–9:30 P.M.
CoRioliS Reception

9:00–11:00 P.M.
AMS Early Career Professional Reception

MONDAY, 11 JANUARY

Book Signings

8:00 A.M.–4:30 P.M.
Poster Viewing

9:00–10:30 A.M.
16th Presidential Forum: Serving Society in Times of Crisis: Past, Present, and Future

9:00–11:00 A.M.
Spouses Coffee

10:30–11:00 A.M.
Coffee Break

12:45–1:05 P.M.
Daily Weather Briefing

1:30–2:30 P.M.
Walter Orr Roberts Lecture

2:30–4:00 P.M.
Formal Poster Viewing with Coffee Break

5:30–7:30 P.M.
Ribbon Cutting, Opening Reception, and Corporate Patron Recognition

7:15–10:00 P.M.
23|5 Talks: The 'Wow' of Weather, Water, and Climate with a screening of the feature-length documentary film, "Merchants of Doubt," based on the 2010 book by Naomi Oreskes and Erik M. Conway

TOWN HALL EVENTS

12:15–1:15 P.M.
"Outside the Box" Skillsets for Staying Relevant and Landing the Next Job

US Community Weather Research Planning

Closing the Gap: Research Strategies to Advance Skill and Value of Subseasonal to Seasonal Predictions of the Earth System

Total Water Prediction

Weather Ready Nations (WRNs)

7:00–8:00 P.M.
Weather, Climate, Water and the New Energy Economy—Integrating and Operationalizing Renewable Energy Forecasts

TUESDAY, 12 JANUARY

Book Signings

8:00 A.M.–6:00 P.M.
Poster Viewing

8:30 A.M.–5:30 P.M.
Mario Molina Symposium

9:30 A.M.–6:00 P.M.
Exhibits Open

9:00–11:00 A.M.
Spouses Coffee

9:45–11:00 A.M.
Formal Poster Viewing with Coffee Break

12:00–1:30 P.M.
Women in the Atmospheric Sciences Luncheon

1:30–2:30 P.M.
Bernhard Haurwitz Memorial Lecture

6:00–8:00 P.M.
Mario Molina Symposium Banquet

12:15–1:15 P.M.
AMS Publications Workshop—A Panel Discussion on Open Access, Ethics, and Other Hot Topics in Scientific Publishing

12:45–1:05 P.M.
Daily Weather Briefing

3:00–3:30 P.M.
Meet the President

Coffee Break in the Exhibit Hall

TOWN HALL EVENTS

12:15–1:15 P.M.
Presidential Town Hall Meeting: Historic Development of Meteorology during the Last 100 Years

NASA Earth Science Division

Contributions of Environmental Satellites to Societal Weather Readiness and Environmental Intelligence and Security

"What if the water can't be stopped?" Tribal Resilience in an Age of Sea Level Rise

NOAA Town Hall

6:00–8:00 P.M.
Spirituality and the Atmospheric Sciences: Ethics and Climate Change from the Perspective of Religion and Faith

WEDNESDAY, 13 JANUARY

Book Signings

8:00 A.M.–6:30 P.M.
Poster Viewing

8:30 A.M.–5:30 P.M.
Peter Lamb Symposium

9:30 A.M.–6:30 P.M.
Exhibits Open

9:00–11:00 A.M.
Spouses Coffee

10:00–10:30 A.M.
Meet the President

Coffee Break in the Exhibit Hall

12:00–1:30 P.M.
Peter Lamb Luncheon

12:45–1:05 P.M.
Daily Weather Briefing

1:30–2:30 P.M.
Robert E. Horton Lecture

2:30–4:00 P.M.
Formal Poster Viewing with Coffee Break

5:30–6:30 P.M.
Awards Banquet Reception

7:00 P.M.
96th AMS Awards Banquet

TOWN HALL EVENTS

12:15–1:15 P.M.
Presidential Town Hall on Demystifying Careers in the Atmospheric Sciences

The 2017–2027 National Academy of Sciences Decadal Survey for Earth Science and Applications from Space

NOAA's Research and Development Enterprise

NSF Division of Atmospheric and Geospace Sciences Strategies and Frontiers in Research: 2016–2020

Total Water, Part II

The Weather Value Chain of the Future: From Commercial Satellites to Crowdsourcing, and Everything In Between

THURSDAY, 14 JANUARY

Book Signings

8:00 A.M.–12:00 P.M.
Poster Viewing

8:30 A.M.–5:30 P.M.
Marvin Geller Symposium

9:30 A.M.–12:00 P.M.
Exhibits Open

9:45–11:00 A.M.
Formal Poster Viewing with Coffee Break

12:45–1:05 P.M.
Daily Weather Briefing

3:00–3:30 P.M.
Meet the President

Coffee Break, Levels 2 and 3 Foyers

6:00–8:00 P.M.
Marvin Geller Banquet

96TH ANNUAL MEETING MOBILE APP

Get the Most from Your 2016 AMS 96th Annual Meeting Experience!

Get the mobile app!

- **View the entire conference program by session, author, or abstract**
- **Create and save your schedule for the conference**
- **Check out a map of the exhibit hall and read exhibitor listings**
- **Locate yourself within the convention center**
- **Look up general info about the meeting**
- **Get updates and information directly from AMS**
- **Connect with AMS 2016 on social media**

Visit the AMS website in early December for instructions on how to download the mobile app.

Preregistration

Everyone attending the 96th AMS Annual Meeting must register and wear a badge. Early registration rates are valid through Tuesday, 1 December 2015. Registration forms faxed or mailed to AMS Headquarters will be accepted until 15 December 2015. Online registrations will be accepted throughout the conference. Preregistration forms must be accompanied by one of the following forms of payment: check (personal/business/traveler's), money order, purchase order, or credit card number (MasterCard/VISA/American Express). Foreign checks must be drawn on a U.S. bank and made payable in U.S. dollars. Confirmation of registration will be sent once the form is processed. Refunds (less a $25 processing fee) will be granted only for cancellations received before 22 December 2015.

Conference Registration

Registrants may choose the Full-Week Registration Package or the One-Day Registration Package. The full-week package includes admission to all conferences, exhibits, coffee breaks, general receptions, and one Annual Meeting Banquet ticket. The one-day package includes admission to all of the above for one calendar day, with the exception of the Annual Meeting Banquet.

Short Course Registration

All short course/workshop attendees must register and wear a badge/ribbon; registration rates are listed below. Short course/workshop registration is not included in the 96th Annual Meeting registration, and short course/workshop registration does not include registration for the 96th AMS Annual Meeting.

REGISTRATION DESK
EXHIBIT HALL D LOBBY

The AMS Registration Desk will be open for the Student Conference and this year's two-day Short Courses on Saturday, 9 January, 7:30–10:00 A.M., and for this year's one-day Short Courses on Sunday, 10 January, 7:30–9:00 A.M.

Annual Meeting registration will be held on Sunday, 10 January, 9:00 A.M.–6:00 P.M.; Monday–Wednesday, 11–13 January, 7:30 A.M.–6:00 P.M.; and Thursday, 14 January, 7:30 A.M.–3:00 P.M.

ABOUT YOUR BADGE

Attendees must carry their badges with them at all times while at the convention center. The badge includes a bar code that contains name and address information provided during registration. With an attendee's approval, exhibitors may scan the bar code to easily obtain the name, postal mail and e-mail addresses, and phone number information for follow-up after the meeting.

Everyone (including children) is required to have a badge for admittance into the Exhibit Hall.

Special Conference Registration

15th Annual AMS Student Conference and Career Fair Registration

An early registration fee of $40 has been set for this conference and registration must be completed online. Starting on 16 December 2015, late registration will be available for $60. On-site registration ($60) may be available as space permits. Attendees must register separately for the 96th AMS Annual Meeting. Please note that the Student Conference is intended for undergraduates and graduate students and that all registrants must be AMS Student Members. Please apply for student membership online (https://www2.ametsoc.org/ams/index.cfm/membership/).

Fourth AMS Conference for Early Career Professionals

Interested attendees are invited to join the Fourth AMS Conference for Early Career Professionals, hosted by the American Meteorological Society and organized by the AMS Board for Early Career Professionals. An early registration fee of $25 has been set for this conference and registration must be completed online. Early registration will be available online until 15 December 2015. Starting on 16 December 2015, late registration will be available for $40. On-site registration ($40) may be available as space permits.

19th Conference of Atmospheric Science Librarians International Registration

All attendees for the 19th Conference of Atmospheric Science Librarians International (ASLI) must register and wear a badge. This year, ASLI Conference attendees should register in advance through the AMS website (http://annual.ametsoc.org/2016/index.cfm/registration/special-conference-registration/) or by fax for $50 until 1 December 2015. Registrations received between 2 December 2015 and the conference dates will be $75. After 15 December 2015,

registration must be done at the meeting or online only. For those registering on site, registration will take place at the AMS Annual Meeting Registration Desk. Registration for the ASLI Conference does not include registration for other 96th AMS Annual Meeting events, but ASLI Conference registrants are encouraged to access the exhibits.

AMS's Teacher Workshop and Share-a-Thon

A registration fee of $25 has been set for the Teacher Workshop and Share-a-Thon. Registration is limited to 100 teachers and must be completed online or through the Teacher Workshop Paper Registration Form. There will be no on-site registration and attendees must register by Friday, 27 November 2015 (space permitting).

Those attending the Workshop will receive a free copy of the AMS Weather Book (valued at $35). This book contains more than 100 graphic illustrations, in full color and with exceptional detail, that serve to illuminate and explain a host of atmospheric phenomena, from the Northern Lights and lake-effect snow to the jet stream and ocean currents. This book will be distributed on-site and only to those who attend the workshop.

NOTE: Registration for the Teacher Workshop does not include registration for the 96th AMS Annual Meeting.

Press Registration

The AMS will operate a Press Room in the Convention Center, Monday–Thursday, 11–15 January 2016.

Press credentials are required for access to all conferences, special programs, and the exhibits. Eligibility for press registration is limited to the working press and freelance science writers with appropriate identification, as well as public information officers of scientific societies, educational institutions, and government agencies. A banquet ticket is not included with a press registration but may be purchased for $50.

All journalists and public information officers can register in advance by sending credentials to Rachel Thomas-Medwid (tel: 617-226-3955; e-mail: rthomas@ametsoc.org) or by registering on site in the Press Room.

Statement on Open Meetings

Throughout the week, AMS Committees, Boards, and the Council will be meeting at various times and locations. These meetings are, in principle, open to all members of the Society, although portions of some meetings may be held in executive session when dealing with personnel issues, awards, or other matters of a confidential nature.

As a matter of courtesy and to ensure adequately sized meeting rooms, members wishing to observe a particular Committee, Board, or Council Meeting should contact its chairperson in advance. Members may request a place on the agenda by following a similar procedure. Please feel free to contact Joyce Annese (tel: 617-226-3902; e-mail: jannese@ametsoc.org) at AMS Headquarters for assistance.

Professional and Respectful Conduct at AMS Meetings

AMS is committed to safe and productive meetings for all attendees. Harassment, intimidation, or discrimination of any kind will not be tolerated at any meeting or event associated with the meeting. All communication should be appropriate for a professional audience including people of many different backgrounds. Those who violate the standards of professional and respectful conduct may be asked to leave the meeting immediately and without refund, may not be consid-

AMS MEETS, TWEETS, AND BLOGS!

With more than 2500 presentations to be given at the 2016 AMS Annual Meeting in New Orleans, the best way to stay up to date with all that is going on is by following all of the AMS social media channels.

Every day during the Annual Meeting, AMS publishes news, interviews, commentaries, updates, photos, and videos across multiple online channels.

The Front Page blog (www.blog.ametsoc.org) extends the reach of attendees and exhibitors beyond the conference center walls to fellow members back home and to the general public. In addition to news and commentary during the week in New Orleans, the blog features special sessions, news about presenters, tips for attendees, and explores the links between AMS science, the meeting agenda, and the world in the months leading up to the meeting.

In addition to The Front Page, follow the breaking stories and ongoing conversations at the Annual Meeting in real time on Facebook and Twitter. To stay up to date, be sure to "like" AMS on Facebook (www.facebook.com/ametsoc) and follow @ametsoc on Twitter. The Twitter hashtag for the Annual Meeting is #AMS2016.

Follow us

CONFERENCE REGISTRATION RATES

	FULL WEEK PACKAGE			ONE-DAY PACKAGE		
Attendee type	Early registration through 1 Dec.	Registration 2 Dec. through 2 Jan.	Late registration onsite	Early registration through 2 Dec.	Registration 3 Dec. through 31 Jan.	Late registration onsite
AMS Full Member; Program/Session Chair	$510	$550	$570	$280	$320	$340
AMS Associate Member; Nonmember Speaker; Nonmember Poster Presenter; Exhibitor Attendee, Cosponsoring Member*	$555	$595	$615	$280	$320	$340
Nonmember	$605	$645	$665	$280	$320	$340
Retired Member	$190	$230	$250	$90	$130	$150
AMS Student Member	$165	$205	$225	$60	$100	$120
Student Nonmember	$195	$235	$255	$90	$130	$150

An additional Annual Meeting banquet ticket may be purchased for $50. Child Annual Meeting Banquet tickets may be purchased by contacting Gillian Peguero (gpeguero@ametsoc.org).

*The following societies are cosponsoring the AMS 96th Annual Meeting: American Academy of Environmental Engineers and Scientists (AAEES), American Geosciences Institute (AGI), American Geophysical Union (AGU), American Society of Agronomy (ASA); American Water Resources Association (AWRA), Atmospheric Science Librarians International (ASLI), Australian Meteorological and Oceanographic Society (AMOS), Canadian Meteorological and Oceanographic Society (CMOS), Crop Science Society of America (CSSA), Indian Meteorological Society (IMS), National Weather Association (NWA), Soil Science Society of America (SSSA), The Oceanography Society (TOS), and World Meteorological Organization (WMO)

On site, attendees who are not AMS members may complete an application for membership and apply the $95 difference for registration to the membership fee for the calendar year 2016. Please stop by the AMS Membership Desk, which is part of the AMS Registration Desk, for assistance in completing the membership application process.

ered for service on AMS Boards and Committees, and may be subject to additional legal action.

Harassment, intimidation, or discrimination includes offensive verbal comments related to gender, sexual orientation, disability, physical appearance, body size, race, religion; sexual images in public spaces; deliberate intimidation, stalking, or following; harassing photography or recording; sustained disruption of talks or other events; inappropriate physical contact; and unwelcome sexual attention.

This statement is meant to cover all meeting-associated events, including those sponsored by organizations other than AMS but held in relation to AMS events. This includes the scientific program and exhibitions, as well as receptions, town hall meetings, and other informal or formal gatherings associated with AMS.

Any attendee who believes he or she may have witnessed or have been subjected to conduct that violates professional and respectful behavior should contact a senior member of the AMS staff. This may be done by talking with any AMS staff (identified with a staff badge) or by sending an e-mail to reportconcern@ametsoc.org or leaving a message at 617-226-3965 with the appropriate contact information. A senior AMS staff member will be in contact in a timely manner. (In the unlikely event a reply is not received within 12 hours of sending an e-mail or leaving a voice-mail message, follow-up with an AMS staff member at the meeting is advised to ensure that the original message has been received.) Anyone witnessing or experiencing behavior that constitutes an immediate and serious threat is advised to call 911 or the local police first.

The AMS takes any breach of professional conduct at an AMS meeting or related function very seriously. Attendees are encouraged to report any unprofessional conduct in the knowledge that AMS staff members will do their best to maintain the confidentiality of all parties to the extent possible

SHORT COURSE REGISTRATION RATES

	By 1 Dec				After 1 Dec			
	AMS Member	Non-Member	Student Member	Student Non-Member	AMS Member	Non-Member	Student Member	Student Non-Member
A Beginner's Course to Using Python in Climate and Meteorology [two-day (Sat–Sun) course]	$375	$415	$265	$295	$415	$455	$205	$335
Coastal Surge and Inundation Modeling [one-day (Sun) course]	$285	$320	$215	$245	$325	$365	$255	$285
Data Management Resource Center [one-day (Sun) course]	$165	$205	$95	$125	$205	$245	$135	$165
GIS Tutorial for Atmospheric Sciences [one-day (Sun) course]	$245	$285	$175	$205	$285	$325	$215	$245
Geostationary Operational Environmental Satellite-R (GOES-R) and Joint Polar Satellite System (JPSS) [one-day (Sun) course]	$50	$50	$50	$50	$50	$50	$50	$50
Introduction to PyNIO and Related Python Tools for Geoscientific Data Analysis [one-day (Sun) course]	$245	$285	$175	$205	$285	$325	$215	$245
Meteorological Measurements and Instrumentation [one-day (Sun) course]	$250	$290	$180	$210	$290	$330	$220	$250
Soil Moisture Data Tutorial [one-day (Sun) course]	$195	$235	$125	$155	$235	$275	$165	$195

AMS MOBILE APP

Want to get the most from your 2016 AMS 96th Annual Meeting experience? Download the mobile app!

With the AMS mobile app attendees can see and do more:

- View the entire conference program by session, author, or abstract
- Create and save schedules for the conference
- Check out a map of the exhibit hall and read exhibitor listings
- Locate yourself within the convention center
- Look up general info about the meeting
- Get updates and information directly from AMS
- Connect with AMS 2016 on social media (#AMS2016)

Visit the AMS website in early December for instructions on how to download the mobile app.

while taking appropriate actions. In situations for which additional action is warranted, the AMS will cooperate fully with the appropriate authorities.

Americans with Disabilities Act

It is the Society's sincere desire to comply fully with both the letter and the spirit of the Americans with Disabilities Act (ADA) of 1990. For questions about accessibility such as real-time captioning (communication access real-time translation; CART), special printing needs, reserved seating, or wheelchair-accessible service for the hotel shuttles, please contact Christine Keane (ckeane@ametsoc.org). Two-week advance notice is necessary to ensure seamless action.

If issues arise on site in New Orleans, please visit the AMS Registration Desk, in the Lobby of Exhibit Hall D, or contact the AMS staff at 504-670-4100 during the following hours: Sunday, 10 January, 12:00–5:30 p.m.; Monday, 11 January, 7:30 a.m.–6:00 p.m.; Tuesday, 12 January, 7:30 a.m.–6:00 p.m.; Wednesday, 13 January, 7:30 a.m.–6:30 p.m.; and Thursday, 14 January, 7:30 a.m.–3:00 p.m.

Special housing needs should also be requested when hotel reservations are made. AMS wants to ensure that each attendee's stay at the 96th Annual Meeting is a pleasant and productive one.

AMS ANNUAL MEETING PROGRAM STAFF

AMS Main number: 617-227-2426

Meetings and Exhibit staff:

Claudia Gorski (ext. 3967)
Marjorie Maloney (ext. 3968)
Jennifer Ives (ext. 3974)
Christine Keane (ext. 3969)
Gillian Peguero (ext. 3971)
Sotiria Qirjazi (ext. 3970)
Jennifer Rosen (ext. 3972)
Ricky Sidla (ext. 3981)
Brenda Ward (ext. 3973)

Publications staff:

Bryan Hanssen (ext. 3951)

LOCAL ATTRACTIONS

New Orleans offers much to see and do beyond the Annual Meeting. Attendees are advised to check out the New Orleans Convention and Visitor's Bureau website (http://www.neworleanscvb.com/ams/) for information on attractions, restaurants, tours, and more!

Photo by Cheryl Gerber

Accessibility at the Ernest N. Morial Convention Center

The New Orleans Ernest N. Morial Convention Center is ADA compliant. The New Orleans Ernest N. Morial Convention Center provides service ramps to entrances and elevated areas, an array of passenger elevators, restroom facilities for the disabled, brailed instructions/directions at strategic locations throughout the building, and pay phones located at each level of the facility with (TDD) hearing-impaired functions. Wheelchairs also are available upon request.

For more information on Mobility Scooter rentals is available from the following website: http://www.neworleansonline.com/tools/transportation/gettingaround/handicap-transportation.html.

Accessibility at the Conference

Attendees with a current functional limitation are encouraged to contact the AMS staff (accessibility@ametsoc.org) with questions about accessibility or to request accommodations to fully participate in this conference. Four weeks advance notice is necessary to ensure seamless action.

CALENDAR OF MEETINGS

The Call for Papers and Calendar sections list conferences, symposia, and workshops that are of potential interest to AMS members. **Complete information about events listed in the calendar can be found on the meetings page of the AMS website, www.ametsoc.org. New additions to the calendar are highlighted.**

To list an event in the calendar, please submit the event name, dates, location, and deadlines for abstracts, manuscripts, and preregistration to amsmtgs@ametsoc.org. For a submission to appear in a given issue, it must be submitted at least eight weeks prior to the month of publication (that is, to appear in the March *Bulletin,* the submission must be received by 1 January).

AMS MEETINGS

2016

JANUARY

AMS Short Course: A Beginner's Course to Using Python in Climate and Meteorology, 9–10 January, New Orleans, Louisiana
Preregistration deadline: 15 December 2015
Initial announcement published: Oct. 2015

AMS Short Course on Meteorological Measurements and Instrumentation, 10 January, New Orleans, Louisiana
Preregistration deadline: 15 December 2015
Initial announcement published: Oct. 2015

AMS Short Course: Introduction to PyNIO and Related Python Tools for Geoscientific Data Analysis, 10 January, New Orleans, Louisiana
Preregistration deadline: 15 December 2015
Initial announcement published: Oct. 2015

AMS Short Course on the Geostationary Operational Environmental Satellite (GOES)-R and Joint Polar Satellite System (JPSS), 10 January, New Orleans, Louisiana
Preregistration deadline: 15 December 2015
Initial Announcement Published: Oct. 2015

AMS Short Course on GIS Tutorial for Atmospheric Sciences, 10 January, New Orleans, Louisiana
Preregistration deadline: 15 December 2015
Initial announcement published: Oct. 2015

AMS Short Course on the Data Management Resource Center, 10 January, New Orleans, Louisiana
Preregistration deadline: 15 December 2015
Initial announcement published: Oct. 2015

AMS Short Course on Coastal Surge and Inundation Modeling, 10 January, New Orleans, Louisiana
Preregistration deadline: 15 December 2015
Initial announcement published: Oct. 2015

15th Annual AMS Student Conference, 9–10 January, New Orleans, Louisiana
Abstract deadline: 1 October 2015
Preregistration deadline: 15 December 2015
Initial announcement published: Feb. 2015

Fourth Annual AMS Conference for Early Career Professionals, 10 January, New Orleans, Louisiana
Preregistration deadline: 15 December 2015
Initial announcement published: May 2015

***16th Presidential Forum: Serving Society in Times of Crisis: Past, Present, and Future, 10–14 January, New Orleans, Louisiana**
Preregistration deadline: 1 December 2015
Initial announcement published: TBD

***Marvin Geller Symposium: A Celebration of His Diverse Contributions to the Atmospheric Sciences, 10–14 January, New Orleans, Louisiana**
Abstract deadline: 3 August 2015
Preregistration deadline: 1 December 2015
Manuscript deadline: 12 February 2016
Initial announcement published: April 2015

***Peter Lamb Symposium, 10–14 January, New Orleans, Louisiana**
Abstract deadline: 3 August 2015
Preregistration deadline: 1 December 2015
Manuscript deadline: 12 February 2016
Initial announcement published: March 2015

***Mario Molina Symposium, 10–14 January, New Orleans, Louisiana**
Abstract deadline: 3 August 2015
Preregistration deadline: 1 December 2015
Manuscript deadline: 12 February 2016
Initial announcement published: March 2015

***32nd Conference on Environmental Information Processing Technologies, 10–14 January, New Orleans, Louisiana**
Abstract deadline: 3 August 2015
Preregistration deadline: 1 December 2015
Manuscript deadline: 12 February 2016
Initial announcement published: Feb. 2015

***30th Conference on Hydrology, 10–14 January, New Orleans, Louisiana**
Abstract deadline: 3 August 2015
Preregistration deadline: 1 December 2015
Manuscript deadline: 12 February 2016
Initial announcement published: Feb. 2015

***28th Conference on Climate Variability and Change, 10–14 January, New Orleans, Louisiana**
Abstract deadline: 3 August 2015
Preregistration deadline: 1 December 2015
Manuscript deadline: 12 February 2016
Initial announcement published: Feb. 2015

*An exhibit program will be held at this meeting.

***25th Symposium on Education, 10–14 January, New Orleans, Louisiana**
Abstract deadline: 3 August 2015
Preregistration deadline: 1 December 2015
Manuscript deadline: 12 February 2016
Initial announcement published: March 2015

23rd Conference Probability and Statistics in the Atmospheric Sciences, 10–14 January, New Orleans, Louisiana
Abstract deadline: 3 August 2015
Preregistration deadline: 1 December 2015
Manuscript deadline: 12 February 2016
Initial announcement published: April 2015

***22nd Conference on Applied Climatology, 10–14 January, New Orleans, Louisiana**
Abstract deadline: 3 August 2015
Preregistration Deadline: 1 December 2015
Manuscript Deadline: 12 February 2016
Initial announcement published: March 2015

***20th Conference on Integrated Observing and Assimilation Systems for Atmosphere, Oceans, and Land Surface (IOAS-AOLS), 10–14 January, New Orleans, Louisiana**
Abstract deadline: 3 August 2015
Preregistration deadline: 1 December 2015
Manuscript deadline: 12 February 2016
Initial announcement published: Feb. 2015

19th Joint Conference on the Applications of Air Pollution Meteorology with the A&WMA, 10–14 January, New Orleans, Louisiana
Abstract deadline: 3 August 2015
Preregistration deadline: 1 December 2015
Manuscript deadline: 12 February 2016
Initial announcement published: April 2015

***19th Conference of Atmospheric Science Librarians International, 10–14 January, New Orleans, Louisiana**
Abstract deadline: 3 August 2015
Preregistration deadline: 1 December 2015
Initial announcement published: March 2015

***18th Conference on Conference on Atmospheric Chemistry, 10–14 January, New Orleans, Louisiana**
Abstract deadline: 3 August 2015
Preregistration deadline: 1 December 2015
Manuscript deadline: 12 February 2016
Initial announcement published: March 2015

***18th Symposium on Meteorological Observations and Instrumentation, 10–14 January, New Orleans, Louisiana**
Abstract deadline: 3 August 2015
Preregistration deadline: 1 December 2015
Manuscript deadline: 12 February 2016
Initial announcement published: Feb. 2015

***14th Conference on Artificial and Computational Intelligence and its Applications to the Environmental Sciences, 10–14 January, New Orleans, Louisiana**
Abstract deadline: 3 August 2015
Preregistration deadline: 1 December 2015
Manuscript deadline: 12 February 2016
Initial announcement published: Feb. 2015

***14th History Symposium, 10–14 January, New Orleans, Louisiana**
Abstract deadline: 3 August 2015
Preregistration deadline: 1 December 2015
Manuscript deadline: 12 February 2016
Initial announcement published: April 2015

***14th Symposium on the Coastal Environment, 10–14 January, New Orleans, Louisiana**
Abstract deadline: 3 August 2015
Preregistration deadline: 1 December 2015
Manuscript deadline: 12 February 2016
Initial announcement published: Feb. 2015

***13th Conference on Space Weather, 10–14 January, New Orleans, Louisiana**
Abstract deadline: 3 August 2015
Preregistration deadline: 1 December 2015
Manuscript deadline: 12 February 2016
Initial announcement published: Feb. 2015

***12th Annual Symposium on New Generation Operational Environmental Satellite Systems, 10–14 January, New Orleans, Louisiana**
Abstract deadline: 3 August 2015
Preregistration deadline: 1 December 2015
Manuscript deadline: 12 February 2016
Initial announcement published: Feb. 2015

***12IMPACTS: Major Weather Events and Societal Impacts of 2015, 12 January, New Orleans, Louisiana**
Abstract deadline: 3 August 2015
Preregistration deadline: 1 December 2015
Manuscript deadline: 12 February 2016
Initial announcement published: March 2015

***11th Symposium on Societal Applications: Policy, Research and Practice, 10–14 January, New Orleans, Louisiana**
Abstract deadline: 3 August 2015
Preregistration deadline: 1 December 2015
Manuscript deadline: 12 February 2016
Initial announcement published: Feb. 2015

***Ninth Annual CCM Forum, 10–14 January, New Orleans, Louisiana**
Abstract deadline: 3 August 2015
Preregistration deadline: 1 December 2015
Manuscript deadline: 12 February 2016
Initial announcement published: April 2015

***Eighth Symposium on Aerosol–Cloud–Climate Interactions, 10–14 January, New Orleans, Louisiana**
Abstract deadline: 3 August 2015
Preregistration deadline: 1 December 2015
Manuscript deadline: 12 February 2016
Initial announcement published: March 2015

***Seventh Conference on Environment and Health, 10–14 January, New Orleans, Louisiana**
Abstract deadline: 3 August 2015
Preregistration deadline: 1 December 2015
Manuscript deadline: 12 February 2016
Initial announcement published: Feb. 2015

* An exhibit program will be held at this meeting.

***Seventh Conference on Weather, Climate, and the New Energy Economy, 10–14 January, New Orleans, Louisiana**
Abstract deadline: 3 August 2015
Preregistration deadline: 1 December 2015
Manuscript deadline: 12 February 2016
Initial announcement published: March 2015

***Sixth Conference on Transition of Research to Operations, 10–14 January, New Orleans, Louisiana**
Abstract deadline: 3 August 2015
Preregistration deadline: 1 December 2015
Manuscript deadline: 12 February 2016
Initial announcement published: Feb. 2015

***Sixth Symposium on Advances in Modeling and Analysis Using Python, 10–14 January, New Orleans, Louisiana**
Abstract deadline: 3 August 2015
Preregistration deadline: 1 December 2015
Manuscript deadline: 12 February 2016
Initial announcement published: Feb. 2015

***Fifth Aviation, Range and Aerospace Meteorology Special Symposium, 13 January, New Orleans, Louisiana**
Abstract deadline: 3 August 2015
Preregistration deadline: 1 December 2015
Manuscript deadline: 12 February 2016
Initial announcement published: Feb. 2015

***Fourth Annual Symposium on the Weather, Water, and Climate Enterprise, 10–14 January, New Orleans, Louisiana**
Abstract deadline: 3 August 2015
Preregistration deadline: 1 December 2015
Manuscript deadline: 12 February 2016
Initial announcement published: Feb. 2015

***Fourth Symposium on Building a Weather-Ready Nation: Enhancing Our Nation's Readiness, Responsiveness, and Resilience to High Impact Weather Events, 10–14 January, New Orleans, Louisiana**
Abstract deadline: 3 August 2015
Preregistration deadline: 1 December 2015
Manuscript deadline: 12 February 2016
Initial announcement published: Feb. 2015

***Fourth Symposium on Prediction of the Madden–Julian Oscillation: Processes, Prediction, and Impact, 10–14 January, New Orleans, Louisiana**
Abstract deadline: 3 August 2015
Preregistration deadline: 1 December 2015
Manuscript deadline: 12 February 2016
Initial announcement published: TBD

***Special Symposium on Hurricane Katrina: Progress in Leveraging Science, Enhancing Response and Improving Resilience, 12 January, New Orleans, Louisiana**
Abstract deadline: 3 August 2015
Preregistration deadline: 1 December 2015
Manuscript deadline: 12 February 2016
Initial announcement published: March 2015

***Special Symposium on Seamless Weather and Climate Prediction—Expectations and Limits of Multi-Scale Predictability, 14 January, New Orleans, Louisiana**
Abstract deadline: 3 August 2015
Preregistration deadline: 1 December 2015
Manuscript Deadline: 12 February 2016
Initial announcement published: March 2015

Special Sessions on U.S.–International Partnerships, 10–14 January, New Orleans, Louisiana
Abstract deadline: 3 August 2015
Preregistration deadline: 1 December 2015
Manuscript deadline: 12 February 2016
Initial announcement published: May 2015

* An exhibit program will be held at this meeting.

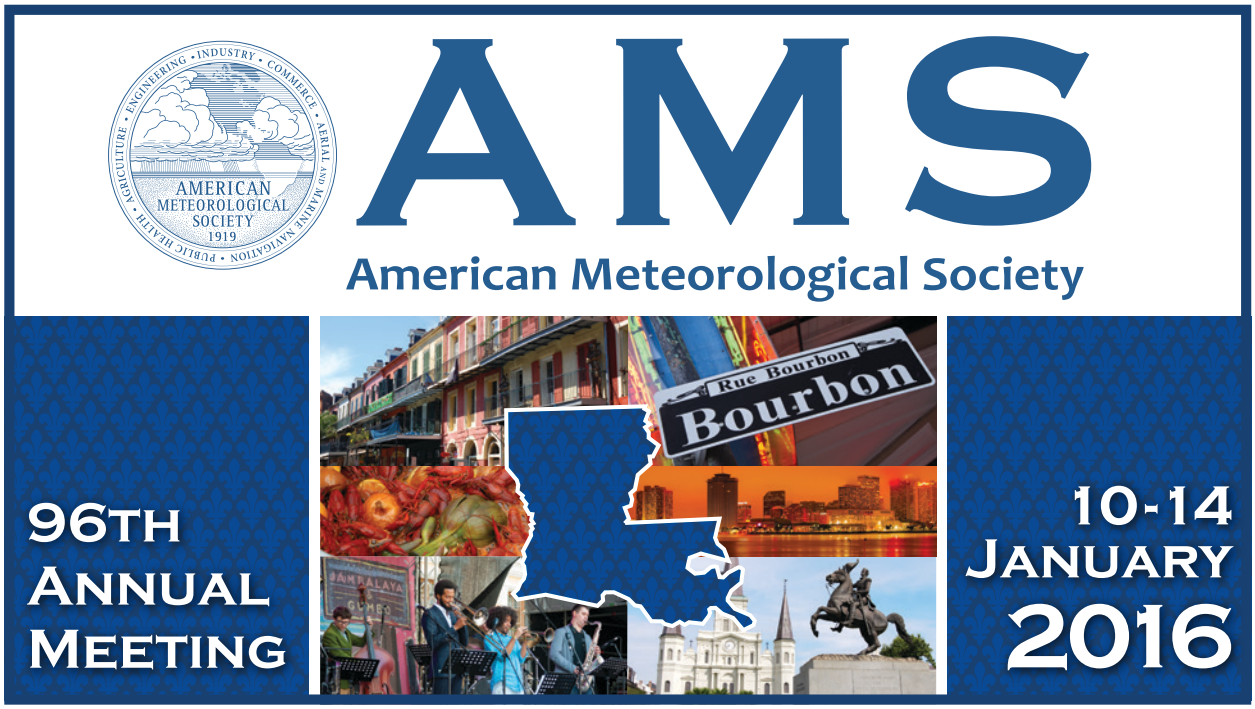

APRIL

32nd Conference on Hurricanes and Tropical Meteorology, 17–22 April, San Juan, Puerto Rico
Abstract deadline: 20 November 2015
Preregistration deadline: 13 March 2016
Manuscript deadline: 17 May 2016
Initial announcement published: Sept. 2015

JUNE

44th Conference on Broadcast Meteorology, 15–17 June, Austin, Texas
Abstract deadline: 3 February 2016
Preregistration deadline: 4 May 2016
Initial announcement published: Sept. 2015

The 32nd Conference on Agricultural and Forest Meteorology, 20–24 June, Salt Lake City, Utah
Abstract deadline: 8 February 2016
Preregistration deadline: 9 May 2016
Manuscript deadline: 22 July 2016
Initial announcement published: Oct. 2015

22nd Symposium on Boundary Layers and Turbulence, 20–24 June, Salt Lake City, Utah
Abstract deadline: 8 February 2016
Preregistration deadline: 9 May 2016
Manuscript deadline: 22 July 2016
Initial announcement published: Oct. 2015

Third Conference on Atmospheric Biogeosciences, 20–24 June, Salt Lake City, Utah
Abstract deadline: 8 February 2016
Preregistration deadline: 9 May 2016
Manuscript deadline: 22 July 2016
Initial announcementpublished: Nov. 2015

17th Conference on Mountain Meteorology, 27 June–1 July, Burlington, Vermont
Abstract deadline: 29 February 2016
Preregistration deadline: 31 May 2016
Manuscript Deadline: 1 August 2016
Initial announcement published: July 2015

AUGUST

Joint 21st American Meteorological Society (AMS) Satellite Meteorology, Oceanography and Climatology Conference and 20th AMS Conference on Air–Sea Interaction, 15–19 August, Madison, Wisconsin
Abstract deadline: 1 April 2016
Preregistration deadline: 1 July 2016
Manuscript deadline: 19 September 2016
Initial announcement published: June 2015

MEETINGS OF INTEREST

2015

OCTOBER

Women in STEM Idea Exchange Summit, 22 October, Waltham, Massachusetts

NOAA's 40th Climate Diagnostics and Prediction Workshop, 26–29 October, Denver, Colorado

NOVEMBER

16th Northeast Regional Operational Workshop (NROW), 4–5 November, Albany, New York

International Workshop for the Implementation of Biometeorological and Bioclimatic Forecasts in Latin America and the Caribbean, 25–28 November, Havana, Cuba

DECEMBER

VIII Cuban Congress of Meteorology the XVI Latin American and Iberian Congress of Societies of Meteorology Seminar-Workshop of Atmospheric Pollution, 1–4 December, Havana City, Cuba

2016

FEBRUARY

AMOS/ARCCCC National Conference 2016, 8–11 February, Melbourne, Australia

APRIL

A&WMA Guideline on Air Quality Models: The New Path, 12–14 April, Chapel Hill, North Carolina

International Radiation Symposium 2016, 17–22 April, Auckland, New Zealand

JULY

17th International Conference on Clouds and Precipitation, 25–29 July, Manchester, Wales, United Kingdom

Radar and Atmospheric Science: A Collection of Essays in Honor of David Atlas

Edited by Roger M. Wakimoto and Ramesh Srivastava

This monograph pays tribute to one of the leading scientists in meteorology, Dr. David Atlas. In addition to profiling the life and work of the acknowledged "Father of Radar Meteorology," this collection highlights many of the unique contributions he made to the understanding of the forcing and organization of convective systems, observation and modeling of atmospheric turbulence and waves, and cloud microphysical properties, among many other topics. It is hoped that this text will inspire the next generation of radar meteorologists, provide an excellent resource for scientists and educators, and serve as a historical record of the gathering of scholarly contributions honoring one of the most important meteorologists of our time.

Radar and Atmospheric Science: A Collection of Essays in Honor of David Atlas

Aug 2003. Meteorological Monograph Series, Vol. 30, No. 52; 270 pp, hardbound; ISBN 1-878220-57-8; AMS code MM52.

Price $75.00 list/$55.00 member

To place an order point your Web browser to www.ametsoc.org/amsbookstore

AMS BOOKS

RESEARCH ◆ APPLICATIONS ◆ HISTORY

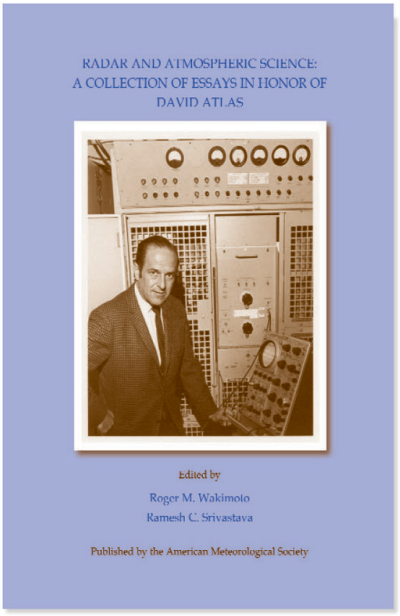

CALL FOR PAPERS

CALL FOR PAPERS

Third Conference on Atmospheric Biogeosciences, 20–24 June 2016, Salt Lake City, Utah

The 3rd Conference on Atmospheric Biogeosciences, sponsored by the American Meteorological Society, will be held 20–24 June 2016 at the Sheraton Downtown Salt Lake City hotel, Salt Lake City, Utah. This conference is organized by the AMS Board on Atmospheric Biogeosciences in collaboration with the Committee on Agricultural and Forest Meteorology, and will be jointly held with the 32nd Conference on Agricultural and Forest Meteorology and the 22nd Symposium on Boundary Layer and Turbulence, including a joint session honoring Bill Massman's contribution to the biometeorology and atmospheric biogeosciences. Preliminary programs, registration, hotel, and general information will be posted on the AMS website by late January 2016.

The conference's theme, in coordination with the Agricultural and Forest Meteorology Conference, is the "Biosphere–atmosphere interactions of natural, agricultural, and urban landscapes in the context of past, current, and future climates." Sample topics for abstracts include biogeochemical–atmosphere processes as affected by climate; biotic influences on atmospheric biogeochemistry (microbial; domesticated animals and plant agroecosystems, urban); trace gas exchanges; atmospheric–biogeochemical cycles in high latitudes; biogenic VOC and organic aerosols; primary biological particles/bioaerosols; aerobiology of spores, pollen, and microbes; palynological studies associated with paleoclimatic simulations; linkages between hydrological cycles and biogeochemical cycles; coupled nitrogen, carbon, and other nutrient studies; emissions and uptake/deposition of trace gases and aerosols; stable isotopic applications to understanding hydrological, biogeochemical, and atmospheric linkages; remote sensing of atmospheric–biosphere processes; and the theory and modelling of coupled biogeochemical, biophysical, ecological, and atmospheric processes.

Please submit your abstract electronically via the web by the deadline date of *8 February 2016* (refer to the AMS web page at http://ams.confex.com/ams/). An abstract fee of $95 (payable by credit card or purchase order) is charged at the time of submission (refundable only if abstract is not accepted). The abstract fee includes the submission of your abstract, the posting of your extended abstract, and the uploading and recording of your presentation that will be archived on the AMS website. We will no longer be producing a CD-ROM, allowing us to extend the deadline for extended abstracts.

Additionally, the Board on Atmospheric Biogeosciences will conduct a student oral and poster competition. Students must be the first author on submissions and be presenting their own, original work.

Authors of accepted presentations will be notified via e-mail by mid-March 2016. All extended abstracts are to be submitted electronically and will be available online via the web. Instructions for formatting extended abstracts will be posted on the AMS website. Manuscripts (up to 10 MB) must be submitted electronically by *22 July 2016*. All abstracts, extended abstracts, and presentations will be available on the AMS website at no cost.

For additional information please contact the Atmospheric Biogeosciences program chairpersons: Richard Grant (e-mail: rgrant@purdue.edu) and Kyaw Tha Paw U (e-mail: ktpawu@ucdavis.edu) or related to the Conference on Agricultural and Forest Meteorology, Heping Liu (e-mail: heping.liu@wsu.edu), Chuixiang Yi (e-mail: chuixiang.yi@qc.cuny.edu), and Brian Viner (e-mail: Brian.Viner@srnl.doe.gov). (11/15)

AMS Short Course on Utilization of Soil Moisture Data from the SMAP mission, 10 January 2016, New Orleans, Louisiana

The AMS Short Course on Utilization of Soil Moisture Data from the SMAP mission, will be held 1:30–5:30 p.m. on 10 January 2016 preceding the 96th AMS Annual Meeting in New Orleans, Louisiana. Preliminary programs, registration, hotel, and general information can be found on the AMS website (www.ametsoc.org).

Soil moisture data are critical for improving applications in weather, climate, drought, flood, fire, human health, and national security. NASA's Soil Moisture Active Passive (SMAP) mission was launched in 2015 and is now providing soil moisture and freeze/thaw measurements from space.

The SMAP Applications Program is working with users to familiarize them with the recently released SMAP data products and to accelerate the use of these data and their impact on applications. The SMAP Project actively supports applied research to leverage fundamental knowledge of how SMAP data products can be scaled and integrated into users' policy, business and management activities to improve decision-making efforts.

The goal of this course is to familiarize the user community with SMAP soil moisture data products—data access, file contents, processing, and usage—and provide an introduction to applications including numerical weather prediction, agricultural forecasts, and extreme events. There will also be a hands-on portion of the

course using SMAP data products. The course will facilitate continuity of satellite soil moisture data utilization from earlier missions (AMSR, SMOS) for regional and global soil moisture research and operational applications. The course will demonstrate data access, data browsing, and use-cases of beta data products publicly available from the SMAP mission. The course is aimed at researchers, modelers, students, and practitioners from the weather and other applications communities. The course is open to all. Existing agencies and organizations involved with SMAP applications include DoD, AFWA, USDA, USGS, ECMWF, NOAA, NIC, and the NRL.

This half-day course will be held on Sunday, 10 January 2016 and will address the following:

- Accessing and opening SMAP data product files via the public-access Data Centers
- Understanding and interpreting product file contents, projections, variables, flags, etc.
- Methods for browsing and data search
- Understanding and usage of data assimilation products based on SMAP measurements and models
- Limitations and caveats in the use of SMAP data; status of product calibration and validation
- Usage of SMAP data in prototype applications

There will be opportunities for interactions between SMAP team scientists and the user community on protocols for assimilating satellite data into operational systems and ways forward for streamlining SMAP data into research to operations.

The course format consists of two hours of lectures and demonstration followed by two hours of hands-on laboratory session with exercises that can be completed any time during the conference.

The instructors for the course are Dara Entekhabi [Science Team Leader of the NASA Soil Moisture Active Passive (SMAP) mission], Simon Yueh, JPL (SMAP Project Scientist), and Eni Njoku (SMAP Soil Moisture Product Team). They will be joined by Narendra Das and Steven Chan from NASA's Jet Propulsion Laboratory and Vanessa Escobar from NASA Goddard Space Flight Center.

The tutorial will begin at 1:30 p.m. and conclude at 5:30 p.m. Internet will be provided for this course. Attendees must bring their own laptops.

For more information please contact Vanessa Escobar at NASA Goddard Space Flight Center, Code 618, 8800 Greenbelt Road, Greenbelt, MD 20771 (tel: 301-614-6654; e-mail: vanessa.escobar@nasa.gov).

NOMINATION SUBMISSIONS

The Council of the American Meteorological Society invites members of the AMS to submit nominations for the Society Awards, Lecturers, Named Symposia, Fellows, Honorary members, and nominees for elective Officers and Councilors of the Society.

Information regarding awards, including award descriptions, listings of previous recipients, and the process for submitting nominations are on the AMS website www.ametsoc.org/awards.

Note: Deadlines differ and some nominations must be submitted on a specific form vs. electronic submission which is available on the AMS website or by request from Headquarters.

2016 AWARDS COMMITTEES

Each committee or commission listed below has the responsibility to select and submit to the Council the names of individuals nominated for the Society's awards listed. The name(s) of individual(s) nominated, a two-page cv, a bibliography of no more than three pages, and three supporting letters should be electronically submitted before **1 May 2016** for the awards that follow, unless stated otherwise. The nominees for awards remain on the committee's active list for three years.

ATMOSPHERIC RESEARCH AWARDS COMMITTEE

The Carl-Gustaf Rossby Research Medal
The Jule G. Charney Award
The Verner E. Suomi Award*
The Remote Sensing Prize (biennial)
The Clarence Leroy Meisinger Award
The Henry G. Houghton Award

OCEANOGRAPHIC RESEARCH AWARDS COMMITTEE

The Sverdrup Gold Medal
The Henry Stommel Research Award
The Verner E. Suomi Award*
The Nicholas P. Fofonoff Award

HYDROLOGIC RESEARCH AWARDS COMMITTEE

Hydrologic Sciences Medal

AWARDS OVERSIGHT COMMITTEE

The Charles Franklin Brooks Award for Outstanding Services to the Society
The Cleveland Abbe Award for Distinguished Service to the Atmospheric Sciences by an Individual
The Joanne Simpson Mentorship Award
The Award for Outstanding Services to Meteorology by a Corporation
Special Awards

EDUCATION AND HUMAN RESOURCES COMMISSION

The Louis J. Battan Author's Award (Adult and K–12)
The Charles E. Anderson Award
The Teaching Excellence Award
Distinguished Science Journalism in the Atmospheric and Related Sciences

PROFESSIONAL AFFAIRS COMMISSION

Outstanding Contribution to the Advance of Applied Meteorology
Award for Broadcast Meteorology
Award for Excellence in Science Reporting by a Broadcast Meteorologist
The Henry T. Harrison Award for Outstanding Contributions by a Consulting Meteorologist

WEATHER AND CLIMATE ENTERPRISE COMMISSION

The Kenneth C. Spengler Award

LOCAL CHAPTER AFFAIRS COMMITTEE

Local Chapter of the Year Award
(nomination form available online at www.ametsoc.org/amschaps/index.html.)

* Recommended by the Atmospheric Research Awards Committee in even-numbered years and by the Oceanographic Research Awards Committee in odd-numbered years.

2016 AWARDS COMMITTEES

SCIENTIFIC AND TECHNOLOGICAL ACTIVITIES COMMISSION

The Charles L. Mitchell Award
The Award for Exceptional Specific Prediction
The Francis W. Reichelderfer Award
The Helmut E. Landsberg Award
The Award for Outstanding Achievement in Biometeorology

- **LECTURERS**
  Robert E. Horton Lecturer in Hydrology
  Bernhard Haurwitz Memorial Lecturer
  Walter Orr Roberts Lecturer
- **PAPER**
  Banner I. Miller
- **STUDENT PAPERS**
  Robert Leviton Student Prize
  Max A. Eaton Student Prize
  Spiros G. Geotis Student Prize
  Peter V. Hobbs Student Prize
- **NAMED SYMPOSIA**
  Section E, of the Policy, Guidelines, and Procedures for Awards and Lectureships provides the Policy on Named Conferences/Symposia and Special Issues of AMS Journals *(full policy description available at www.ametsoc.org/awards):*

> Recognition of scientists in the fields served by the AMS, living or deceased, in the form of a named conference or symposium or a named special issue of one of the Society's journals is an honor reserved for only the most outstanding of our colleagues. It should be awarded only to those individuals who are completing a career, or who have recently died having completed a career, of significant achievements in their field and whose contributions would make them worthy of consideration for Honorary Member of the AMS…

2016 FELLOWS COMMITTEE

The Committee's function is to submit to the Council the names of individuals for election to Fellow.

> Article III, Section 6, of the AMS Constitution provides that those eligible for election to Fellow shall have made outstanding contributions to the atmospheric or related oceanic or hydrologic sciences or their applications during a substantial period of years. The nominees for Fellow must be a member of the Society and remain on the committee's active list for three years.

A nomination letter and three supporting letters should be electronically submitted before 1 May 2016. A list of Fellows and the process for submitting nominations are on the AMS website (www.ametsoc.org/awards).

2016 NOMINATING COMMITTEE

The Committee's function is to submit to the Council the names of individuals for 1) the office of President-Elect for a term of one-year starting at the close of the 97th Annual Meeting (January 2017) and 2) four positions on the Council for a term of three-years starting at the close of the Annual Meeting. Nominations must be submitted prior to 1 April 2016 to the Nominating Committee.

HONORARY MEMBERS

Article III, Section 5, of the AMS Constitution provides that Honorary Members shall be persons of acknowledged preeminence in the atmospheric or related oceanic or hydrologic sciences, either through their own contributions to the sciences or their application or through furtherance of the advance of those sciences in some other way. They shall be exempt from all dues and assessments. The nominees for Honorary member remain on an active list for three years.

Deadline: 1 June 2016; a form and list of Honorary Members is available at www.ametsoc.org/awards.

EYEWITNESS

Evolution of the Atmospheric Sciences

by ROBERT G. FLEAGLE

Eyewitness: Evolution of the Atmospheric Sciences describes how the atmospheric sciences were transformed in the span of the author's professional career from its origins in primitive weather forecasting to its current focus on numerical modeling of environmental change. It describes the author's observations of persons, events, and institutions beginning with graduate study during the Second World War and moving on to continuing expansion of the atmospheric sciences and technologies, through development of a major university department, development of new scientific and professional institutions, and to the role that the science of the atmosphere now plays in climate change and other issues of social and political policy.

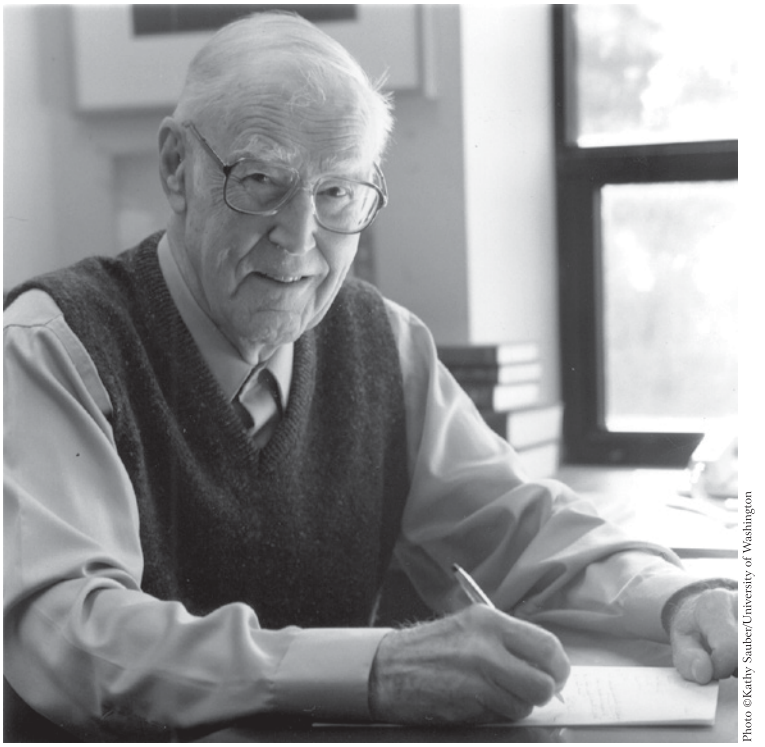

Photo ©Kathy Sauber/University of Washington

EYEWITNESS: EVOLUTION OF THE ATMOSPHERIC SCIENCES

ISBN 1-878220-39-X, 129 pp., hardbound, $75 list/$55 member.

Order online: www.ametsoc.org/amsbookstore

or see the order form at the back of this issue.

ABOUT THE AUTHOR

Robert G. Fleagle earned degrees in physics and meteorology at The Johns Hopkins University and New York University and began his professional career in 1948 at the University of Washington (UW). His research has focused on the structure of midlatitude cyclones, the physics and structure of the surface boundary layer, and processes of air–sea interaction. He is the author of about 100 papers published in scientific journals and of books on atmospheric physics and global environmental change. Applications of science to social and political policy have been important motivations for his career and have occupied his attention increasingly as the decades passed.

Fleagle participated at close range in the beginnings and growth of a major university department and of the University Corporation for Atmospheric Research (UCAR). In 1963 and 1964 he served as a staff specialist in the Office of Science and Technology, Executive Office of the President, and in 1977–78 he served as consultant to the National Oceanic and Atmospheric Administration. He has held many administrative posts including chairman of the UW Department of Atmospheric Sciences (1967–77), chairman of the National Academy of Sciences Committee on Atmospheric Sciences (1969–73),

CORPORATION AND INSTITUTIONAL MEMBERS

SUSTAINING MEMBERS

Ball Aerospace & Technologies Corporation
Baron Services, Inc.
Exelis
Harris Corporation
Lockheed Martin Corporation
Northrop Grumman Corporation
The Aerospace Corporation
The Boeing Company
University Corporation for Atmospheric Research
Vaisala, Inc.

REGULAR MEMBERS

AccuWeather, Inc.
Aerospace & Marine International Corporation
All Weather, Inc.
Atmospheric and Environmental Research, Inc.
Atmospheric Technology Services Company, LLC
Belfort Instrument Company
Botswana Meteorological Services
Campbell Scientific, Inc.
CLS America, Inc.
Coastal Environmental Systems
CSIRO Marine and Atmospheric Research
Davis Instruments Corporation
Earth Networks
EKO Instruments Company, Ltd.
Enterprise Electronics Corporation
Environmental Systems Research, Inc.
ERT, Inc.
EWR Weather Radar Systems
Global Hydrology and Climate Center
Global Science & Technology, Inc.
Global Weather Corporation
I. M. Systems Group
Johns Hopkins University, Applied Physics Laboratory
Kipp & Zonen USA Inc.
Meteorological Technology International
MeteoSwiss
Murray & Trettel, Inc.
National Centre for Medium Range Weather Forecasting
Orbital ATK, Inc.
Panasonic Weather Solutions
Pelmorex Media Inc.
ProSensing, Inc.
Radiometrics Corporation
Raytheon Company
R. M. Young Company
Riverside Technology, inc.
Royal Netherlands Meteorological Institute
Schneider Electric Weather
Science Applications International Corporation
Science Systems and Applications, Inc.
Scintec AG
SeaSpace Corporation
SGT, Inc.
Sonalysts, Inc.
SpectraSensors, Inc.
Sutron Corporation
The Weather Channel
U.S. Department of Energy, Office of Science
Unisys Corporation
University of Alabama in Huntsville, Earth System Science Ctr
University of Illinois, Department of Atmospheric Sciences
University of Wisconsin—Madison, SSEC
Vieux, Inc.
Weather Decision Technologies
Weather Modification, Inc.
Weather Services International, Inc.

SMALL BUSINESS MEMBERS

Advances in Atmospheric Sciences
Climadata Corporation
Geonor, Inc.
Hwind Scientific, LLC
National Council of Industrial Meteorologists
National Weather Service Employees Organization
PCE Americas, Inc.
Remtech, Inc.
Tempus Global Data, Inc.
WeatherSTEM, Inc.
www.WeatherVideoHD.TV
Yankee Environment Systems, Inc.

PUBLICATIONS MEMBERS

Abdus Salam International Centre for Theoretical Physics
Air Force Weather Agency
ARPA FVG, Osservatorio Meteorologico Regionale
Bureau of Meteorology
Civil Aeronautics Administration, MOTC
Colorado State University Libraries
Columbia University, Lamont-Doherty Geological Observatory

For questions relating to corporation and institutional membership, please contact Maria Sarantopoulos at AMS Headquarters—telephone: 617-227-2426, x3912; fax: 617-742-8718; e-mail: msarantopoulos@ametsoc.org; or write to American Meteorological Society, Attn: Maria Sarantopoulos, 45 Beacon St., Boston, MA 02108-3693.

CORPORATION AND INSTITUTIONAL MEMBERS

Membership in the American Meteorological Society does not imply AMS endorsement of an organization's products or services.

Creighton University Reinert/Alumni Memorial Library
Dartmouth College Baker Library
Desert Research Institute
Deutscher Wetterdienst
Embry Riddle Aeronautical University
Environment Canada Library, Downsview
EUMETSAT Library
Finnish Meteorological Institute
Florida International University Library
Florida State University, Department of EOAS
Geophysical Institute/International Arctic Research Center
Harvard University, Gordon McKay and Blue Hill Libraries
Hong Kong Observatory Library
India Meteorological Department
Indian Institute of Technology Bhubaneswar
Indian Institute of Tropical Meteorology
Indiana University Library
Instytut Meteorologii I Gospodarki Wodnej
Irish Meteorological Service
Japan Weather Association
Joint Typhoon Warning Center
Los Alamos National Laboratory
Lyndon State College, Samuel Read Hall Library
MBL/WHOI Library
Meteo-France
Meteorological Service of New Zealand Ltd.
Meteorologisk institutt
Millersville University, Department of Earth Sciences
MIT, Lincoln Laboratory
National Centers for Environmental Information
National Environment Agency
National Weather Center Library
Naval Postgraduate School, Dudley Knox Library
New York University
NIWA Wellington Library
NOAA - GLERL Library
NOAA AOML Library
NOAA Central Library
NOAA Seattle Library
North Carolina State University Hunt Library
Pennsylvania State University, Paterno Library
Purdue University Libraries
Republic of Korea Air Force, Headquarters
South African Weather Service
St. Louis University, Dept. of Earth & Atmospheric Sciences
Swedish Meteorological & Hydrological Institute
U.K. National Meteorological Library
U.S. Army Corps of Engineers, Library - ERDC
U.S. Department of Commerce, Boulder Labs Library
U.S. EPA Main Library
Universitatsbibliothek Innsbruck
Universitatsbibliothek Trier
University of Colorado Libraries
University of Copenhagen, Niels Bohr Institute Library
University of Delaware Library
University of Frankfurt Library
University of Hawaii at Manoa, Library
University of Maryland, McKeldin Library
University of Melbourne, Baillieu Library
University of New South Wales Library
University of North Carolina, Ramsey Library
University of North Dakota, Chester Fritz Library
University of Northern Colorado, Michener Library
University of Oklahoma, School of Meteorology
University of Washington Libraries
WeatherPredict Consulting Inc.
Weizmann Institute of Science
Yale University, Geology Library
Zentralanstalt fur Meteorologie und Geodynamik

Color indicates new or reinstated member

FELLOWSHIP AND SCHOLARSHIP SPONSORS

FELLOWSHIPS
AMS Giving Program
DOE, Atmospheric System Research
Lockheed Martin Corporation*
NASA Earth Science
NOAA's Climate Program Office
NOAA's National Weather Service

FRESHMAN AND UNDERGRADUATE SCHOLARSHIPS
Baron Services Inc.
Earth Networks
CLS America, Inc.
Harris Corporation
Lockheed Martin MS2
Naval Weather Service Association
Raytheon Company
R. M. Young Company
SAIC, Center for Atmospheric Physics
Science and Technology Corporation
Stinger Ghaffarian Technologies
Vaisala, Inc.
Jerome Namias Memorial Endowed Scholarship
Edgar J. Saltsman Endowed Scholarship
Bernard Vonnegut and Vincent Schaefer Endowed Scholarship
Percival D. Wark and Clara B. (Mackey) Wark Endowed Scholarship

*Corporate Patron

MINORITY SCHOLARSHIPS
AMS Giving Program

SENIOR SCHOLARSHIPS
AMS 75th Anniversary Endowed Scholarship
Bhanwar Lal Bahethi Scholarship
Om and Saraswati Bahethi Scholarship
Saraswati (Sara) Bahethi Scholarship
Werner A. Baum Undergraduate Endowed Scholarship
Loren W. Crow Memorial Scholarship
The Dr. Robert Fraser Scholarship
Karen Hauschild Friday Endowed Scholarship
Bob Glahn Endowed Scholarship in Statistical Meteorology
The Jerry C. Glover Scholarship
Dr. Pedro Grau Undergraduate Scholarship
Richard and Helen Hagemeyer Scholarship
John R. Hope Endowed Scholarship in Atmospheric Sciences
David S. Johnson Endowed Scholarship
Larry R. Johnson Scholarship
Dr. Yoram Kaufman Scholarship
Carl W. Kreitzberg Endowed Scholarship
Ethan and Allan Murphy Endowed Memorial Scholarship
The Naval Weather Service Association Scholarship Award
K. Vic Ooyama Endowed Scholarship
The Orville Family Endowed Scholarship in Meteorology
The Ken Reeves Scholarship
Michael J. Roberts, Jr. Scholarship
Guillermo Salazar Rodriguez Undergraduate Scholarship
Mark J. Schroeder Endowed Scholarship in Meteorology

The Life Cycles of Extratropical Cyclones

Edited by Melvyn A. Shapiro and Sigbjørn Grønås

Containing expanded versions of the invited papers presented at the International Symposium on the Life Cycles of Extratropical Cyclones, held in Bergen, Norway, 27 June–1 July 1994, this monograph will be of interest to historians of meteorology, researchers, and forecasters. The symposium coincided with the 75th anniversary of the introduction of Jack Bjerknes's frontal-cyclone model presented in his seminal article, "On the Structure of Moving Cyclones." The monograph's content ranges from a historical overview of extratropical cyclone research and forecasting from the early eighteenth century into the mid-twentieth century, to a presentations and reviews of contemporary research on the theory, observations, analysis, diagnosis, and prediction of extratropical cyclones. The material is appropriate for teaching courses in advanced undergraduate and graduate meteorology.

***The Life Cycles of Extratropical Cyclones* is available for $75 list/$55 members.**
To order, visit www.ametsoc.org/amsbookstore, or see the order form at the back of this issue.

SPACE RESERVED FOR CERTIFIED CONSULTING METEOROLOGISTS

MURRAY AND TRETTEL, INCORPORATED

THOMAS R. PIAZZA

Certified Consulting Meteorologist

Operational Forecasting • Media • Air Quality/Meteorological/PSD Monitoring/Wind Assessment/Studies • Forensic Research • Dispersion Modeling • Nuclear Emergency Support

600 First Bank Drive, Suite A
Palatine, IL 60067
847-934-8230
FAX: 847-963-0199
E-mail: Thomas.Piazza@WeatherCommand.com

NORTH AMERICAN WEATHER CONSULTANTS

DON A. GRIFFITH, PRESIDENT

Certified Consulting Meteorologist

Weather Modification • Air Quality Surveys & Field Studies • Applied Research • Forensic Meteorology

8180 South Highland Dr., Suite B-2
Sandy, UT 84093
801-942-9005
FAX 801-942-9007
E-mail: nawc@nawcinc.com

WEATHER RESEARCH CENTER JOHN C. FREEMAN WEATHER MUSEUM

JILL F. HASLING, DIRECTOR

Certified Consulting Meteorologist

Worldwide Weather & Oceanographic Forecasting • Climatology • Training • Expert Testimony • Research in Meteorology & Oceanography • Wave Spectra • Software Development • The WRC Weather Museum

5090 Richmond #467
Houston, Texas 77056
Phone: 713-529-3076
E-mail: WRC@wxresearch.org
website: www.wxresearch.com

TRC ENVIRONMENTAL CORP.

GALE F. HOFFNAGLE
DOUGLAS R. MURRAY
PIETRO A. CATIZONE
DAVID FOX
ELIZABETH STANKO

Certified Consulting Meteorologists

Environmental Consulting & Research • Applied Meteorology • Air Quality and Meteorological Monitoring • Diffusion Modeling • Tracer Studies • Air Toxics Monitoring • Expert Testimony

1-800-TRC-5601
Offices in major industrial centers throughout the United States

McVEHIL-MONNETT ASSOCIATES, INC.

GEORGE E. McVEHIL, Ph.D.
KENDALL C. NECKER

Certified Consulting Meteorologists

Air Quality Analysis and Monitoring • Permitting • Dispersion Modeling • Air Toxics • Meteorological Analysis • Industrial Meteorology • Litigation Support • Expert Testimony

44 Inverness Drive East
Building C
Englewood, CO 80112
303-790-1332
FAX 303-790-7820
www.mcvehil-monnett.com

APPLIED METEOROLOGY, INC.

JOHN W. HATHORN

Certified Consulting Meteorologist

Meteorological Consulting & Analysis • Air Quality Modeling & Monitoring • Site Selection & Permitting • Environmental Data Acquisition Systems & Network with Remote-Control

9110 Weymouth Dr.
Houston, TX 77031-3034
713-995-5004
E-mail: hathorn.ami@gmail.com

SIMPSON WEATHER ASSOCIATES, INC.

M. GARSTANG, Ph.D.
G. D. EMMITT, Ph.D.
R.H. SIMPSON, Ph.D. (retired)

Certified Consulting Meteorologists

Environmental Risk Assessment • Air Quality Modeling/Monitoring • Instrumentation Development/Deployment • Lidar simulation/application

809 E. Jefferson St.
Charlottesville, VA 22902
434-979-3571
FAX: 434-979-5599

AEROCOMP

JOSEPH A. CATALANO

Certified Consulting Meteorologist

Expert Testimony • Climatological Analysis • Industrial Meteorology & Air Impact • Atmospheric Modeling • Wind & Ice Loading • Data Management Software & Services

P.O. Box 26109
Santa Ana, CA 92799-6109
714-964-3672
FAX: 714-964-1357
E-mail: ccm299@aerocomp.com

ACCUWEATHER ENTERPRISE SOLUTIONS, INC.

MICHAEL R. SMITH, SENIOR VICE PRESIDENT AND CHIEF INNOVATION EXECUTIVE
STEPHEN P. PRYOR, EXPERT SENIOR FORENSIC METEOROLOGIST

Certified Consulting Meteorologists

• Premier Meteorological Consultants Serving All Industries • Forensic Services • Forecast Services • Expert Testimony • Exclusive Technology • Extensive Database • Comprehensive Studies

100 North Broadway, Suite 750
Wichita, KS 67202
www.accuweather.com/enterprisesolutions
Phone: 316-266-8000
Fax: 316-366-4934
salesmail@accuweather.com

METEOROLOGICAL EVALUATION SERVICES, CO. INC. (MES)

PATRICK T. BRENNAN, PRESIDENT

Certified Consulting Meteorologist

Air-Quality Consulting • Expert Testimony • Industrial Meteorology • Nuclear Licensing Studies • Weather Investigations for Legal and Insurance Firms

165 Broadway
Amityville, NY 11701
631-691-3395
E-mail: pbrennan@mesamity.com

Certified Consulting Meteorologist: The certification program of the American Meteorological Society is aimed at fostering the establishment and maintenance of a high level of professional competency, and mature and ethical counsel, in the field of consulting meteorology. Requirements of knowledge, experience, and character are determined by a five-person board. Objectives of the program and application procedures are described in full detail in the August 2001 *Bulletin* (pp. 1689–1694).

PROFESSIONAL DIRECTORY

SPACE RESERVED FOR CERTIFIED CONSULTING METEOROLOGISTS

ACCUWEATHER, INC.

ELLIOT ABRAMS, SENIOR VICE PRESIDENT
STEPHAN M. WISTAR, SENIOR METEOROLOGIST

Certified Consulting Meteorologists

Meteorological Consultants Serving Industry, Government and the Media • Forensic Services • Forecast Services • Expert Testimony • Complete Database • Applied Information Technologies

385 Science Park Road
State College, PA 16803
www.AccuWeather.com

814-235-8626
Fax: 814-235-8769
E-mail: forensics@accuweather.com

Superior Accuracy™

TRINITY CONSULTANTS

GEORGE J. SCHEWE, PRINCIPAL CONSULTANT
ANTHONY J. SCHROEDER, MANAGING CONSULTANT

Certified Consulting Meteorologists

Air Quality Consulting • Regulatory Modeling • Meteorology/Climatology • Dispersion Modeling Courses Worldwide • BREEZE® Dispersion Modeling Software • Litigation Support

Covington, KY 859-341-8100
Indianapolis, IN 317-451-8100

gschewe@trinityconsultants.com
tschroeder@trinityconsultants.com

www.trinityconsultants.com
Offices Nationwide 800-229-6655

ANTHONY (ANDY) JOHNSON

Certified Consulting Meteorologist

Expert Testimony • Weather Investigations for Legal and Insurance Firms • Forensic Meteorology • Consultant since 1979

3912 West Dale Ave.
Tampa, FL 33609

Phone: 813-310-3865
Alt: 813-878-2929
FAX: 813-878-2939
E-mail: AJohnsonWX@gmail.com

METEOROLOGICAL SOLUTIONS INC.

GEORGE W. WILKERSON, PRINCIPAL CONSULTANT
DAN A. RISCH, MANAGING CONSULTANT

Certified Consulting Meteorologists

Ambient Monitoring • Meteorological Towers (2 to 100 m) • AERMOD & CALPUFF Modeling • Permitting • Performance Audits • Remote Data Management and Web Hosting • Applied Meteorology • Forensic Meteorology • Field Studies

4525 Wasatch Blvd., Suite 200
Salt Lake City, Utah 84124
www.metsolution.com

Ph/Fax: 801-272-3000/3040
drisch@trinityconsultants.com
gwilkerson@trinityconsultants.com

HOW THE WEATHERWORKS

H. MICHAEL MOGIL, PRESIDENT AND CEO

Certified Consulting Meteorologist

Forensic Meteorology • Expert Testimony • Weather Investigations for Legal and Insurance Firms • Data Analysis • Educational Design • Weather-based Training and Educational Courses • Science Writing • Weather Photography.

5644 Tavilla Circle - Suite #201
Naples, FL 34110
www.weatherworks.com
hmmogil@weatherworks.com

Phone: 239-591-2468
Cell: 240-426-2900
Fax: 202-742-2806

AIR WEATHER & SEA CONDITIONS, INC.

JAY ROSENTHAL, PRESIDENT

Certified Consulting Meteorologist

Expert testimony and data analysis for legal and insurance matters • Accident weather reconstruction • Satellite Interpretation • Air Pollution Transport • Excellent Client References • Emergency Response

P. O. Box 512
Pacific Palisades, CA 90272
website: www.weatherman.org

Phone: 818-645-8632
310-454-7549
FAX: 310-454-7569
E-mail: AirWeather@aol.com

MAYACAMAS WEATHER CONSULTANTS

JOHN P. MONTEVERDI, Ph.D., DIRECTOR

Certified Consulting Meteorologist

Forensic Meteorology • Climate Studies • Litigation Support • Expert Testimony • Operational Forecasts and Nowcasts

4425 View Street
Oakland, CA 94611

415-882-9898
Fax: 510-653-4320

E-mail: montever@comcast.net
website: www.mayacamaswx.com

CLIMATE PHYSICS, LLC

EDWIN X BERRY, Ph.D.

Certified Consulting Meteorologist

Consulting Services • Modeling Analyses and Studies • Forensic Meteorology • Research and Development • Expert Testimony • Climatology • Weather Modification • Climate Change • CCM #180

439 Grand Dr., #147
Bigfork, MT 59911

406-471-1464
ed@edberry.com

WEATHER DECISION TECHNOLOGIES, INC.

RICHARD L. CARPENTER, JR., Ph.D.
J. WILLIAM CONWAY
E. DeWAYNE MITCHELL
BRENT L. SHAW

Certified Consulting Meteorologists

Radar Meteorology • Severe Weather Nowcasting and Analysis • Mesoscale and Microscale Numerical Modeling • Aviation Weather • Forensic Meteorology • Expert Testimony

201 David L. Boren Blvd., Ste. 270
Norman, OK 73072
405-579-7675

www.wdtinc.com
info@wdtinc.com

AECOM

HOWARD BALENTINE

Certified Consulting Meteorologists

Air Quality Modeling • Air Pollution and Meteorological Studies • Air Toxic Risk Assessment • Clean Air Act Regulatory Analysis • Climate Change Analyses • Emission Inventory Development • Expert Testimony • Greenhouse Gas Footprint • Risk Management and Process Safety • Toxic and Flammable Hazards Assessment • Weather and Air Quality Forecasting

1220 Avenida Acaso
Camarillo, CA 93012

(805) 388–3775

For professional card rates, please apply to:
Executive Director, American Meteorological Society, 45 Beacon St., Boston, MA 02108-3693

SPACE RESERVED FOR CERTIFIED CONSULTING METEOROLOGISTS

Certified Consulting Meteorologist: The certification program of the American Meteorological Society is aimed at fostering the establishment and maintenance of a high level of professional competency, and mature and ethical counsel, in the field of consulting meteorology. Requirements of knowledge, experience, and character are determined by a five-person board. Objectives of the program and application procedures are described in full detail in the August 2001 *Bulletin* (pp. 1689–1694).

PROFESSIONAL DIRECTORY

SPACE RESERVED FOR MEMBERS

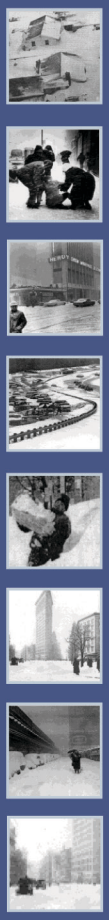

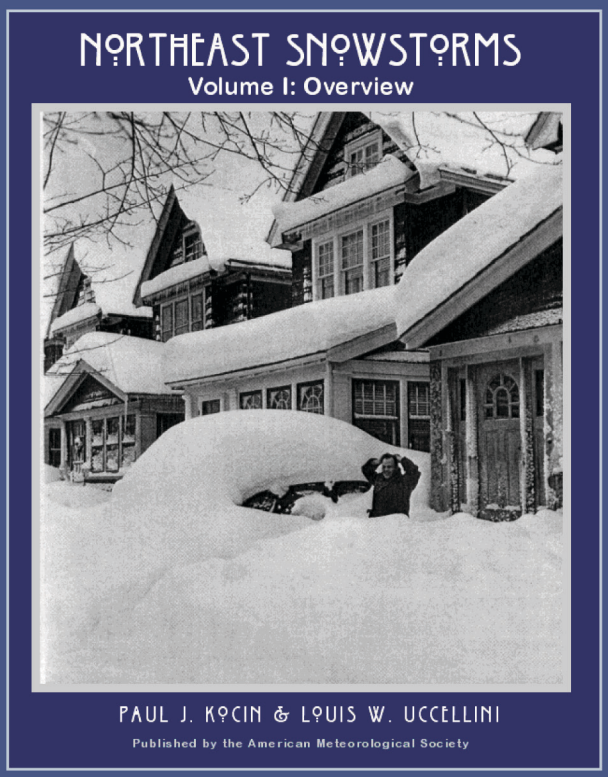

NORTHEAST SNOWSTORMS

Volume I: Overview

Volume II: The Cases

Paul J. Kocin and Louis W. Uccellini

Northeast Snowstorms offers the most comprehensive treatment on winter storms ever compiled: more than 50 years of professional experience in the form of a two-volume compendium of insights, examples, photographs, over 200 color figures, and a DVD of added material.

American Meteorological Society; 818 pages, hardbound;
AMS code MM54

Price: $100.00 list/$80.00 member/ $60.00 student member

ORDER ONLINE!

www.ametsoc.org/amsbookstore

or see the order form at the back of this issue.

EMPLOYMENT

Director of the Cooperative Institute for Mesoscale Meteorological Studies
University of Oklahoma

The University of Oklahoma invites nominations and applications for a dynamic, visionary leader to serve as Director of the highly successful Cooperative Institute for Mesoscale Meteorological Studies (CIMMS).

CIMMS was established in 1978 as a cooperative program that unites the scientific and technical resources of National Oceanic and Atmospheric Administration (NOAA) and The University of Oklahoma (OU) into a center of research excellence. CIMMS was created to support NOAA's Mission of Science, Service and Stewardship and thereby contribute to NOAA's long-term goal of building a Weather-Ready Nation that is prepared for and responds to weather-related events. CIMMS research areas include weather radar, hydrometeorology, observations and numerical modeling of high-impact weather including severe storms, forecast and warning improvements, regional climate variations, the societal and socioeconomic impacts of weather and climate, and related subject areas.

The Director of CIMMS is expected to play a leadership role in fostering the development of collaborative research between NOAA and OU and work to realize the transitions of these research benefits to NOAA's operational mission. The successful applicant must also have a dedicated commitment to the academic and research mission of the University of Oklahoma. Qualifications include an earned doctorate degree in atmospheric sciences or a related field or equivalent experience; strong evidence of exceptional leadership skills, such as managing a large, multi-disciplinary organization; a record of personal research; strong evidence of success in developing and executing a bold vision for collaborative research, including demonstrated success in resource mobilization; evidence of research breadth and/or substantial intellectual curiosity given the breadth of CIMMS activities; outstanding communication skills; leadership in professional service and recognized national and international visibility within the professional community; an understanding of strategies regarding the translation of research outcomes into operations; experience working at or familiarity with a comprehensive research university and an understanding of graduate student involvement in research; working knowledge of how policies are developed within NOAA or similar organizational entities including experience of successfully working with administrators, funding managers and the legislative process to develop and sustain programs and projects. Director of CIMMS will also be appointed as a tenured Professor in the School of Meteorology of the College of Atmospheric and Geographic Sciences or in the appropriate academic department or school. The salary (commensurate with qualifications) and starting date are negotiable. This position will remain open until filled. References will be contacted only upon approval. Every effort will be made to ensure confidentiality in the process until the interview stage.

CIMMS is a unit within the National Weather Center at OU (http://www.nwc.ou.edu), the world's largest facility that brings together academic, operational, research, and support organizations in a uniquely synergistic fashion. The Center is part of OU's Research Campus (http://urc.ou.edu), which co-locates and strategically builds linkages among private sector, government, and academic organizations.

The NWC houses several NOAA operational and research organizations, including the National Severe Storms Laboratory (NSSL), the Storm Prediction Center (SPC), the National Weather Service (NWS) Forecast Office, the Weather Decision Training Division, and components of the Radar Operations Center that manages the Nation's WSR-88D radar systems. NSSL and CIMMS pioneered development and use of Doppler radars to monitor convective storms and detect signatures of severe weather, which eventually led to the establishment of the national network of WSR-88D Doppler radars and more recently, the introduction of polarimetric radar capabilities to improve precipitation estimates and identify hydrometeor types. NSSL and CIMMS scientists have worked closely over the past two decades with the SPC, NWS Forecast Offices and research experts world-wide at the Hazardous Weather Testbed to demonstrate the value of cutting-edge ensemble weather prediction systems in forecasting the probability of severe weather.

The School of Meteorology, also located in the NWC within the College of Atmospheric and Geographic Sciences, is the largest academic atmospheric science program in the nation, with more than 250 undergraduates, nearly 100 graduate students and 25 faculty. The School is most well-known for international leadership in the areas of severe storms, mesoscale dynamics, convective-scale modeling and radar research. However, the expertise of the faculty also includes atmospheric chemistry, polar studies, boundary layer and urban meteorology, climate, monsoon circulations, data assimilation, tropical meteorology, lightning, dynamics and cloud physics. Other OU organizations located in the NWC or housed nearby on the research campus include the Advanced Radar Research Center (ARRC), the Center for Analysis and Prediction of Storms (CAPS) and the Department of Interior's South Central Climate Science Center (CSC). A unique aspect of the School is the presence of numerous adjunct and affiliate scientists from these co-located research centers, CIMMS and from NOAA.

To apply, please submit a letter of interest including a statement that addresses one's leadership philosophy, research goals and teaching vision, a current curriculum vitae, and the names of four or more people who can serve as references (with full mailing and e-mail addresses, telephone, and fax numbers). Please address all correspondence to:

Dean Berrien Moore III
Vice President for Weather and Climate
College of Atmospheric and Geographic Sciences
Search Committee Chairperson
University of Oklahoma
120 David L. Boren Blvd.
Norman, OK 73072
Phone: 405-325-3095/Fax: 405-325-1180/E-mail: berrien@ou.edu
All E-mail correspondence should be copied to
Ms. Tracy Reinke: treinke@ou.edu
and
Ms. Lee Anne Sallee: lasallee@ou.edu

The University of Oklahoma is an Affirmative Action, Equal Opportunity Employer.
Women and minorities are encouraged to apply.

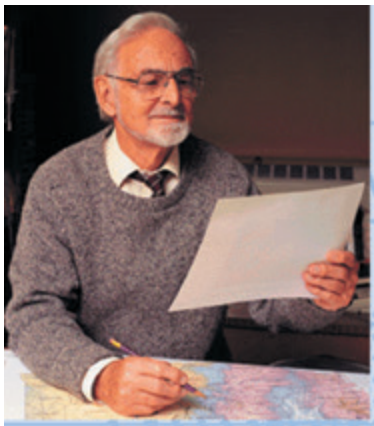

A Half Century of Progress in Meteorology: A Tribute to Richard Reed

edited by Richard H. Johnson and Robert A. Houze Jr.

with selections by: Lance F. Bosart, Robert W. Burpee, Anthony Hollingsworth, James R. Holton, Brian J. Hoskins, Richard S. Lindzen, John S. Perry, Erik A. Rasmussen, Adrian Simmons, Pedro Viterbo

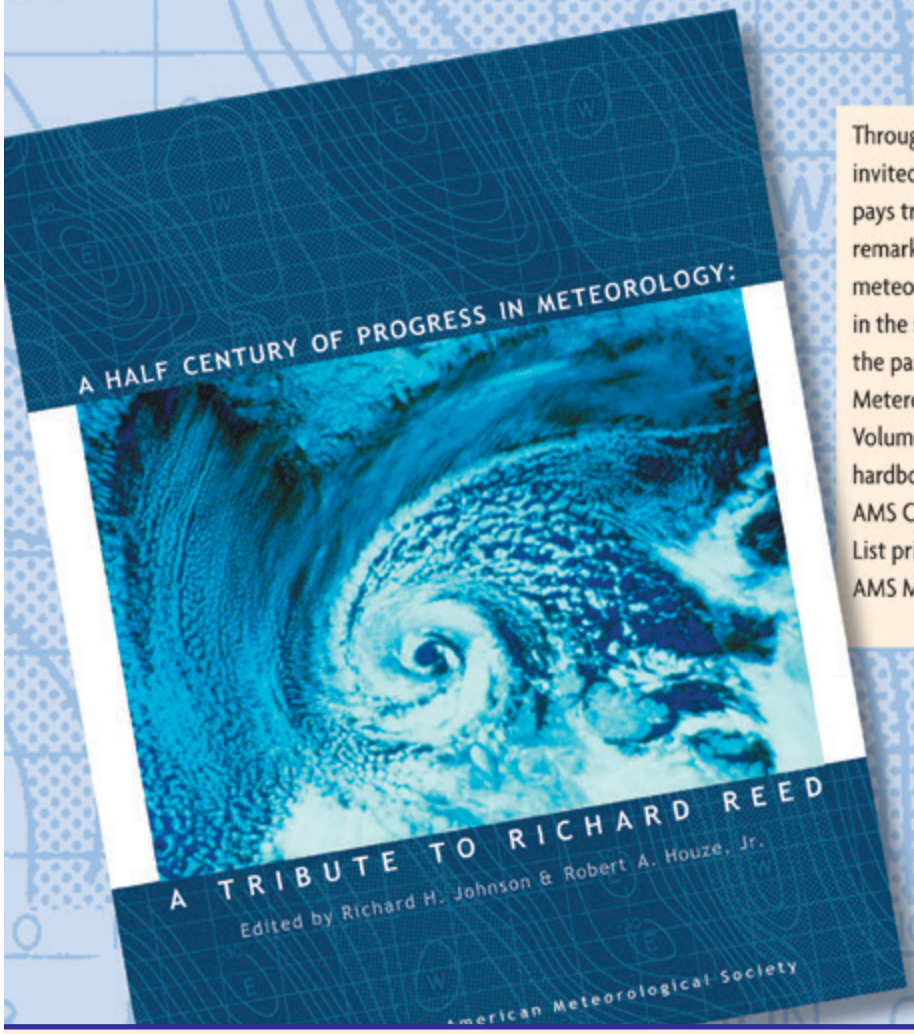

Through a series of reviews by invited experts, this monograph pays tribute to Richard Reed's remarkable contributions to meteorology and his leadership in the science community over the past 50 years. 2003. Meterological Monograph Series, Volume 31, Number 53; 139 pages, hardbound; ISBN 1-878220-58-6; AMS Code MM53.
List price: $80.00
AMS Member price: $60.00

ORDER ONLINE: bookstore.ametsoc.org or see the order form at the back of this issue

AMERICAN METEOROLOGICAL SOCIETY

A gift for every season.

(PLUS FREE SHIPPING!)

Fleece Scarf $17

COLOR: **Charcoal with AMS emblem**

Ceramic Mug $7

COLORS: **Navy with white AMS seal**
White with navy AMS seal

Umbrella with weather symbols $14

COLOR: **Navy with white symbols**

Silk Tie with weather symbols $17

COLORS: **Navy with white symbols and Burgundy with gold symbols**

Cotton T-Shirt

Adult: S, M, L, XL, XXL **$12**
Child: S, M, L **$10**

COLORS: **Navy with white AMS seal**
White with navy AMS seal

Travel Mug $8

COLOR: **Blue stainless steel with white AMS seal**

Membership Lapel Pins $10

COLOR: **Gold**

Soft Briefcase $27

COLOR: **Black with white AMS seal**
DIMENSIONS: **16"L, 12.5"H, 3.75"W (expands to 5")**

Silk Scarf with weather symbols $17

COLORS: **Navy with white symbols**
Burgundy with gold symbols

Long Sleeve T-Shirt

Mens: S, M, L, XL, XXL **$15**
COLOR: **Navy with white AMS seal**
Womens: S, M, L, XL **$15**
COLORS: **Gray with blue AMS seal**

12 Pocket CD Case $9

COLOR: **Blue with white AMS seal**

ORDER TODAY! Prepay by check/money order, Visa, MC, or AMEX

CALL 617-226-3998 FAX 617-742-8718

MAIL AMS, 45 Beacon Street, Boston, MA 02108-3693

FOR MORE GIFT IDEAS check out the new AMS Online Bookstore (weather books, biographies, histories, monographs and more) at www.ametsoc.org/amsbookstore.

INDEX TO ADVERTISERS

ONLINE CAREER CENTER

The AMS Online Career Center may be accessed through the AMS Web site at www.ametsoc.org/careercenter/index.html. In addition to posting positions, advertisers may search and view job seekers' résumés.

Job Posting Rates:
$375 (30-day posting)

$1593.75 (5 pack of jobs) Usable for 30-day job postings. Buy 5 job posting credits at a 15% discounted rate. These credits may be used at anytime during the next 12 months.

$3000 (10 pack of jobs) Usable for 30-day job postings. Buy 10 job-posting credits at a 20% discounted rate. These credits may be used at anytime during the next 12 months.

$3375 (12 pack of jobs) Usable for 30-day job postings or a continual 12-month posting. Buy 12 job-posting credits at a 25% discounted rate. These credits may be used at anytime during the next 12 months.

Advertisers may upload a company logo free of charge.

Résumés: View complete resumes for free! If you find any candidates you are interested in, submit your interest to them. If the candidate is interested in your opportunity, we connect you for just $20.00. If the candidate is not interested, you pay nothing!

AMS Corporation Member Discounts: Active AMS Corporation Members (small business, regular, or sustaining) receive a 25% discount when posting a position. Contact Kelly G. Savoie (ksavoie@ametsoc.org) to receive a coupon code. To receive the discount, the code must be entered when you post a position. The discount code is non-transferable.

AMS Member Benefit: AMS Members will be given 14-days advance access to a job listing. A member-only symbol will appear next to the posting. After 14 days, the job posting is open to all.

Submission of Ads: Advertisers must create an online account and submit ad text through the AMS Career Center site. Ad text may be entered at any time.

Payment Information: Prepayment is required by credit card or valid purchase order.

Contact Information: If you have questions, please contact Customer Service at 888-575-WORK (9675) (inside U.S.) or 860-440-0635 (outside U.S.).

ADVERTISING POLICY

The AMS will accept tasteful and accurate advertisements for products and services of professional interest to AMS members from organizations that are actively involved in the atmospheric and related sciences. The AMS also accepts advertising from organizations that have an interest in the atmospheric and related sciences and services, but are not actively involved in them. These organizations may promote their contributions to AMS activities and other good works, but may not directly promote products or services. The AMS reserves the right to refuse advertising that does not meet these criteria. Acceptance of advertising does not constitute the Society's endorsement of the product or service being advertised.

ORDER FORM

FOR AMS PUBLICATIONS ADVERTISED IN THIS ISSUE

Name: _____

Address: _____

City, State: _____ ZIP: _____

Province: _____ Country: _____

☐ Member (# _____)

☐ Nonmember

	Qty.	Member Price*	Nonmember Price*	Total
		(Please circle appropriate price)		
Eloquent Science: A Practical Guide to Becoming a Better Writer,				
Speaker, and Atmospheric Scientist (p. 1972)		$30.00	$45.00	
A Half Century of Progress in Meteorology:				
A Tribute to Richard Reed, MM No. 53 (p. 2021)		$60.00	$80.00	
Life Cycles of Extratropical Cyclones (p. 2014)		$55.00	$75.00	
Living on the Real World: How Thinking and Acting				
Like Meteorologists Will Help Save the Planet (p. 1943)		$22.00	$30.00	
Northeast Snowstorms, MM No. 54 (p. 2019)		$80.00	$100.00	
Student member price:		$60.00		
Radar and Atmospheric Science: A Collection of Essays				
in Honor of David Atlas (p. 2005)		$80.00	$100.00	
A Scientific Peak: How Boulder Became a World Center for				
Space and Atmosphric Science (p. 1844)		$25.00	$35.00	
Taken by Storm, 1938: A Societal and Meteorological History				
of the Great New England Hurricane (p. 1967)		$30.00	$40.00	
The Thinking Person's Guide to Climate Change (p. 1928)		$20.00	$30.00	
**** Shipping and handling: Please add $8 PER ORDER for delivery within the U.S. and $15 PER ITEM for deliveries outside the U.S. There is no shipping and handling charge on DVDs or CD-ROMs for either U.S. or foreign orders. Shipping prices subject to change.***		**SHIPPING**		
		TOTAL		

I am paying by: ☐ Check/money order ☐ Credit Card No. _____ Exp. date:_____

☐ Visa ☐ Mastercard ☐ American Express

Name on Card:_____ Billing address: _____

Signature: _____ _____

_____

☐ Please include an AMS membership application with my order.

Please send prepaid orders to Order Department, American Meteorological Society, 45 Beacon St., Boston, MA 02108-3693